PHOTOISOMERIZATION STUDIES OF SOME HYDRAZONE COMPOUNDS

OPAS TOJIRA

A THESIS SUBMITTED IN PARTIAL FULFILLMENT
OF THE REQUIREMENTS FOR
THE DEGREE OF MASTER OF SCIENCE
(PHYSICAL CHEMISTRY)
FACULTY OF GRADUATE STUDIES
MAHIDOL UNIVERSITY
2000

ISBN 974-664-103-4

Thesis

entitled

PHOTOISOMERIZATION STUDIES OF SOME HYDRAZONE COMPOUNDS

Opas Tojira

Mr. Opas Tojira
Candidate

Assoc. Prof. Prapin Wilairat, Ph.D.
Major-advisor

Prof. Orapin Rangsiman, Dr.rer.nat.
Co-advisor

Prof. Sauvarop Limcharoen, Dr.rer.nat.
Co-advisor

Prof. Liangchai Limlomwongse,
Ph.D.
Dean
Faculty of Graduate Studies

Prof. Sauvarop Limcharoen, Dr.rer.nat.
Chairman
Master of Science Programme
in Physical Chemistry
Faculty of Science

Thesis

entitled

PHOTOISOMERIZATION STUDIES OF SOME HYDRAZONE COMPOUNDS

was submitted to the Faculty of Graduate Studies, Mahidol University
for the degree of Master of Science (Physical Chemistry)
on
May 12, 2000

Opas Tojira
.....
Mr. Opas Tojira
Candidate

.....
Assoc. Prof. Prapin Wilairat, Ph.D.
Chairman

.....
Prof. Orapin Rangsiman, Dr.rer.nat.
Member

S. Benjavongkulchai
.....
Soontaree Benjavongkulchai, Ph.D.
Member

Sauvarop Limcharoen
.....
Prof. Sauvarop Limcharoen, Dr.rer.nat.
Member

.....
Prof. Liangchai Limlomwongse,
Ph.D.
Dean
Faculty of Graduate Studies
Mahidol University

.....
Assoc. Prof. Rassmidara Hoonsawat,
Ph.D.
Acting Dean
Faculty of Science
Mahidol University

ACKNOWLEDGEMENT

The author would like to express his sincere gratitude and deep appreciation to his advisor, Dr. Prapin Wilairat, for scientific thinking, valuable guidance and helpful discussion throughout the course of this work. His appreciation also goes to Dr. Sauvarop Limcharoen and Dr. Orapin Rangsiman for facilities, assistance, and their valuable comments and suggestions in the completion on this thesis.

Special words of thanks go to Dr. Soontaree Benjavongkulchai for her kindness and valuable suggestions. Additionally, he is especially grateful to Dr. Pramuan Tangboriboonrat for her kindness and encouragement.

For financial support during this project, he gratefully acknowledges the National Science and Technology Development Agency (NSTDA) and Faculty of Science, Mahidol University for the "Institutional Strengthening Programme" scholarship.

Finally, the author wishes to use this opportunity to express his grateful thanks to his family and friends for their kindness and encouragement.

Opas Tojira

3936141 SCPC/M: MAJOR: PHYSICAL CHEMISTRY; M.Sc. (PHYSICAL CHEMISTRY)
KEY WORDS : PHOTOISOMERIZATION / ZWITTERIONIC FORM / THERMAL CIS-TRANS ISOMERIZATION REACTION / PYRIDOXAL ISONICOTINOYL HYDRAZONE / KINETICS

OPAS TOJIRA: PHOTOISOMERIZATION STUDIES OF SOME HYDRAZONE COMPOUNDS. THESIS ADVISORS: PRAPIN WILAIRAT, Ph.D., SAUVAROP LIMCHAROEN, Dr.rer.nat., ORAPIN RANGSIMAN, Dr.rer.nat., 187 p. ISBN 974-664-103-4.

The photosensitive imine compound, pyridoxal isonicotinoyl hydrazone (PIH), and structural analogues, pyridoxal benzoyl hydrazone (PBH), pyridoxal salicyloyl hydrazone (PSH), benzaldehyde isonicotinoyl hydrazone (BIH), benzaldehyde benzoyl hydrazone (BBH), benzaldehyde salicyloyl hydrazone (BSH), salicylaldehyde isonicotinoyl hydrazone (SIH), salicylaldehyde benzoyl hydrazone (SBH) and salicylaldehyde salicyloyl hydrazone (SSH) were synthesized and characterized using electronic absorption, fluorescence excitation and emission, and infrared absorption spectroscopic techniques.

The existence of tautomeric forms of PIH in the solid state was investigated and confirmed using recrystallization, infrared spectroscopy and X-ray diffraction. There is formation of the zwitterionic form of the pyridoxal due to the transfer of the phenolic proton to the pyridoxal nitrogen when PIH crystallizes in the hydrated structure (1:1 PIH-to-water). UV-Visible and fluorescence spectral data indicate that the Schiff-base/pyridinium phenolate tautomeric forms only occur in the solid state. In solution state, the compound is readily converted to the normal Schiff-base (non-dipolar) form.

The configurational change of the two diastereomers associated with the carbon-nitrogen double bond of PIH and analogues has been observed via the change in electronic absorption spectra when their methanolic solutions are exposed to light. Upon keeping in the dark, the spectra slowly convert to the initial state at ambient temperature. In solid state, this behaviour does not occur to any significant extent.

The kinetics of the thermal cis-trans isomerization reactions of all the hydrazones in methanolic solutions have been investigated at four temperatures: 25.0, 30.0, 35.0 and 40.0 °C using UV-visible spectrophotometry. The results show that these reactions are first order, with the activation energies of 10–19 kcal mol^{-1} (42–80 kJ mol^{-1}) and logarithm of preexponential factors of 3–10. The temperature dependence of the first-order rate constant has also been analyzed using the Activated Complex Theory of reaction rate.

The activation energies and the preexponential factors are related to the *cis*-molecular structures of the hydrazones. It is difficult to directly compare the rates of the thermal cis-trans isomerizations of the various hydrazones. However, with hydrazones having the same value of the preexponential factors, their rates of reactions can be compared.

3936141 SCPC/M: สาขาวิชา: ฟิสิคัลเคมี; วท.ม. (ฟิสิคัลเคมี)

โอภาส โตจิระ: การศึกษาการเปลี่ยนรูปไอโซเมอร์ของสารประกอบไฮดราโซนบางชนิดเมื่อกระตุ้นด้วยแสง (PHOTOISOMERIZATION STUDIES OF SOME HYDRAZONE COMPOUNDS). คณะกรรมการควบคุมวิทยานิพนธ์: ประพิณ วิไลรัตน์, Ph.D., เสาวรภย์ ลิ้มเจริญ, Dr.rer.nat., อรพินท์ รังสิมันต์, Dr.rer.nat. 187 หน้า. ISBN 974-664-103-4

งานวิจัยนี้ได้ทำการสังเคราะห์สารประกอบซึ่งไวต่อแสง pyridoxal isonicotinoyl hydrazone (PIH) และสารประกอบที่มีโครงสร้างสัมพันธ์กับ PIH ได้แก่ pyridoxal benzoyl hydrazone (PBH), pyridoxal salicyloyl hydrazone (PSH), benzaldehyde isonicotinoyl hydrazone (BIH), benzaldehyde benzoyl hydrazone (BBH), benzaldehyde salicyloyl hydrazone (BSH), salicylaldehyde isonicotinoyl hydrazone (SIH), salicylaldehyde benzoyl hydrazone (SBH) และ salicylaldehyde salicyloyl hydrazone (SSH) และทำการตรวจสอบโดยใช้เทคนิคทางแสง electronic absorption, fluorescence excitation กับ emission และ infrared absorption

การศึกษาโครงสร้างของ PIH ในสถานะของแข็ง โดยการใช้ recrystallization, infrared spectroscopy และ X-ray diffraction พบว่า PIH สามารถเกิดผลึกแบบมีน้ำรวมอยู่ในโครงสร้างในสัดส่วนระหว่างโมเลกุลของ PIH กับ น้ำเป็นหนึ่งต่อหนึ่ง ในโครงสร้างนี้ไฮโดรเจนอะตอมจะเคลื่อนย้ายจาก phenolic-hydroxyl group ไปยังไนโตรเจนอะตอมของ pyridoxal เกิดเป็น zwitterion ผลจากสเปกตราของ UV-visible และ fluorescence ยังแสดงให้เห็นว่าโครงสร้างผสมระหว่าง Schiff base และ pyridinium phenolate เกิดขึ้นเฉพาะในของแข็งเท่านั้น ในสารละลาย PIH จะเปลี่ยนไปอยู่ในรูปของ Schiff base ทั้งหมด

เมื่อโดนแสง PIH และไฮดราโซนที่มีโครงสร้างสัมพันธ์ในสารละลายเมธานอล จะเกิดการเปลี่ยนรูปไอโซเมอร์ โดยหมุนรอบพันธะคู่ระหว่างคาร์บอนกับไนโตรเจน ซึ่งมีผลทำให้เกิดการเปลี่ยนแปลงในสเปกตราของ electronic absorption แต่เมื่อนำสารละลายเหล่านี้มาเก็บไว้ในที่มืด สเปกตราจะเปลี่ยนกลับสู่สภาวะเดิมอย่างช้าๆ คุณสมบัติดังกล่าวนี้ไม่มีการเกิดขึ้นเมื่อสารประกอบอยู่ในสถานะของแข็ง

การศึกษาจลนศาสตร์ของการเปลี่ยนรูปไอโซเมอร์จาก cis เป็น trans โดยอาศัยความร้อนของไฮดราโซนทั้งหมดในสารละลายเมธานอลที่อุณหภูมิ 25.0, 30.0, 35.0 และ 40.0 °C โดยการใช้ UV-visible spectrophotometry แสดงว่า ปฏิกิริยาเหล่านี้เป็นปฏิกิริยาอันดับหนึ่ง ซึ่งมีพลังงานกระตุ้น 10–19 กิโลแคลอรีต่อโมล (42–80 กิโลจูลต่อโมล) และมีค่าแฟคเตอร์แห่งความถี่ในรูปของลอการิทึมเป็น 3–10 ในงานวิจัยนี้มีการวิเคราะห์ผลของอุณหภูมิที่มีต่ออัตราเร็วของปฏิกิริยา โดยใช้ทฤษฎี Activated Complex ด้วย

การพิจารณาค่าพลังงานกระตุ้นและค่าแฟคเตอร์แห่งความถี่ของทุกไฮดราโซนในสัมพันธ์กับโครงสร้างของโมเลกุล แสดงว่าการเปรียบเทียบอัตราเร็วของปฏิกิริยาโดยตรงจากค่าทั้งสองเป็นไปไม่ได้ ยกเว้นสำหรับบางปฏิกิริยาซึ่งมีค่าของแฟคเตอร์แห่งความถี่ใกล้เคียงกัน

CONTENTS

LIST OF TABLES

LIST OF FIGURES

Figure **Page**

Figure **Page**

Figure **Page**

Figure **Page**

Figure **Page**

LIST OF ABBREVIATIONS

DF	Desferrioxamine (Desferal®)
HBED	*N*, *N*′-bis(2-Hydroxybenzoyl)ethylenediamine-*N*, *N*′-diacetic acid
HP	3-Hydroxypyridin-4-one
PIH	Pyridoxal isonicotinoyl hydrazone
PBH	Pyridoxal benzoyl hydrazone
PSH	Pyridoxal salicyloyl hydrazone
BIH	Benzaldehyde isonicotinoyl hydrazone
BBH	Benzaldehyde benzoyl hydrazone
BSH	Benzaldehyde salicyloyl hydrazone
SIH	Salicylaldehyde isonicotinoyl hydrazone
SBH	Salicylaldehyde benzoyl hydrazone
SSH	Salicylaldehyde salicyloyl hydrazone
PpMBH	Pyridoxal *p*-methoxybenzoyl hydrazone
PmFBH	Pyridoxal *m*-fluorobenzoyl hydrazone
IIH	3-Hydroxyisonicotinaldehyde isonicotinoyl hydrazone
EDTA	Ethylenediaminetetraacetic acid
PPH	Pyridoxal 2-pyridyl hydrazone
MPH	1-(*N*-Methyl-pyridoxylidenium)-2-(2′-pyridyl)hydrazine iodide
EPH	1-(*N*-Ethoxy-carbonylmethylpyridoxylidenium)-2-(2′-pyridyl) hydrazine bromide
DMSO	Dimethyl sulfoxide

pycPIH	Pale yellow crystal PIH
docPIH	Deep orange crystal PIH
dopPIH	Deep orange powder PIH
oypPIH	Orange-yellow powder PIH
pysPIH	Pale yellow sheet PIH
oycPIH	Orange-yellow crystal PIH
IR	Infrared
FT-IR	Fourier transform infrared spectroscopy
^{1}H-NMR	Hydrogen-1 nuclear magnetic resonance
^{13}C-NMR	Carbon-13 nuclear magnetic resonance
UV	Ultraviolet
s.d.	Standard deviation
HPLC	High-performance liquid chromatography

pycPIH	Pale yellow crystal PIH
docPIH	Deep orange crystal PIH
dopPIH	Deep orange powder PIH
oypPIH	Orange-yellow powder PIH
pysPIH	Pale yellow sheet PIH
oycPIH	Orange-yellow crystal PIH
IR	Infrared
FT-IR	Fourier transform infrared spectroscopy
^{1}H-NMR	Hydrogen-1 nuclear magnetic resonance
^{13}C-NMR	Carbon-13 nuclear magnetic resonance
UV	Ultraviolet
s.d.	Standard deviation
HPLC	High-performance liquid chromatography

CHAPTER I

INTRODUCTION

After the potential of pyridoxal isonicotinoyl hydrazone as a physiological iron chelator was accidentally discovered by Ponka *et al.* in 1979 [1,2], its efficacy and those of other structurally related compounds were extensively studied with the view of development as new oral drugs for use in iron overload diseases. The only current clinical iron-chelating drug is desferrioxamine which is not effective when given orally and is also expensive.

From results of these studies, several interesting chemical properties of pyridoxal isonicotinoyl hydrazone and related compounds were found. These include the occurrence of the thermal- and photo-interconversions of the cis and trans isomers associated with the carbon-nitrogen double bond which can be observed from changes in optical absorption of compounds [3]. In addition, photochromic and thermochromic behaviours may also be significant for some compounds which have a hydroxyl group ortho to the carbon-nitrogen double bond [4-13]. Although the photochemistry of the imine system has been studied for a long time [14], this subject is still of interests, especially their photochromic and thermochromic properties.

In this research, certain chemical properties of these hydrazones are investigated in some detail.

1.1 Iron overload in man

While disturbances of iron balance almost invariably result in a reduction of total body iron content, a number of special situations occur in which iron overload occurs [15]. A human absorb about 1 mg of iron per day and excrete about the same amount. This is due to our very poor capacity to absorb dietary iron and to our relatively limited capacity to rid ourselves of iron compared to other mammals. This means that man lives on a knife-edge, where the slightest dis-equilibrium in iron homeostasis between absorption and excretion can lead to either iron deficiency or iron overload. Although the term **haemosiderosis** or **siderosis** can be used to indicate any increase in tissue iron, the term **iron overload** is preferable [16], and will be used here to describe the deposition of large amounts of storage iron in either or both reticuloendothelial cells and parenchymal tissues of the body. The term **haemochromatosis** will be reserved for conditions of massive iron overload, with cirrhosis and/or other tissue damage attributable to iron, and in which body iron stores are increased to 15 g or more [16].

Normal iron stores in human subjects represent up to 2,000 mg, present in roughly equal amounts between the macrophages of the reticuloendothelial system, the hepatic (liver) parenchymal cells, and the skeletal muscle. Although the concentration in skeletal muscle is low (15–30 μg), because of the large mass of muscle tissue (about 30 kg in an average man), muscular tissue still accounts for about one third of the normal body reserve. In iron overload, although muscle iron increases, it does so to a much lesser degree than do hepatic or reticuloendothelial bone marrow iron stores. Iron loading can be either parenchymal or reticuloendothelial, and may occur either by oral or parenteral routes. Parenchymal loading is seen in idiopathic haemochromatosis,

due to excess iron absorption from diets with normal amounts of bioavailable iron, and in the parenteral iron overloading due to the treatment of refractory, non-haemorrhagic anaemias with multiple blood transfusions. At the other extreme, patients with aplastic anaemia and hypocellular erythroid marrows tend to deposit most of the iron they receive by blood transfusions directly in reticuloendothelial cells [16].

Table 1.1 Causes of iron overload

I.	Increased iron absorption
	A. From diets with normal amounts of bioavailable iron
	1. Hereditary (HLA-linked) haemochromatosis
	2. Iron-loading anaemias (refractory anaemias with hypercellular erythroid marrow)
	3. Chronic liver disease (cirrhosis, portacaval shunt)
	4. Porphyria cutanea tarda
	5. Congenital defects (atransferrinemia and other disorders)
	B. From diets with increased amounts of bioavailable iron
	1. African dietary overload
	2. Kaschin-Beck (Urov) disease
	3. Medicinal iron ingestion
II.	Parenteral iron overload
	A. Transfusional iron overload
	B. Inadvertent iron overload from therapeutic injections
III.	Neonatal iron overload
	A. Hereditary tyrosinaemia
	B. Zellweger's cerebrohepatorenal syndrome
	C. Neonatal haemochromatosis
IV.	Focal sequestration of iron
	A. Idiopathic pulmonary haemosiderosis
	B. Hallervorden-Spatz syndrome
	C. Renal haemosiderosis

The causes of iron overload are summarized in Table 1.1 [17]. In both adults and children, iron overload may be produced by an increased absorption of dietary iron, by parenteral administration of iron, or both. Increased absorption of iron may be the result of (i) an inappropriately elevated absorption of iron from a diet containing normal amounts of iron (this occurs in idiopathic haemochromatosis [18], in the iron-loading anaemias and a number of other disorders), (ii) consumption of large amounts of dietary iron, as has been reported, for example for the South African Bantu population [19], and perhaps also, the prolonged ingestion of medicinal iron. Parenteral iron loading is produced by repeated blood transfusions, of which the thalassaemias represent the classic example, and much less often, by injections of therapeutic iron preparations. A number of iron overload conditions have been observed in the neonate and infant, presumably due to a disturbance in the regulation of maternal-foetal iron balance, although the pathogenesis of such disorders is not clear. Rarely, as in pulmonary haemosiderosis, sequestration of iron may lead to a focal iron overload. In all such disorders of iron overload the magnitude, rate and distribution of iron accumulation will influence the onset and the severity of the complications that are observed. While a number of estimates of the magnitude of the body burdens associated with clinical manifestations in iron overload can be made, it is also important to insist on a number of other factors. These include the distribution of the iron load between relatively harmless reticuloendothelial sites and potentially toxic parenchymal locations, internal redistribution of iron, the amounts of circulating non-transferrin-bound iron in serum, ascorbate status, and other factors which may influence the extent of tissue damage.

1.1.1 The thalassaemias

The name **thalassaemia** (Greek: *thalassa*, sea) was introduced to define miscellaneous cases of syndromes associated with chronic anaemias in individuals of Mediterranean origin [20]. As research into haemoglobin diseases expanded, it became apparent that the thalassaemias are a heterogeneous group of inherited blood disorders. Their underlying cause is a genetic mutation that affects the synthesis of α- or β-chains of haemoglobin [20,21]. For this reason, they are classified broadly into the α- and β-thalassaemias. The clinical severity is directly related to the extent of imbalance in α- or β-chain production and, in the case of β-thalassaemias, to the degree of compensation by γ-chain production.

The α-thalassaemias result from a very heterogeneous series of molecular defects of α-chain production. These fall into several groups which result from either deletions involving the α-globin genes or from so far ill-defined defects in which the globin genes are intact but their output is markedly reduced. There is a third group of α-thalassaemias which result from chain termination mutations which involve the α-globin genes.

The consequences of defective α-chain production are seen both in foetal and adult life because haemoglobins F and A share α-globin chains directed by the same gene loci. The structure of normal human foetal and adult haemoglobin is written $\alpha_2\gamma_2$ and $\alpha_2\beta_2$, respectively. When α-chain synthesis is defective in the foetus, excess γ-chains are produced which form γ_4 tetramers called **haemoglobin Bart's**. In adult life, defective α-chain synthesis leads to the production of β_4 tetramers or **haemoglobin H**. Haemoglobins Bart's and H remain as soluble molecules in the red cell precursors in

the marrow and after reticulocytes are delivered into the peripheral circulation, but because of their inherent instability gradually precipitate as the red cells age, and hence cause damage to the red cell membrane resulting in a haemolytic anaemia. Hence the anaemia of α-thalassaemia is mainly due to a shortened red cell survival and erythropoiesis is relatively effective.

The situation in β-thalassaemia, which is equally heterogeneous at the molecular level, is quite different. In all the β-thalassaemias, there is excess α-chain production but unpaired α-chains cannot form a soluble homotetramer like γ- and β-chains. Hence they rapidly precipitate in the red cell precursors. This leads to intramedullary death of a large number of the latter and thus to a marked degree of ineffective erythropoiesis. The resulting anaemia leads to erythropoietin production which stimulates erythroid expansion and hence there is a markedly expanded but grossly dyserythropoietic marrow mass.

Since iron absorption from the gastrointestinal tract is increased in dyserythropoietic states, the β-thalassaemias are characterized by progressive iron accumulation. If the associated anaemia requires regular transfusion, this adds a further source of iron and hence all the β-thalassaemias are characterized by marked iron-loading. On the other hand, those forms of α-thalassaemia which are compatible with foetal survival usually result in a relatively mild degree of anaemia in adult life (e.g., haemoglobin H disease) and are associated with relatively effective erythropoiesis. Hence iron-loading in α-thalassaemia is not a serious clinical problem.

1.1.2 Oral iron chelators

Iron overload is a serious problem in patients who undergoes blood transfusion regime necessary for the clinical management of certain chronic blood disorders such as the genetic anaemias generally known as the thalassaemia syndromes. The quality of life of the thalassaemia patients is greatly improved if a high transfusion regime is followed: the haemoglobin is maintained at a normal level rather than just above the safe limit. On the other hand with each blood transfusion up to 250 mg of iron is introduced as transfused erythrocytes. Siderosis will develop as iron(III) starts to accumulate as insoluble deposits of haemosiderin. Eventually this condition will be fatal as vital organs such as the liver and the heart suffer irreversible damage. The importance of chelation therapy therefore becomes apparent.

In principle, an iron-chelating drug mobilizes the excess of body iron in an excretable form thus reversing the iron balance. In practice the development of such a compound is a complicated task and despite widespread interest in the problem, no compound so far assayed has fulfilled all the requirements that an iron chelating drug should meet [3,15,21-24].

The desirable properties of chelators for the treatment of iron overload have been described by several authors. They include a high affinity and selectivity for iron (III) under physiological conditions, and a correspondingly low affinity for other metal ions (Ca, Mn, Cu, Mg, etc.) of biological importance. The drug must have accessibility to bind iron from a small, slowly replenished, chelatable iron pool and not interfere with heme synthesis. To minimize toxicity, it requires a limited lipophilicity of the iron-free chelator, rapid elimination of the iron-ligand complex from the body, no re-distribution or re-absorption of iron from the iron-ligand complex, low penetration of

the cerebro-spinal fluids by the iron-ligand complex, and no facilitation by the iron-ligand complex of microbial growth. In addition, the iron-chelating drug should be inexpensive, easy to take and should have no acute or long-term toxicity.

The iron chelating drug that has provided the most hope for patients with thalassaemia is **desferrioxamine** (Desferal®). Introduced in 1960 [25], it has been extensively evaluated in laboratory [26-28] and clinical studies [26,29] and is now the reference drug to which new chelators are compared. Desferrioxamine (DF, Figure 1.1), a naturally occurring sideramine of *Streptomyces pilosus*, is a hexadentate ligand comprised of three hydroxamic acid moieties which can bind to all of the coordination sites of iron in a 1:1 complex. Hydroxamates have a particularly high affinity for iron which explains their wide distribution among the siderophores. This particular compound has been used in iron-chelation therapy for more than 15 years. Until recently, however, its lack of oral effectiveness together with other drawbacks, such as pain at the site of injection, severely limited its acceptance.

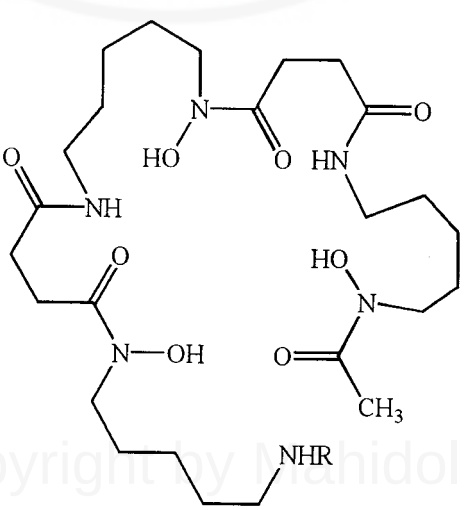

Figure 1.1 Structural formula of the hydroxamate-containing siderophore desferrioxamine (alternating $NH_2-(CH_2)_n-NHOH$ and succinate).

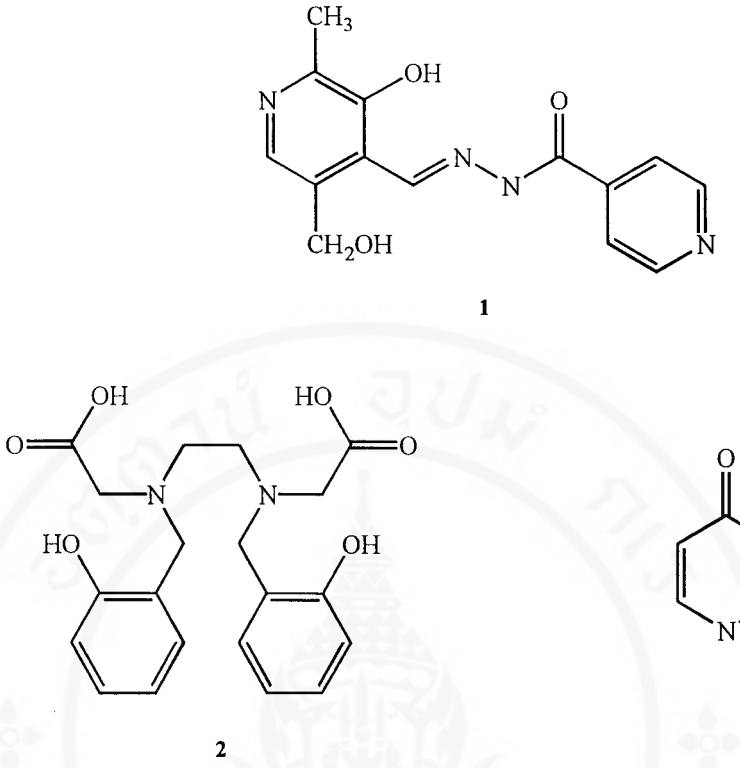

Figure 1.2 Structural formulas of orally effective candidates 1. pyridoxal isonicotinoyl hydrazone (PIH), 2. *N,N'*-bis(2-hydroxybenzoyl)ethylenediamine-*N,N'*-diacetic acid (HBED) and 3. 3-hydroxypyridin-4-one (HP) being currently studied for their possible use as iron chelating drugs.

Research into improved iron chelators is therefore warranted with particular emphasis on their oral effectiveness.

A number of orally active candidates are being tested [15,21,23,24], notably derivatives of pyridoxal isonicotinoyl hydrazone (PIH), derivatives of *N,N'*-bis(2-hydroxybenzoyl)ethylenediamine-*N,N'*-diacetic acid (HBED) and hydroxypyridones (HP), as shown in Figure 1.2. They are characterized by good intestinal absorption, lipophilicity and preferential mobilization of parenchymal (i.e. the most toxic) liver iron deposition. However, as yet, they are not ready for clinical use. Among the candidates most worthy of consideration, are derivatives of the bidentate 3-hydroxypyridin-4-one series, aryl hydrazone derivatives of pyridoxal isonicotinoyl

hydrazone as well as prodrug forms of DF. Two major obstacles stand in the way of the development of effective oral substitutes for DF. These are the availability of appropriate animal models for drug testing, and the possibility of ensuring that candidate chelators are given the degree of toxicological screening that is obviously necessary for a drug that will be used continuously throughout the life of the patient.

1.2 Coordination chemistry of pyridoxal isonicotinoyl hydrazone and related compounds towards iron ions

After the preliminary report of Ponka and co-workers in 1979 [1,2], the potential of PIH and structural analogues as physiological iron chelators has been extensively examined and confirmed in a variety of biological and biochemical assays [30-33]. Although the biological properties of these chelating agents were becoming well documented, little was known of the coordination chemistry underlying interactions between these agents and iron ions. Since such chemical information is important in understanding the *in vivo* behaviour of these chelators therefore it prompted many investigators to study these properties in detail.

The iron(III) complexes of PIH and some analogues have been characterized. In the early work by Ponka [2], a possible structure of a bis-PIH–iron(III) complex was proposed: each ligand uses the carbonyl oxygen, aldimine nitrogen and phenolate oxygen to coordinate to the iron. Such a coordination mode was suggested on the basis of the effect of chemical modifications of the hydrazone on its iron-binding capacity.

In 1982, the first structural analysis of iron(III) complexes of PIH based on single crystal X-ray diffraction was reported by Murphy *et al.* [34,35]. In this work,

the 1:1 ligand-to-metal complex of $[FeCl_2(H_2pih)]Cl$ (**1**) which were red-brown crystals, were obtained directly from methanol solutions with equal molar amounts of $FeCl_3 \cdot 6H_2O$ and PIH present. In the presence of water, this complex converts to the red-brown crystals of *cis*-$[FeCl_2(H_2pih)(H_2O)]Cl \cdot H_2O$ (**2**). The mother liquor from which the both crystals deposited was highly acidic (pH ~ 2).

The structures of **1** and **2** consist of discrete cations, chloride anions, and, in **2**, water molecules held together by electrostatic interactions and hydrogen bonds as shown in Figure 1.3. In **1** the iron penta-coordination polyhedron is roughly square-pyramidal, the least-squares plane defined by O(1), N(3), O(2), and Cl(2) lying 0.54 Å below Fe and Cl(1) at the apex above. The structure of the $[FeCl_2(H_2pih)(H_2O)]^+$ complex is similar except for the addition of a water molecule to the polyhedron, which becomes roughly octahedral. The iron atom is slightly displaced (0.09 Å) toward Cl(1) from the least-squares plane of O(2)–Cl(2)–O(1)–N(3).

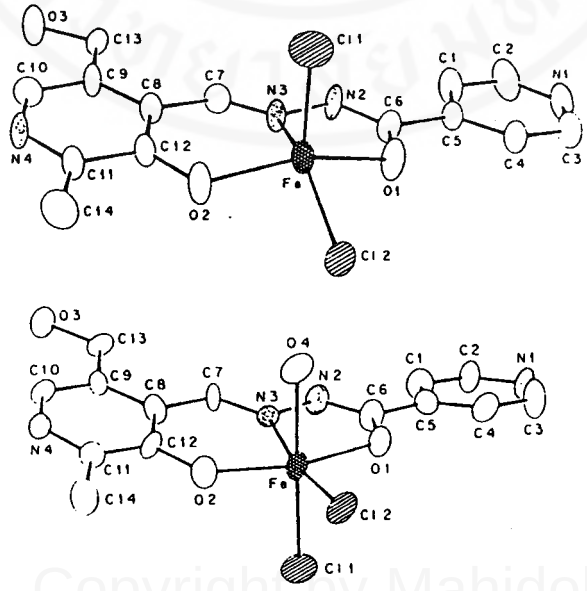

Figure 1.3 ORTEP drawing of a) $[FeCl_2(H_2pih)]^+$ cation (**1**) and b) $[FeCl_2(H_2pih)(H_2O)]^+$ cation (**2**), showing the 50% probability thermal ellipsoids. The hydrogen atoms, the chloride counter-ion and, for **2**, the uncoordinated water molecule have been omitted for clarity.

In both crystals PIH acts as a neutral, planar, tridentate ligand and the Cl^-: Fe(III) ratio is three. In each case two chloride ions are bonded to the iron and the remaining chloride ion is merely a counter-ion, being hydrogen bonded to N(1), N(4) and O(3) of three adjacent ions in **1** and to N(1), N(4) and O(4) of adjacent ions in **2**. The coordinated ligand retains the neutrality characteristic of its free form by a transfer of protons from the phenolic oxygen atom, O(2), and the hydrazidic nitrogen atom, N(2), to the pyridine nitrogen atoms N(1) and N(4). Thus the actual ligand in **1** and **2** is a zwitterion, a pattern seen in other complexes containing vitamin B_6 moieties. In the free ligand the hydrazidic linkage between the two pyridine rings is neutral and ideally represented as C(7)=N(3)–N(2)H–C(6)=O(1). Upon complexation to a metal ion, the ligand can either lose or retain the hydrazidic proton. If it retains the proton, the pattern of bond distances will vary little from those in the free ligand as shown in Figure 1.4a. This is seen in the seven-coordinate structure and in the SBH complex, in both of which the hydrazidic hydrogen atom is retained, although involved in hydrogen bonding. In the PIH complexes, however, the hydrazidic hydrogen atom has been lost. Therefore the linkage of ligand in these complexes are uninegative and represented as $C(7)=N(3)–N(2)=C(6)–O(1)^-$ as shown in Figure 1.4b. Given that this latter unit is planar and conjugated in both **1** and **2** and in similar complexes, it may safely be assumed that folded forms of coordinated PIH are energetically unfavourable and thus unlikely [2]. Given that **1** and **2** are formed from solutions of high acidity, it is clear that O(2) and N(2) are readily deprotonated in the presence of iron(III), as is not unexpected. It seems likely that the tridentate Fe–PIH linkage is independent of pH over a wide range, limited on the low side by reprotonation and on the high side by intrusion of OH^- and eventual formation of hydrous iron(III) oxide.

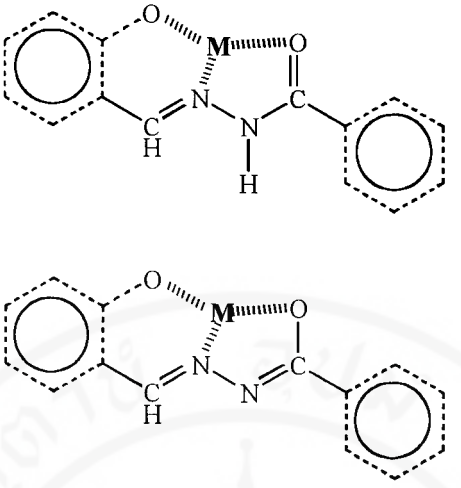

Figure 1.4 Hydrazidic linkages of aryl hydrazones in complexation to a metal ion for a) retaining and b) losing of the hydrazidic proton.

The infrared spectra of the both PIH complexes show the broad absorption between 3500 and 2600 cm^{-1}, attributed to O–H group involved in intramolecular hydrogen bonding. The complexes also show weak absorptions near 2000 cm^{-1}. Bands like these have been associated with the zwitterionic form of pyridoxal [] and of amino acids [] and have been attributed to vibrational modes of the pyridinium group. In these complexes the amide I band of the ligand disappears, indicative of coordination of the carboxylate oxygen atom to the iron ion.

In neutral aqueous media, the 2:1 complex of $[Fe(pih)(Hpih)]\cdot 3H_2O$ is formed. This is consistent with the observations of Ponka *et al.* [1] who conducted spectrophotometric studies with iron(III) and PIH showing that a 2:1 ligand-to-metal complex is formed at pH 7.4. No crystals suitable for X-ray diffraction were obtained.

The chelating agent PIH and structural analogues have attracted considerable attention in the search for high affinity iron chelators due to its high activity in mobilizing cellular iron in a variety of cellular and animal-based bioassays [30-33].

Consideration of the high activity of these chelators has prompted systematic studies examining their chemical properties.

In 1990, Richardson *et al.* reported the results of solution studies of the protonation constants and the formation constants with iron(III) of PIH and some structural analogues by using potentiometry and UV-visible spectrophotometry [38]. They show that, in case of protonation constants, PIH has four pK_a values: 2.95, 4.41, 7.86 and 10.25. The assignment of these pK_a values to ionizable sites on the ligands was made by comparison with pyridoxal, the acid hydrazide and related compounds. For PIH, these values attribute to pyridinium proton of isoniazide ring, phenolic proton of pyridoxal ring, pyridinium proton of pyridoxal ring and hydrazidic proton respectively. In case of other structural analogues *viz* pyridoxal benzoyl hydrazone (PBH), pyridoxal *p*-methoxybenzoyl hydrazone (PpMBH), pyridoxal *m*-fluorobenzoyl hydrazone (PmFBH), 3-hydroxyisonicotinaldehyde isonicotinoyl hydrazone (IIH) and salicylaldehyde isonicotinoyl hydrazone (SIH) (Figure 1.5), their results are summarized in Table 1.2.

From examination of the pK_a values of PIH and PBH, it is evident that the extra ring nitrogen in PIH acts in an analogous way to a nitro group by withdrawing electron density. In the case of PIH, a pK_a of 10.25 is associated with the ionization of the hydrazidic proton which is almost one unit lower than that of PBH (11.19). A comparable, although less dramatic increase, in acidity of the NH–N group is seen when comparing PBH and PmFBH, due to the electron withdrawing fluoro group. On the other hand, the *p*-methoxy group does not have any substantial effect on the pK_a values obtained (compare PBH and PpMBH).

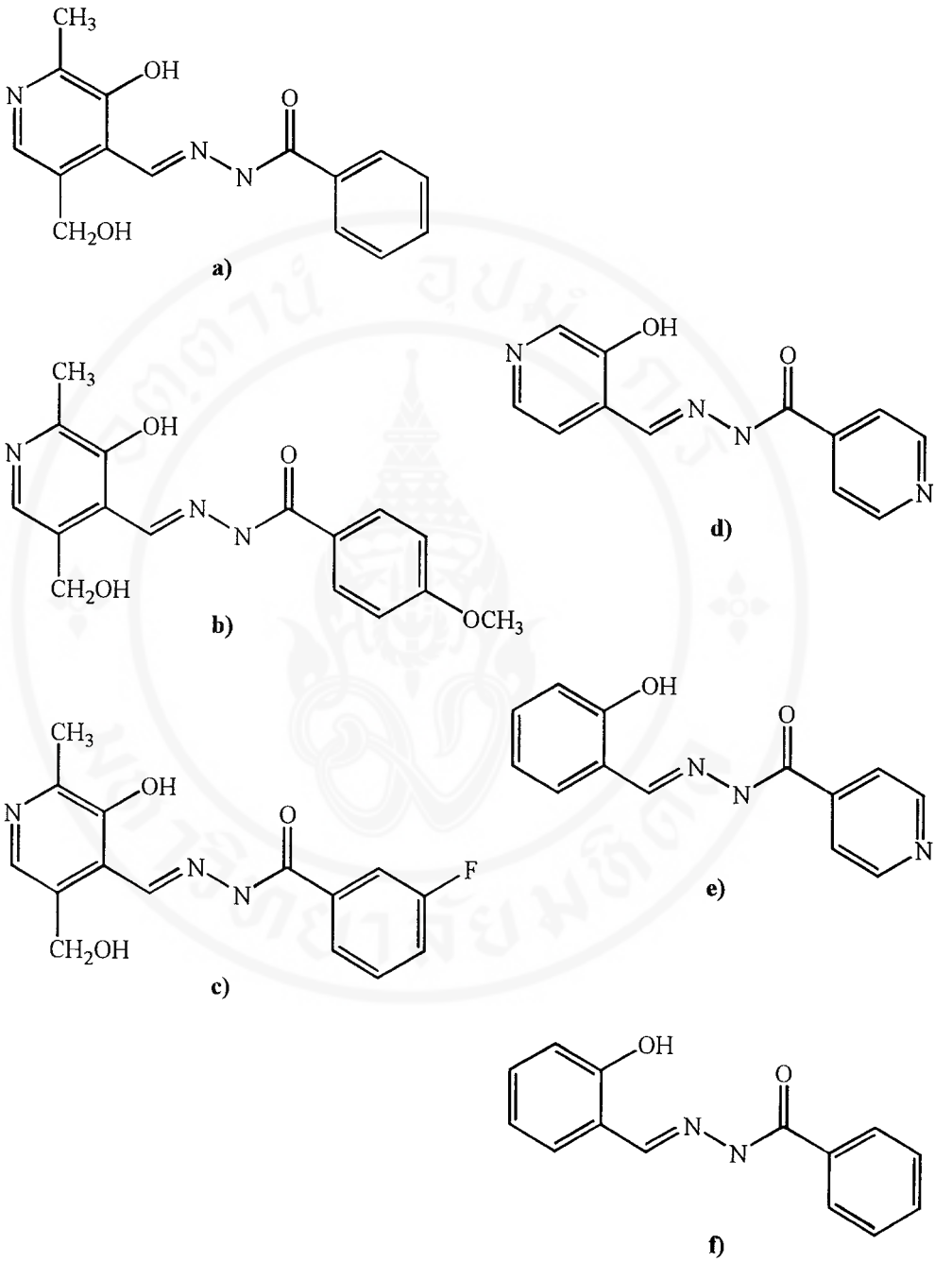

Figure 1.5 Structures of the chelating agents: a) pyridoxal benzoyl hydrazone (PBH), b) pyridoxal *p*-methoxybenzoyl hydrazone (PpMBH), c) pyridoxal *m*-fluorobenzoyl hydrazone (PmFBH), d) 3-hydroxyisonicotinaldehyde isonicotinoyl hydrazone (IIH), e) salicylaldehyde isonicotinoyl hydrazone (SIH) and f) salicylaldehyde benzoyl hydrazone (SBH).

Table 1.2 Protonation constants of pyridoxal isonicotinoyl hydrazone (PIH) and analogues

Ligand	pK_i (± s.d.)	Assignment[a]
PIH	2.95 ± 0.02	INH ring N
	4.41 ± 0.01	PYR ring OH
	7.86 ± 0.01	PYR ring N
	10.25 ± 0.01	–NH–N
PBH	4.24 ± 0.02	PYR ring OH
	8.15 ± 0.01	PYR ring N
	11.19 ± 0.01	–NH–N
PpMBH	4.14 ± 0.07	PYR ring OH
	8.28 ± 0.06	PYR ring N
	11.06 ± 0.03	–NH–N
PmFBH	4.378 ± 0.008	PYR ring OH
	8.087 ± 0.007	PYR ring N
	10.828 ± 0.005	–NH–N
IIH	2.97 ± 0.002	INH ring N
	3.97 ± 0.002	PYR ring OH
	7.93 ± 0.15	PYR ring N
	10.0 ± 0.9	–NH–N
SIH	3.43 ± 0.11	INH ring N
	8.29 ± 0.04	PYR ring OH
	9.8 ± 1.6	–NH–N

[a]INH and PYR refer to the pyridine rings derived from isoniazide and pyridoxal respectively.

The distribution of the species of some chelating agents are shown in Figure 1.6. It is seen that all the chelating agents are present as a mixture of neutral and a singly charged anionic species at near-physiological pH (7.4). This suggests that the chelating agents would be orally effective and lipophilic in that they would be able to diffuse through cell membranes, allowing absorption from the gut and access to intracellular iron pools. From examination of the above data, the presence of the neutral species is maximal at pH 6 and hence maximal absorption of these ligands would probably occur in the small intestine where the pH is in this range.

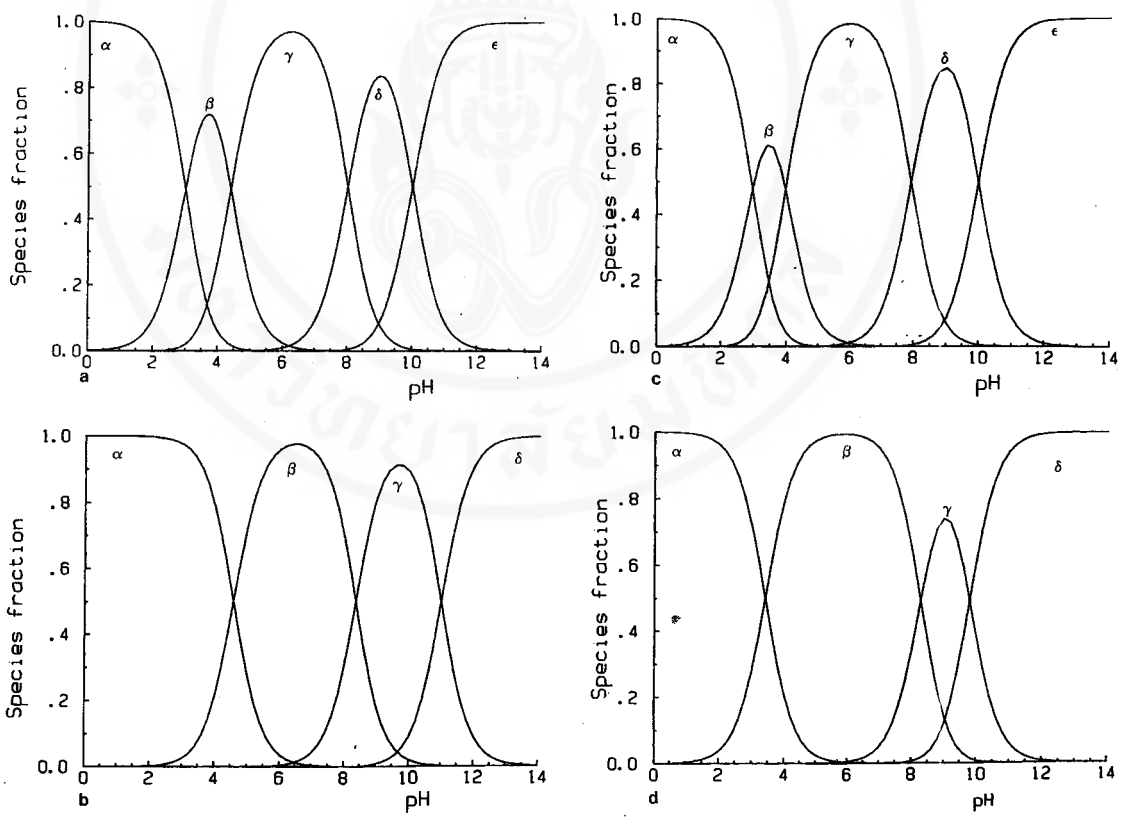

Figure 1.6 Species distribution as a function of pH for a) pyridoxal isonicotinoyl hydrazone ($\alpha = H_4L^{2+}$, $\beta = H_3L^{+}$, $\gamma = H_2L^{0}$, $\delta = HL^{-}$ and $\varepsilon = L^{2-}$), b) pyridoxal benzoyl hydrazone ($\alpha = H_3L^{+}$, $\beta = H_2L^{0}$, $\gamma = HL^{-}$ and $\delta = L^{2-}$), c) 3-hydroxyisonicotinaldehyde isonicotinoyl hydrazone ($\alpha = H_4L^{2+}$, $\beta = H_3L^{+}$, $\gamma = H_2L^{0}$, $\delta = HL^{-}$ and $\varepsilon = L^{2-}$) and d) salicylaldehyde isonicotinoyl hydrazone ($\alpha = H_3L^{+}$, $\beta = H_2L^{0}$, $\gamma = HL^{-}$ and $\delta = L^{2-}$).

In addition, due to the similarities in protonation and the increased lipophilicity of PpMBH and PmFBH when compared to PIH and PBH, absorption from the gut should be similar to, if not better than, that which has been reported for these latter two chelating agents [31,32]. Since the ratio of neutral to charged species is approximately the same for all four chelating agents, the differences in activity seen in the foetal hepatocyte screen and *in vivo* in rats [33] cannot be attributed simply to a difference in the charged state of the ligands.

For studies of the interaction of iron(III) with PIH and three analogues PBH, IIH and SIH [39], it is found that, in the pH range 1.5–3.2, both PIH and IIH associate with iron(III) with the loss of two or three protons from their fully protonated form H_4L^{2+}, giving $Fe(H_2L)^{3+}$, $Fe(H_2L)_2^{3+}$ and $Fe(HL)_2^{+}$. The species $Fe(HL)^{2+}$ forms with IIH but not PIH. In the case of the other two ligands PBH and SIH, only the two species $Fe(HL)^{2+}$ and $Fe(HL)_2^{+}$ are detected. At pH > 3.2, the iron(III) is present almost exclusively as the bis-complexes for all of the ligands studies. By potentiometric pH titrations, the species $Fe(HL)^{2+}$, $Fe(HL)_2^{+}$, $Fe(HL)L^{0}$ and FeL_2^{-} are observed for PBH, IIH and SIH, and for PIH, $Fe(HL)_2^{+}$, $Fe(HL)L^{0}$, and FeL_2^{-} are only detected.

The results of studies show that the affinities of PIH and IIH for Fe(III) are comparable, indicating that the $-CH_3$ and $-CH_2OH$ side chains on the pyridoxal ring have little influence on metal-binding. However, the substitution of a benzene for a pyridine ring results in a dramatic increase in iron-binding capability as in case of PBH and SIH.

The distributions of the complex species as a function of pH and in the presence of a 1000-fold molar excess of ligand over iron(III) are shown in Figure 1.7. At

physiological pH (7.4), the complex with PIH exists as the singly charged anion FeL_2^- but the other three ligands occur as a mixture of this anionic species and the neutral species $Fe(HL)L^0$. This is consistent with the fact that the excretion of the Fe(III)–PIH complex occurs primarily in bile [32].

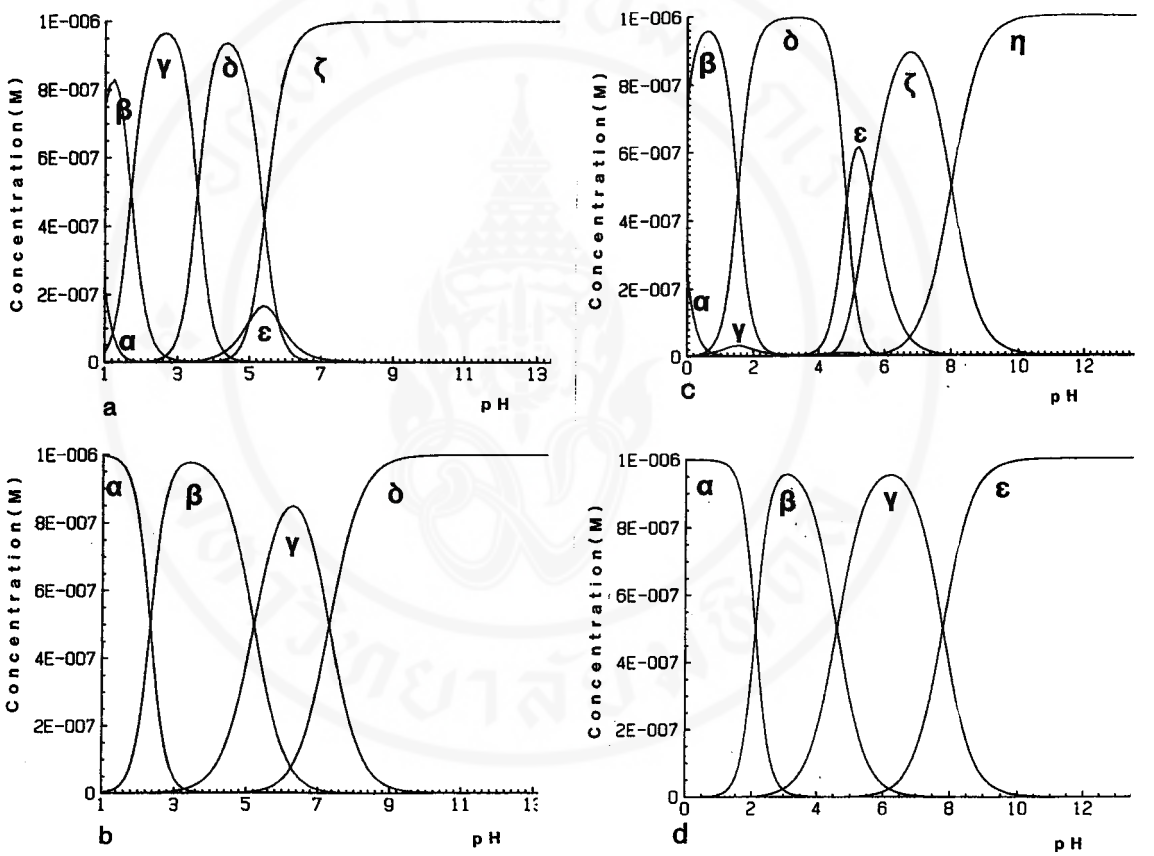

Figure 1.7 Distribution of iron(III) complex species as a function of pH for [Fe(III)] = 10^{-6} M, [Ligand] = 10^{-3} M when ligand is a) pyridoxal isonicotinoyl hydrazone (α = uncomplexed Fe(III), β = $Fe(H_2L)^{3+}$, γ = $Fe(HL)^{2+}$, δ = $Fe(H_2L)_2^{3+}$, ε = $Fe(HL)_2^+$, ξ = $Fe(HL)(L)^0$ and η = FeL_2^-), b) pyridoxal benzoyl hydrazone (α = $Fe(HL)^{2+}$, β = $Fe(HL)_2^+$, γ = $Fe(HL)(L)^0$ and δ = FeL_2^-), c) 3-hydroxyisonicotinaldehyde isonicotinoyl hydrazone (α = uncomplexed Fe(III), β = $Fe(H_2L)^{3+}$, γ = $Fe(HL)^{2+}$, δ = $Fe(H_2L)_2^{3+}$, ε = $Fe(HL)_2^+$, ξ = $Fe(HL)(L)^0$ and η = FeL_2^-) and d) salicylaldehyde isonicotinoyl hydrazone (α = $Fe(HL)^{2+}$, β = $Fe(HL)_2^+$, γ = $Fe(HL)(L)^0$ and δ = FeL_2^-).

Comparison of the metal-binding affinities of ligands that form complexes of different stoichiometries can best be achieved by calculation of their pM (= –log[M]) values, where M is the uncomplexed or *free* metal ion. Such values for PIH and its analogues are shown in Table 1.3 together with those for the serum iron-transport protein transferrin and three high affinity siderophores: desferrioxamine (currently in clinical use), rhodotorulic acid and enterobactin. The pM values for the PIH ligands are greater than that for transferrin, indicating that these ligands are thermodynamically able to mobilize transferrin-bound iron. A kinetic barrier, however, inhibits this exchange process, as in the case of desferrioxamine. The rates of mobilization of iron from transferrin by desferrioxamine and PIH are comparable [2].

Table 1.3 Unbound iron concentrations at pH 7.4, [Fe(III)] = 10^{-6} M, [Ligand] = 10^{-3} M

Compound	**pM**[a]
PIH	27.7
PBH	39.7
IIH	24.5
SIH	50
Transferrin	25.6[b]
Desferrioxamine	28.6[b]
Rhodotorulic acid	25.0[b]
Enterobactin	37.6[b]

[a]pM = –log [uncomplexed metal]
[b]Taken from reference 38

A large number of spectroscopic and physicochemical analyses were performed mostly on PIH [34,35,40]. They showed that two ligands are usually involved in the complex with one iron(III) [34,35], with an estimated average constant log $K \sim 8.7$ [40]. Moreover, it seems that even if iron(II) is involved in the complexation process, in the final complex the metal is always in the iron(III) form. The oxidation of iron(II) to iron(III) is probably enhanced by complex formation, as observed with some other ligands such as EDTA, oxalates, phosphates, citrates, etc. In addition, PIH and its analogues probably exist as several species related to the acidity of the medium. Each of these can complex iron differently. This associates complex formation and mobilization *in vivo* with the acidity of the cell compartments in which it occurs. These can be the mildly acidic (pH < 6) vesicles responsible for the transport of the iron-loaded transfer protein transferrin from the plasma membrane to its iron-demanding targets inside the cell. Nonheme iron mostly occurs *in vivo* as iron(III). However, the latter is reduced to iron(II) by an enzyme (reductase) before its natural mobilization from the transferrin-loaded vesicles. This mobilization process also requires the presence of a reductant such as ascorbate and a iron(II) cytoplasmic carrier. Moreover, iron(II) is considered as the form in which iron reacts *in vivo* with the chelating ligands of PIH and structural analogues. This can explain the fact that, for example, PIH can mobilize iron from transferrin though the affinity of the latter for iron(III) is about 10^{12} times greater than that of the chelate (affinity to transferrin is 10^{21} mol^2 dm^{-6} and that to PIH $10^{8.7}$ mol^2 dm^{-6}) [33,41]. All these arguments, which confirm the importance of complex formation with iron(II) in the metabolism of iron led to kinetic and thermodynamic study of complex formation between iron(II) and PIH and its structural analogues PBH, SIH and SBH (salicylaldehyde benzoyl

hydrazone, Figure 1.5f) by Dubois *et al.* [41], and the results of this study was reported in 1992.

In neutral aqueous media PIH and other chelating agents form bicomplexes with iron(II) in two-step mechanism. The first is fast and is ascribed to complex formation with a single ligand; second-order rate constants are 1.65×10^5, 1.70×10^5, 0.85×10^5 and 0.60×10^5 mol^{-1} dm^3 s^{-1} for PIH, PBH, SIH and SBH, respectively. Bicomplex formation is slower and occurs for the same ligands with second-order rate constants 2.45×10^4, 3.05×10^4, 4.00×10^4 and 1.50×10^4 mol^{-1} dm^3 s^{-1}. The affinities of these chelates to iron(II) are shown in Table 1.4.

Table 1.4 Affinity constants for complex formation of iron(II) and 2 equivalent of pyridoxal isonicotinoyl hydrazone and analogues

Ligand	$10^5 K_{c,1}$ (mol dm^{-3})	$10^5 K_{c,2}$ (mol dm^{-3})	$10^{-9} (1 / K_{c,1}K_{c,2})$ (mol^{-2} dm^6)
PIH	1.30	1.00	7.7 ± 1.2
PBH	1.00	0.80	12.5 ± 1.5
SIH	8.50	2.00	0.60 ± 0.10
SBH	10.80	4.00	0.25 ± 0.05

X-ray and IR analyses seem to indicate that, in the crystal of the Fe(III)–PIH complex, the ligands are in a tridentate conformation where phenol and hydrazide protons are transferred to the pyridine nitrogen atoms on the pyridoxal and the isonicotinoyl rings [34,35]. Therefore, these latter are both in a zwitterionic form. However, in aqueous media and in the absence of a metal ion, if the hydrazide proton

transfer to the pyridine nitrogen of isonicotinoyl were to occur, the related zwitterion would have a stability range in the pH 6 region (between the deprotonation pK_a of the hydrazone (pK_a = 10.1) and that of the pyridinium (pK_a = 2.26)). This is quite unlikely, because of the large difference between both of pK_a (about 8). Additionally, in PBH, the isonicotinoyl is replaced by a benzoyl, which prevents the hydrazide-pyridine prototautomerism and would, therefore, lead to a less stable complex with iron. Nonetheless, affinity constants of PIH and PBH for iron(II) are of the same order of magnitude (Table 1.4). This indicates that with Fe(II), in both complexes, PIH and PBH have a similar tridentate configuration which excludes the existence of a hydrazide-pyridine zwitterion in the Fe(II)–PIH complex. Therefore, the isonicotinoyl is probably engaged in the bis-PIH–Fe(II) complex in a neutral nonzwitterionic configuration. This analysis does not apply to SIH for which the difference between the pK_a of pyridine protonation (pK_a = 3.33) and that of phenolate protonation (pK_a = 8.30) is about 5. This can lead to a zwitterion with a stability range in the pH 6 region and which can be involved in complex formation. This zwitterion cannot, of course, occur with SBH, which can explain the lower affinity of the latter for iron as compared to that of SIH (Table 1.4). As for the pyridoxal moiety in neutral aqueous media, it is zwitterionic and is probably directly involved in the iron(II) and iron(III) complexes with PIH and PBH. This can also explain the higher stabilities of these complexes as compared to those of SIH and SBH.

Infrared studies of iron(III) complexes of PIH, and three similar chelating agents PBH, SIH and SBH have been reported [42]. This technique was used to examine and confirm the structural modification of these chelators in solid state during the complexation of iron(III) by Colonna *et al.*, in 1993.

The most significant result of this study is the difference existing between the spectra of SBH and SIH complexes on one hand, and PBH and PIH complexes on the other hand. IR spectra of the iron complexes reveal the permanence of the O=C–NH amide group identity for SBH and SIH, but not for PBH and PIH. A strong modification affects this O=C–NH group of PBH and PIH during complexation corresponding to deprotonation of the O=C–NH linkage as shown in Figure 1.4b. The drastic shift of the amide I band by the complexation of SBH and SIH proves the engagement of the carbonyl group in the association with iron.

Besides, for all the complexes, the normal mode corresponding to $\nu C–O + \delta O–H$ is absent, and no band with a comparable intensity can be found in the area of study. This fact proves the deprotonation of phenolic hydroxyl through complexation. These results present a good correlation with structures known through crystallographic studies [35].

In 1994, infrared studies of seven siderophores which differ from SBH by only one *para*-substituent on the benzoyl moiety were reported [43]. The shifts of the main bands and the intensity variations of substituted ring characteristic vibrations of these compounds were investigated and discussed specially according to the nature of the substituents. Their IR spectra which obtain from both solution (DMSO solvent) and solid state (KBr pellet) were compared, as well.

Vibrational spectroscopy is a tool particularly well adapted to the study of the permanence of identity of the O–H phenolic link on one hand, and of the O=C–NH amide group on the other hand.

In 1995, Colonna *et al.* reported the results of infrared studies of complexes between iron, SBH and seven analogous derivatives [44]. The amide I and Φ−O band shifts indicate that the ligand oxygen atoms are directly linked to iron ion. The analogy between iron(II) and iron(III) complexes in the mid-IR range and the chiefly identical frequencies in the far-IR range provide evidence that oxidation of iron(II) has occurred. The bands directly involved in complexation are shifted compared to the free hydrazones, and all are medium or weak.

Chemical properties of other iron-chelating agents apart from above compounds were also reported. In 1995, the proton binding constants (pK_a) and species distribution over pH range of two types of biologically active iron chelators (*a*) pyridoxal type (L_x)—pyridoxal 2-pyridyl hydrazone (PPH) and pyridoxal isonicotinoyl hydrazone (PIH); (*b*) pyridoxal-betaine type (L_y)—1-(*N*-methyl-pyridoxylidenium)-2-(2′-pyridyl)hydrazine iodide (MPH) and 1-(*N*-ethoxy-carbonylmethylpyridoxylidenium)-2-(2′-pyridyl)hydrazine bromide (EPH) determined by several techniques such as a combination of *ab initio* calculations and pH-dependence of ^{13}C-NMR spectroscopy, and glass electrode potentiometry were reported by Doungdee *et al.* [45,46].

Both of these techniques give similar results. For all ligands included in this study, the pK_a values invariably increase in the order: pyridinium protonation < pyridoxylidenium protonation < phenolate protonation < amine-hydrazone protonation. At pH < 2, all ligands exist in the respective protonated forms ($H_4L_x^{2+}$, $H_3L_y^{2+}$ and $H_3L_x^{+}$) and at pH > 11, in the fully deprotonated forms (L_x^{2+} and L_y^{-}).

1.3 Photoisomerization of imine system

Many photoreactions are known to interconvert isomeric compounds. The term *rearrangement* is more general than *isomerization* [47]. For convenience, we shall classify *primary* photochemical rearrangements as the following reaction types:

1. Cis-trans isomerization.
2. Sigmatropic rearrangements.
3. Electrocyclic rearrangements.
4. Structural rearrangements which result from intramolecular cycloadditions.

In a broad sense all four of these classes are special cases of *pericyclic* rearrangements and, for concerted reactions, they all may be treated under a unifying framework guided by the rules derived from orbital-symmetry considerations.

1.3.1 Cis-trans isomerization of unsaturated compounds

Absorption of a photon by a compound containing an olefinic link often results in cis-trans geometrical isomerization [48]. In many simple systems the trans isomer absorbs light of longer wavelength more intensely than the cis isomer; consequently, if long wavelength light is employed a photostationary condition is reached in which the cis isomer predominates. The rates of conversion of trans to cis and cis to trans isomers are equal at the **photostationary state**. Cis-trans isomerization may also be effected by photosensitization and is one of the most general photoreactions of ethylenes and other unsaturated linkages capable of geometrical isomerization, (e.g., C=N, N=N, etc.).

It is important to note that numerous photoreactions of compounds containing cyclic double bonds, such as linear additions, cycloadditions, electrocyclic reactions, rearrangements, etc., are, in fact, photoinduced cis-trans isomerizations followed by reaction of a reactive trans-cyclic isomer. For example, the solvent addition reaction (Equation 1.1) and the fragmentation reaction (Equation 1.2) both involve an initial photochemical cis-trans isomerization to form highly reactive trans-cyclic ethylenes (**1** and **2**) which proceed to products via secondary thermal reactions.

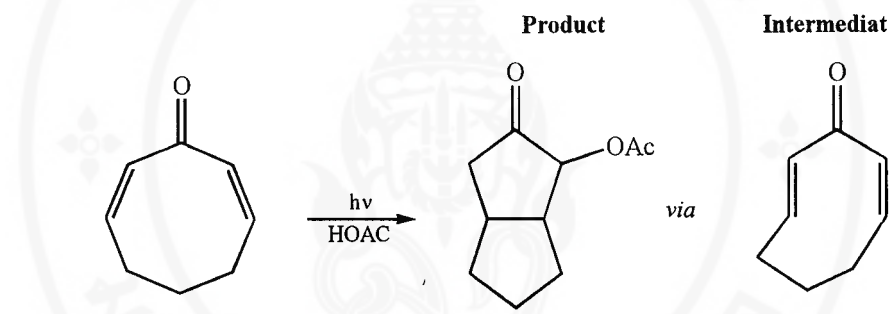

(1.1)

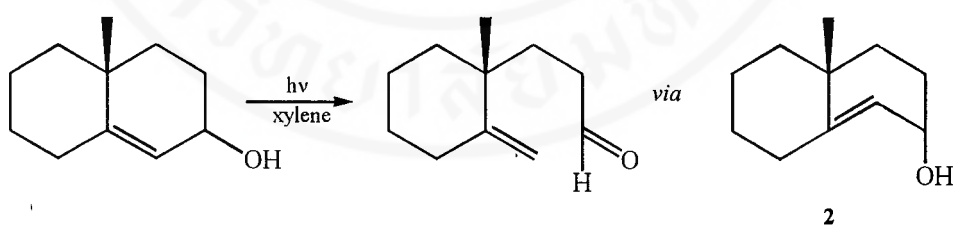

(1.2)

1.3.2 Photochemical cis-trans isomerization of imine system

The thermal- and photo-interconversions of the cis and trans isomers of imines are a subject of long-standing interest [14]. The mechanism for the thermal interconversion of imine diastereomers is currently the subject of considerable debate and has been considered in terms of either a planar inversion mechanism or a rotation mechanism [14]. The *rotation* or *torsion* mechanism involves a twisting about the C–N double bond. In order to bring about this change in geometry, there must be a reduction in the

double bond character of the imine bond in the transition state relative to the ground state. The C=N–C bond angle remains constant at 120° on proceeding through the transition state, as does the sp^2 conjugation of the lone pair of electrons on nitrogen. The *inversion* mechanism, on the other hand, is characterized by an increase in the angle of the C=N–C bond from approximately 120° in the ground state to 180° in the transition state. The double bond character of the imine bond remains intact in the transition state, as the lone pair of electrons on nitrogen rehybridizes from sp^2 to sp. With this mechanism, the nonbonding electrons on nitrogen become available as p electrons for conjugative interaction with other π-electron systems attached to the nitrogen atom in the transition state. Evidence obtained from studies of substituent effects (steric and electronic) suggests that most simple imines interconvert by the inversion mechanism, although some of the results obtained have been considered to be inconclusive [49].

Recent investigations into the factors influencing the ease of thermal isomerization about the C–N double bond have shown that the interconversion barrier is remarkably sensitive to the attached substituent groups [50]. For example, among imino compounds derived from benzophenone, changes in groups attached to nitrogen produce a range of rates of uncatalyzed isomerizations of greater than 14 powers of 10 [50]. Attempts to elucidate the mechanisms (lateral shift, rotational, or intermediate possibilities) of individual thermal imine isomerizations continue to challenge the ingenuity of various research groups and provide fuel for controversy.

The mechanism by which the cis and trans isomers of imines are interconverted in the excited state is even more complicated. Whether isomerization about the C–N double bond proceeds by rotation or linear inversion remains to be clarified. A major complication with the photochemical studies is that the thermal barrier between the

two diastereomers of most imines is sufficiently low that the photochemically induced shift in the configurational equilibrium is only temporary at ambient temperatures and is frequently followed by a rapid, thermal relaxation which reestablishes the initial configurational equilibrium between the cis and trans isomers.

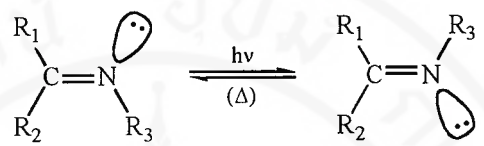

3 4 (1.3)

Even before the turn of the century, evidence was available which showed that ultraviolet light causes the rearrangement in oximes from one geometric isomer to the other [14]. Sporadic studies of this reaction have since been undertaken. Its use for the chemical synthesis of the pharmacologically active isomer has been described for *trans*-isonicotinaldehyde oxime.

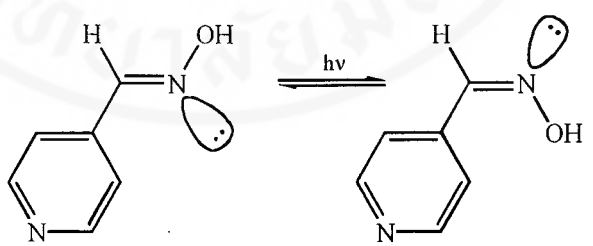

5 6 (1.4)

In addition to undergoing cis-trans photoisomerization, oximes are known to afford other products on electronic excitation. For example, Calas and co-workers observed that the oxime of 9-anthraldehyde not only photoisomerized but also underwent a competing [4 + 4] cyclodimerization [14]. These workers did not pursue the more mechanistic features of the photoisomerization process.

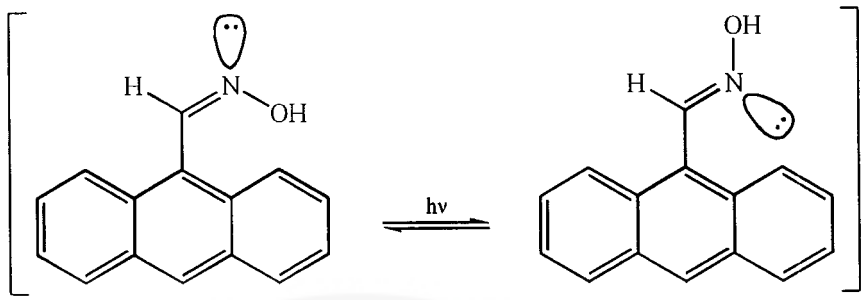

7 8 (1.5)

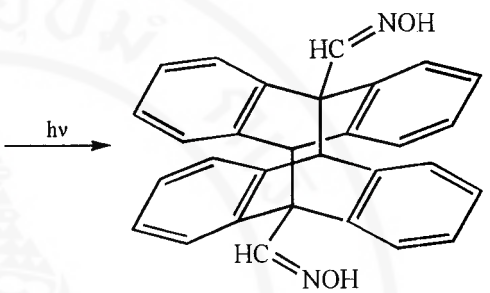

9

Padwa and Albrecht have investigated the solution-phase cis-trans photoisomerization of oxime ethers in order to clarify the mechanistic details of the C–N double bond photoisomerization. The great configurational stability of oxime ethers at room temperature stands in striking contrast to the behaviour of *N*-aryl- and -alkylimines [50]. These oximes ethers are attractive candidates for mechanistic photostudies since the presence of the alkoxyl group drastically reduces the rate of thermal interconversion ($k < 10^{-13}$ at 60 °C) and allows mechanistic studies to be carried out at ambient temperatures. The results obtained by Padwa and Albrecht with oxime ethers **10** and **11** are of fundamental interest by virtue of the superficial parallels to and mechanistic differences from the corresponding situation in olefin photochemistry.

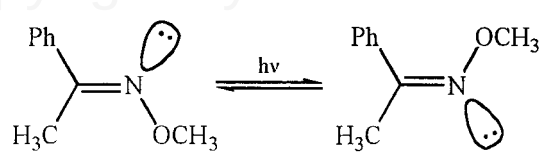

10 11 (1.6)

Photochemical cis-trans isomerization of hydrazones has also been reported in the literature [14]. The quinonoid system, 1,2-naphthoquinone-2-diphenylhydrazone (**12**), gave rise to remarkably large spectral changes; a wavelength shift of the absorption peak of 100 nm was reported [14].

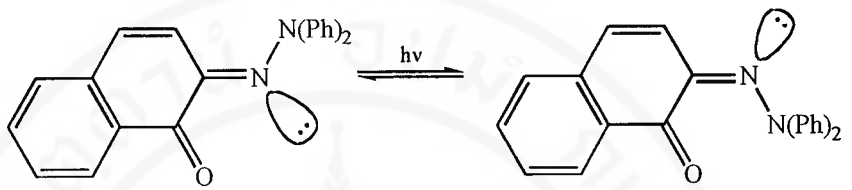

12 **13** (1.7)

The photochemical interconversion of the cis and trans isomers of Schiff bases is of recent origin [51]. Initial reports appeared in the literature claiming that the geometric isomers could be separated. Soon afterwards, however, other authors stated that they were unable to repeat the experiment or that the isomerism in question was a case of dimorphism [49]. In 1957, Fischer and Frei, working at temperatures below −100 °C, were able to detect distinct changes in the absorption spectra of *N*-benzylideneaniline, *N*-(α-naphthylidene)-α-naphthylamine, and related compound [52]. The extent of these changes depends on the wavelength of the light used for irradiation, with a definite equilibrium attained at each wavelength. These spectroscopic changes were found to be reversed on warming to room temperature. The thermal relaxation was measured in the range −70 to −40 °C and was estimated to have an activation energy of 16–17 kcal mol^{-1}, which should be compared with the values of 23 and 42 kcal mol^{-1} which apply to the isoelectronic molecules azobenzene and stilbene, respectively. The spectral changes observed with the naphthylimine system were attributed to the formation of the thermally unstable cis isomer (**15**) which isomerized to the thermodynamically more stable trans isomer (**14**) on warming.

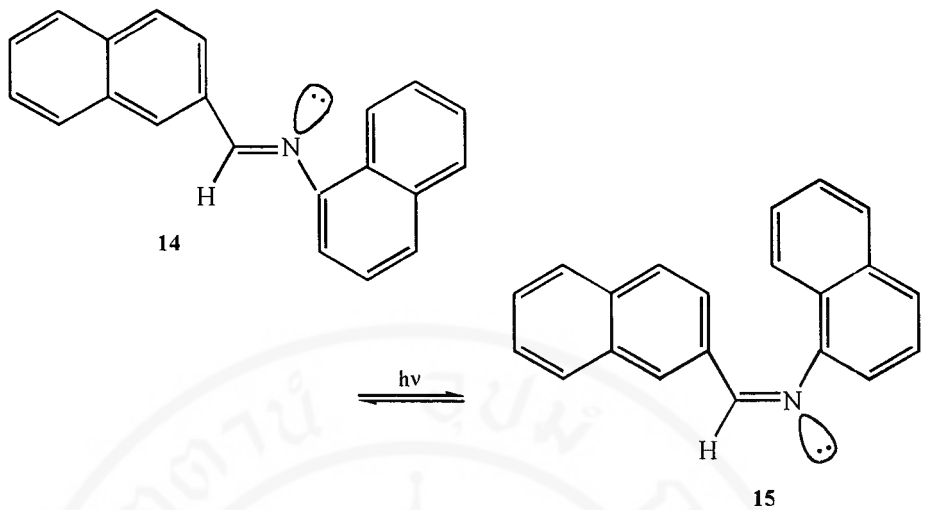

14 15 (1.8)

Wettermark and co-workers were able to demonstrate the cis-trans photoisomerization of other substituted *N*-benzylideneanilines such as *N*-(*o*-hydroxybenzylidene)aniline, *N*-(*o*-hydroxybenzylidene)-*β*-naphthylamine etc., even at room temperature, using flash photolysis techniques [4,5]. They found that in each of these compounds there appears to be a light-induced formation of cis isomer (**17**) from the more stable trans isomer (**16**). The existence of cis isomer was evidenced by a decreased absorption at wavelengths below 400 nm. In the dark, this species decayed following first-order kinetics and had a half-life of about one second at room temperature. The activation energy of 14 to 17 kcal mol^{-1} for this relaxation agrees quite well with results obtained previously by Fischer and Frei [52]. More recent work showed that the rate constant for the thermal relaxation of photoisomerized aromatic Schiff bases follows the bond order about the C–N double bond [4,5].

Ar = phenyl or *β*-naphthyl

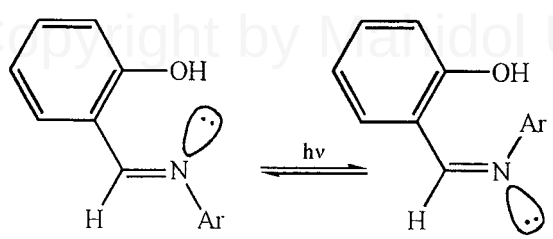

16 17 (1.9)

The above results clearly indicate that the thermal barrier between the two diastereomers of most imines is sufficiently low that the photochemically induced shift in the configurational equilibrium is only temporary at ambient temperatures and is frequently followed by a rapid, thermal relaxation which reestablishes the initial configurational equilibrium between the cis and trans isomers. Photoisomerization about the C–N double bond is undoubtedly a major path responsible for the high rate and efficiency of radiationless decay of the excited state of simple imines and accounts for the lack of photoreactivity of a large number of systems possessing a C–N double bond.

1.4 The scope of this thesis

There are two main parts of this research. One is to explain the difference in crystalline colour of PIH which was synthesized by two different methods. Infrared spectroscopy and single-crystal X-ray crystallography are used to investigate and characterize the PIH crystal. The second part is to study the rates of the thermal cis-trans isomerization reactions of PIH and other structurally related compounds, namely PBH, PSH, BIH, BBH, BSH, SIH, SBH and SSH in methanolic solutions. The rate constants of these isomerization reactions are measured at four temperatures: 25.0, 30.0, 35.0 and 40.0 °C, and the activation energy and the logarithm of preexponential factor calculated. UV-Visible spectrophotometry is used to follow the change of isomeric forms of these hydrazones in solution for this study.

For this research work, all compounds under investigation are hydrazones, formed from a carbonyl compound and an acid hydrazide by nucleophilic addition and

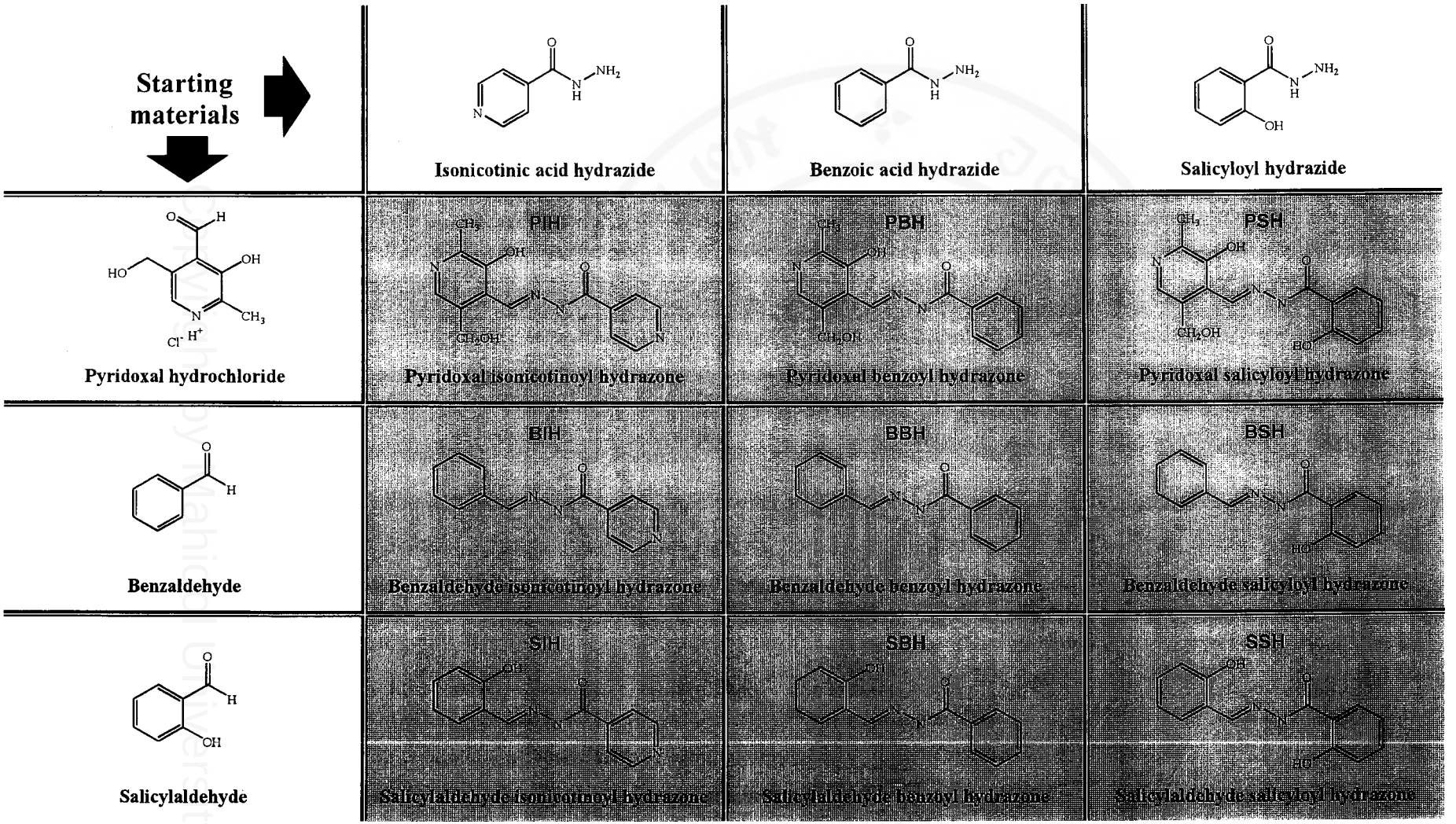

Figure 1.8 Starting materials and hydrazone products studied in this research.

subsequent elimination reaction. Figure 1.8 shows all the starting materials and the products prepared for study.

CHAPTER II

EXPERIMENTAL SECTION

In this chapter, chemicals, instruments and methods for synthesis of compounds are presented. In addition, experimental procedures for spectroscopic, photochromic, crystallographic and kinetic studies will be described in detail.

2.1 Chemicals

The chemicals used in this research and their purity are listed below.

Chemicals	**Manufacturer**	**Grade**
Acetonitrile	Eastman	AR
Ammonium hydroxide	Merck	Pro analysi
Benzaldehyde	Merck	Synthesis
Benzoic acid hydrazide	Fluka	Purum
Chloroform	Merck	Pro analysi
Ethanol	Merck	Pro analysi
Ethyl acetate	Merck	Pro analysi
Isonicotinic acid hydrazide	Sigma	AR

Chemicals	Manufacturer	Grade
Manganese oxide activated	Fluka	Akiviert
Methanol	Merck	HPLC
Methanol	Merck	Pro analysi
Potassium bromine	Baker	AR
iso-Propyl alcohol	BDH	AR
n-Propyl alcohol	Amend	AR
Pyridoxal hydrochloride	Sigma	AR
Pyridoxine hydrochloride	Merck	Commercial
Salicyloyl hydrazide	Sigma	AR
Salicylaldehyde	Merck	Synthesis
Sodium acetate anhydrous	BDH	AR
Titriplex III (Na_2-EDTA)	Merck	AR

2.2 Instrumentation

2.2.1 UV-Visible spectrophotometer

A Jasco Uvidec-650 double beam spectrophotometer, thermostatted by Eyela Digital Uniace UA 100 waterbath, was used for the kinetic studies of the cis to trans isomerization reactions and to obtain the UV-visible absorption spectra of solutions.

2.2.2 Fluorescence spectrometer

A Jasco spectrofluorometer model FP-770 was used to obtain the fluorescence emission and excitation spectra of solutions.

2.2.3 Infrared spectrometer

A Perkin Elmer fourier transform infrared spectrometer model PE System 2000 was used to record infrared spectra.

2.2.4 Single-crystal X-ray diffractometer

Automated Nonius FR 591 Mach 3 four-circle diffractometer with Zr-filtered, graphite-monochromated Mo$K\alpha$ radiation (λ = 0.70930 Å) was used for data collection. Crystallographic computations were performed on a Silicon Graphics computer with programmes provided with the X-ray system, MaXus version 2.1.p5 Copyright © 1997–1999, from the Laboratory for Crystallography, Department of Chemistry, Mahidol University.

2.2.5 Light sources

Sunlight and a Philips mercury arc model 93136E, 0.9–1 A, Holland were used to initiate the photochemical isomerization reaction for the kinetic studies.

2.2.6 Computer

A IBM compatible personal computer was used to collect and analyse the experimental data, and to report the research work.

2.3 Preparation and purification of materials

For this research work, pyridoxal isonicotinoyl hydrazone (PIH) and other structurally related compounds: pyridoxal benzoyl hydrazone (PBH), pyridoxal salicyloyl hydrazone (PSH), benzaldehyde isonicotinoyl hydrazone (BIH), benzaldehyde benzoyl hydrazone (BBH), benzaldehyde salicyloyl hydrazone (BSH), salicylaldehyde isonicotinoyl hydrazone (SIH), salicylaldehyde benzoyl hydrazone (SBH) and salicylaldehyde salicyloyl hydrazone (SSH) were synthesized and purified by the methods described below.

2.3.1 Pyridoxal isonicotinoyl hydrazone

Two methods were used in the preparation of this compound.

Method 1 [53]

10 g pyridoxine hydrochloride in 140 ml water was treated with 4.8 g H_2SO_4 and 5 g MnO_2. The mixture was heated at 60–70 °C for about 2.5 hours until the MnO_2 dissolved. The solution was filtered, and then heated on a waterbath. 6.85 g isonicotinic acid hydrazide in 50 ml water was added, and the mixture was filtered after 0.5 hour to yield 9.7 g of the manganese salt. 7.4 g Titriplex III (Na_2-EDTA) in 50 ml of water was made slightly basic with NH_4OH in order to dissolve the salt and the solution added to the manganese salt of PIH dissolved in 50 ml of water. After 0.5 hour PIH precipitated out to yield 6.2 g of product. The product was recrystallized from hot methanol to give pale yellow crystals.

Method 2 [3,33,54]

PIH was prepared in a good yield by mixing together equimolar quantities of nearly saturated solutions of isonicotinic acid hydrazide and pyridoxal hydrochloride, both in 0.1 M sodium acetate buffer (pH 4–5). The mixture was then heated for 2–3 minutes at 100 °C. The relatively insoluble condensation product was filtered from the cooled solution, washed with water and air dried. The hydrazone is quite soluble in dilute hydrochloric acid. The crude product was recrystallized from hot methanol, giving orange crystals.

2.3.2 Pyridoxal benzoyl hydrazone

PBH was prepared by mixing together equimolar quantities of nearly saturated methanolic solutions of pyridoxal hydrochloride and benzoic acid hydrazide in a beaker. The mixture was then heated on hot plate to about 45–50 °C for 20 minutes and allowed to stand for 24 hours at room temperature. The crude crystalline product was filtered from the solution, washed with cold methanol and air dried. The product was recrystallized from hot methanol to yield pale yellow crystals.

2.3.3 Other hydrazones

The method for the preparation of PBH (Section 2.3.2) was used for synthesizing PSH, BIH, BBH, BSH, SIH, SBH and SSH but with the starting materials listed in Table 2.1.

Table 2.1 Starting materials for synthesis of hydrazones

Starting materials	Product (color)
Pyridoxal HCl / isonicotinic acid hydrazide	PIH (pale yellow / deep orange crystals)
Pyridoxal HCl / benzoic acid hydrazide	PBH (pale yellow crystal)
Pyridoxal HCl / salicyloyl hydrazide	PSH (pale yellow sheet)
Benzaldehyde / isonicotinic acid hydrazide	BIH (white crystal)
Benzaldehyde / benzoic acid hydrazide	BBH (white crystal)
Benzaldehyde / salicyloyl hydrazide	BSH (white crystal)
Salicylaldehyde / isonicotinic acid hydrazide	SIH (white crystal)
Salicylaldehyde / benzoic acid hydrazide	SBH (yellow crystal)
Salicylaldehyde / salicyloyl hydrazide	SSH (pale yellow crystal)

2.3.4 Stock solutions

Crystals of PIH or other structurally related compounds were ground finely on a mortar to facilitate dissolving. The methanolic stock solution of 1×10^{-3} M was prepared by heating at 45–50 °C with stirring for about 2 hours until all the solids dissolved before making up to volume. Each solution was stored in a refrigerator for less than 7 days before use.

2.4 Experimental procedures

2.4.1 UV-Visible spectrophotometric study

The methanolic solution of all starting materials, *viz* pyridoxal hydrochloride, benzaldehyde, salicylaldehyde, isonicotinic acid hydrazide, benzoic acid hydrazide and salicyloyl hydrazide, and products, namely PIH, PBH, PSH, BIH, BBH, BSH,

SIH, SBH and SSH were prepared at suitable concentration (absorbance < 1.00 at all wavelengths) and UV-visible absorption spectra were measured with 1-cm pathlength quartz cuvette at wavelength 200–500 nm.

2.4.2 Photochromic study of PIH and related compounds

Methanolic solutions of PIH and the other hydrazones, *viz* PBH, PSH, BIH, BBH, BSH, SIH, SBH and SSH were prepared with absorbance at λ_{max} < 1.00. The UV-visible absorption spectra were then measured at time intervals of 15 minutes until the absorbance no longer changed with time.

Photochromic studies were carried out by irradiating the methanolic solutions of PIH and related compounds with the UV-light at wavelength 296 nm, with 20 nm band width, in the Jasco spectrofluorometer. The result of irradiation was monitored spectrophotometrically every 15 minutes for 1.5 hours.

After final irradiation, the methanolic solutions of PIH and related compounds were kept in the dark at room temperature. Then their spectral changes were measured 20 times at regular time intervals of 15 minutes.

2.4.3 Fluorescence spectroscopic study

In the experiment, 2.0×10^{-6} M methanolic solutions of PIH and structurally related compounds, namely PBH, PSH, BIH, BBH, BSH, SIH, SBH and SSH were prepared for fluorometric measurements.

0.05 ml of 1.0×10^{-3} M stock solution was pipetted into 25 ml volumetric flask and the solution was made up to volume with methanol (HPLC grade). The solution was stored in the dark until the measurement was made. The fluorescence excitation

and emission spectra of these compounds were obtained with a Jasco spectrofluorometer using 1-cm pathlength quartz cell.

2.4.4 Infrared spectroscopic study

The IR spectra were obtained from neat liquids or KBr pellets on a FT-IR spectrometer, with a 4.00 cm^{-1} resolution and 200 accumulations.

2.4.5 Single-crystal X-ray crystallographic study

To obtain suitable crystals for X-ray diffraction studies, PIH and eight structural analogues PBH, PSH, BIH, BBH, BSH, SIH, SBH and SSH were recrystallized in the dark from various solvents such as methanol, ethanol, *n*-propyl alcohol, *iso*-propyl alcohol, acetonitrile and ethyl acetate. With variation of solvent vapourization, good crystals could be probably obtained.

In X-ray crystal analysis, intensity measurements were made at ambient temperature on a Nonius diffractometer using the ω–2θ scan techniques. The data were corrected for Lorentz and polarization effects but not for absorption and extinction. Reflections with $I > 3\sigma(I)$ were regarded as observed. In this experiment, the crystal structures were solved by the direct method with the programme SHELXL-97. The structure refinements were carried out by the full-matrix least-squares technique with the programme SHELXL-97. The experimental conditions are summarized in Table 3.6 (Section 3.5).

2.4.6 Kinetic study

In this research work, the kinetics of the cis to trans isomerization reactions of PIH and structurally related compounds in methanolic solutions were investigated at four temperatures, namely 25.0, 30.0, 35.0 and 40.0 °C, using a Jasco UV-visible spectrophotometer.

The 5.0×10^{-5} M methanolic solution was prepared by pipetting 1.25 ml of the 1.0×10^{-3} M stock solution into 25 ml volumetric flask and making up to volume with methanol. The solution was then stored in the dark for 1 night before the measurement was carried out.

After the sample and reference cell holder in the cell compartment of UV-visible spectrophotometer attained the required temperature, 3.0 ml of the solution was transferred into 1-cm pathlength quartz cuvette. To prevent evaporation of methanol solvent during the kinetic studies, the cuvette was covered with a teflon cap. The trans to cis photoisomerization reaction was carried out by placing the cuvette in sunlight. After 5–7 minutes, the cuvette was placed in the sample holder of the spectrophotometer. The kinetics of the cis to trans isomerization was followed when the cuvette had attained the temperature of the thermostatted cell temperature (after 6–10 minutes). The reaction was followed until the equilibrium state was established, i.e. until the absorbance was nearly constant with respect to time. The measurement of the isomerization reaction was repeated at least three times.

When isomerization reaction was found to be rather rapid ($t_{1/2}$ < 10 minutes) as in the case of PBH, PSH and BIH, a different photoisomerization technique was employed. In this case, the cuvette with the methanol solution was placed in the sample holder of the cell compartment and thermostatted at required temperature for

20 minutes. The cuvette was then irradiated with a UV-lamp for 5 seconds to initiate the photoisomerization reaction. To maintain the temperature throughout the process, the irradiation must be rapidly carried out in less than 10 seconds. After the irradiation, the measurement was immediately started after the cell was returned to the holder. The change in absorbance with time was followed until the absorbance was nearly constant.

2.5 Treatment of kinetic data

In this study, the thermal cis-trans isomerization reactions of all hydrazones were continuously followed using UV-visible spectrophotometer. The experimental kinetic data were obtained as plots of the optical absorbance of the reacting system versus time. Since these reactions are first-order, the variation of absorbance versus time corresponds with the rate equation of $\ln(A_\infty - A)/(A_\infty - A_0)$ versus time. This model equation is fitted directly to the data using the principle of least-squares via **Enzfitter**, a non-linear regression data analysis programme, in IBM compatible microcomputer and the values of the parameters, *viz* the observed rate constant and the difference in absorbance at $t = \infty$ and $t = 0$, and the best-fit curve are able to obtain from this calculation. The Microsoft® Excel 97 (version 8.0) programme was also employed. The reported rate constants were the averaged values of at least three kinetic runs.

CHAPTER III

RESULTS

3.1 UV-Visible spectrophotometric study

Electronic absorption spectra of methanolic solutions of all starting materials and products are shown in Figures 3.1 and 3.2, respectively. From the UV-visible spectra, there are no absorption at wavelengths greater than 500 nm, so spectra were recorded at wavelengths between 200–500 nm.

In UV-visible spectroscopy, it is useful to compare spectra of related simple molecules with spectra of more complex compounds. Therefore the electronic absorption spectra of the starting materials were measured to help in interpretation [55-64]. From the spectrum of benzaldehyde as shown in Figure 3.1b, three major bands at 244, 280 and 328 nm are observed. These absorptions can be attributed to aromatic $\pi \rightarrow \pi^*$ (*K* band), aromatic $\pi \rightarrow \pi^*$ (*B* band) and $n \rightarrow \pi^*$ (*R* band) transitions, respectively. These are shifted to longer wavelengths by effect of conjugation. For salicylaldehyde, the addition of hydroxyl group at the ortho position of aromatic ring increases both the wavelength and the intensity of *K* and *B* bands because of extended conjugation. From Figure 3.1c, its the *K* and *B* bands occur at wavelengths 254 and 325 nm, respectively.

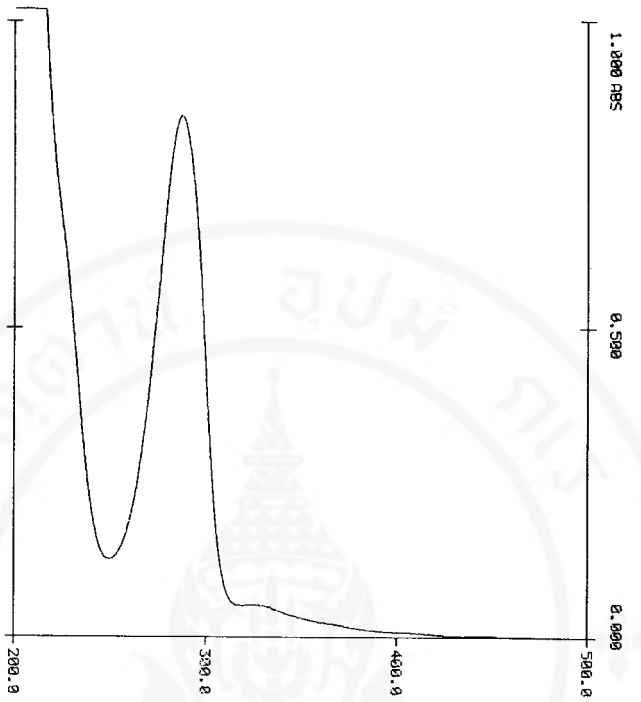

a)

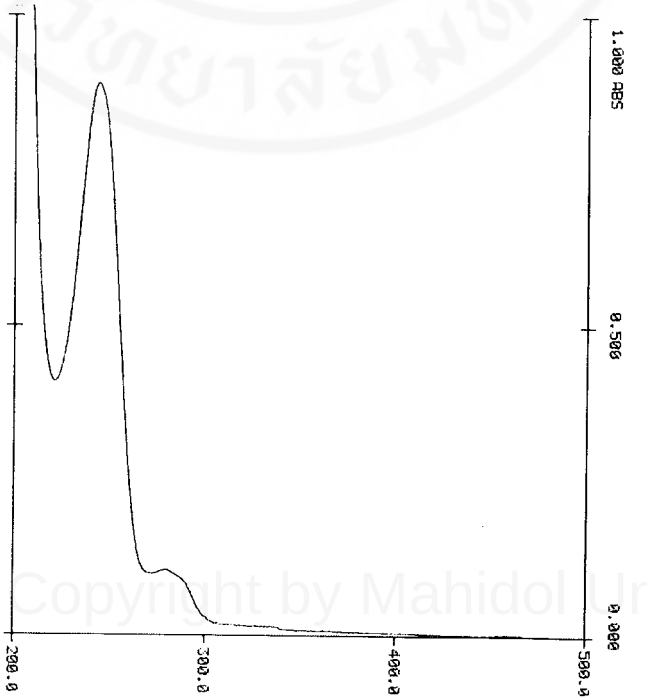

b)

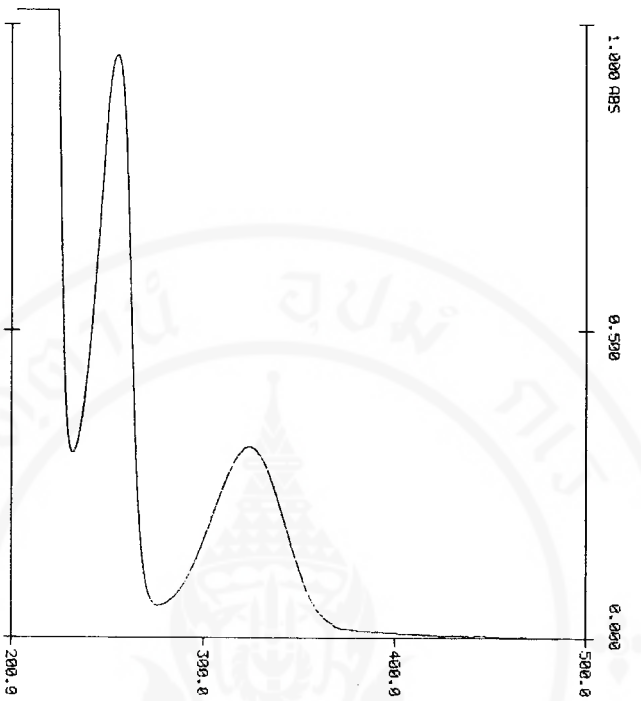

c)

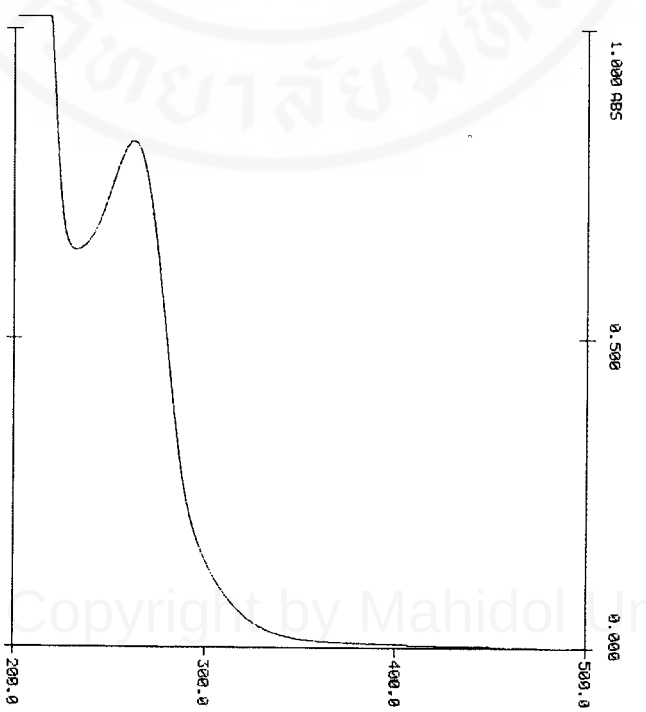

d)

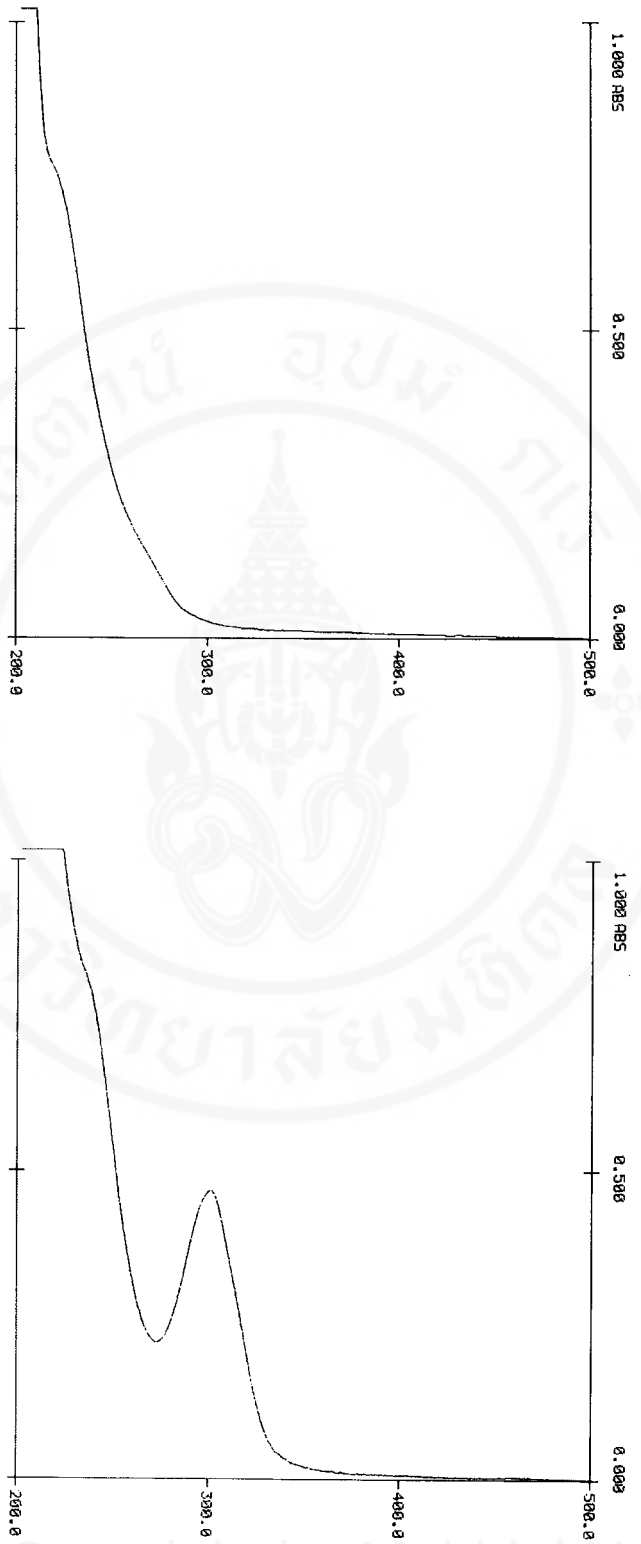

Figure 3.1 Electronic absorption spectra of a) pyridoxal hydrochloride, b) benzaldehyde, c) salicylaldehyde, d) isonicotinic acid hydrazide, e) benzoic acid hydrazide and f) salicyloyl hydrazide in methanol.

In the case of benzoic acid hydrazide, its absorption spectrum consists of $\pi \rightarrow \pi^*$ (*K* band) and $\pi \rightarrow \pi^*$ (*B* band) transitions like those of benzaldehyde but both bands appear at wavelengths 220 and 270 nm, lower than of benzaldehyde. This result shows that the hydrazide substituent gives rise to shifts in *K* and *B* bands which are less than the carbonyl substituent of benzaldehyde, as shown in Figure 3.1e. With the addition of hydroxyl group, the *K* and *B* bands of salicyloyl hydrazide are shifted to longer wavelengths, 235 and 300 nm respectively, with increase in the molar absorptivity of *B* band, as shown in Figure 3.1f.

For pyridoxal hydrochloride and isonicotinic acid hydrazide, electronic $\pi \rightarrow \pi^*$ transition (*B* band) of heteroaromatic ring is involved. This band is somewhat intense because it is an allowed transition. Isonicotinic acid hydrazide shows one band at 262 nm, attributed to $\pi \rightarrow \pi^*$ transition or *B* band. For pyridoxal hydrochloride, very intense band at wavelength 287 nm, connected with $\pi \rightarrow \pi^*$ transition (*B* band), and weak band near 325 nm, attributed to $n \rightarrow \pi^*$ transition (*R* band), are observed.

3.1.1 Pyridoxal isonicotinoyl hydrazone

For PIH, both pale yellow crystals and deep orange crystals purified using Sep-pak C-18 cartridge (Millipore®, U.S.A), give UV-visible absorption spectra that are not different in methanol, as shown in Figure 3.2a and 3.2b. From the spectra, three major absorption bands near 296, 340 and 400 nm are observed. These bands correspond to $\pi \rightarrow \pi^*$ (*K* band), $\pi \rightarrow \pi^*$ (*B* band) and $n \rightarrow \pi^*$ (*R* band) transitions, respectively. For heteroaromatic compound, the *B* band is somewhat intense because this transition is allowed. Besides the *B* band from pyridoxal part near 340 nm, the *B* band of isonicotinic acid hydrazide part are also observed as a shoulder near 305 nm.

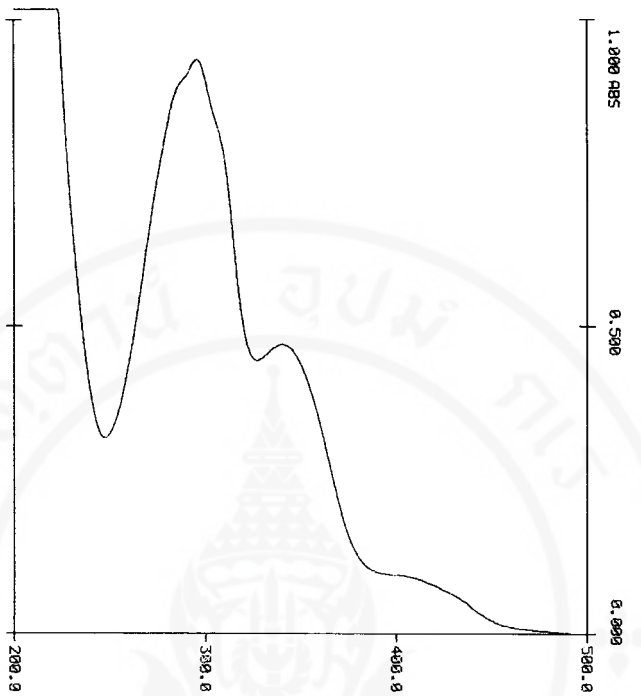

a)

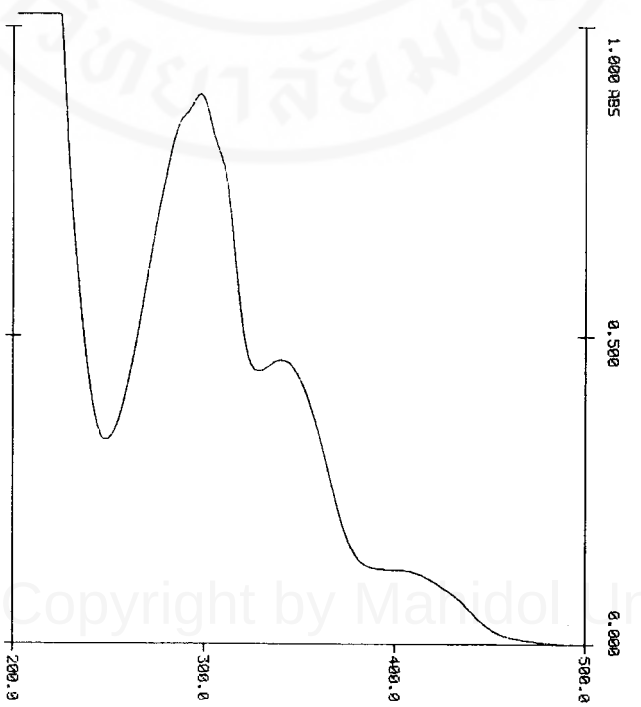

b)

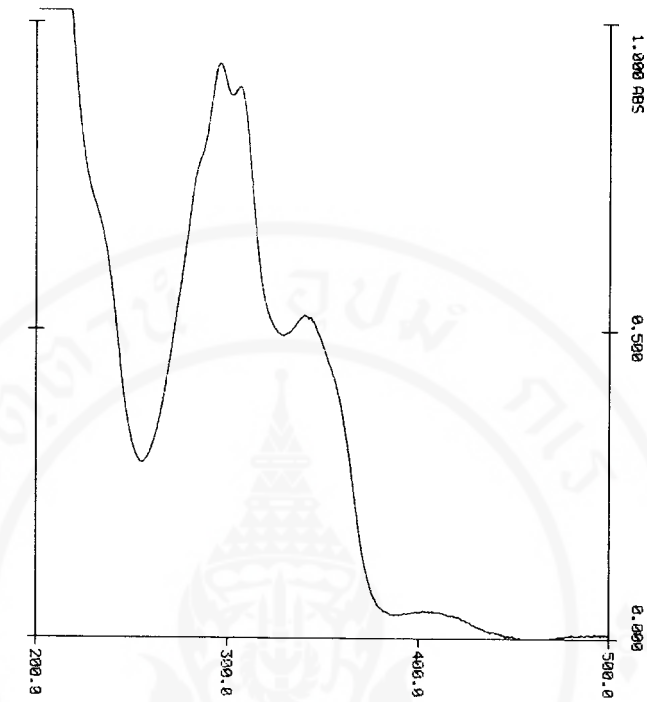

c)

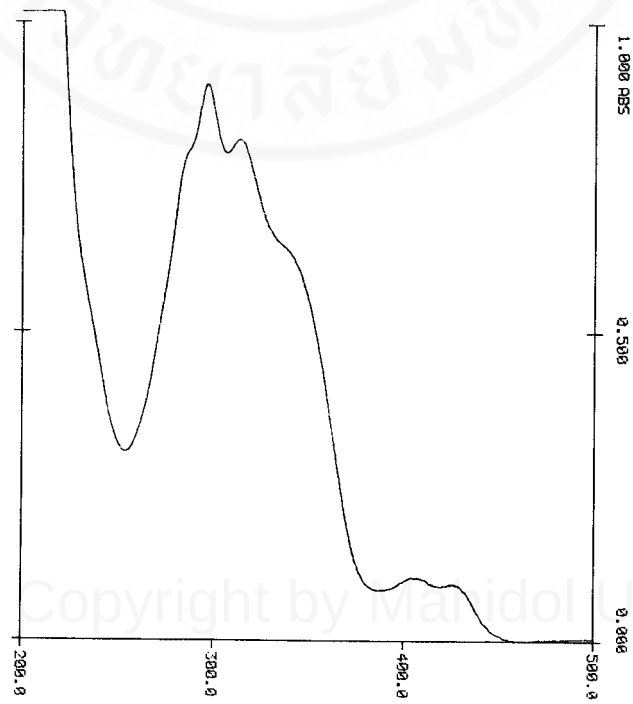

d)

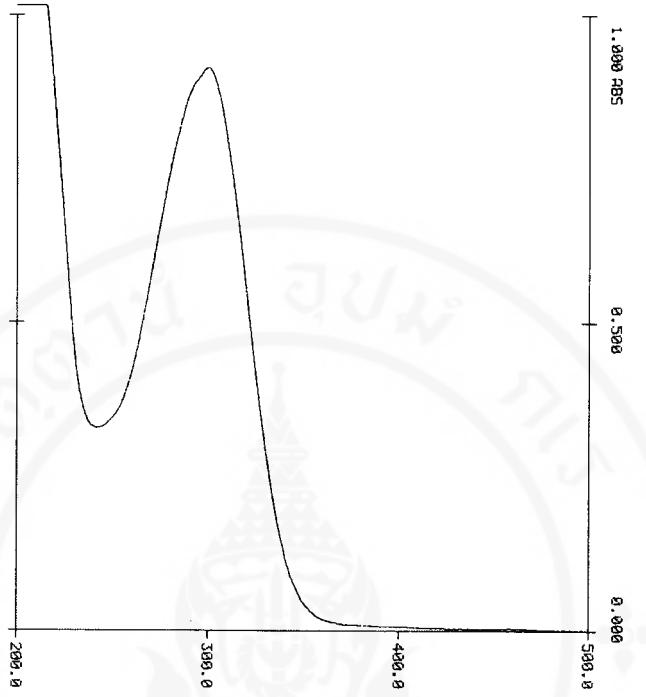

e)

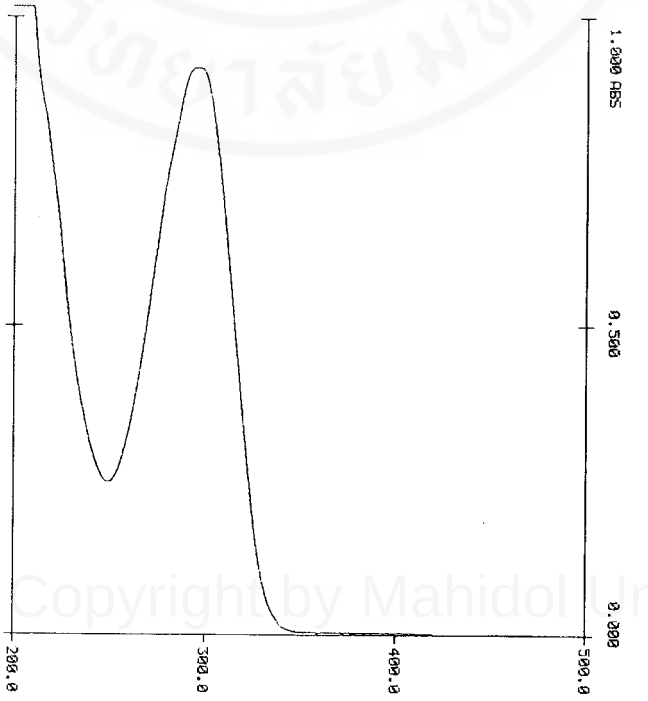

f)

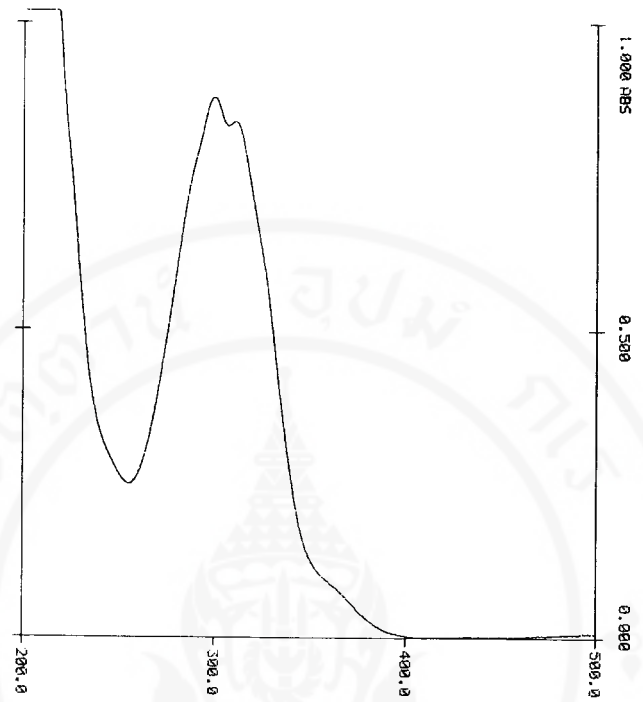

g)

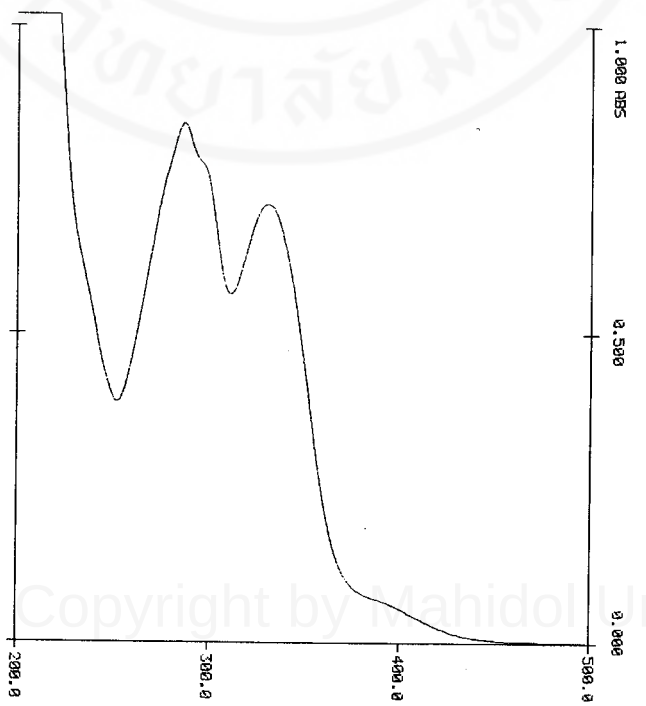

h)

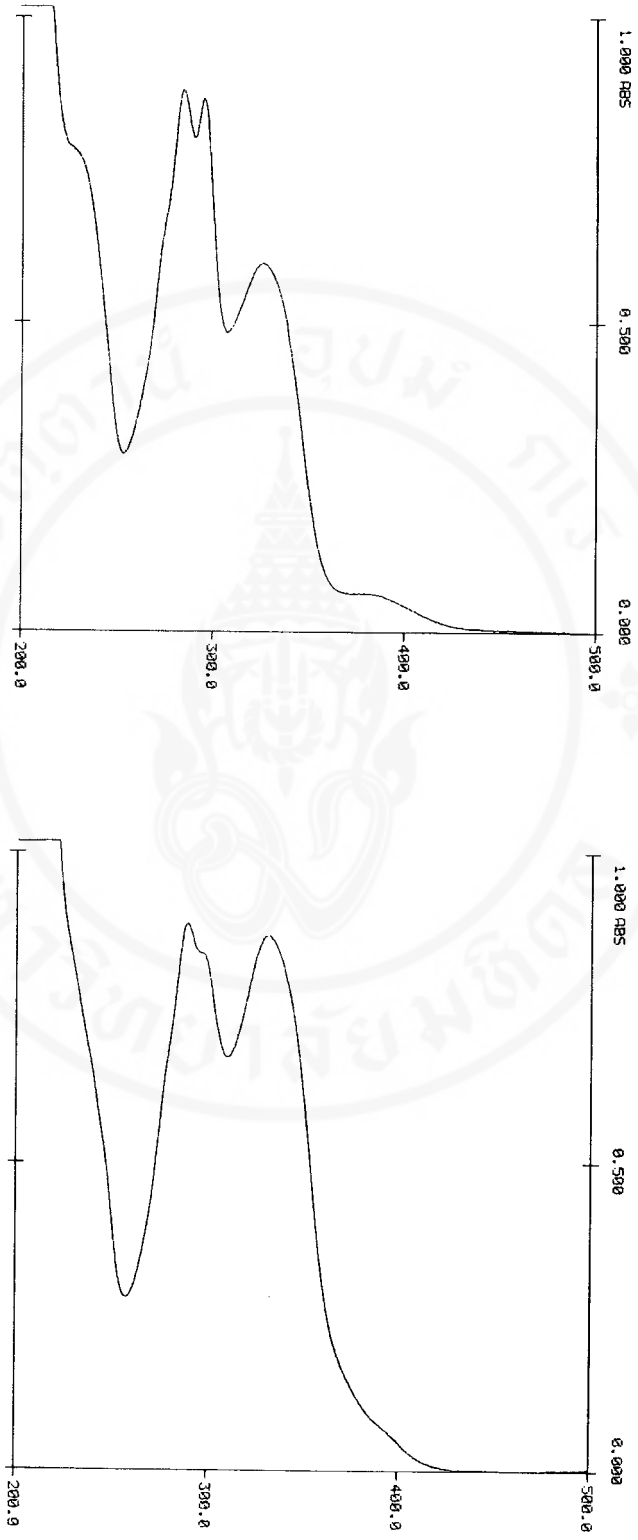

Figure 3.2 Electronic absorption spectra of a) pale yellow crystal PIH, b) deep orange crystal PIH, c) PBH, d) PSH, e) BIH, f) BBH, g) BSH, h) SIH, i) SBH and j) SSH in methanol.

3.1.2 Pyridoxal benzoyl hydrazone

The electronic absorption spectrum of PBH is shown in Figure 3.2c. The spectrum consists of four major bands and two shoulders. The intense bands at 295 and 306 nm correspond to $\pi \rightarrow \pi^*$ (*K* bands) transitions. For the bands near 340 and 405 nm, they are attributed to heteroaromatic $\pi \rightarrow \pi^*$ (*B* band) and $n \rightarrow \pi^*$ (*R* band) transitions, respectively. The shoulders near 235 and 285 nm probably correspond to $\pi \rightarrow \pi^*$ transitions.

3.1.3 Pyridoxal salicyloyl hydrazone

The UV-visible spectrum of PSH is shown in Figure 3.2d. The intense band at 297 and 315 nm result from $\pi \rightarrow \pi^*$ (*K* bands) transitions of pyridoxal and salicyloyl hydrazide, whereas the medium and weak bands near 338 and 410 nm result from $\pi \rightarrow \pi^*$ (*B* band) transition of the heteroaromatic ring of pyridoxal and $n \rightarrow \pi^*$ (*R* bands) transitions, respectively. The shoulders at 235 and 285 nm may correspond to $\pi \rightarrow \pi^*$ transitions.

3.1.4 Benzaldehyde isonicotinoyl hydrazone

BIH spectrum displays one major absorption band at 301 nm, as shown in Figure 3.2e. This band results from $\pi \rightarrow \pi^*$ (*K* band) transition of the heteroaromatic ring, whereas the shoulder near 295 nm corresponds to $\pi \rightarrow \pi^*$ transition. For the very weak band at about 395 nm, this results from $n \rightarrow \pi^*$ transition (*R* band).

3.1.5 Benzaldehyde benzoyl hydrazone

In Figure 3.2f, UV-visible spectrum of BBH shows one major absorption band at 296 nm. From the spectra of benzaldehyde and benzoic acid hydrazide, the starting materials for synthesis of BBH, this band may consist of several minor absorption bands such as *K* bands at about 295 and 298 nm, corresponding to $\pi \rightarrow \pi^*$ transitions of each aromatic ring in BBH molecule and E_2 band around 280 nm, corresponding to aromatic $\pi \rightarrow \pi^*$ transition.

3.1.6 Benzaldehyde salicyloyl hydrazone

The intense bands near 300 and 310 nm result from aromatic $\pi \rightarrow \pi^*$ (*K* bands) transitions, whereas the weaker band near 365 nm results from $n \rightarrow \pi^*$ (*R* band) transition, as shown in Figure 3.2g.

3.1.7 Salicylaldehyde isonicotinoyl hydrazone

Electronic absorption spectrum of SIH is shown in Figure 3.2h. The most intense band at 288 nm results from aromatic $\pi \rightarrow \pi^*$ transition (*K* band). Its shoulder near 297 nm is due to $\pi \rightarrow \pi^*$ transition (*B* band) of the heteroaromatic ring of the isonicotinic acid hydrazide. Besides the *K* band, aromatic $\pi \rightarrow \pi^*$ transition (*B* band) of salicylaldehyde is also seen at 332 nm. Weak absorption at 390 nm is due to $n \rightarrow \pi^*$ transition (*R* band).

3.1.8 Salicylaldehyde benzoyl hydrazone

From the spectrum of SBH, four major bands and two shoulders are observed as shown in Figure 3.2i. These bands partially overlap each other. The broad weak band at 377 nm is attributed to $n \rightarrow \pi^*$ (*R* band) transition. For medium and high intensity bands at 327, 297 and 286 nm, they correspond to aromatic $\pi \rightarrow \pi^*$ transition, i.e. secondary (*B*) band, and *K* bands from salicylaldehyde and benzoic acid hydrazide, respectively. Shoulders at about 229 and 275 nm are connected with aromatic $\pi \rightarrow \pi^*$ transitions of E_1 and E_2 bands, respectively.

3.1.9 Salicylaldehyde salicyloyl hydrazone

From Figure 3.2j, two major absorption bands of SSH are observed. The intense band near 331 nm corresponds to $\pi \rightarrow \pi^*$ (*B* band) transition of aromatic ring. Increase in intensity of this band results from the overlap of the *B* bands from benzene rings of salicylaldehyde and salicyloyl hydrazide. The *R* band in the spectrum of SSH is observed as shoulder of *B* band near 395 nm. This band is nearly submerged by the intense *B* band. The most intense band at 289 nm results from aromatic $\pi \rightarrow \pi^*$ (*K* band) transition of salicyloyl hydrazide part, whereas its shoulder results from $\pi \rightarrow \pi^*$ (*K* band) transition of aromatic ring of salicylaldehyde part. The other shoulders at about 235 and 275 nm are attributed to E_1 and E_2 $\pi \rightarrow \pi^*$ transitions of aromatic ring, respectively.

The electronic absorption bands of these hydrazones are summarized in Table 3.1.

Table 3.1 Absorption data for the hydrazones studied

Compound	λ_{max} (nm)[a]	Electronic transition	Band[b]
PIH	285 (sh)	$\pi \rightarrow \pi^*$	
(pale yellow and	**296**	Heteroaromatic $\pi \rightarrow \pi^*$	*K*
deep orange	305 (sh)	Heteroaromatic $\pi \rightarrow \pi^*$	*B*
crystals)	340	Heteroaromatic $\pi \rightarrow \pi^*$	*B*
	400 (br)	$n \rightarrow \pi^*$	*R*
PBH	235 (sh)	$\pi \rightarrow \pi^*$	
	285 (sh)	$\pi \rightarrow \pi^*$	
	295	$\pi \rightarrow \pi^*$	*K*
	306	$\pi \rightarrow \pi^*$	*K*
	340	Heteroaromatic $\pi \rightarrow \pi^*$	*B*
	405 (br)	$n \rightarrow \pi^*$	*R*
PSH	235 (sh)	$\pi \rightarrow \pi^*$	
	285 (sh)	$\pi \rightarrow \pi^*$	
	297	$\pi \rightarrow \pi^*$	*K*
	315	$\pi \rightarrow \pi^*$	*K*
	338 (sh)	Heteroaromatic $\pi \rightarrow \pi^*$	*B*
	406 and 426	$n \rightarrow \pi^*$	*R*
BIH	295 (sh)	$\pi \rightarrow \pi^*$	
	301	Aromatic $\pi \rightarrow \pi^*$	*K*
	395 (br)	$n \rightarrow \pi^*$	*R*
BBH	220 (sh)	Aromatic $\pi \rightarrow \pi^*$	E_1
	280 (sh)	Aromatic $\pi \rightarrow \pi^*$	E_2
	296	Aromatic $\pi \rightarrow \pi^*$	*K*

Table 3.1 (continued)

Compound	λ_{max} (nm)[a]	Electronic transition	Band[b]
BSH	285 (sh)	Aromatic $\pi \rightarrow \pi^*$	E_2
	300	Aromatic $\pi \rightarrow \pi^*$	K
	310	Aromatic $\pi \rightarrow \pi^*$	K
	365 (sh)	$n \rightarrow \pi^*$	R
SIH	240 (sh)	$\pi \rightarrow \pi^*$	
	275 (sh)	$\pi \rightarrow \pi^*$	
	288	Aromatic $\pi \rightarrow \pi^*$	K
	297 (sh)	Heteroaromatic $\pi \rightarrow \pi^*$	B
	332	Aromatic $\pi \rightarrow \pi^*$	B
	390 (sh)	$n \rightarrow \pi^*$	R
SBH	229 (sh)	Aromatic $\pi \rightarrow \pi^*$	E_1
	275 (sh)	Aromatic $\pi \rightarrow \pi^*$	E_2
	286	Aromatic $\pi \rightarrow \pi^*$	K
	297	Aromatic $\pi \rightarrow \pi^*$	K
	327	Aromatic $\pi \rightarrow \pi^*$	B
	377 (br)	$n \rightarrow \pi^*$	R
SSH	235 (sh)	Aromatic $\pi \rightarrow \pi^*$	E_1
	275 (sh)	Aromatic $\pi \rightarrow \pi^*$	E_2
	289	Aromatic $\pi \rightarrow \pi^*$	K
	297 (sh)	Aromatic $\pi \rightarrow \pi^*$	K
	331	Aromatic $\pi \rightarrow \pi^*$	B
	395 (sh)	$n \rightarrow \pi^*$	R

[a]Shoulder and broad band inflections are represented by (sh) and (br), respectively.
[b]*R* band, German *radikalartig*; *K* band, German *konjugierte*; *B* band, benzenoid; *E* band, ethylenic; see: A. Burawoy, *Berichte*, **63**, 3155 (1930); *J. Chem. Soc.*, 1177 (1939) and E. A. Braude.

3.2 Photochromic study of PIH and related compounds

Photochromic behaviours of the two solid forms of PIH, namely pale yellow crystal and deep orange crystal purified using Sep-pak C-18 cartridge (Millipore®, U.S.A), and structurally related compounds, namely PBH, PSH, BIH, BBH, BSH, SIH, SBH and SSH were investigated under the same experimental conditions for comparison. The UV-irradiation of methanolic solutions of these compounds were followed spectrophotometrically over a time period of about 15 minutes. It was found that there were spectral changes around 400 and 300 nm.

When the PIH was irradiated by UV-irradiation for about 15 minutes, the absorption spectrum increased in intensity at 400 nm but decreased at 250–350 nm. These changes in the absorbance increased with further irradiation, as shown in Figure 3.3a1 and 3.3b1, respectively. The existence of isosbestic points at 263, 268 and 410 nm indicate the formation of two species, *cis*- and *trans*-isomers. The deep orange crystal PIH (docPIH) from Sep-pak C-18 shows photosensitivity comparable to the pale yellow crystal PIH (pycPIH), as shown in Figure 3.3a and 3.3b.

After the irradiated PIH solution was kept in the dark, it was found that the absorption spectrum gradually returned to their initial values, with a decrease of the 400 nm band and an increase of the 250–350 nm band, as shown in Figure 3.3a2 and 3.3b2. The changes in absorbances of the solutions of deep orange crystal and pale yellow crystal exhibited similar behaviours.

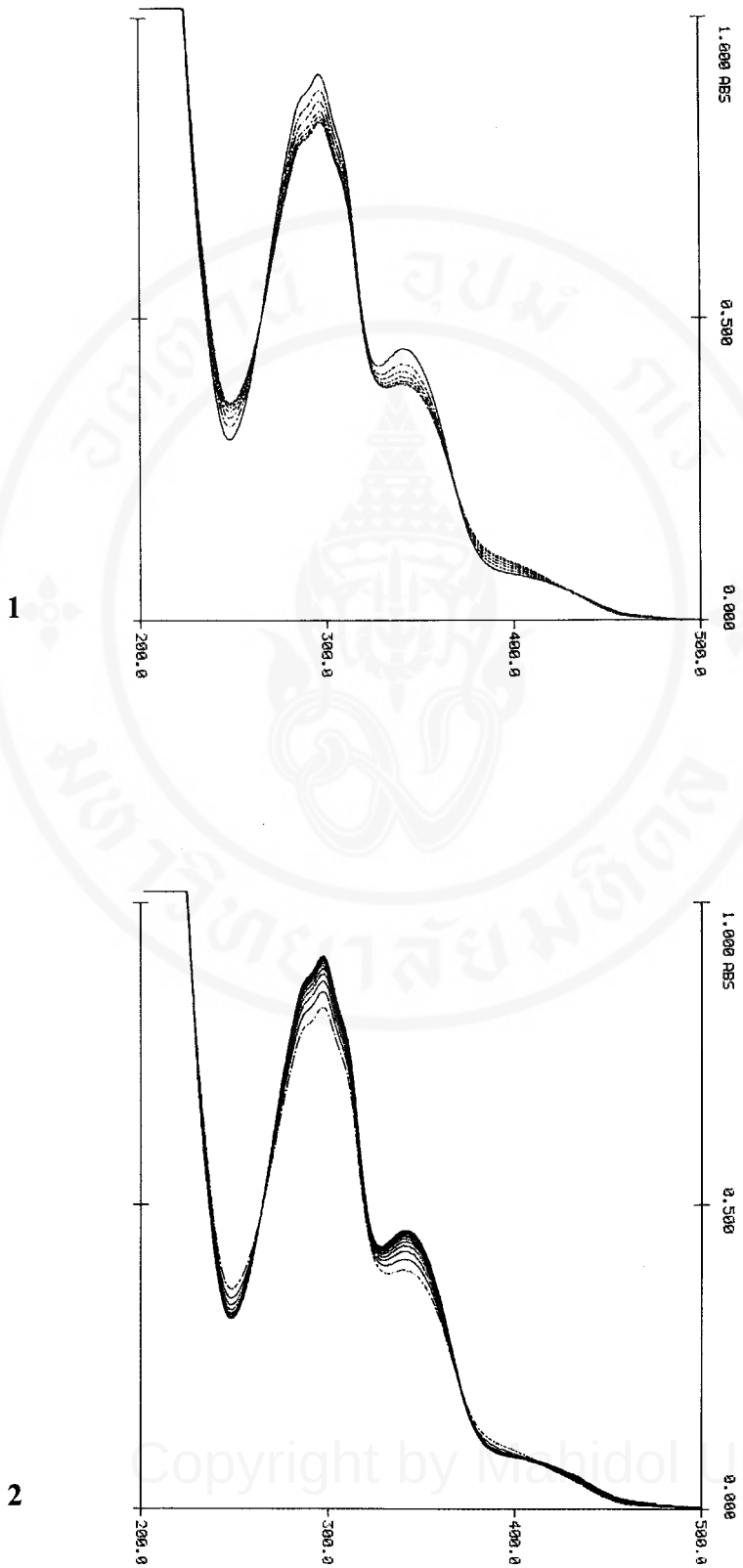

a)

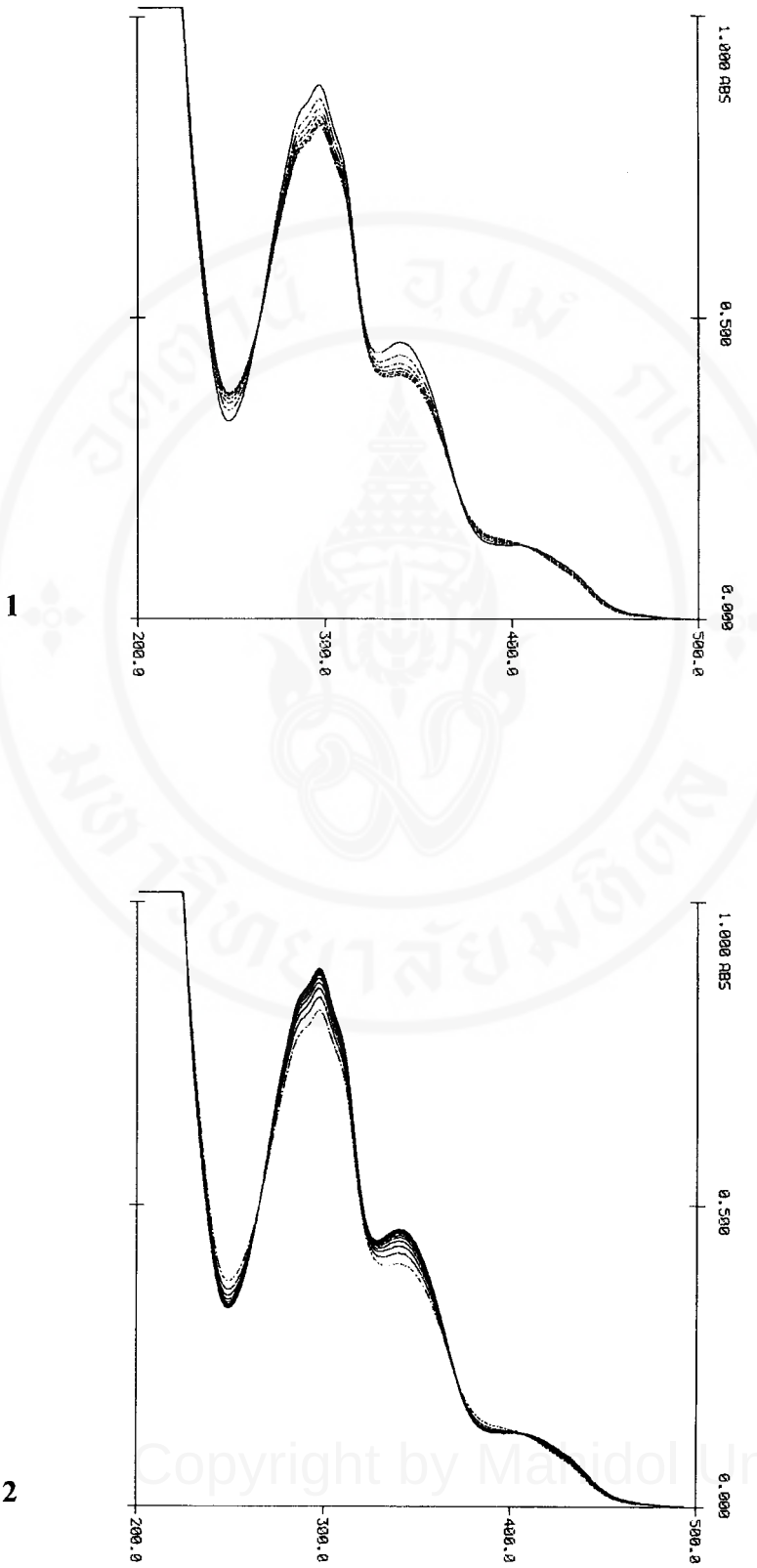

b)

1

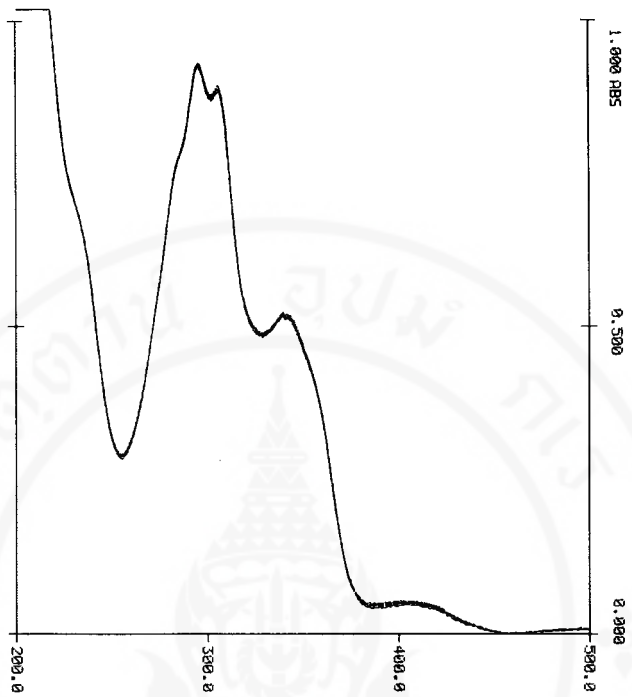

2

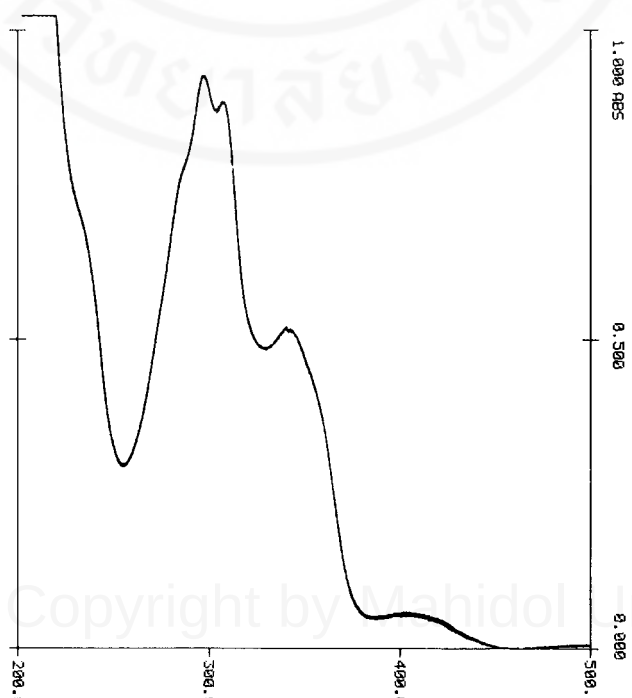

c)

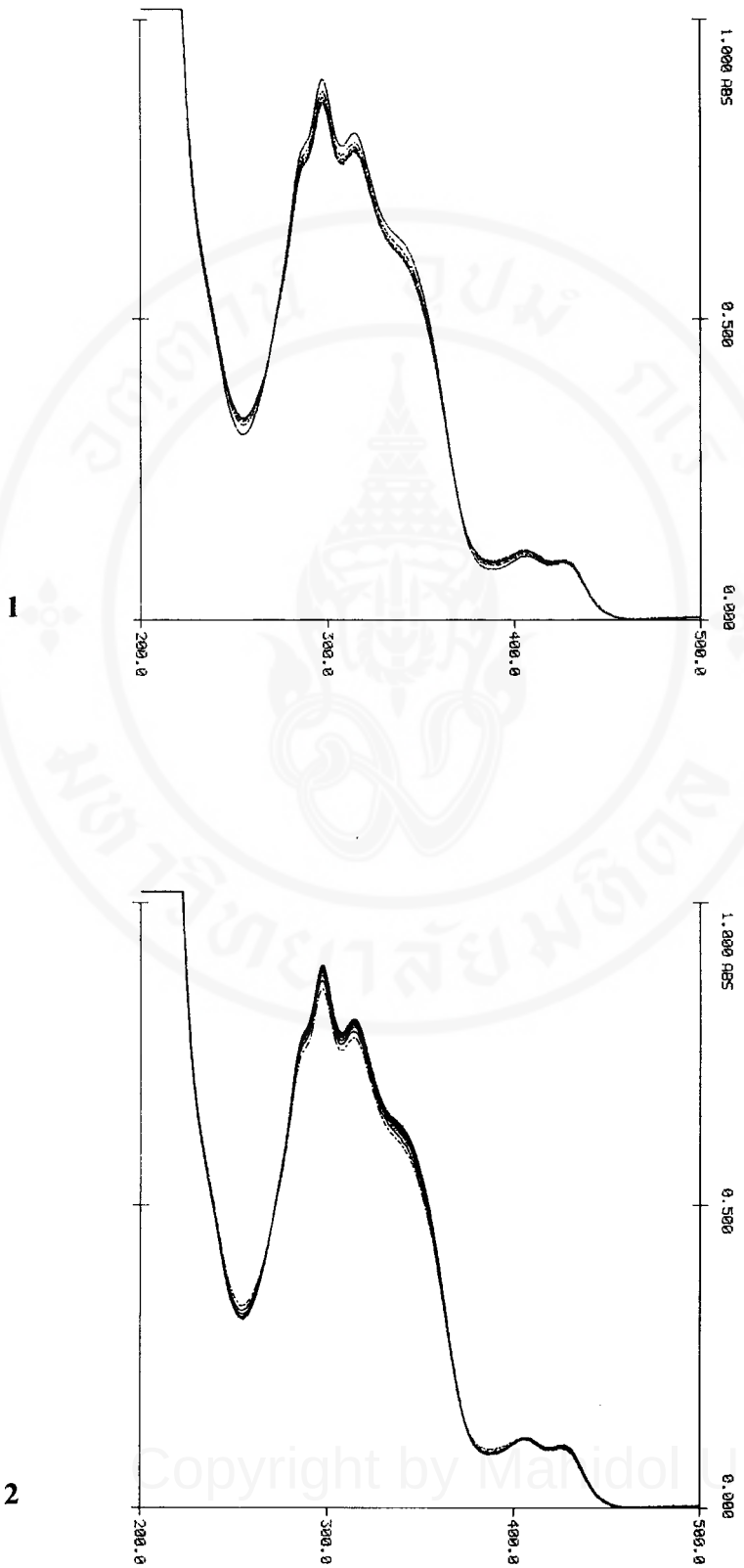

d)

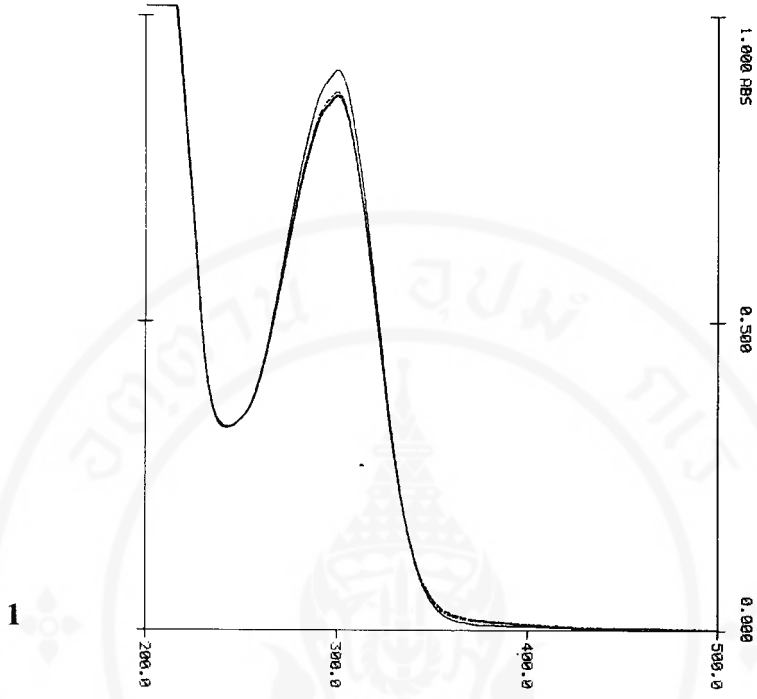

1

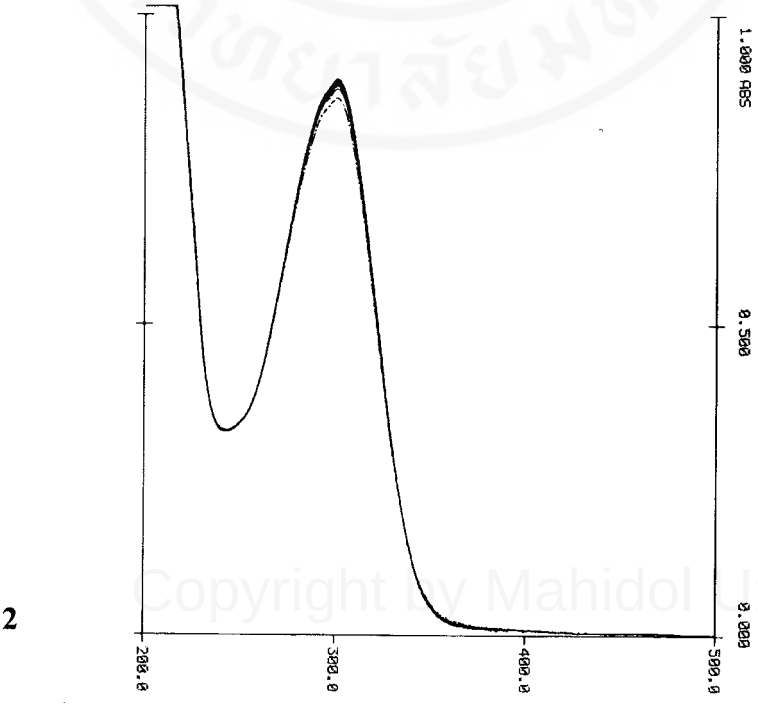

2

e)

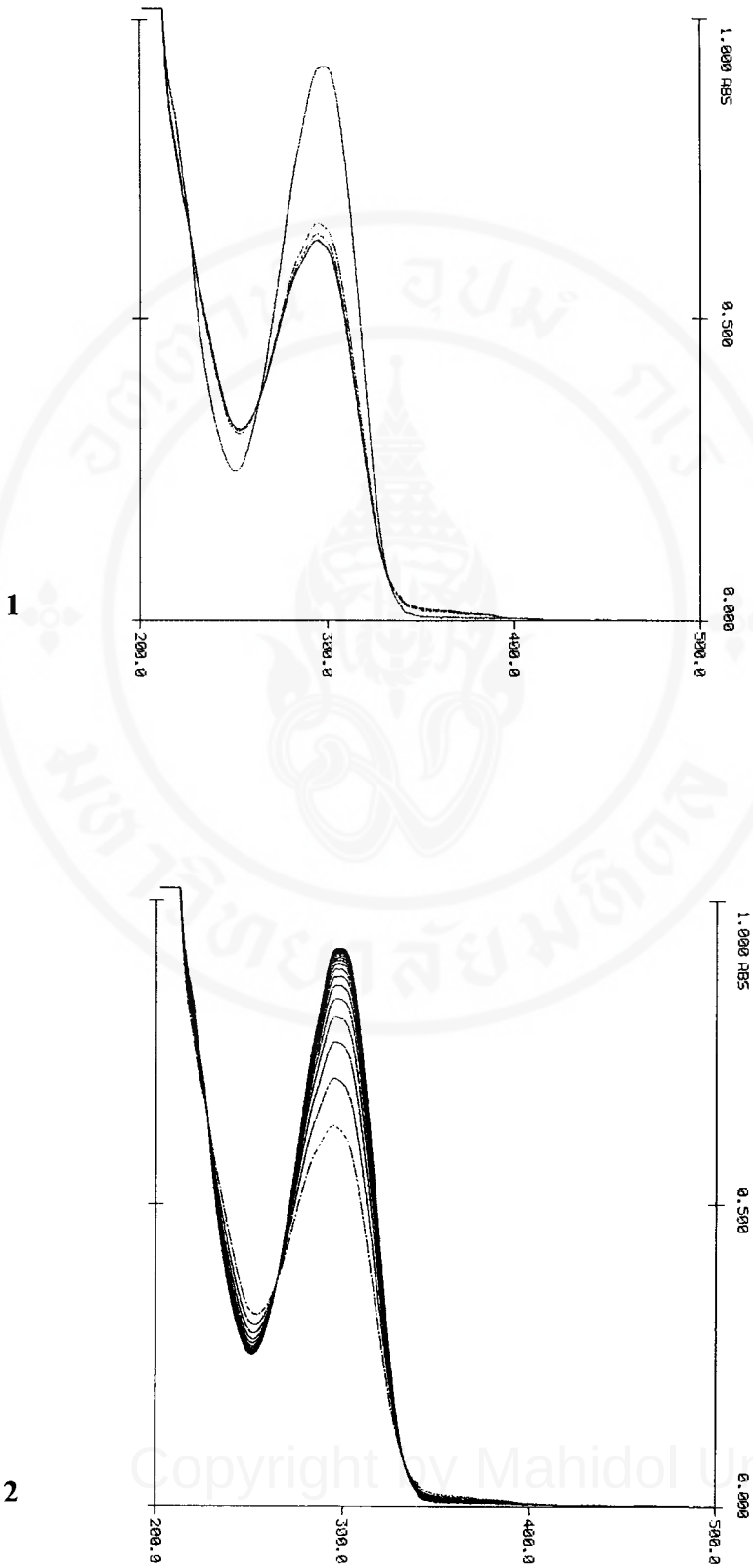

f)

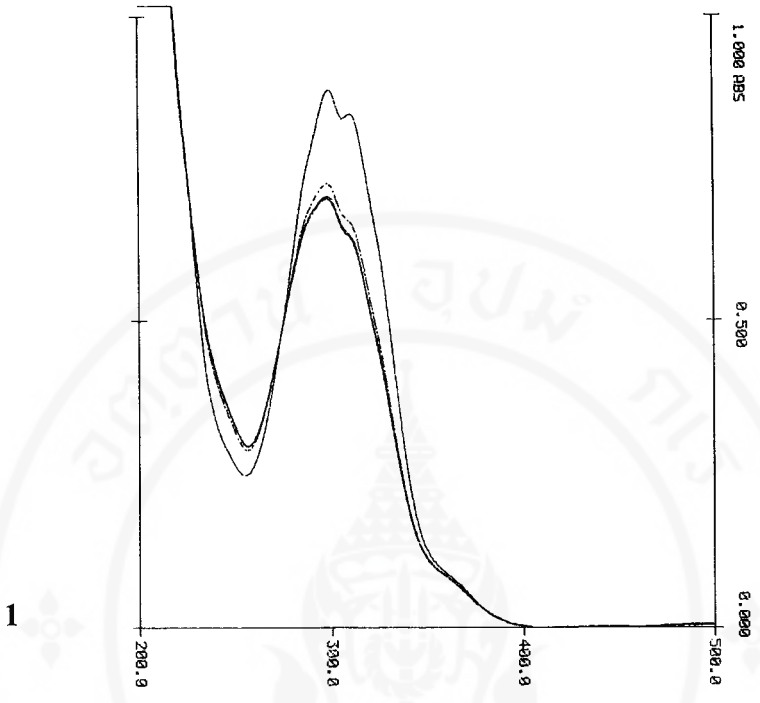

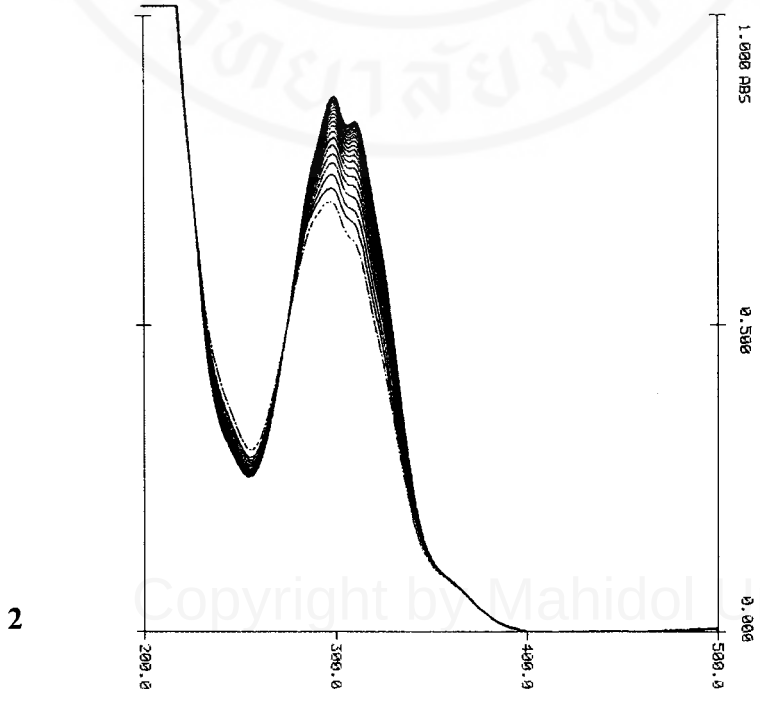

g)

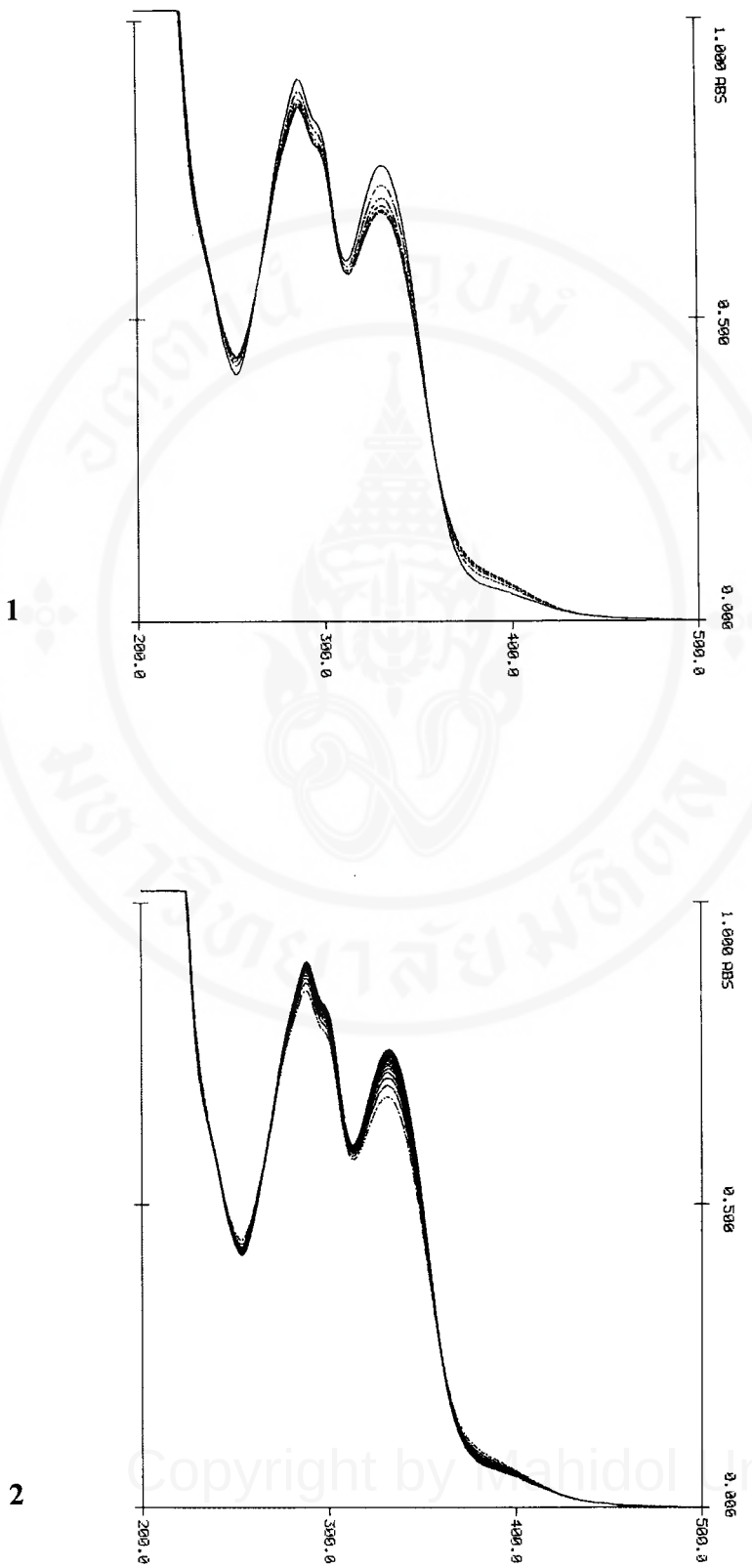

h)

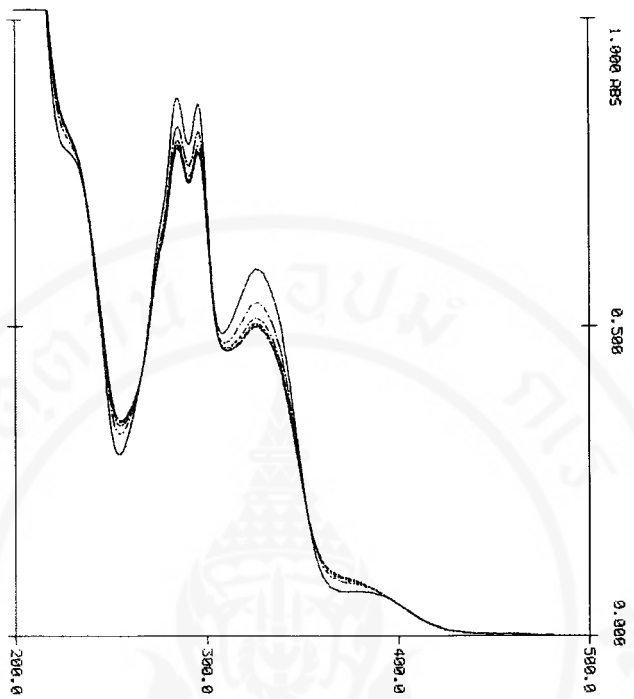

1

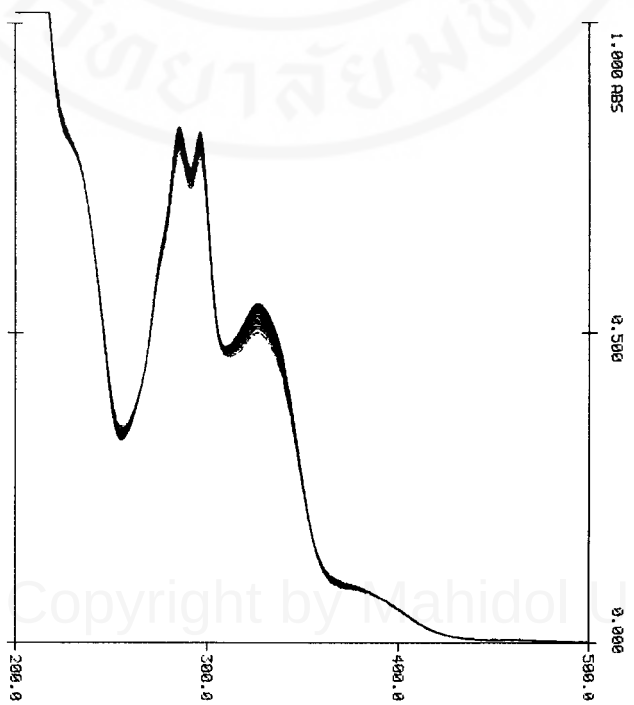

2

i)

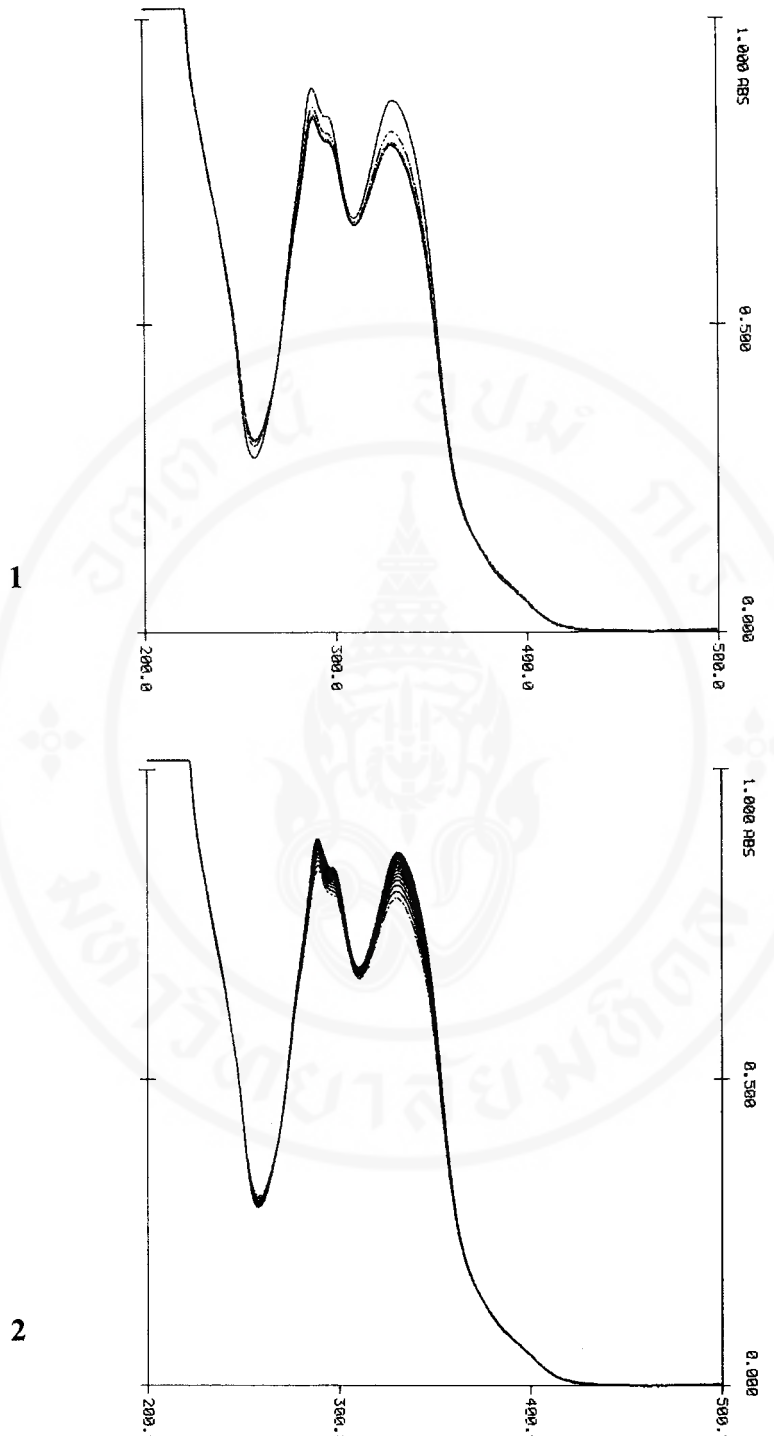

Figure 3.3 Electronic absorption spectra of a) pycPIH, b) docPIH, c) PBH, d) PSH, e) BIH, f) BBH, g) BSH, h) SIH, i) SBH and j) SSH in methanol. **1** before (——) and after (–·–·–) irradiation at 296 nm for 15, 30, 45, 60, 75 and 90 minutes (from top to bottom); **2** after 90 minutes UV-irradiation (–·–·–) and after keeping in the dark (——), measuring every 15 minutes for 5 hours, from bottom to top, respectively.

Table 3.2 Photochromic behaviours of hydrazones

Compound	Isosbestic point (nm)	Spectral change	
		Under light	In dark
BBH	226	Increase	Decrease
	263		
	333	Decrease	Increase
BSH	274	Decrease	Increase
	380		
SBH	266	Decrease	Increase
	353		
	400	Increase	Decrease
pycPIH	263	Decrease	Increase
	368		
	430	Increase	Decrease
docPIH	263	Decrease	Increase
	369		
	407	Increase	Decrease
SSH	268	Decrease	Increase
	372		
	410	Increase	Decrease
SIH	265	Decrease	Increase
	359		
BIH	248	Decrease	Increase
	335		
PSH	269	Decrease	Increase
	368		
PBH	270	Decrease	Increase
	365		

For the other hydrazones, time interval about 15 minutes was used to follow the changes of the absorption spectra in both light and dark. The results are shown in Figure 3.3c–3.3j. The isosbestic points and the increase or decrease of the spectra of these substances are summarized in Table 3.2. In the table, the hydrazones are arranged in order from the maximum spectral changes to the minimum spectral changes.

3.3 Fluorescence spectroscopic study

The excitation and emission fluorescence spectra of the two types of PIH and structurally related compounds in methanol are shown in Figure 3.4. The maximum excitation and emission wavelengths are shown in Table 3.3.

Table 3.3 Fluorescence data for the hydrazones studied

Compound	Maximum spectra (nm)		Sensitivity[a]
	λ_{ex}	λ_{em}	
pycPIH	320, 410	503	×100
docPIH	320, 410	503	×100
PBH	294, 408	489	×10
PSH	297, 406	482	×10
BIH	323	420	×100
BBH	218	287	×100
BSH	300	471	×100
SIH	313, 391	505	×100
SBH	300, 382	496	×100
SSH	302, 386	466	×10

[a]Sensitivity scale setting of instrument

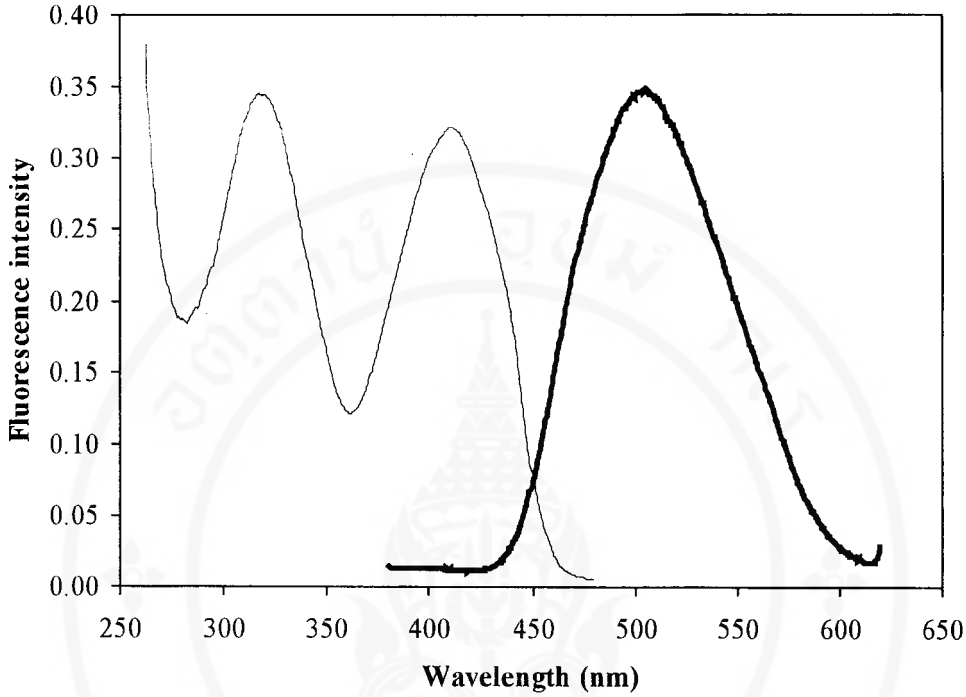

a)

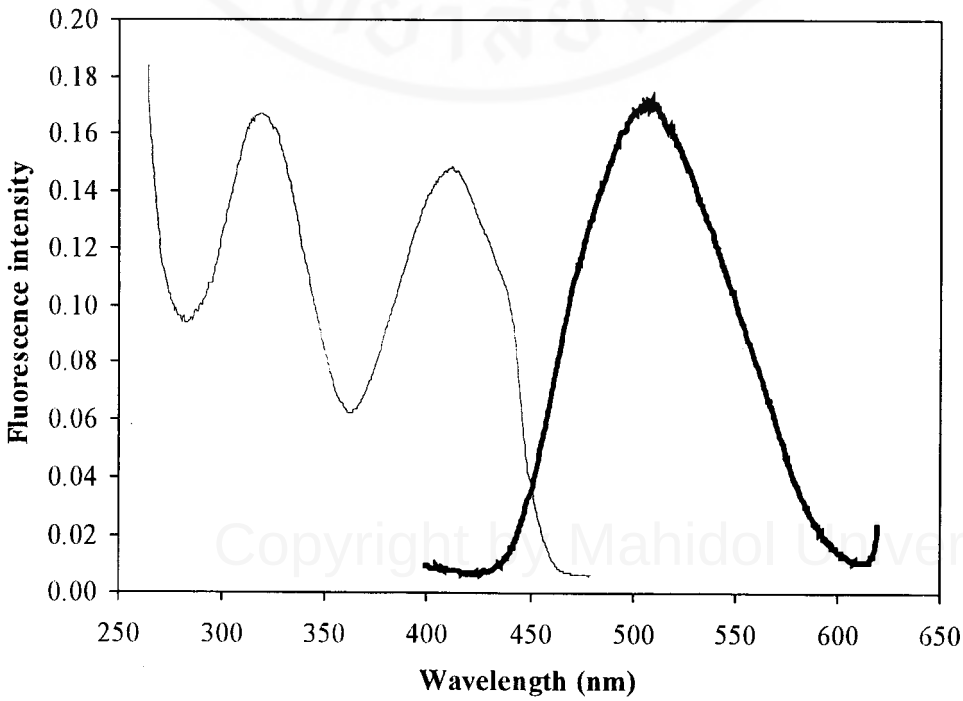

b)

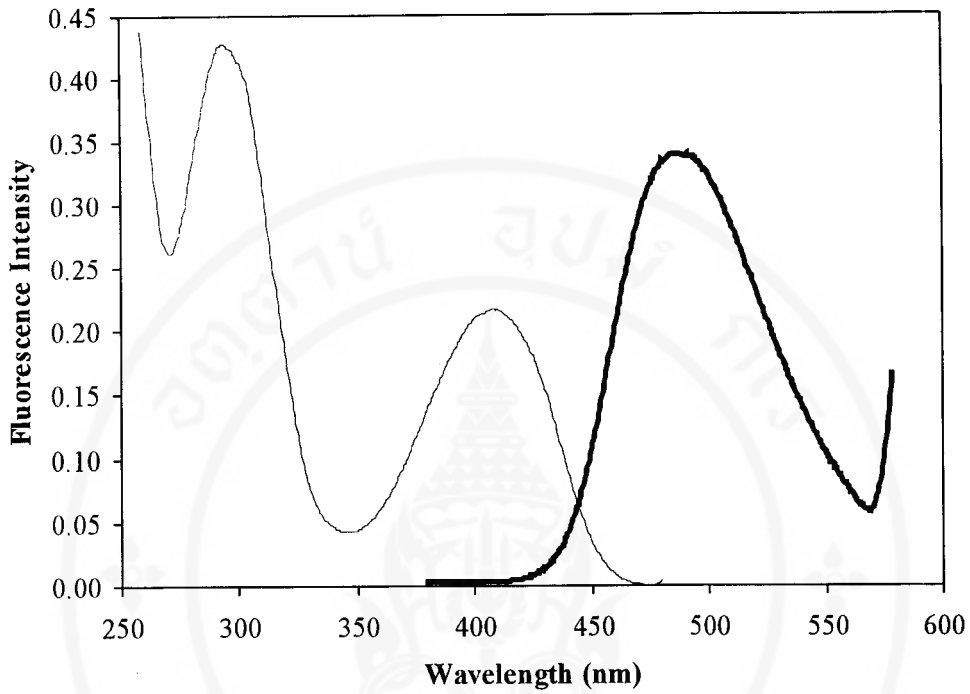

c)

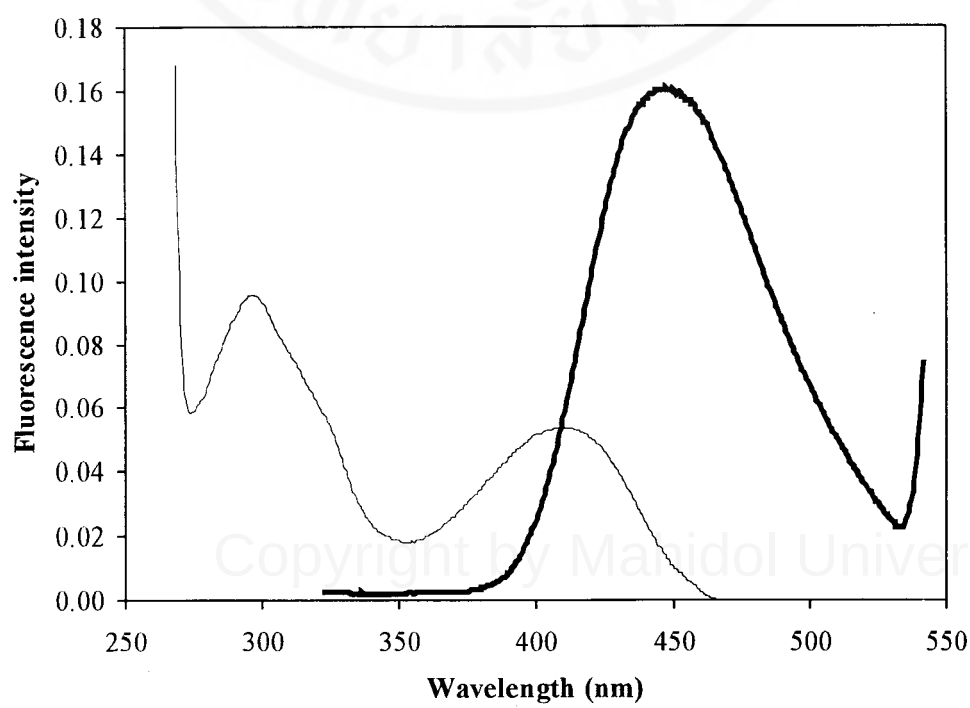

d)

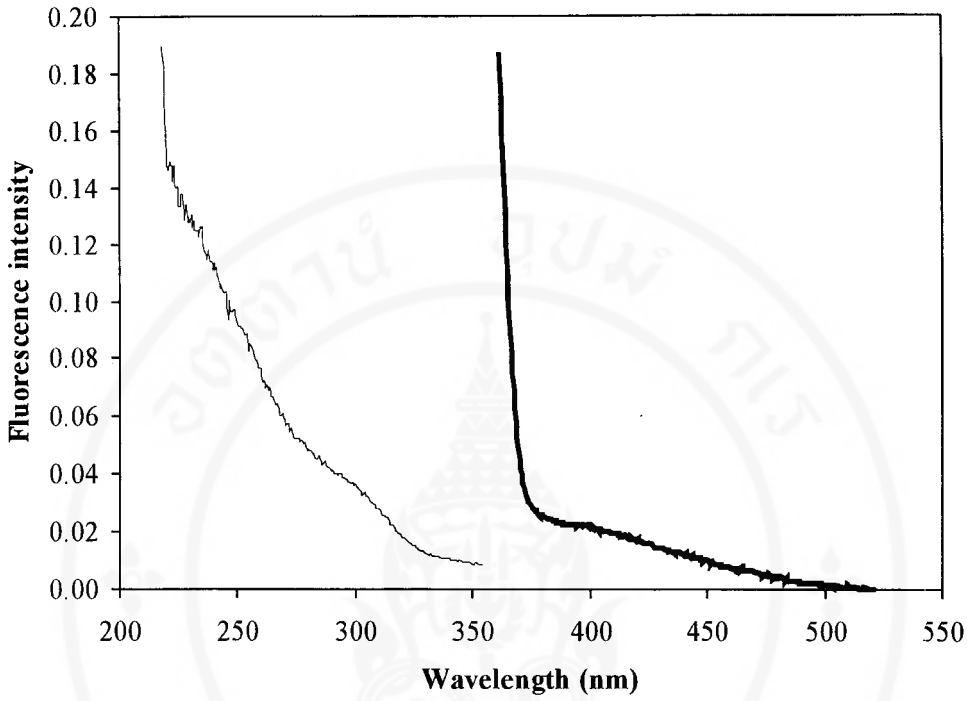

e)

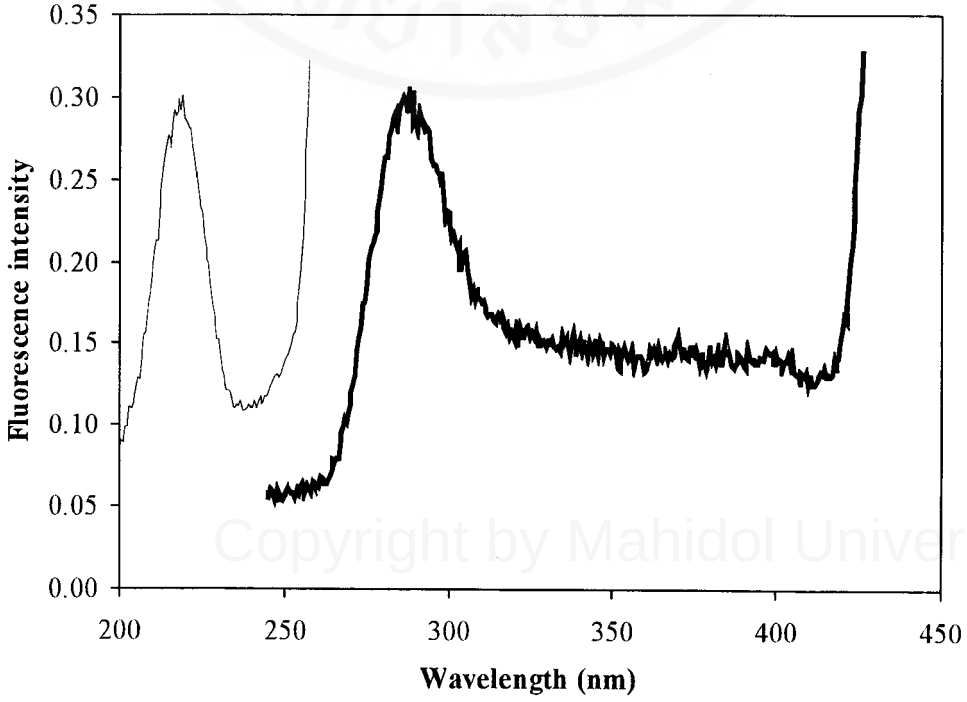

f)

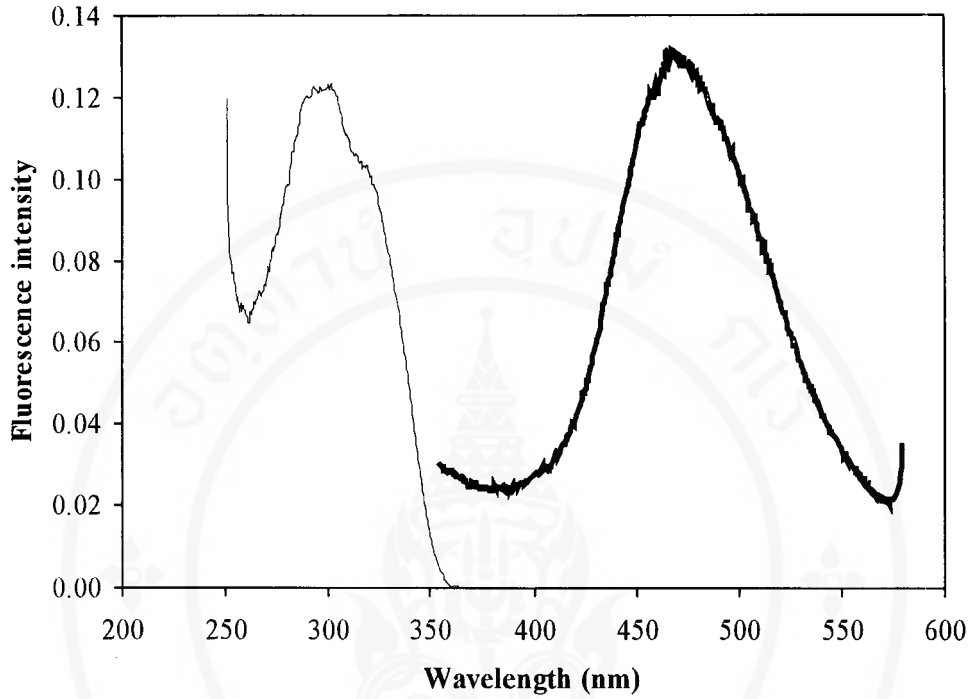

g)

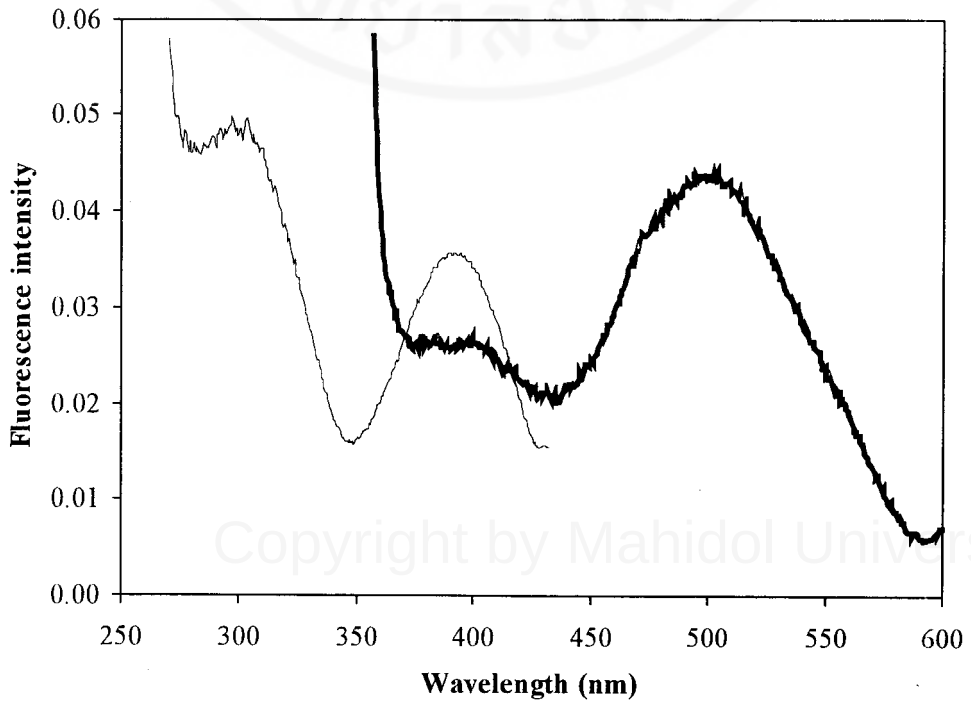

h)

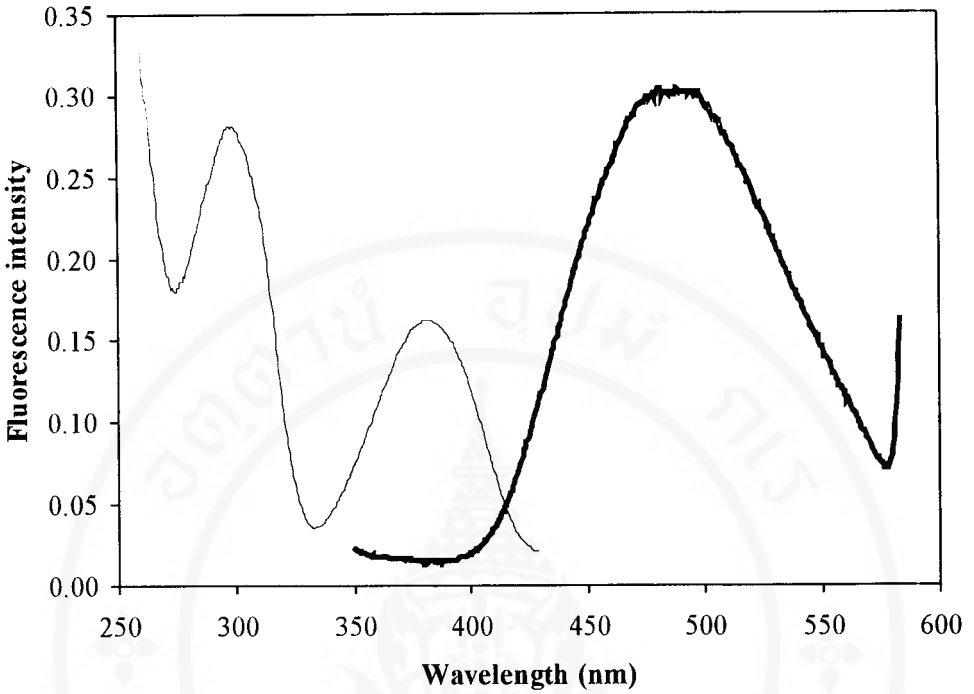

i)

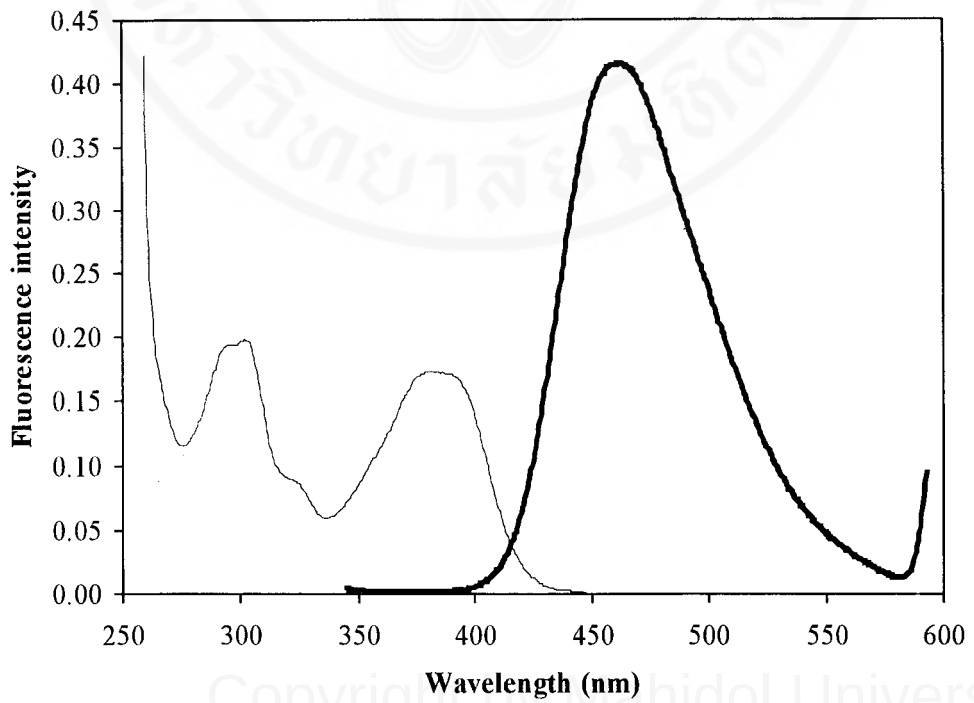

j)

Figure 3.4 Fluorescence excitation (——) and emission (▬▬) spectra of a) pycPIH, b) docPIH, c) PBH, d) PSH, e) BIH, f) BBH, g) BSH, h) SIH, i) SBH and j) SSH in methanol (2.0×10^{-6} M), with excitation and emission band width of 20 nm.

3.4 Infrared spectroscopic study

Infrared spectra of the starting materials and the hydrazones were measured as neat liquids or as KBr discs. The spectra are shown in Figure 3.5–3.21 and 3.23–3.30, and the relevant assignments of the vibrational absorption bands of each compound are described in Section 3.4.1 and 3.4.2, and given in Table 3.4 and 3.5 [35-37,42-44,63-70].

3.4.1 Starting materials

As for electronic absorption spectra, infrared spectra of the starting materials were recorded to help in the interpretation of the spectra of the compounds studied. The infrared spectrum of pyridoxal hydrochloride is shown in Figure 3.5. The weak C=O stretching vibration is at approximately 1645 cm^{-1}. The shift of this band to the lower frequency may result from the intramolecular hydrogen bonding between the carbonyl group with the *ortho*-hydroxyl group. The aldehydic C–H stretching bands appear in the 2850–2700 cm^{-1} region. Their intensity is pronounced by the broad hydrogen-bonded O–H stretching band at about 2900 cm^{-1}. Besides this band, the hydroxyl group shows an O–H in-plane bending absorption at 1361 cm^{-1}. The absorption bands near 1286 and 1019 cm^{-1} may involve with the C–O stretching vibrations. The heteroaromatic ring C–H stretching bands appear near 3050 cm^{-1} and are pronounced by the O–H stretching band, as well. Ring stretching vibrations occur in the general region between 1600 and 1400 cm^{-1}. These absorptions involve stretching and contraction of all of the bonds in the ring and interaction between these stretching modes. In the spectrum, the two heteroaromatic ring, C=C and C=N,

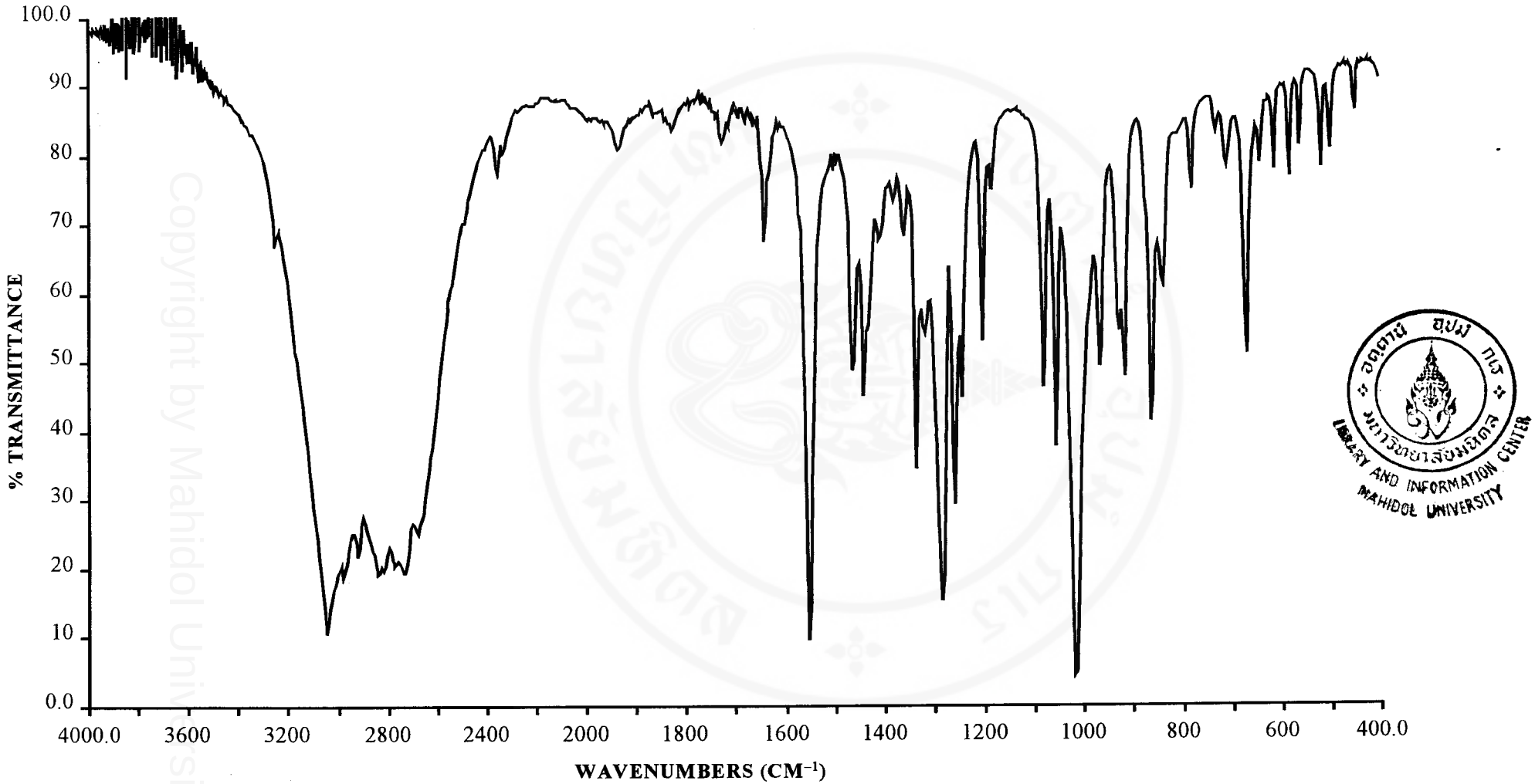

Figure 3.5 Infrared spectrum of pyridoxal hydrochloride (KBr pellet).

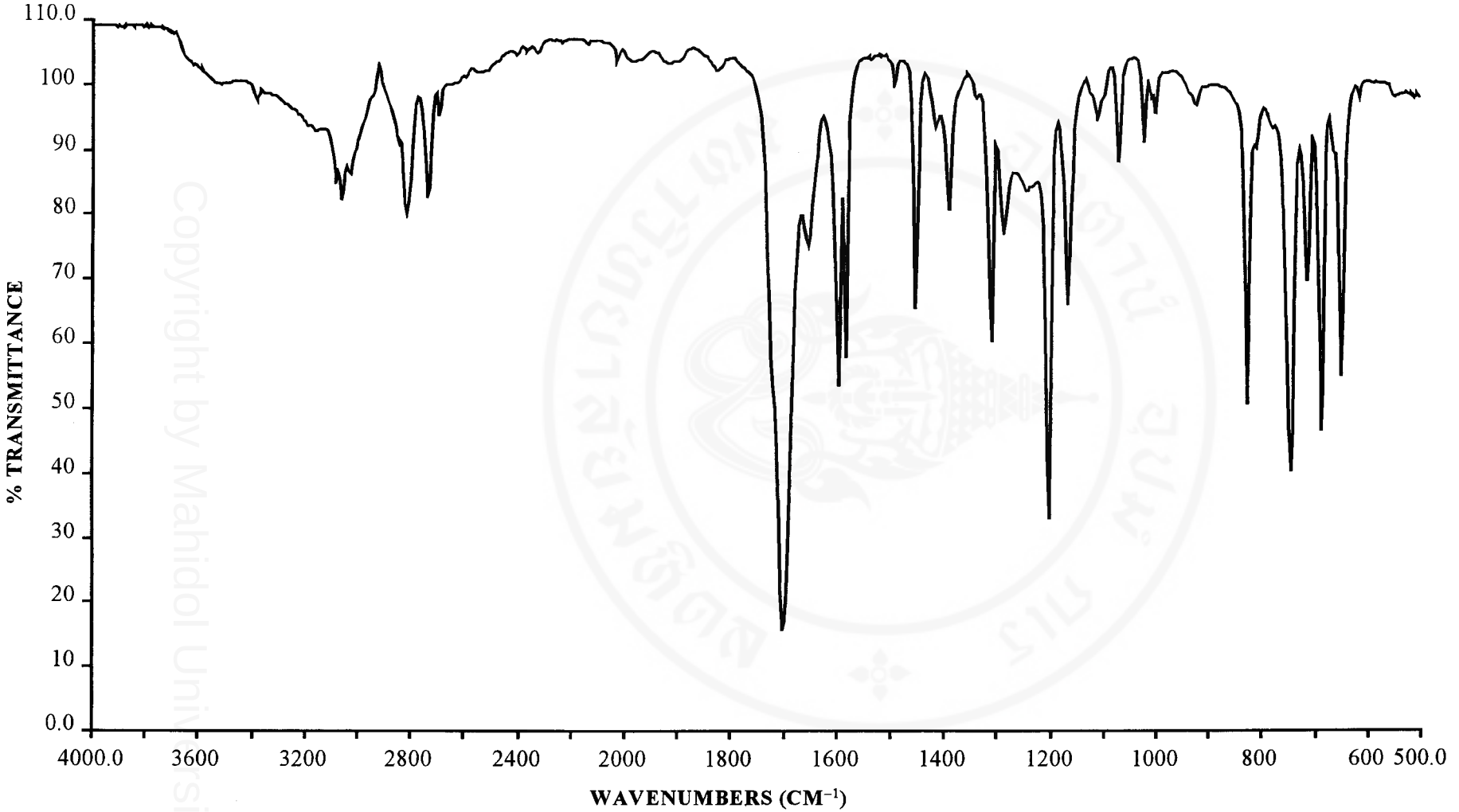

Figure 3.6 Infrared spectrum of benzaldehyde (neat liquid).

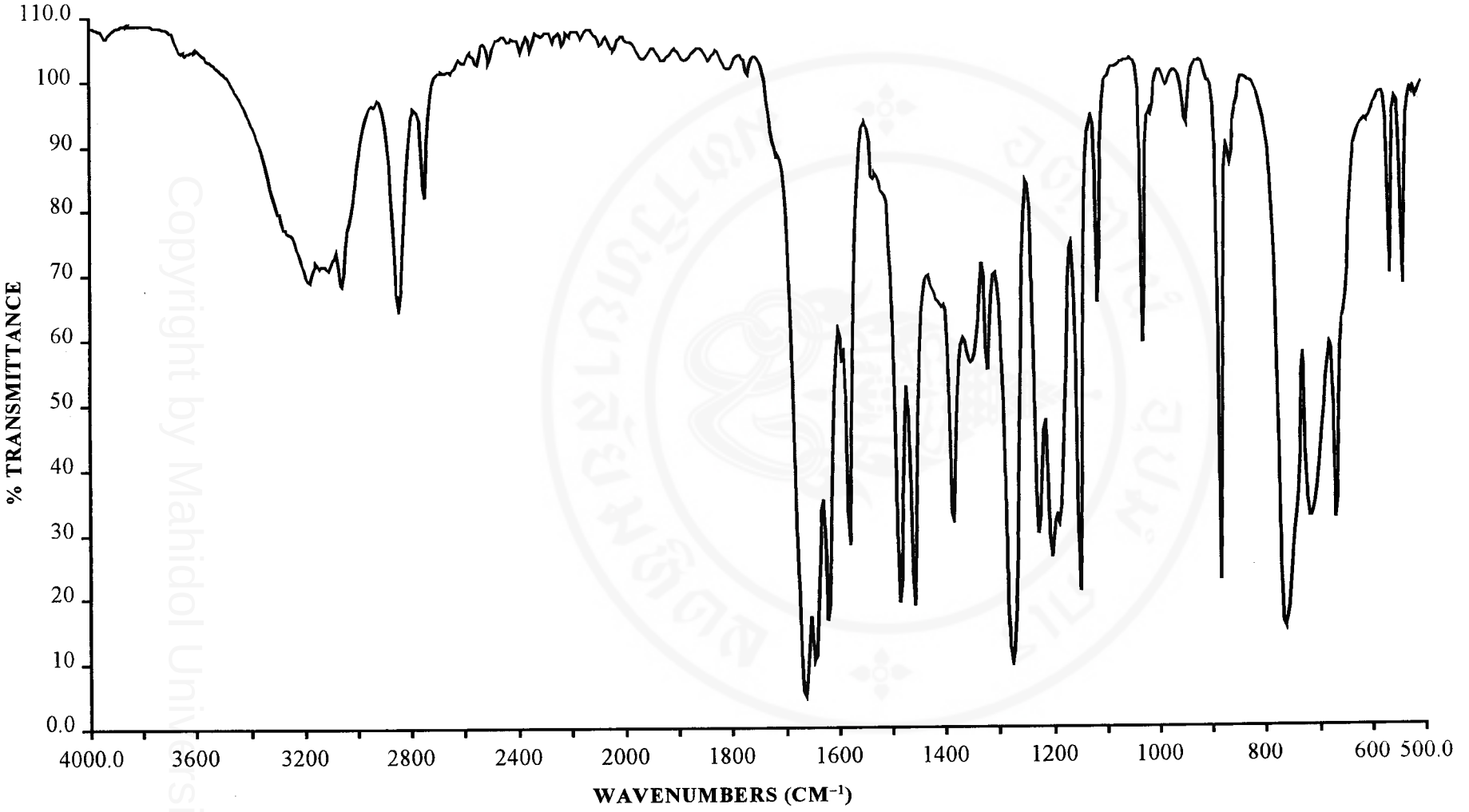

Figure 3.7 Infrared spectrum of salicylaldehyde (neat liquid).

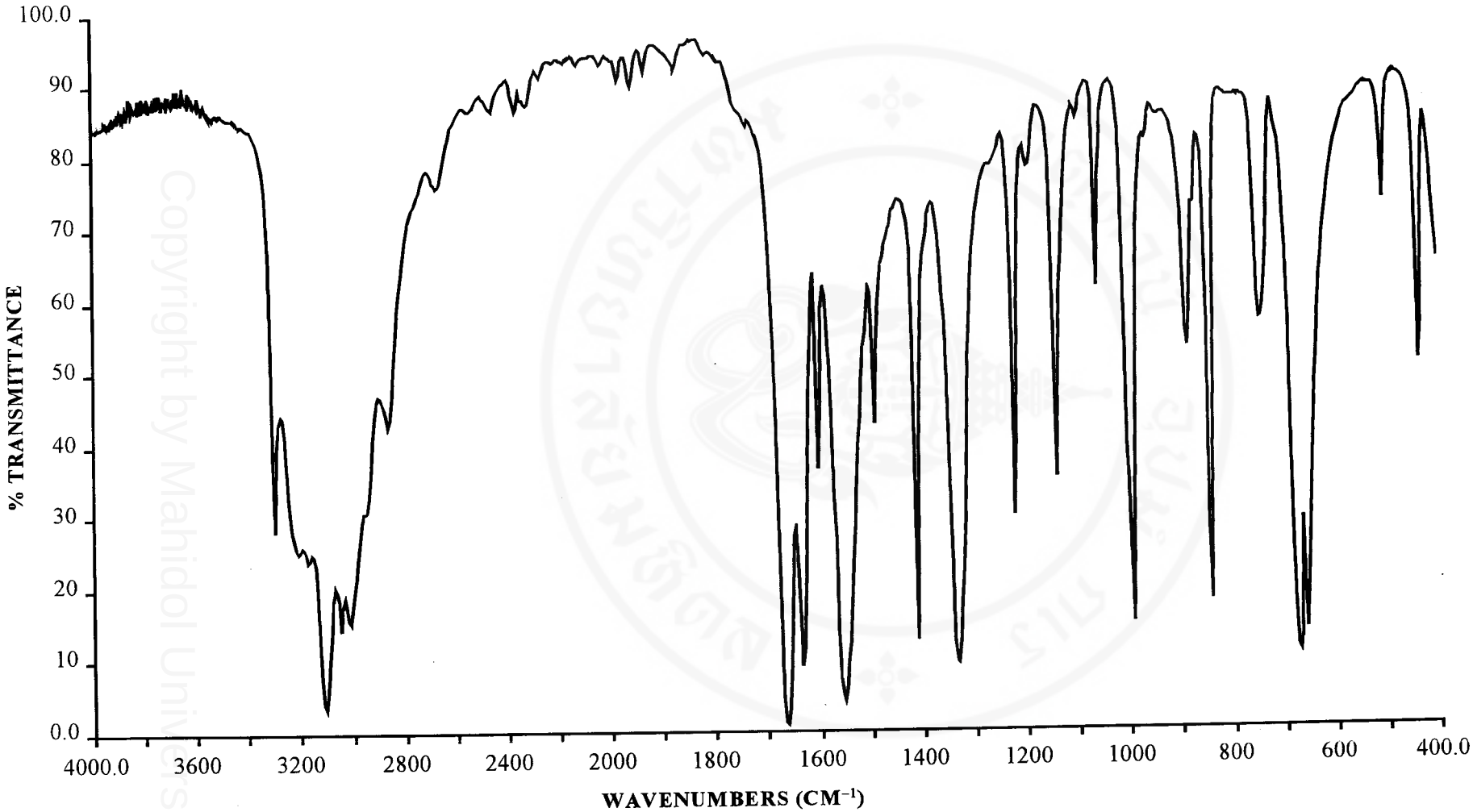

Figure 3.8 Infrared spectrum of isonicotinic acid hydrazide (KBr pellet).

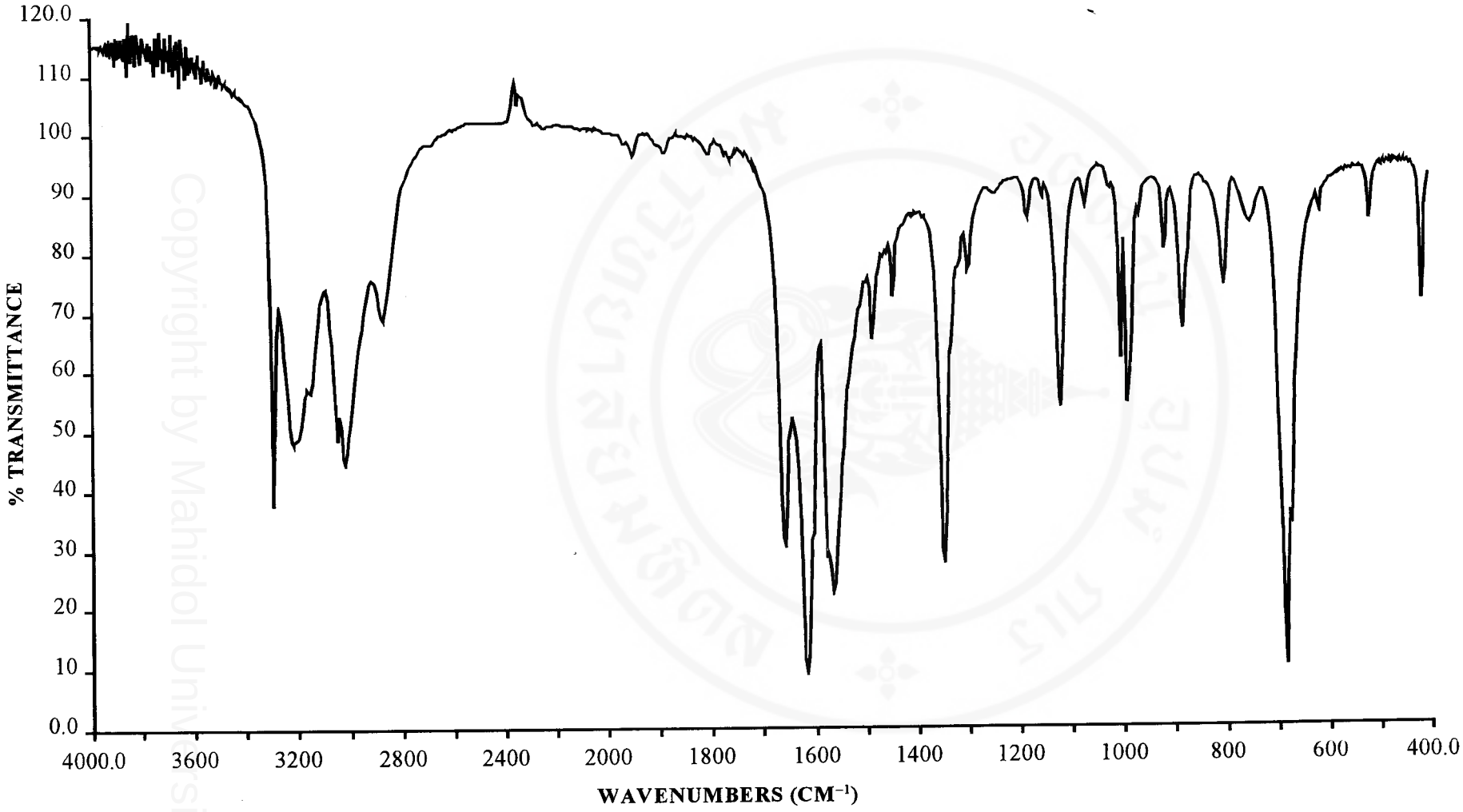

Figure 3.9 Infrared spectrum of benzoic acid hydrazide (KBr pellet).

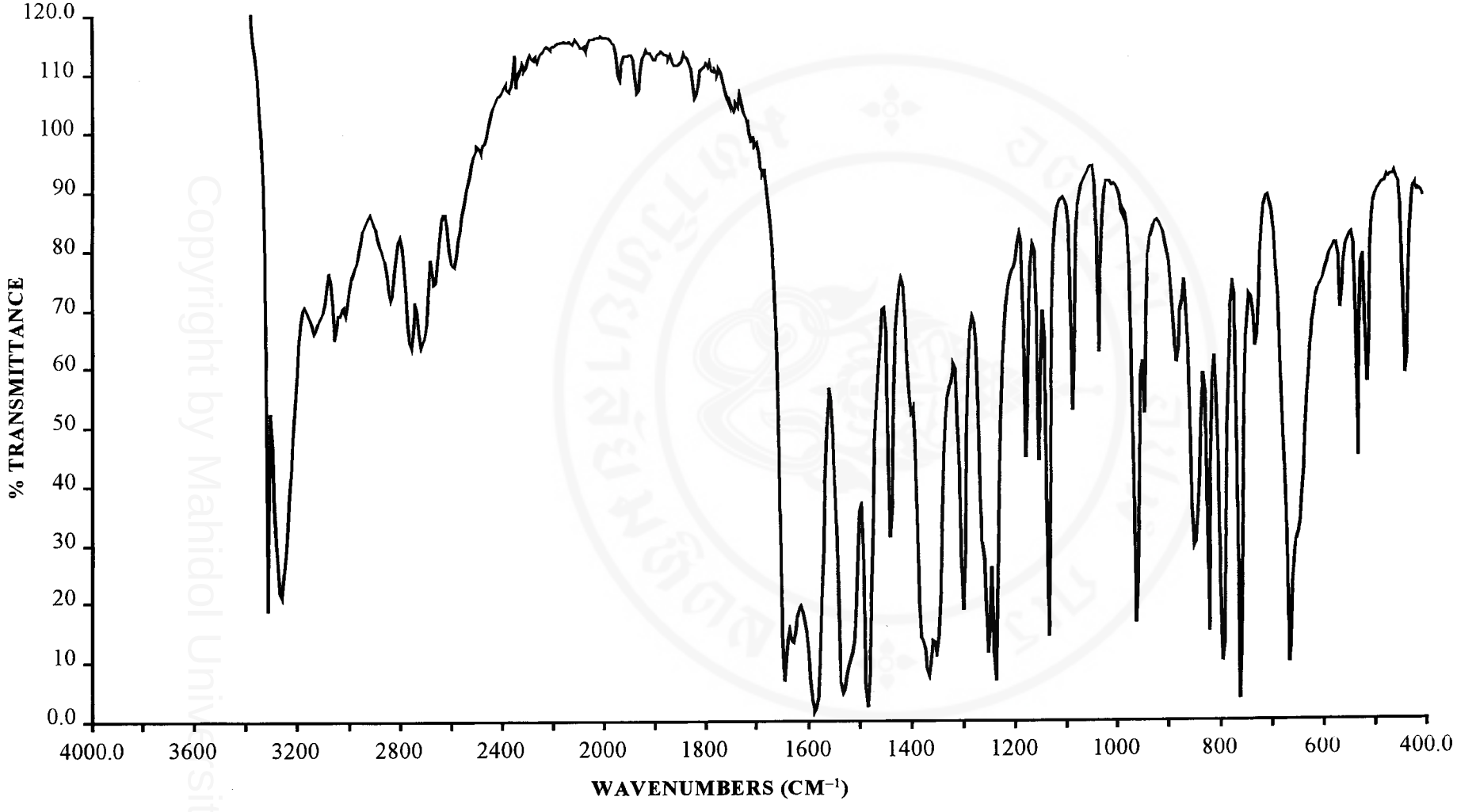

Figure 3.10 Infrared spectrum of salicyloyl hydrazide (KBr pellet).

stretching bands are observed near 1506 and 1443 cm^{-1}. The C–H stretching bands occur at about 2985 and 2922 cm^{-1}. Methylene (CH_2) and methyl (CH_3) groups have a characteristic bending mode absorption at approximately 1465 and 1381 cm^{-1}, respectively. As for the 3255 and 1556 cm^{-1} absorption bands, they may correspond to the N–H stretching and in-plane bending vibrations at heteroaromatic ring, respectively. The position of absorption with this general region depends on the degree of hydrogen bonding.

Since they are liquids at room temperature, the infrared spectra of benzaldehyde and salicylaldehyde were obtained using neat liquids and are shown in Figure 3.6 and 3.7, respectively. Both show a similar absorption spectrum, with additional bands related to hydroxyl group in the spectrum of salicylaldehyde. The carbonyl groups of benzaldehyde and salicylaldehyde absorb at approximately 1702 and 1665 cm^{-1}, respectively. The strong C=O absorption of salicylaldehyde is shifted to lower wavenumbers, due to the internal hydrogen bonding between the carbonyl group with the hydroxyl group of the molecule. For aldehydic and aromatic C–H vibrational absorptions, both benzaldehyde and salicylaldehyde show the C–H stretching, in-plane and out-of-plane bending bands in the 3100–2700, 1300–1000 and 900–650 cm^{-1} regions, respectively. The difference in the C–H (and C–C) out-of-plane bending bands of the both compounds results from the substitution pattern on aromatic ring. For monosubstituted ring, as in the case of benzaldehyde, the two strong absorptions are near 746 and 688 cm^{-1}. For salicylaldehyde, the *ortho*-disubstituted ring gives one strong band near 766 cm^{-1}. In addition to these vibrational bands, salicylaldehyde displays the hydrogen-bonded O–H and C–O stretching bands at about 3200 and 1278 cm^{-1}, respectively.

The vibrational absorption spectrum of isonicotinic acid hydrazide is shown in Figure 3.8. From this spectrum, the most intense absorption band at 1667 cm^{-1} is assigned as the C=O stretching vibration (amide I). Its position depends on the degree of hydrogen bonding and, thus, on the physical state of the compound. For the vibrational absorptions near 1635 and 1557 cm^{-1}, they are assigned as the strong N–H bending (NH_2, NH) bands. These absorptions involve coupling between N–H bending and other fundamental vibrations and require a trans geometry. The N–H stretching vibrational bands of isonicotinic acid hydrazide absorb in the 3350–3150 cm^{-1} region. As for the strong band at about 3112 cm^{-1}, it is attributed to a Fermi resonance overtone of the 1557 cm^{-1} band. The other absorption bands in spectrum near 3051 and 3016; and 1602, 1493 and 1413 cm^{-1} correspond to the heteroaromatic C–H and C=C (and C=N) stretching vibrational bands, respectively.

Benzoic acid hydrazide and salicyloyl hydrazide give infrared spectra similar to isonicotinic acid hydrazide but with the additional bands related to the hydroxyl group in the case of salicyloyl hydrazide. From Figure 3.9 and 3.10, their C=O stretching (amide I) bands absorb near 1661 and 1647 cm^{-1}, respectively. As in the case of isonicotinic acid hydrazide, the N–H stretching bands of benzoic acid hydrazide and salicyloyl hydrazide appear in the 3350–3150 cm^{-1} region. The strong N–H bending bands absorb at about 1618 and 1566 cm^{-1} for benzoic acid hydrazide, and at about 1630 and 1533 cm^{-1} for salicyloyl hydrazide. The other absorption bands in the spectrum of benzoic acid hydrazide are concerned with the mononuclear aromatic group. The aromatic C–H stretching and the skeletal vibrations give absorption in the 3060–3020 and 1600–1400 cm^{-1} regions. In the latter region, the absorption bands are

at approximately 1600, 1578, 1488 and 1447 cm^{-1}. For the monosubstituted benzoic acid hydrazide, the spectrum also shows vibrational bands near 752 and 685 cm^{-1}, related to the aromatic C–H and C–C out-of-plane bending absorptions. For salicyloyl hydrazide, the aromatic C–H stretching and the skeletal vibrations absorb in the same regions as observed for benzoic acid hydrazide. There is also a broad hydrogen-bonded O–H stretching and C–O stretching bands near 3000 and 1245 cm^{-1}.

3.4.2 PIH and related compounds

Differences in the colour of the solid PIH compounds are reflected in differences in the infrared spectra. In this research, four different infrared spectra of PIH are observed, as shown in Figure 3.11–3.21.

When PIH compound was synthesized using the method 2 (Section 2.3.1), deep orange powder PIH (dopPIH) was obtained. This compound gives the infrared spectrum as shown in Figure 3.11. After recrystallization in hot methanol and water, dopPIH gave the deep orange crystal PIH (docPIH) and the orange-yellow powder PIH (oypPIH), respectively. The infrared spectra of these compounds are shown in Figure 3.12 and 3.13. In additional experiments, after dopPIH was recrystallized after passing through Sep-pak C-18 cartridge, it was found that crystals come in many forms, both irregular and needle-shape crystals. These crystals exhibit colours from deep orange to yellow but their infrared spectra are similar to the docPIH or the oypPIH obtained from hot methanol or water as typically shown in Figure 3.14. For PIH crystals obtained after passing through Sep-pak, mostly docPIH were obtained after repeated recrystallization with hot methanol. In some cases, but rarely, PIH could be found in two forms, namely deep orange crystal and pale yellow sheet. The infrared

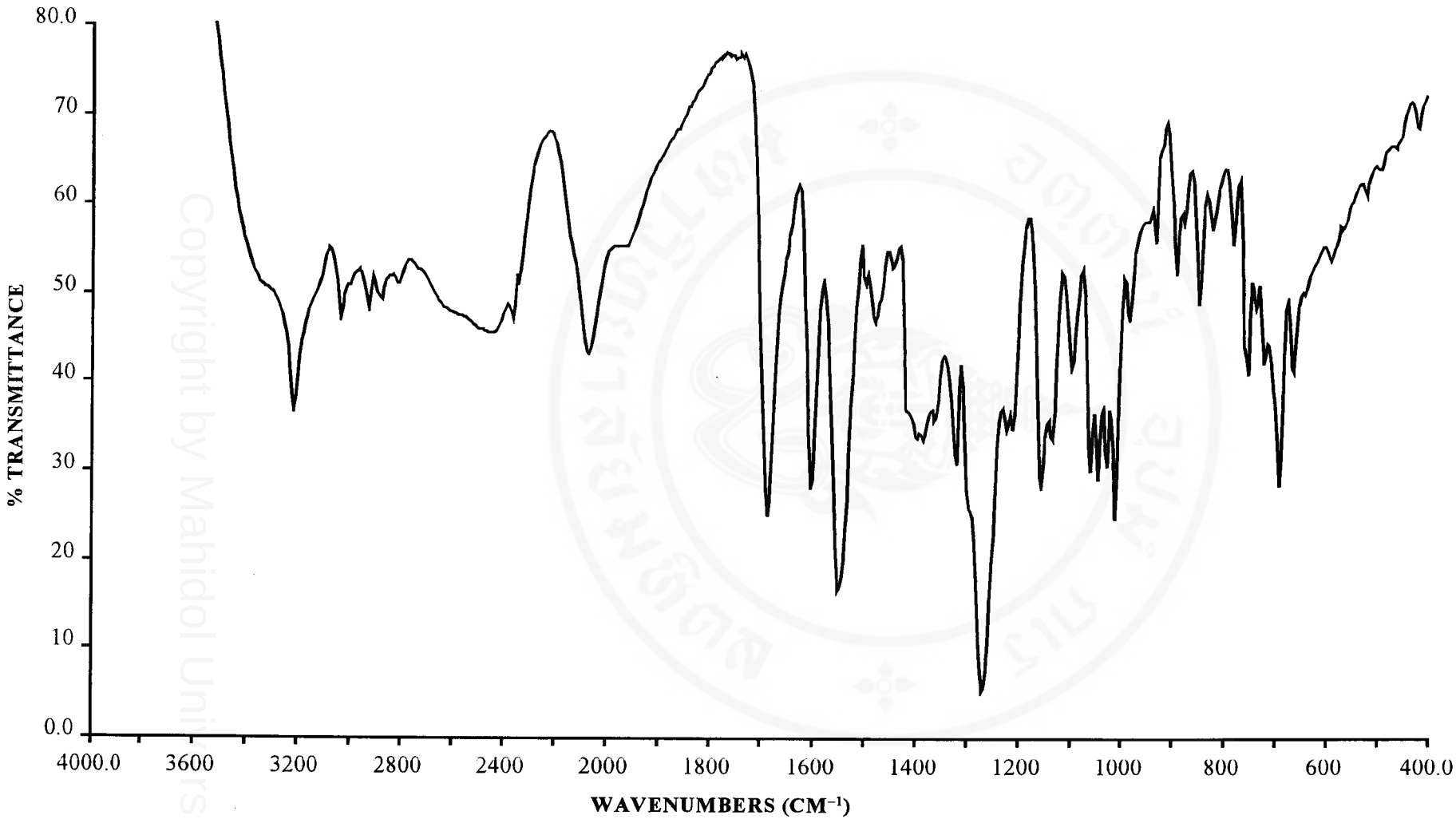

Figure 3.11 Infrared spectrum of deep orange powder PIH (KBr pellet).

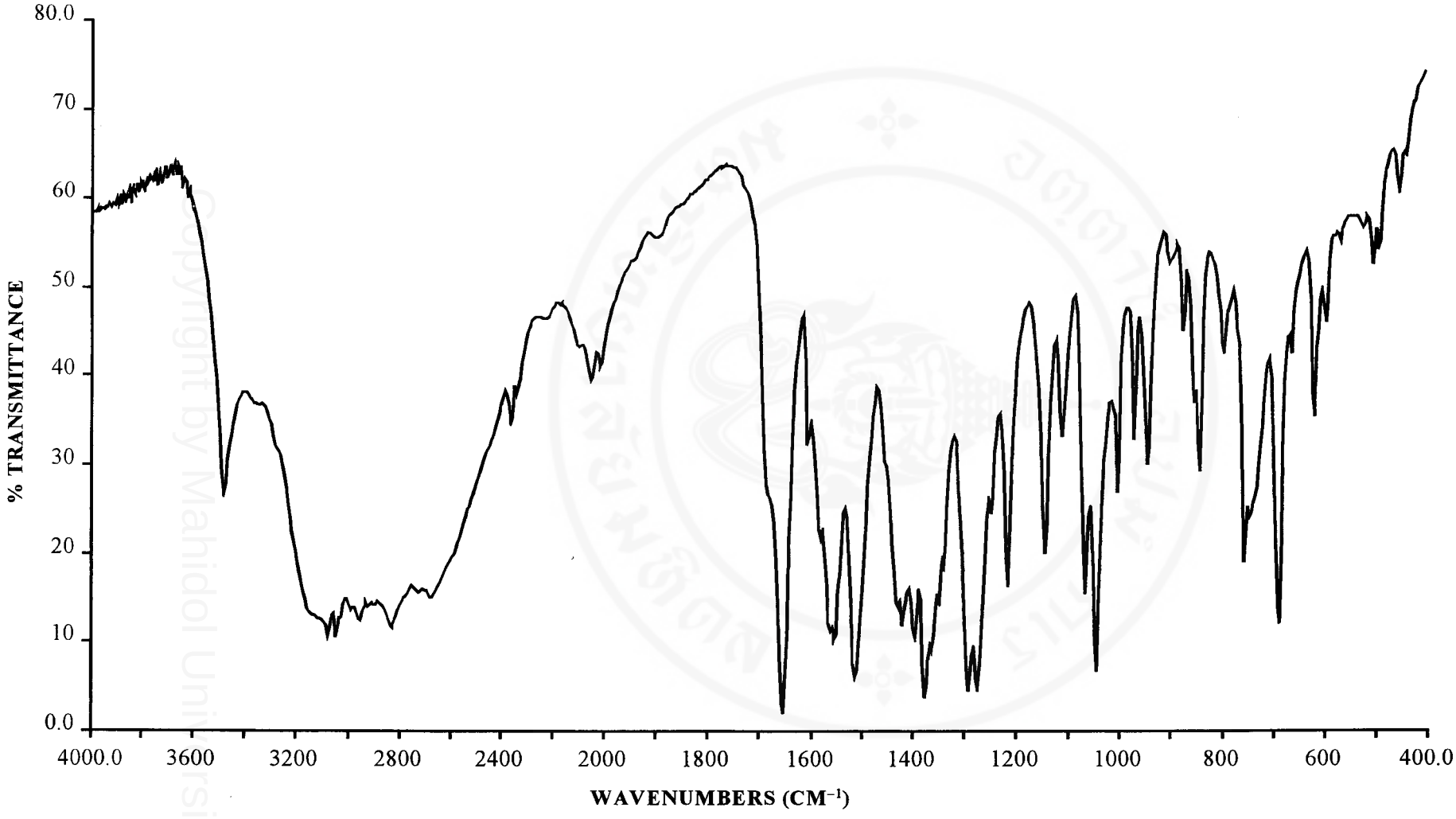

Figure 3.12 Infrared spectrum of deep orange crystal PIH obtained from recrystallization of deep orange powder PIH in hot methanol (KBr pellet).

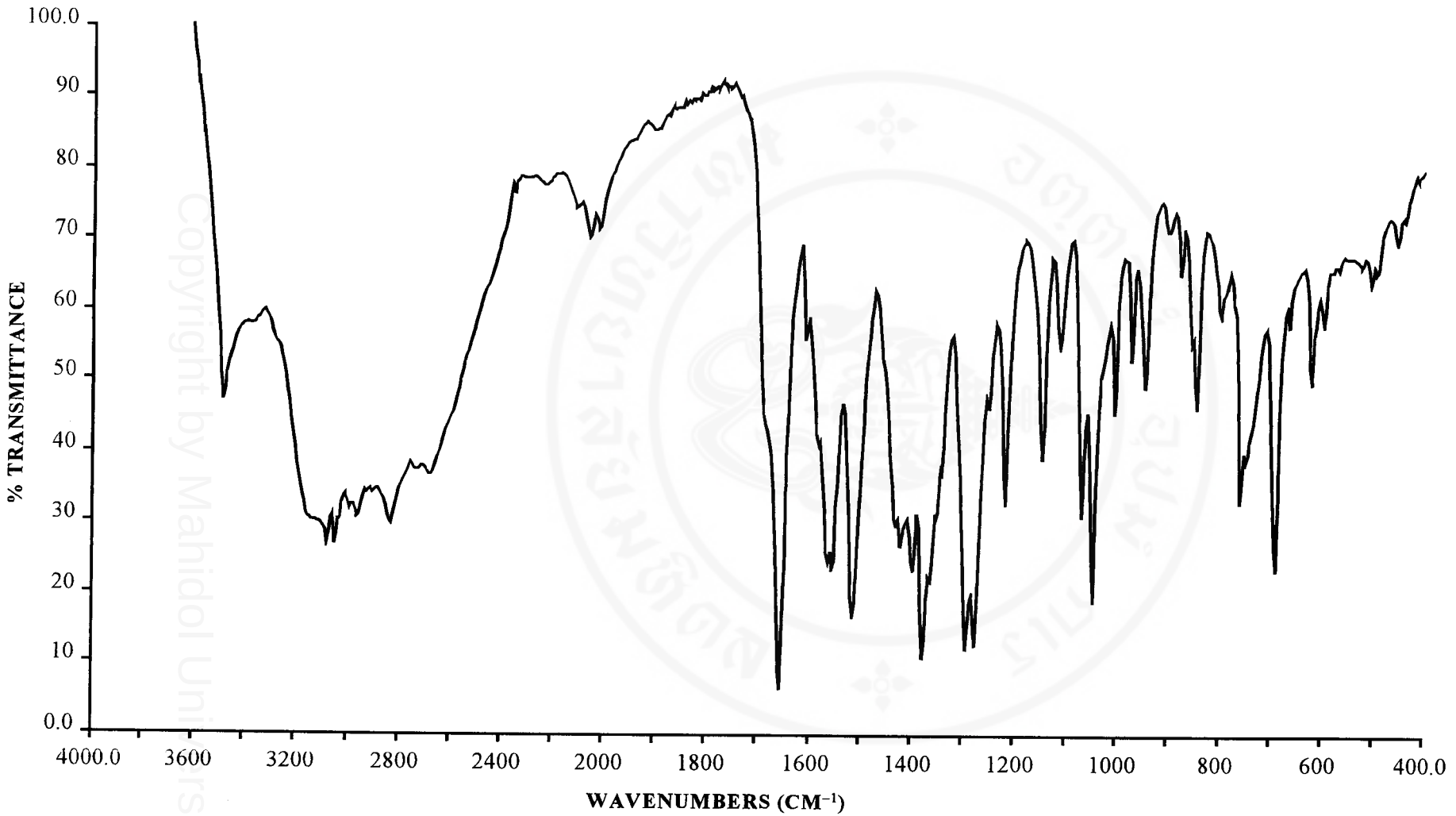

Figure 3.13 Infrared spectrum of orange-yellow powder PIH obtained from recrystallization of deep orange powder PIH in hot water (KBr pellet).

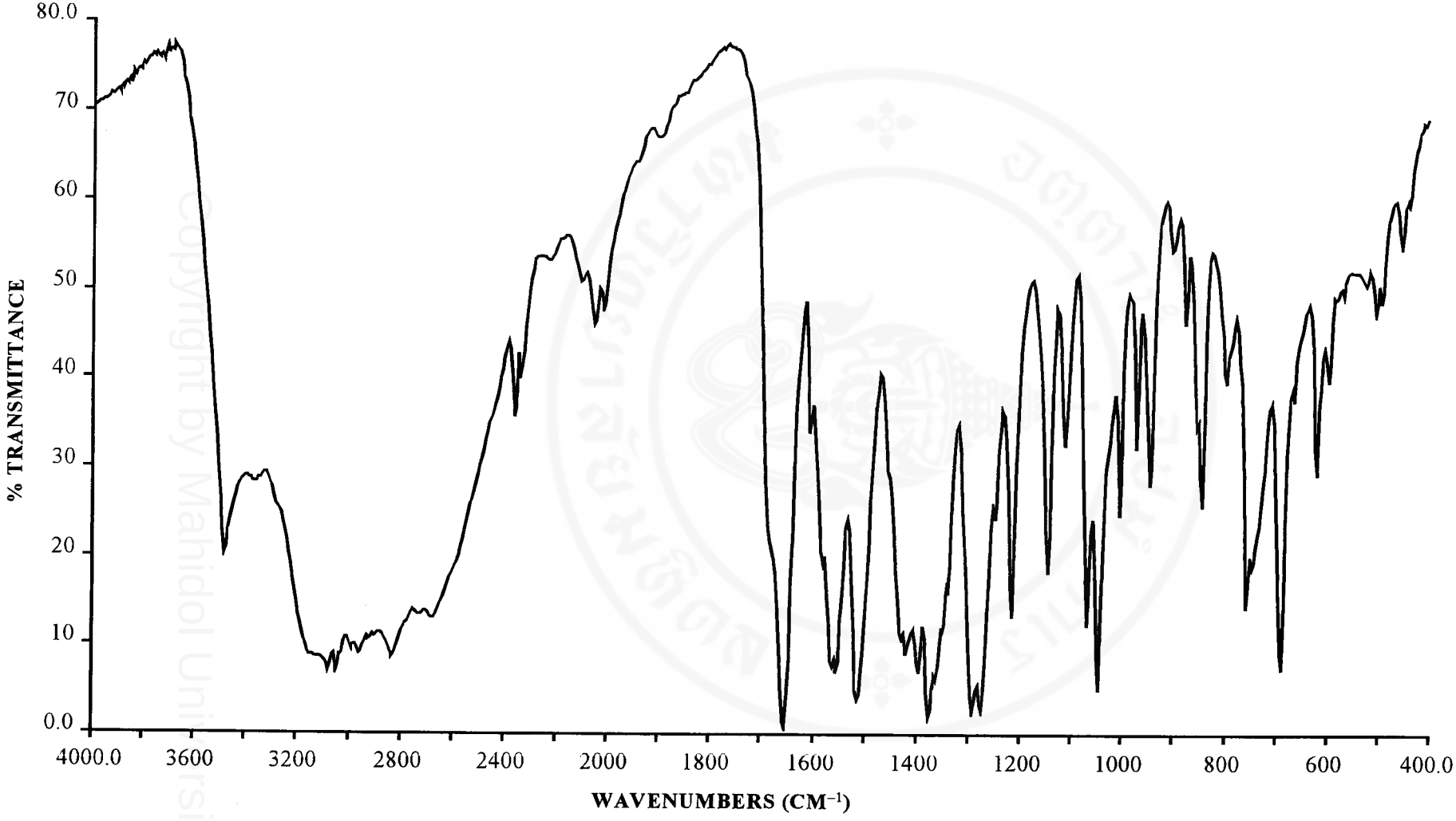

Figure 3.14 Infrared spectrum of typically deep orange crystal PIH obtained from deep orange powder PIH passed through Sep-pak C-18 cartridge (KBr pellet).

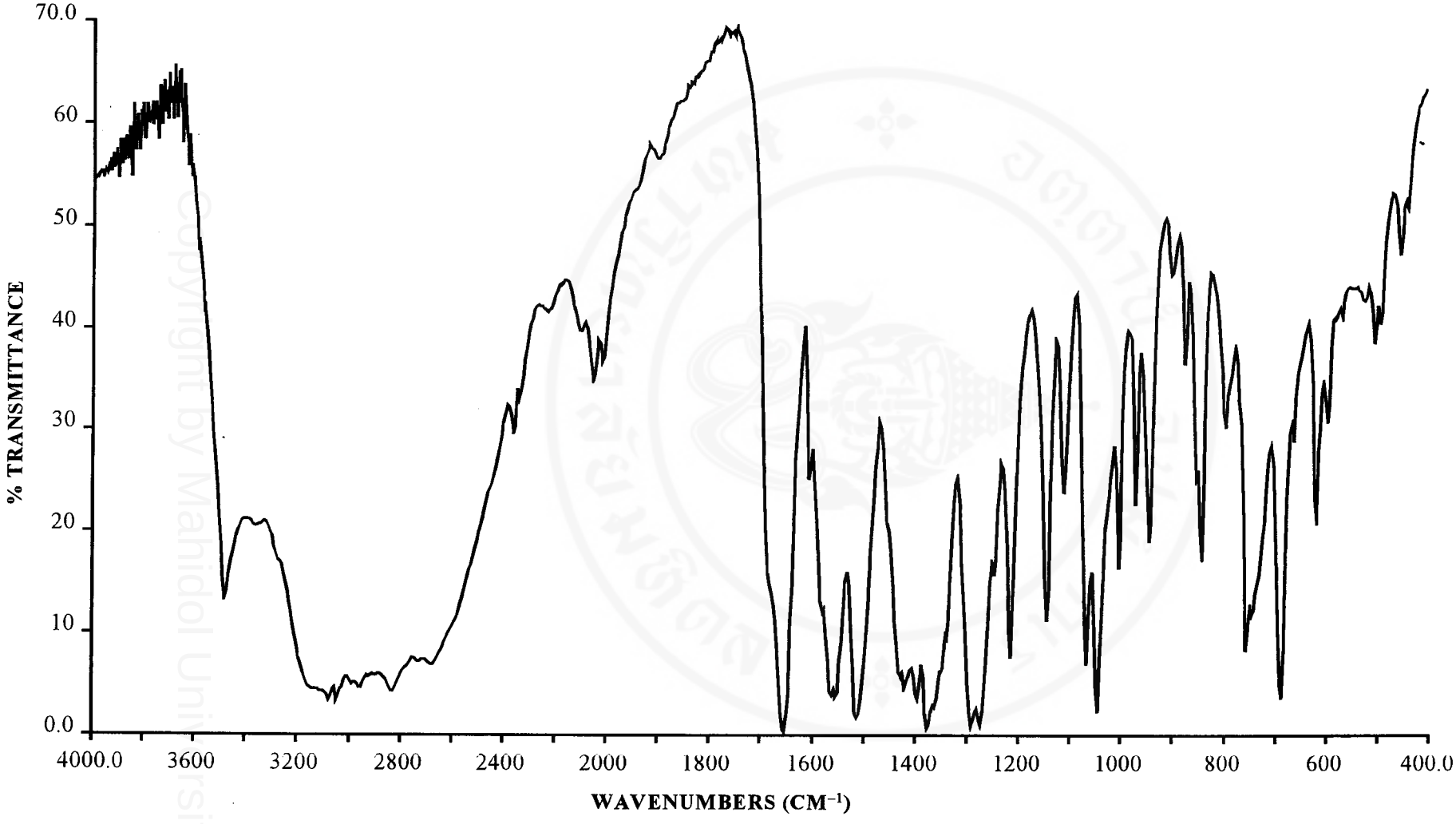

Figure 3.15 Infrared spectrum of deep orange crystal PIH obtained from recrystallization of deep orange crystal PIH (Sep-pak) in hot methanol several times (KBr pellet).

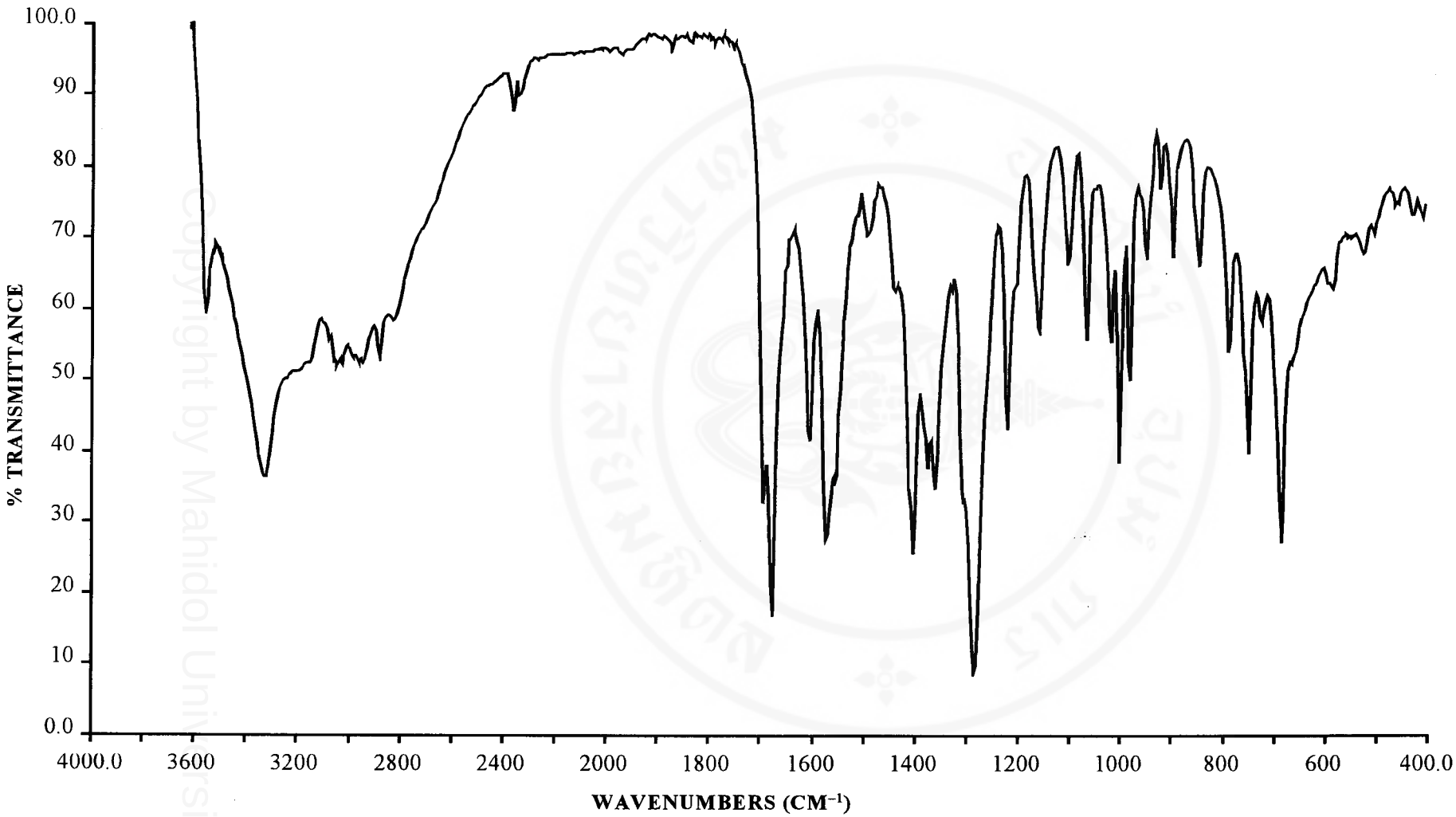

Figure 3.16 Infrared spectrum of pale yellow sheet PIH obtained from recrystallization of deep orange crystal PIH (Sep-pak) in hot methanol several times (KBr pellet).

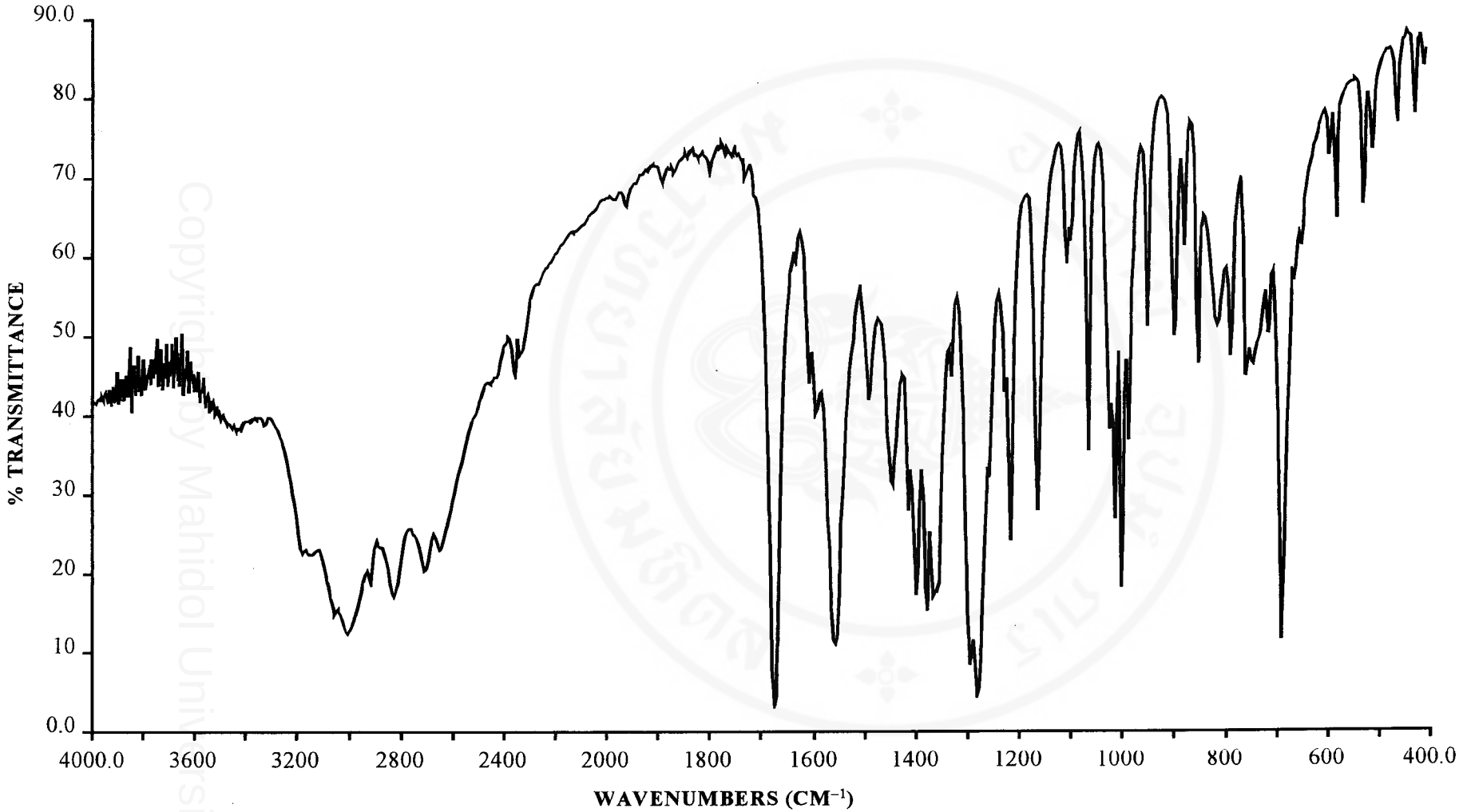

Figure 3.17 Infrared spectrum of pale yellow crystal PIH (KBr pellet).

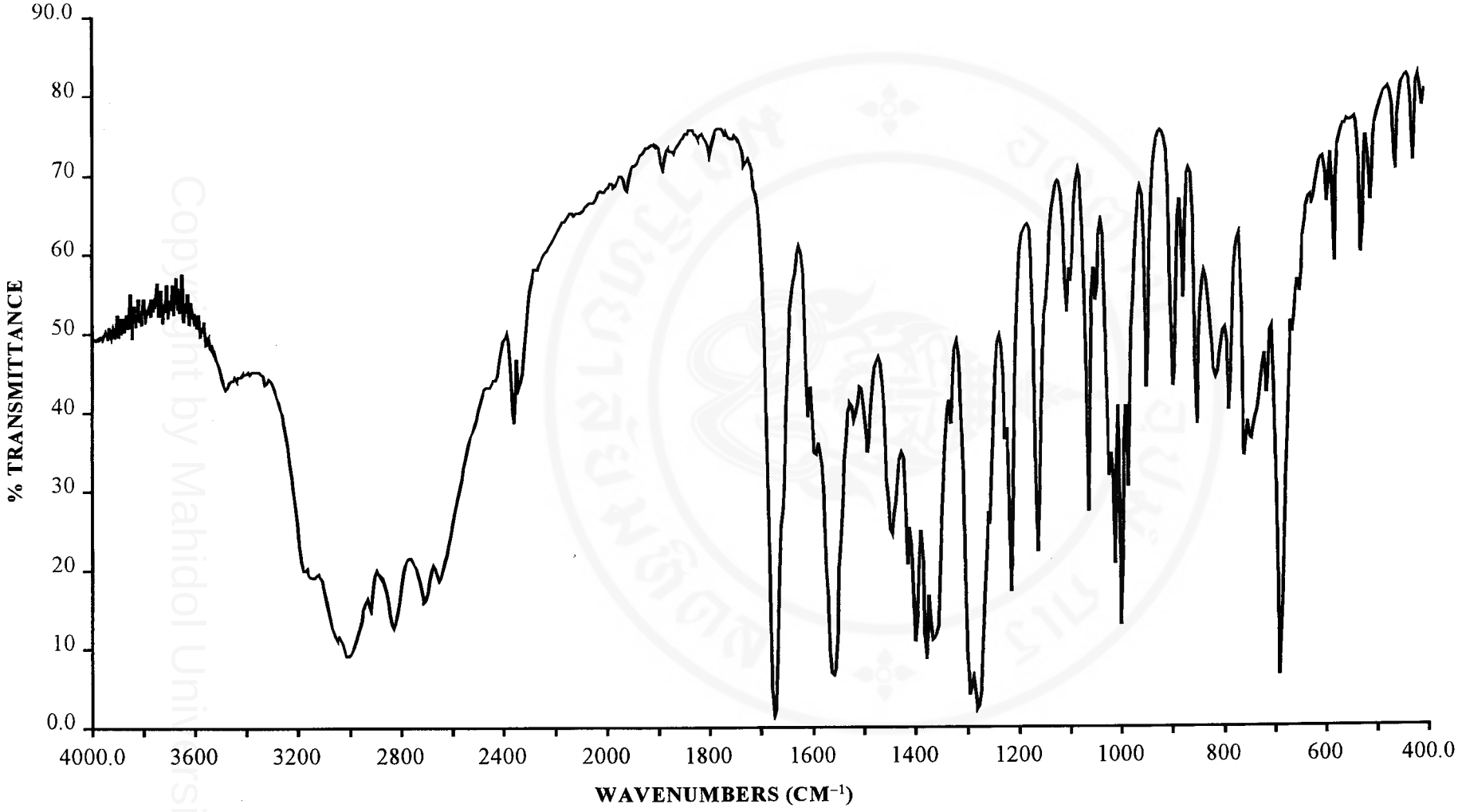

Figure 3.18 Infrared spectrum of slightly orange-yellow crystal PIH (KBr pellet).

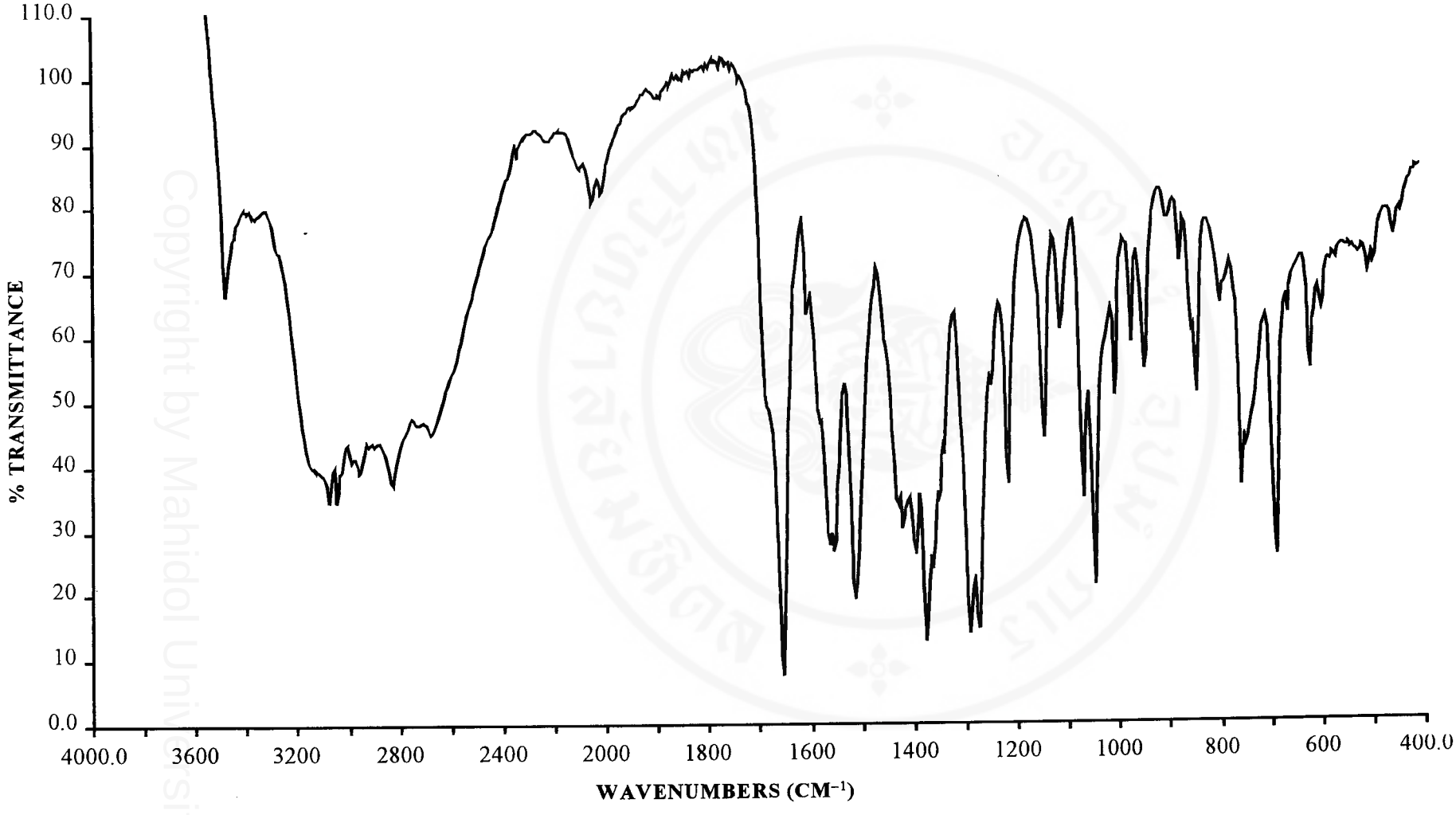

Figure 3.19 Infrared spectrum of orange-yellow crystal PIH obtained from recrystallization of pale yellow crystal PIH in hot methanol (KBr pellet).

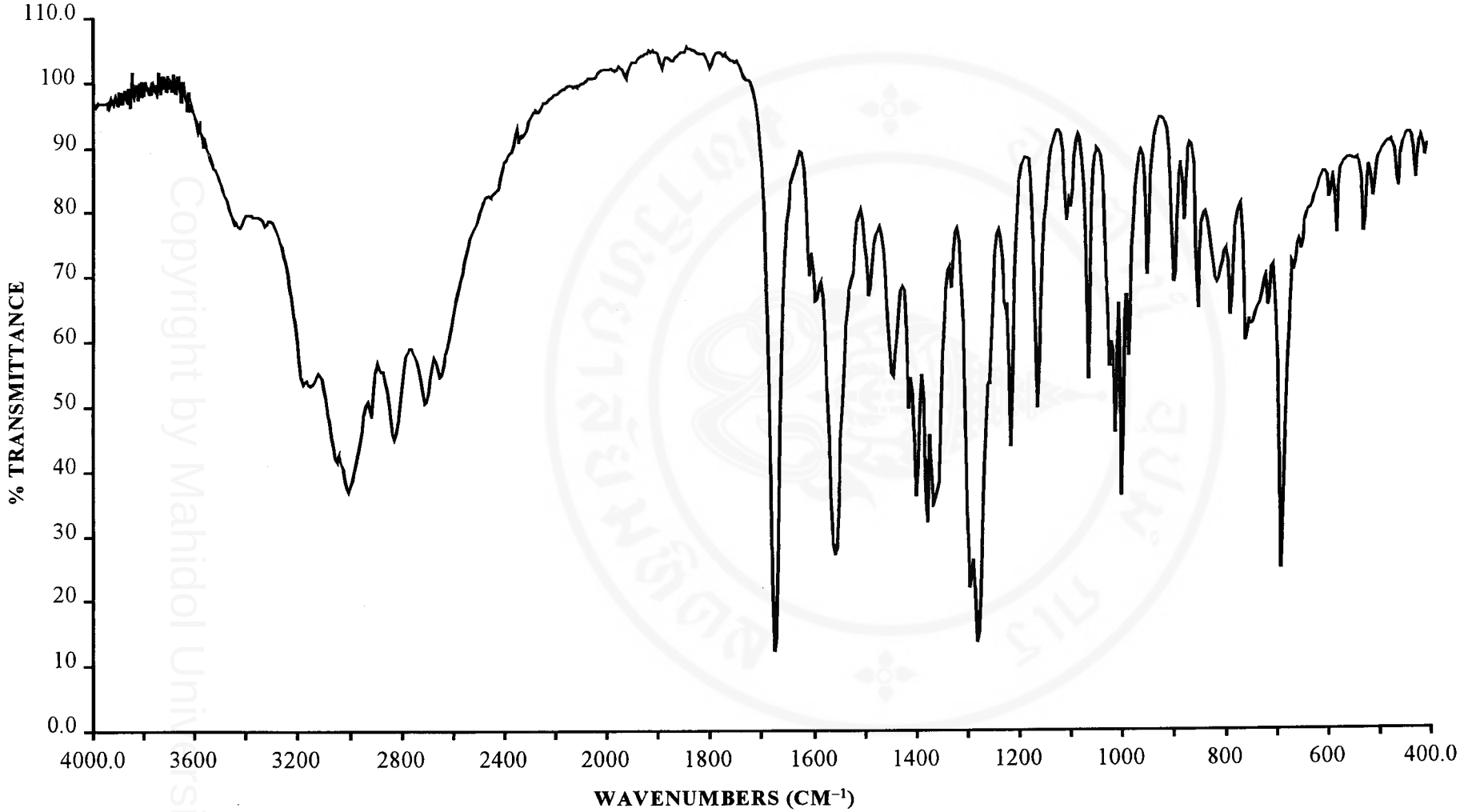

Figure 3.20 Infrared spectrum of tiny pale yellow crystal PIH obtained by crystallization of deep orange crystal PIH (Sep-pak) in methanol seeded with 2–3 crystals of pale yellow crystal PIH (KBr pellet).

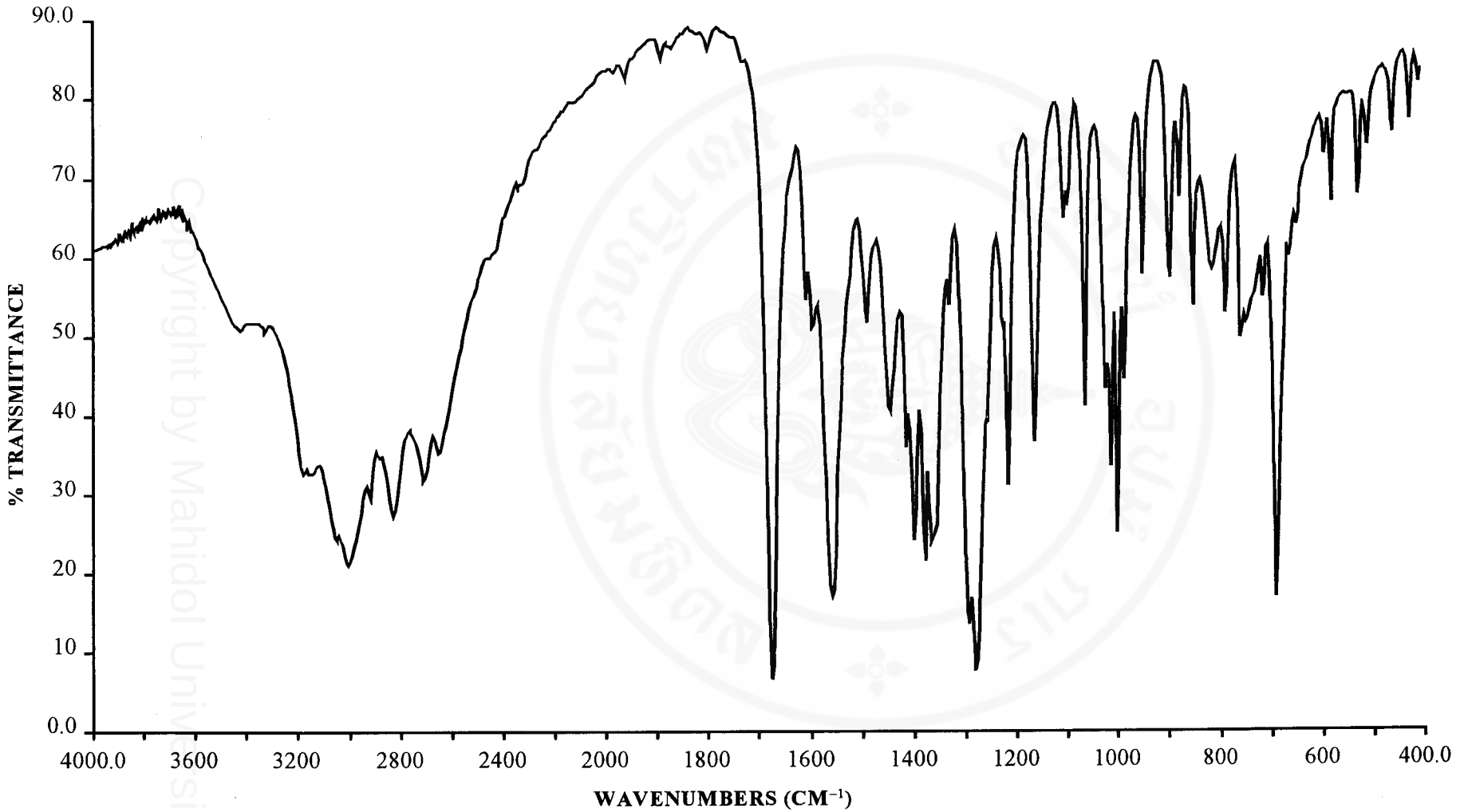

Figure 3.21 Infrared spectrum of fine pale yellow crystal PIH obtained by crystallization of deep orange crystal PIH (Sep-pak) in methanol seeded with 2–3 crystals of pale yellow crystal PIH (KBr pellet).

spectra of the both forms are shown in Figure 3.15 and 3.16, respectively. From infrared spectrum of the pale yellow sheet PIH (pysPIH), it is observed that it is intermediate between infrared spectra of the docPIH and the pale yellow crystal PIH (pycPIH) (see Figure 3.14 and 3.17).

When the method 1 (Section 2.3.1) was used for preparation, pycPIH was obtained and its infrared spectrum is displayed in Figure 3.17. In some samples of pycPIH some crystals are slightly orange-yellow in colour. Its infrared spectrum is exhibited in Figure 3.18. The infrared spectra of both are slightly different from each other, especially the bands at 1676 and 1518 cm^{-1}. The first band is broad a bit in the latter like the overlapping of two bands and the second disappears in the spectrum of the former. For pycPIH, it is observed that the recrystallization in methanol can give rise to orange-yellow crystal PIH (oycPIH) and its infrared spectrum is shown in Figure 3.19. It is seen that this infrared spectrum is similar to the docPIH obtained from dopPIH synthesized by condensation reaction (method 2).

pycPIH can be obtained by crystallization of docPIH (purified from Sep-pak C-18 cartridge) in methanol, seeded with 2–3 crystals of pycPIH. The tiny and fine crystals obtained from this crystallization are pale yellow and their infrared spectra are shown in Figure 3.20 and 3.21, respectively. It is seen that these infrared spectra are similar to the pycPIH prepared by the method 1. The steps in the crystallizations of the various types of PIH are summarized as flow chart, Figure 3.22.

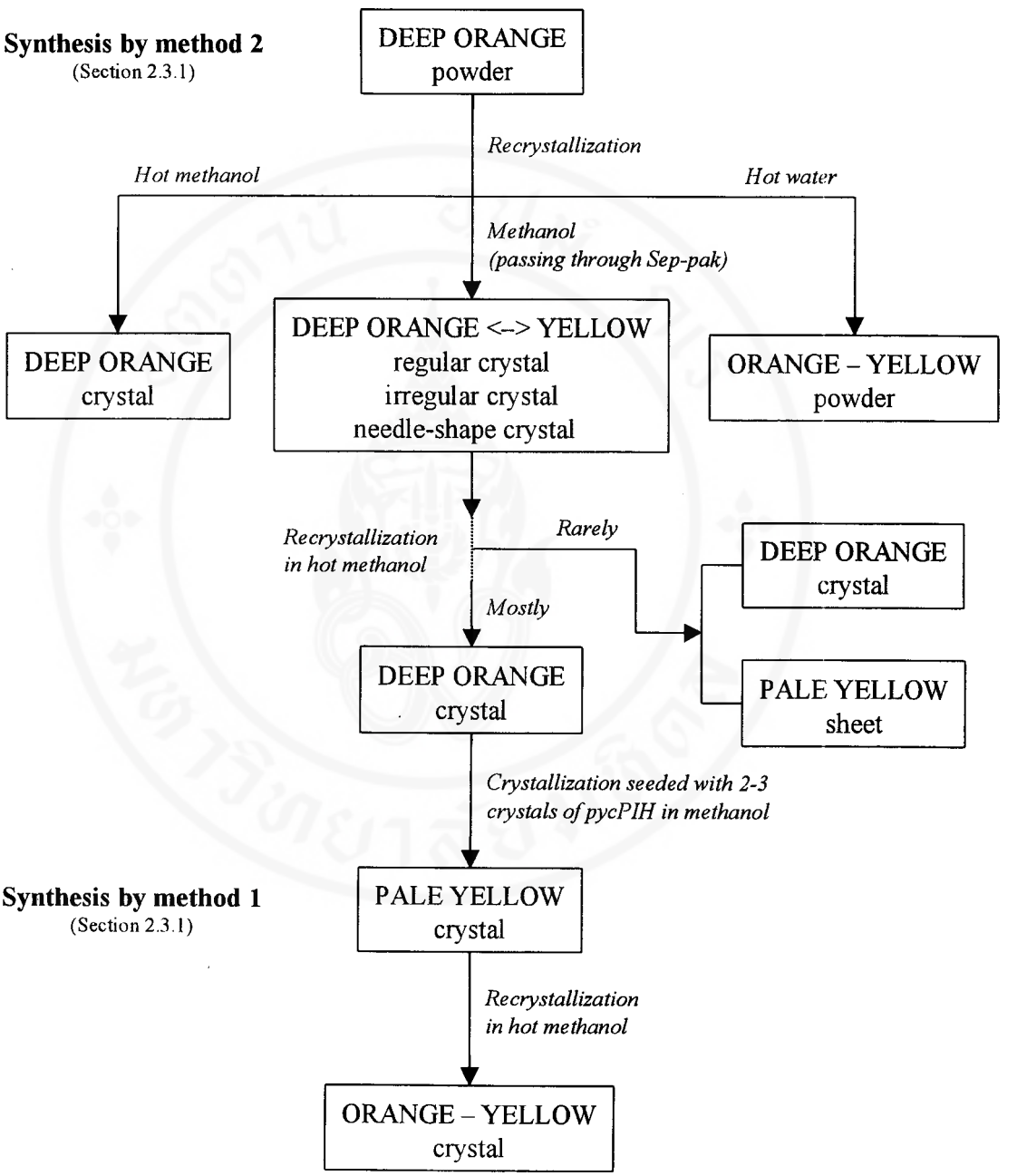

Figure 3.22 Flow chart of the crystallization steps for the various types of PIH.

Infrared spectra of the various types of PIH all show a strong band at approximately 1680 cm^{-1}, corresponding to a carbonyl absorption and assigned as the amide I band. Its position depends on the degree of hydrogen bonding and, thus, on the physical state. The amide II band absorbs in the region of 1570–1520 cm^{-1}. This band results from interaction between the N–H bending and the C–N stretching of the C–N–H group and requires a trans geometry. For the absorption bands in the 3340–3000 cm^{-1} region, these are attributed to the N–H and C–H heteroaromatic ring stretching vibrations in PIH molecule. Besides these bands, the vibrational bands corresponding to the amide III and the coupled C–O stretching and O–H bending also appear in the 1370 to 1200 cm^{-1} region of the spectra. It can be seen that these spectra are slightly different. The significant difference is the presence of medium broad bands around 2450 and 2050 cm^{-1} in the dopPIH whereas it is absent in the pycPIH. The other bands in these forms are quite similar with exception at around 1500 and 1050 cm^{-1}. Although the dopPIH was recrystallized from hot methanol or water, the infrared spectra are still different from the pycPIH in the region of 2050, 1500 and 1200–1000 cm^{-1}. The docPIH and the dopPIH, recrystallized from hot methanol as well as from hot water, not only exhibits a band at 2050 cm^{-1} but the carbonyl band is also shifted to the lower frequency, *viz* 1656 cm^{-1}. In addition, the single band at 1559 cm^{-1} in pycPIH is split into two bands at 1560 and 1515 cm^{-1} in docPIH. Another difference is the band at 1060 cm^{-1} in docPIH which corresponds to the band at about 1000 cm^{-1} for the pycPIH as shown in Figure 3.11–3.21.

Some major absorption bands for the various types of PIH along with their possible assignments are given in Table 3.4.

Table 3.4 Selected infrared bands and band assignments for the various types of PIH

Wavenumbers (cm^{-1})											Assignment
dopPIH (F3.11)	docPIH (F3.12)	oypPIH (F3.13)	docPIH (F3.14)	docPIH (F3.15)	pysPIH (F3.16)	pycPIH (F3.17)	pycPIH (F3.18)	oycPIH (F3.19)	pycPIH (F3.20)	pycPIH (F3.21)	
	3485	3484	3485	3484	3561	3445	3486	3484	3429	3429	
					3328	3330			3329	3329	
3221									3182	3183	N–H stretching
						3157			3158	3157	N–H stretching
	3079	3079	3080	3080	3078			3079			sp^2 C–H ring stretching
3036	3048	3048	3048	3048	3048	3056		3048	3055	3055	sp^2 C–H ring stretching
3000					3028	3009	3008		3008	3009	sp^2 C–H ring stretching
2927	2958	2959	2959	2959	2950	2921	2921	2959	2920	2920	sp^3 C–H stretching
2878					2882						sp^3 C–H stretching
	2833	2833	2834	2833	2830	2831	2831	2833	2831	2831	sp^3 C–H stretching
2450											$C{=}\overset{\overset{|}{H}}{N^+}{-}H$ Ammonium band
				2104							$C{-}\overset{\overset{|}{H}}{N^+}{-}H$ Immonium band
2071	2052	2052	2052	2052				2052			$C{=}\overset{\overset{|}{H}}{N^+}{-}H$ Immonium band
	2015	2014	2015	2014				2014			$C{-}\overset{\overset{|}{H}}{N^+}{-}H$ Immonium band
					1694						
1687	1656	1656	1656	1656	1677	1676	1676	1656	1676	1676	C=O stretching (amide I)
					1649	1634					C–N stretching
1602	1605	1606	1606	1606	1604	1608	1608	1606	1608	1608	C=C, C=N ring stretching (skeletal vibration)
	1582		1581		1573	1594	1594		1594	1594	C–C, C=N ring stretching (skeletal vibration)
		1562	1563	1563				1562			
1550	1553	1553	1554	1554	1554	1559	1559	1553	1559	1559	N–H in-plane bending (amide II)
	1515	1515	1515	1514			1518	1515			
1498					1491	1490	1491		1490	1490	C–C, C=N ring stretching (skeletal vibration)
1478											
1443	1431	1431	1431		1438	1446	1446	1431	1446	1446	C–C, C=N ring stretching (skeletal vibration)
1420	1421	1421	1421	1421		1414	1415	1421	1414	1414	C=C, C=N ring stretching (skeletal vibration)
1398	1397	1397	1397	1397	1403	1400	1400	1397	1400	1400	
1385	1377	1378	1377	1377	1375	1380	1380	1378	1379	1379	CH_3 in-plane bending
1362	1363	1363			1361	1366	1366	1363	1366	1366	C–N stretching (amide III)
	1350	1350	1350					1350			
	1340	1340	1340	1340		1331	1331	1340	1331	1331	
1321					1327						
1295	1294	1294	1294	1294	1306	1296	1296	1294	1296	1296	cycle-CH_2
1270	1276	1276	1276	1276	1285	1281	1281	1276	1281	1281	C–O stretching and O–H in-plane bending
	1248	1248	1248	1248		1257	1257	1248	1257	1257	C–O stretching and O–H in-plane bending
1223					1221	1226	1226		1226	1226	

Table 3.5 Selected infrared bands and band assignments for the hydrazones studied

Wavenumbers (cm^{-1})								Assignment
PBH	PSH	BIH	BBH	BSH	SIH	SBH	SSH	
3432		3449			3449	3449		
3358	3353	3352			3348	3332		
3221	3223	3198	3200	3239	3201	3271		N–H stretching
	3173		3181		3182		3187	N–H stretching
			3154	3163		3159		
3089					3081			sp^2 C–H ring stretching
3057	3050		3061	3069	3065	3058		sp^2 C–H ring stretching
				3042			3044	sp^2 C–H ring stretching
3028		3027	3029	3027		3022		sp^2 C–H ring stretching
				3004	3005			sp^2 C–H ring stretching
2968								sp^2 C–H stretching
2936								sp^3 C–H stretching
			2930	2934				
	2928							sp^3 C–H stretching
		2917			2914		2915	
				1659				
1676	1649	1693	1642	1630	1685	1674	1638	C=O stretching (amide I)
1630			1618		1625	1621	1619	C=N stretching
1596	1604	1606	1601	1611	1614	1607	1611	C=C, C=N ring stretching (skeletal vibration)
		1599						C=C, C=N ring stretching (skeletal vibration)
1587				1585				C=C, C=N ring stretching (skeletal vibration)
			1577	1577		1579	1572	C=C, C=N ring stretching (skeletal vibration)
1542	1548	1565	1553	1565	1568	1540	1557	N–H in-plane bending (amide II)
1512			1502	1509				C=C, C=N ring stretching (skeletal vibration)
1491	1489	1492	1487	1491	1491	1488	1488	C=C, C=N ring stretching (skeletal vibration)
1473	1471							CH_3 in-plane bending
		1468	1460	1457			1454	C=C, C=N ring stretching (skeletal vibration)
1450	1458	1449	1447	1448	1459	1442		C=C, C=N ring stretching (skeletal vibration)
1428	1426	1412		1412	1408	1414	1412	C=C, C=N ring stretching (skeletal vibration)
1400			1390		1393	1401		
1384	1384							CH_3 in-plane bending
				1381			1374	C–N stretching (amide III)
1366	1368							
1348	1356	1355	1365		1355	1357		C–N stretching (amide III)
1327		1330	1330		1331			
		1315	1322					
1302	1295		1305	1312			1307	
					1291	1274	1272	C–O stretching and O–H in-plane bending
		1285	1288					
					1275	1262		C–O stretching and O–H in-plane bending
1256	1257							C–O stretching and O–H in-plane bending
			1252		1243			
				1236			1231	C–O stretching and O–H in-plane bending
		1230	1229		1224	1220		
1216	1217			1216			1214	C–O stretching and O–H in-plane bending
					1209	1208		

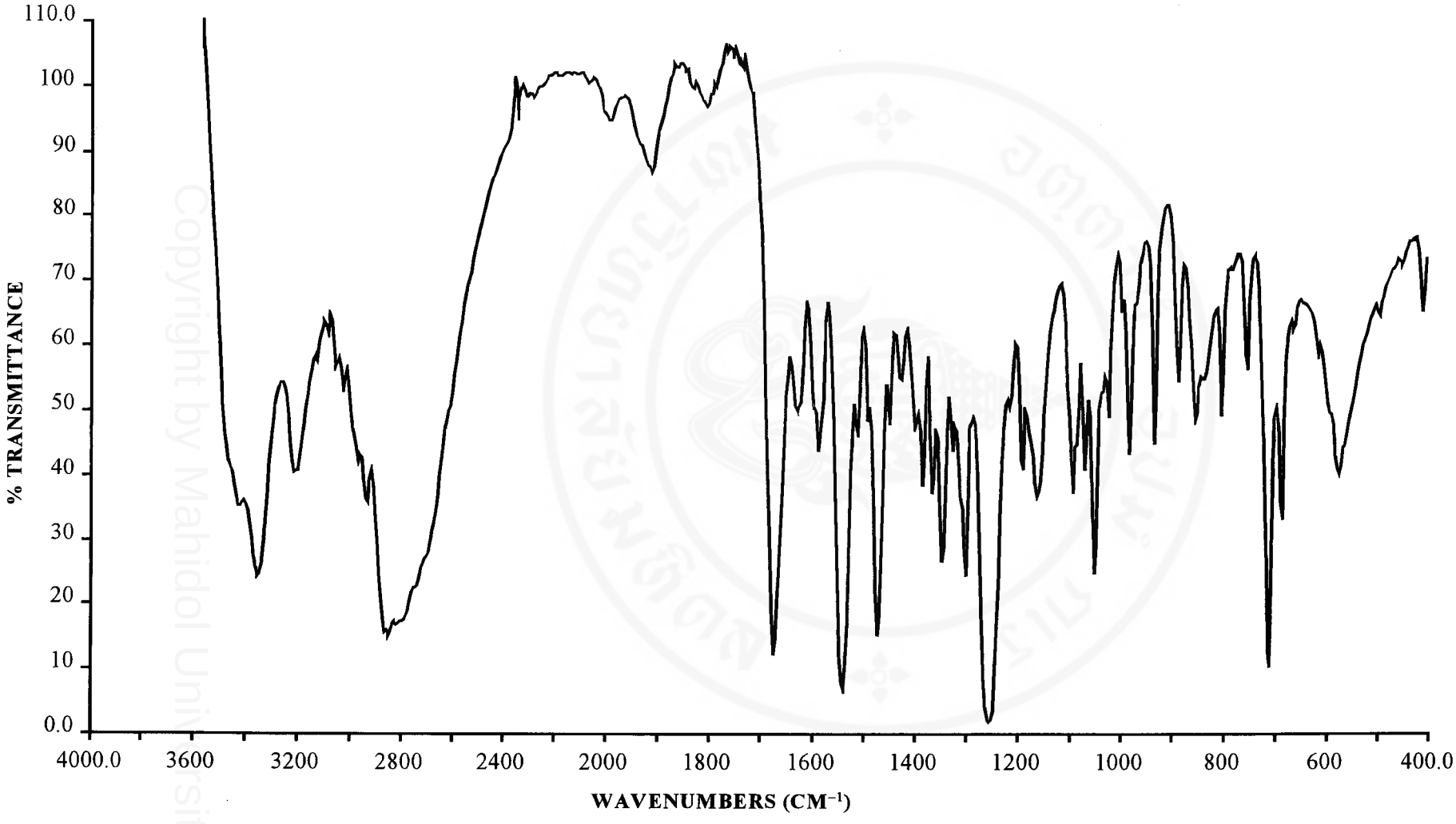

Figure 3.23 Infrared spectrum of pyridoxal benzoyl hydrazone (KBr pellet).

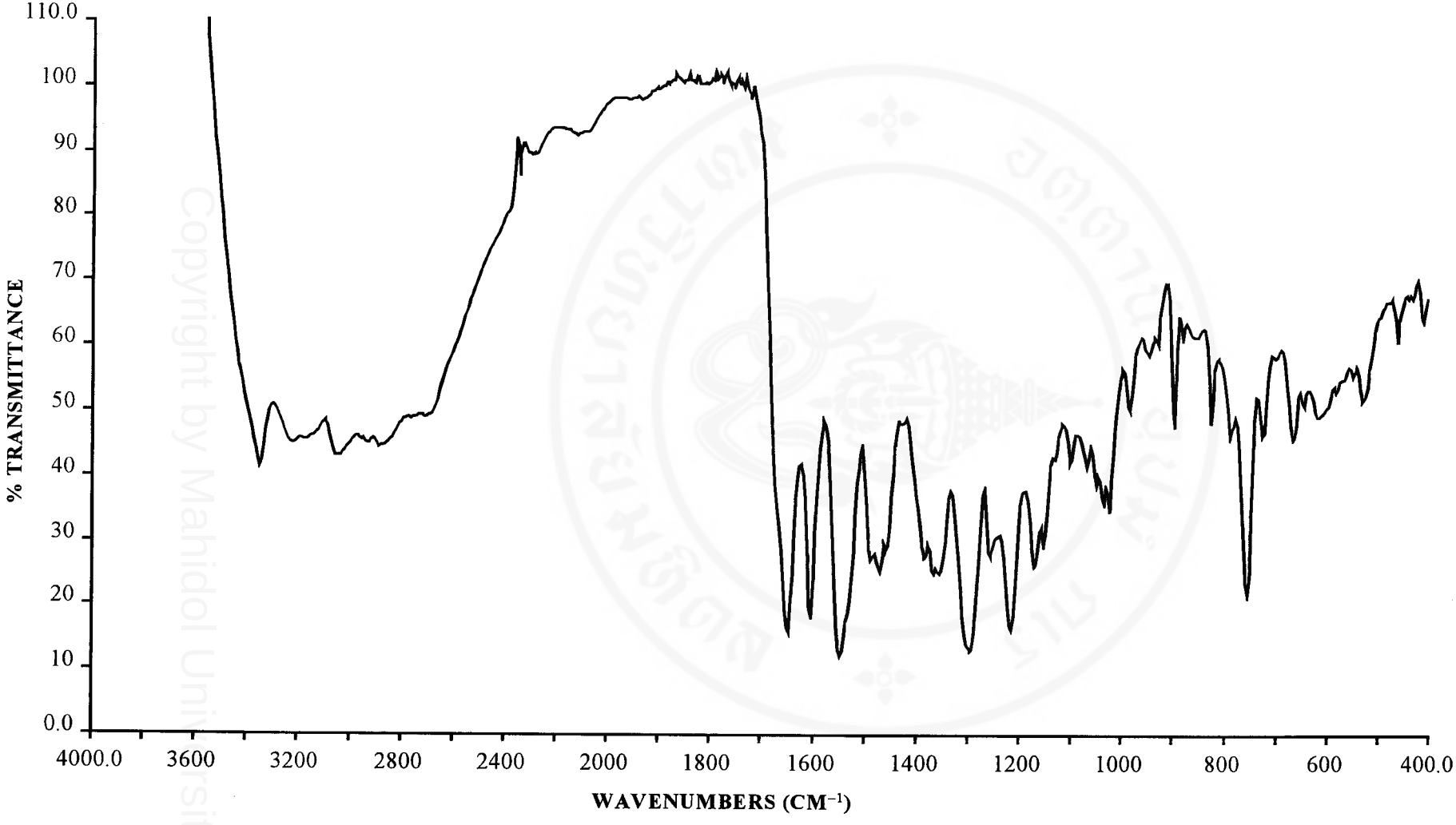

Figure 3.24 Infrared spectrum of pyridoxal salicyloyl hydrazone (KBr pellet).

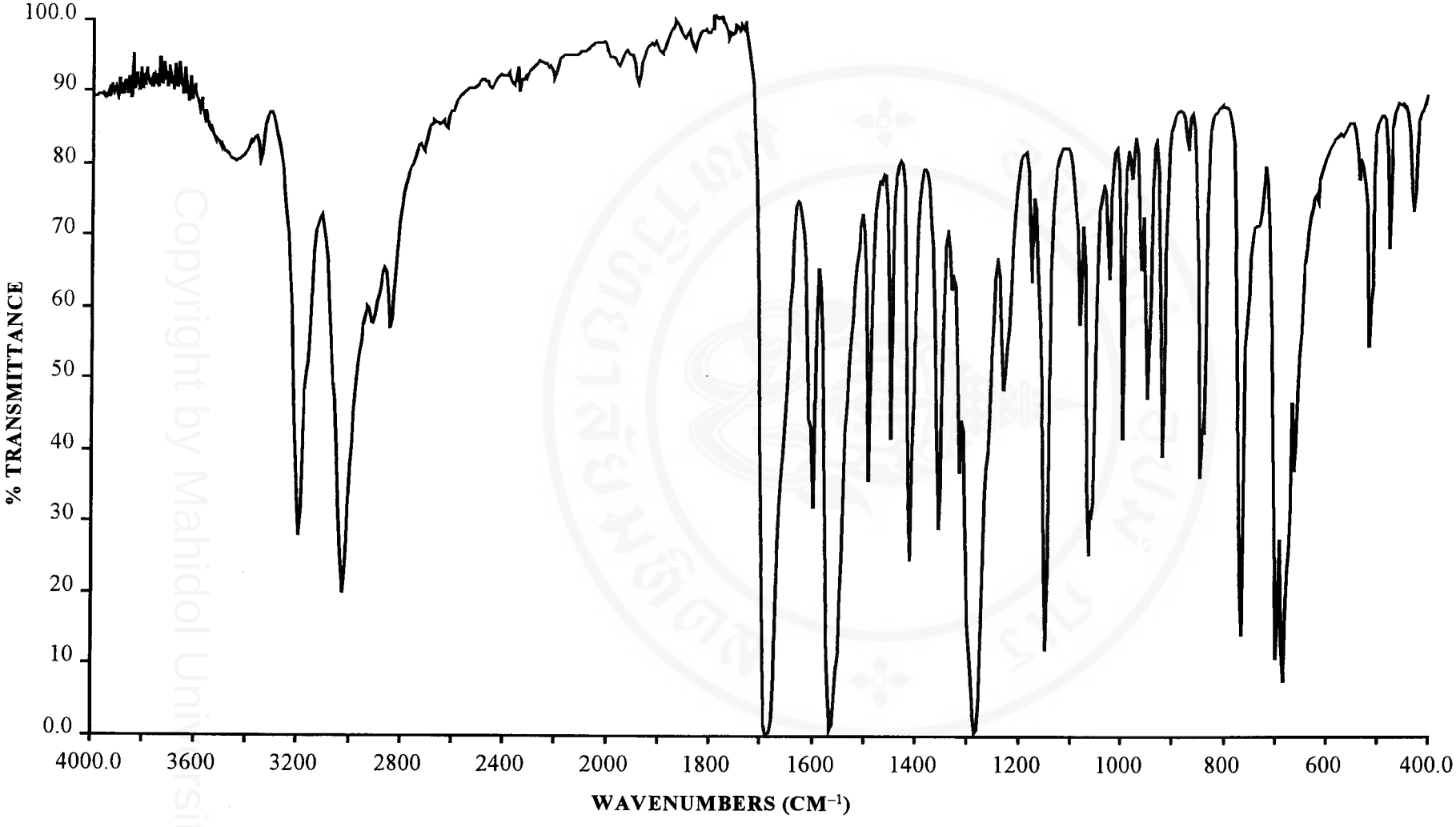

Figure 3.25 Infrared spectrum of benzaldehyde isonicotinoyl hydrazone (KBr pellet).

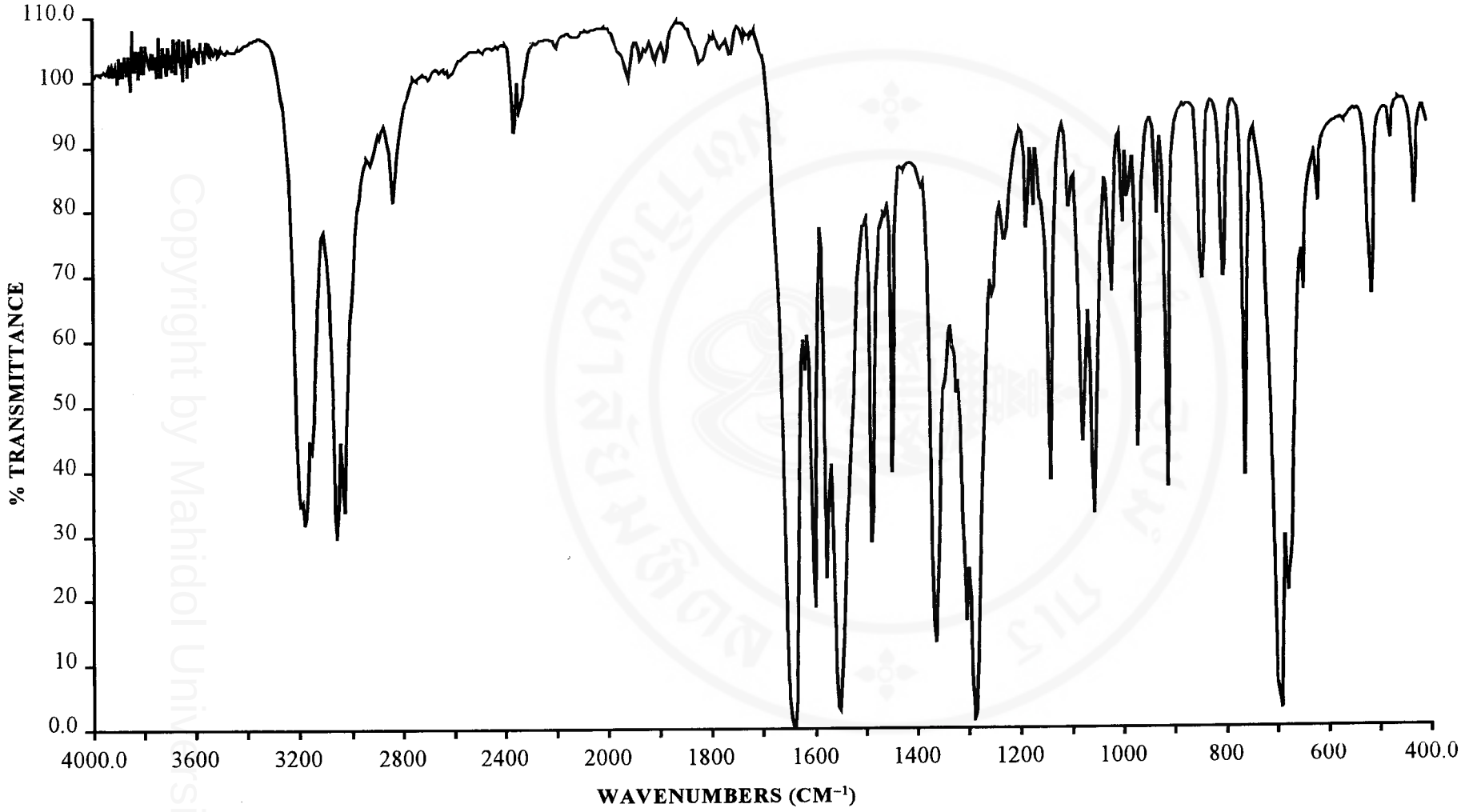

Figure 3.26 Infrared spectrum of benzaldehyde benzoyl hydrazone (KBr pellet).

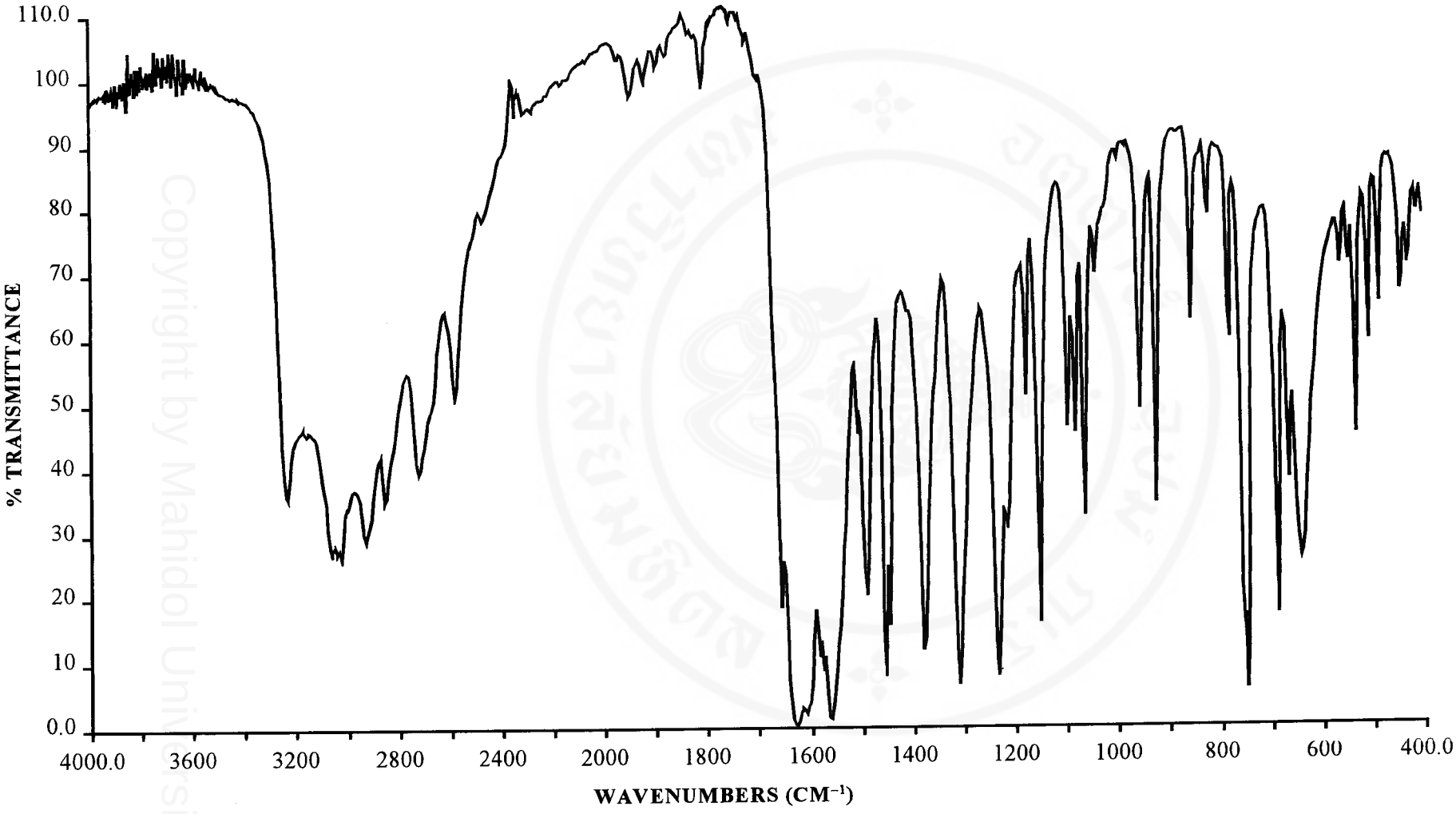

Figure 3.27 Infrared spectrum of benzaldehyde salicyloyl hydrazone (KBr pellet).

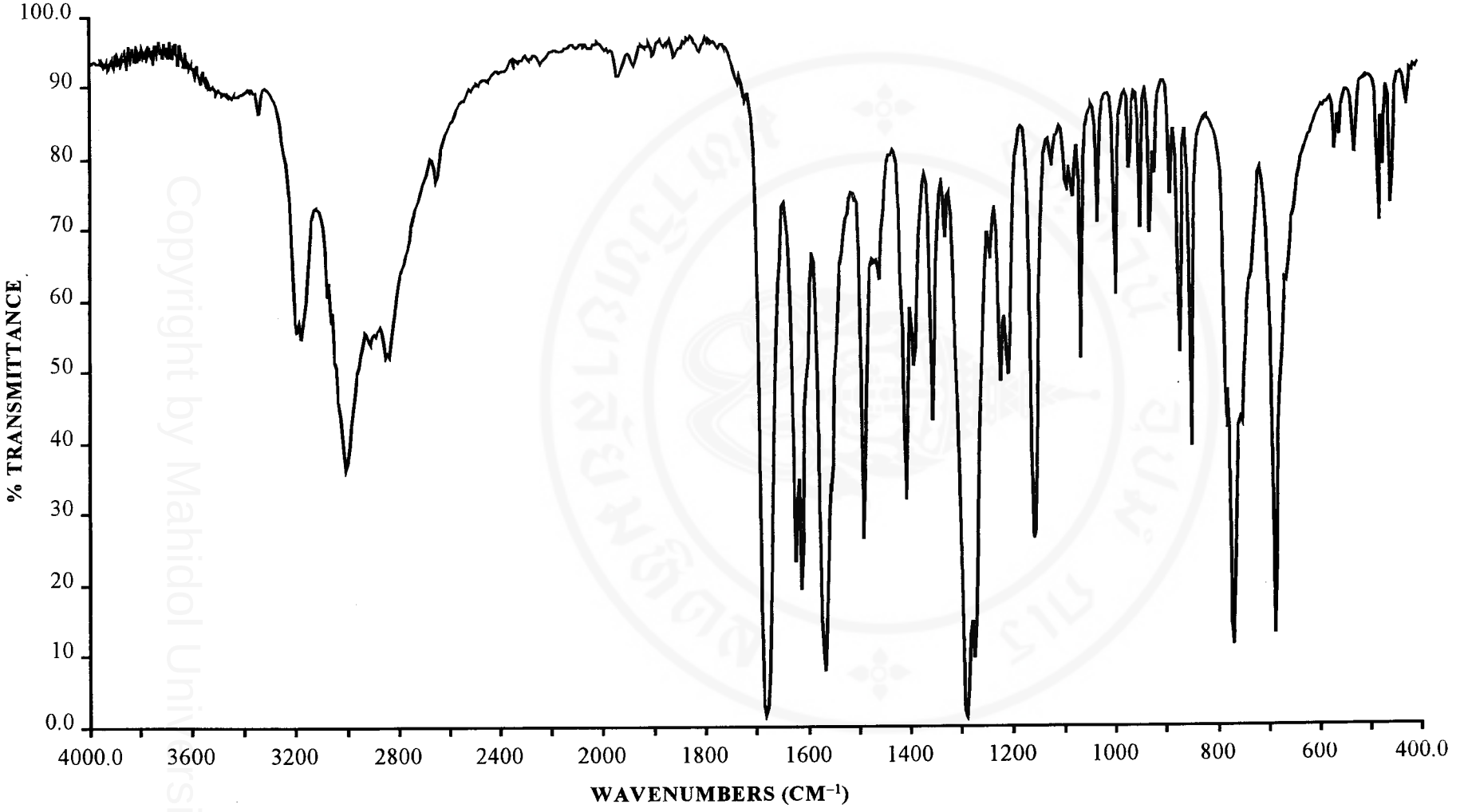

Figure 3.28 Infrared spectrum of salicylaldehyde isonicotinoyl hydrazone (KBr pellet).

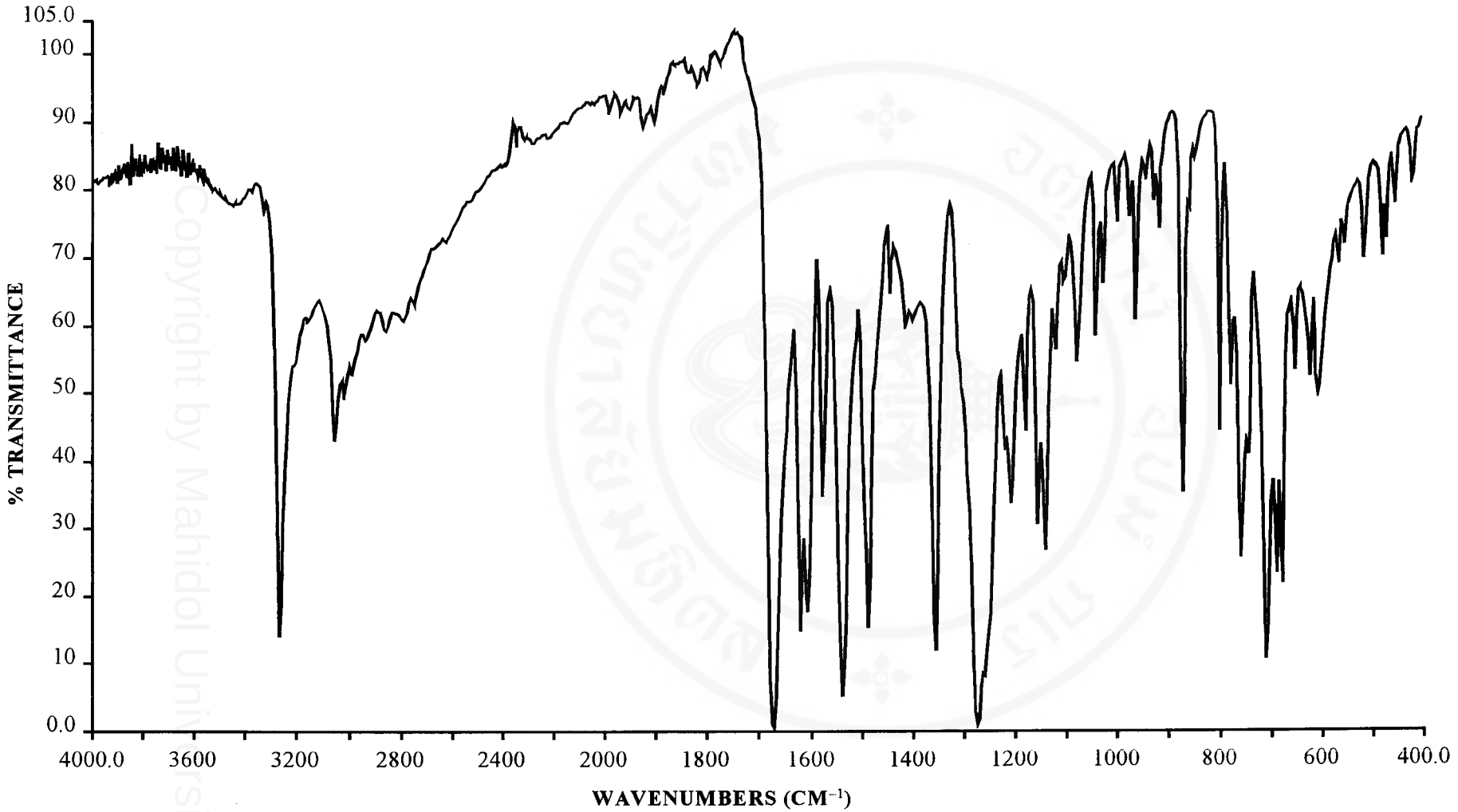

Figure 3.29 Infrared spectrum of salicylaldehyde benzoyl hydrazone (KBr pellet).

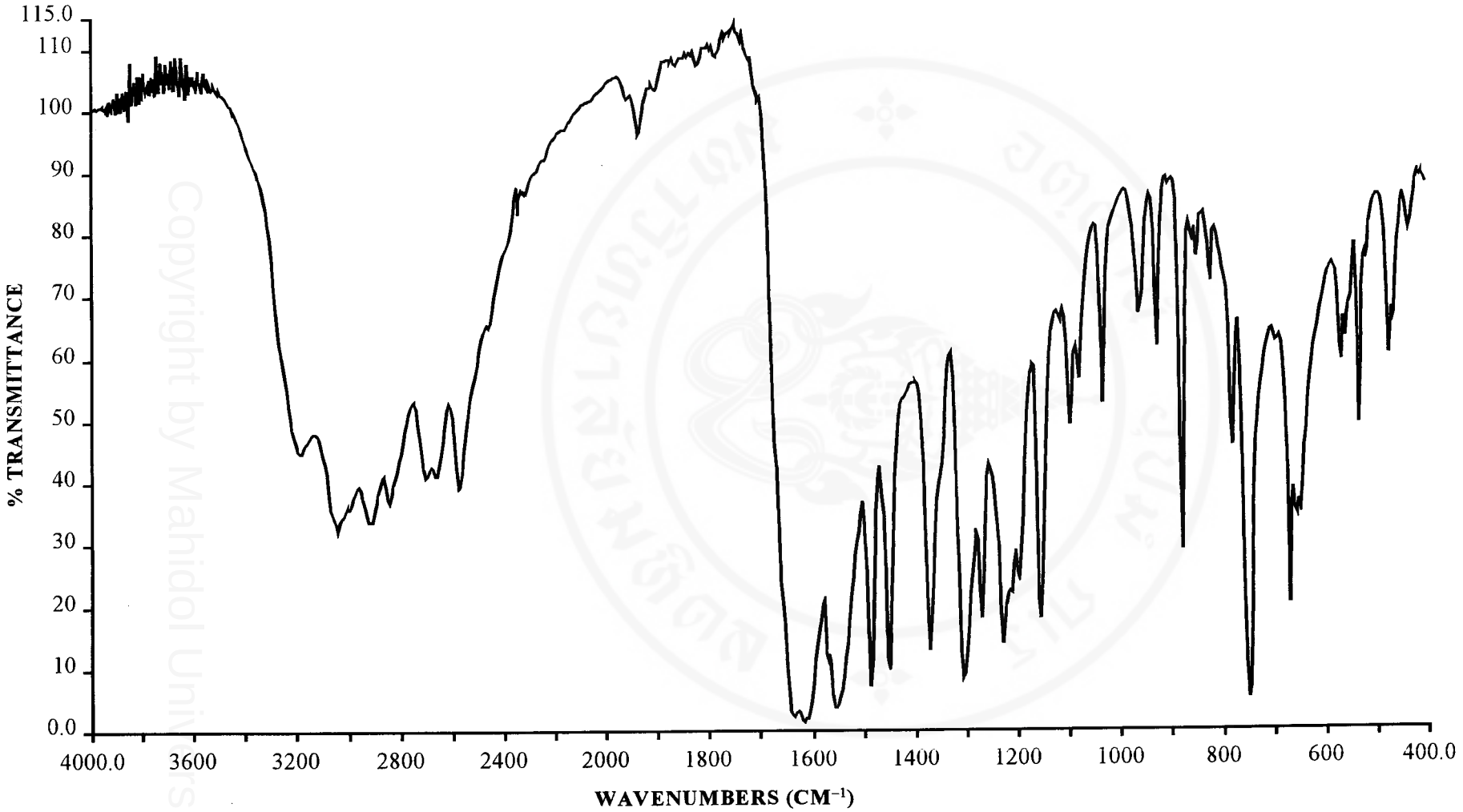

Figure 3.30 Infrared spectrum of salicylaldehyde salicyloyl hydrazone (KBr pellet).

For the other structurally related compounds, *viz* PBH, PSH, BIH, BBH, BSH, SIH, SBH and SSH, their infrared spectra are shown in Figure 3.23--3.30 and the vibrational absorption bands and band assignments are summarized in Table 3.5. These compounds show major absorption bands which are related to the absorption bands of PIH. Therefore consideration of these assignments in some detail may be helpful for prediction of the various forms of PIH in solid state.

3.5 Single-crystal X-ray crystallographic study

In this experiment, the molecular and crystal structures of PIH (both the pale yellow and deep orange crystals) and structurally related compounds were determined using a Nonius single-crystal X-ray diffractometer at ambient temperature. However, only pycPIH, SIH and SBH gave crystals suitable for X-ray diffraction studies. For the other hydrazones, attempts to recrystallize these compounds from various solvents (in which they are reasonable soluble [71]) did not give suitable crystals.

In all cases, the structures were solved by the direct method. In subsequent successive and difference electron-density maps the positions of the remaining non-hydrogen atoms were obtained. Non-hydrogen atoms were refined by full-matrix least-squares method, assuming anisotropic thermal motions. In this present refinement, the three coordinates x, y and z, and the six anisotropic thermal parameters of each atom were found. Their values are given in Table 3.7–3.9. For hydrogen atoms, difference Fourier syntheses revealed hydrogen atom sites and these were included at calculated positions on the atom to which they were attached with one overall isotropic thermal parameter (U = 0.05 Å^2). In all structures, refinements were done on F with $1/\sigma^2(F_o)$ weights. For typical pycPIH, the values of R and weighted R indices, goodness-of-fit, with maximum and average shift/e.s.d. for the final refinement cycle were 0.054, 0.054, 1.101, 0.307 and 0.016, respectively, for the 193 parameters and 1509 data for which $I > 3\sigma(I)$; $F(000)$ = 600. The function minimized was $\Sigma w(|F_o|-|F_c|)^2$ with the weight, w, being defined as $1/\sigma^2(F_o)$. The crystal data and experimental details of pycPIH, SIH and SBH are summarized in Table 3.6. The bond distances and

Table 3.6 Crystal data and experimental details

	pycPIH	SIH	SBH
Crystal data			
Empirical formula	$C_{14}H_{14}O_3N_4$	$C_{13}H_{11}O_2N_3$	$C_{14}H_{12}O_2N_2$
Chemical formula weight	286.3	241.2	240.3
Crystal form	Prismatic	Prismatic	Plate
Crystal colour	Pale yellow	White	Yellow
Crystal size/mm		0.20×0.20×0.20	0.20×0.20×0.20
Temperature/K	← Ambient temperature →		
Crystal system	Monoclinic	Monoclinic	Monoclinic
Space group	$P2_1/n$	$P2_1/n$	$P2_1/n$
Unit-cell dimensions			
a/Å	8.155	8.146	8.143
b/Å	13.005	15.553	15.547
c/Å	13.029	9.573	9.578
α/degrees	90.00	90.02	90.04
β/degrees	90.00	105.76	105.77
γ/degrees	90.00	89.99	89.96
Cell volume/Å^3	1381.8	1167.3	1167.0
Z	4	4	4
Density (obs.)/g cm^{-3}	1.30	1.30	1.30
Density (cal.)/g cm^{-3}	1.37	1.37	1.37
Linear-absorption coefficient/cm^{-1}	1.00	0.96	0.93
F(000)	600	504	504
Radiation type	Mo*Kα*	Mo*Kα*	Mo*Kα*
Wavelength/Å	0.70930	0.70930	0.70930
Data collection			
Diffractometer	← Nonius FR 591 Mach 3 →		
Data collection method	*ω*–2*θ* scans	*ω*–2*θ* scans	*ω*–2*θ* scans

Table 3.6 (continued)

	pycPIH	SIH	SBH
Absorption correction	None	None	None
Extinction correction	None	None	None
No. of measured reflections	7631	4263	3505
No. of independent reflections	2429	1878	1541
θ range/degrees	1.56–24.96	1.31–24.91	1.31–22.89
Range of h, k and l	$-9 \le h \le 9$	$-9 \le h \le 9$	$-8 \le h \le 8$
	$-15 \le k \le 15$	$-18 \le k \le 18$	$-17 \le k \le 17$
	$-15 \le l \le 15$	$-11 \le l \le 11$	$-10 \le l \le 10$
Refinement			
Refinement method	Full-matrix least-squares of F		
***R* indices (all data)**			
R [$R=\Sigma\|\|F_o\|-\|F_c\|\|/\Sigma\|F_o\|$]	0.097	0.078	0.090
wR [$wR=[\Sigma w(F_o-F_c)^2/\Sigma wF_o^2]^{1/2}$]	0.081	0.086	0.099
$wR(F^2)$ [$wR(F^2)=[\Sigma w(F_o^2-F_c^2)^2/\Sigma w(F_o^2)^2]^{1/2}$]	0.053	0.236	
Final *R* indices [$I > 3\sigma(I)$]			
R [$R=\Sigma\|\|F_o\|-\|F_c\|\|/\Sigma\|F_o\|$]	0.054	0.065	0.079
wR [$wR=[\Sigma w(F_o-F_c)^2/\Sigma wF_o^2]^{1/2}$]	0.054	0.081	0.095
$wR(F^2)$ [$wR(F^2)=[\Sigma w(F_o^2-F_c^2)^2/\Sigma w(F_o^2)^2]^{1/2}$]	0.053	0.236	
Goodness-of-fit [GOF=$\Sigma w(F_o-F_c)^2/(n-m)$]	1.101	1.358	1.715
No. of reflections used in refinement	1509	1556	1325
No. of parameters refined	193	163	164
No. of matrix elements	18721	13366	13530
Least-squares weight	$1/\sigma^2(F_o)$	$1/\sigma^2(F_o)$	$1/\sigma^2(F_o)$
$(\Delta/\sigma)_{max}$	0.307	0.159	0.200
$(\Delta/\sigma)_{av}$	0.016	0.026	0.005
Extinction coefficient	0.000	0.000	0.000

Table 3.7 Final atomic coordinates and anisotropic mean-square displacement parameters ($Å^2$) for non-hydrogen atoms of pycPIH

Atom	x	y	z	U_{11}	U_{22}	U_{33}	U_{12}	U_{13}	U_{23}
O(1)	0.5825(3)	0.0989(2)	0.1162(2)	0.038(1)	0.043(1)	0.053(1)	−0.00004(143)	0.012(1)	0.012(1)
O(2)	−0.1027(3)	−0.2177(2)	0.0520(2)	0.043(1)	0.052(1)	0.042(1)	−0.012(1)	0.016(1)	−0.014(1)
N(3)	0.1120(3)	−0.0689(2)	0.0738(2)	0.031(1)	0.028(1)	0.035(1)	0.00014(151)	−0.001(1)	−0.002(1)
N(4)	0.1260(3)	−0.1369(2)	−0.0065(2)	0.031(1)	0.028(1)	0.032(1)	−0.001(1)	−0.002(1)	−0.010(1)
O(5)	−0.0339(3)	−0.0150(2)	0.2371(2)	0.036(1)	0.054(2)	0.056(2)	−0.012(1)	0.015(1)	−0.008(1)
N(6)	0.0569(4)	−0.4496(2)	−0.2354(2)	0.042(2)	0.038(2)	0.045(2)	−0.003(1)	0.002(1)	−0.015(1)
C(7)	0.2063(4)	0.0710(2)	0.1718(2)	0.030(2)	0.027(2)	0.034(2)	0.004(1)	−0.004(1)	0.00002(176)
C(8)	0.1298(4)	−0.2818(3)	−0.1766(3)	0.030(2)	0.034(2)	0.043(2)	−0.004(1)	0.002(1)	−0.00091(195)
C(9)	0.2205(4)	0.0010(3)	0.0842(2)	0.028(2)	0.031(2)	0.034(2)	0.000(1)	0.001(1)	−0.002(1)
C(10)	0.0825(4)	0.0589(3)	0.2447(3)	0.033(2)	0.033(2)	0.040(2)	0.004(1)	0.003(1)	−0.002(1)
N(11)	0.1817(6)	0.1989(3)	0.3413(3)	0.070(2)	0.048(2)	0.045(2)	0.008(2)	−0.005(2)	−0.020(2)
C(12)	0.3179(4)	0.1523(3)	0.1860(3)	0.035(2)	0.028(2)	0.043(2)	−0.00032(177)	−0.010(1)	−0.00038(194)
C(13)	0.0337(4)	−0.2930(3)	−0.0896(2)	0.025(1)	0.031(2)	0.032(2)	−0.00075(167)	−0.00041(158)	−0.002(1)
C(14)	0.0109(4)	−0.2127(3)	−0.0083(2)	0.032(2)	0.034(2)	0.031(2)	0.003(1)	−0.00055(172)	−0.003(1)
C(15)	0.0749(5)	0.1240(3)	0.3294(3)	0.049(2)	0.041(2)	0.041(2)	0.006(2)	0.001(2)	−0.008(2)
C(16)	−0.0496(5)	−0.3846(3)	−0.0781(3)	0.044(2)	0.043(2)	0.039(2)	−0.010(2)	0.009(1)	−0.006(2)
C(17)	0.4550(5)	0.1733(3)	0.1127(3)	0.041(2)	0.034(2)	0.050(2)	−0.007(1)	−0.003(2)	0.008(2)
C(18)	−0.0329(5)	−0.4606(3)	−0.1514(3)	0.051(2)	0.035(2)	0.048(2)	−0.013(2)	0.007(2)	−0.008(2)
C(19)	0.1356(4)	−0.3610(3)	−0.247(3)	0.033(2)	0.045(2)	0.039(2)	−0.00020(203)	0.007(1)	−0.008(2)
C(20)	0.3004(5)	0.2126(3)	0.2718(3)	0.048(2)	0.034(2)	0.055(2)	−0.005(2)	−0.009(2)	−0.009(2)
C(21)	−0.0573(6)	0.1121(4)	0.4077(4)	0.074(3)	0.067(3)	0.059(3)	0.008(3)	0.024(2)	−0.014(2)

Table 3.8 Final atomic coordinates and anisotropic mean-square displacement parameters ($Å^2$) for non-hydrogen atoms of SIH

Atom	x	y	z	U_{11}	U_{22}	U_{33}	U_{12}	U_{13}	U_{23}
O(1)	0.5724(4)	0.1425(2)	0.1783(3)	0.039(2)	0.038(1)	0.047(2)	−0.013(1)	0.00062(164)	−0.002(1)
O(2)	0.7982(4)	0.0195(2)	0.5292(4)	0.051(2)	0.034(2)	0.053(2)	−0.010(1)	−0.013(1)	0.008(1)
N(3)	0.5912(4)	−0.0692(2)	0.3948(3)	0.036(2)	0.031(2)	0.024(1)	0.005(1)	−0.002(1)	0.005(1)
N(4)	0.5366(4)	−0.0047(2)	0.2931(3)	0.035(2)	0.029(2)	0.028(2)	0.006(1)	0.002(1)	0.002(1)
N(5)	0.9205(4)	−0.2588(2)	0.8039(4)	0.037(2)	0.032(2)	0.032(2)	0.004(1)	−0.00051(178)	0.003(1)
C(6)	0.7899(5)	−0.1251(2)	0.6102(4)	0.032(2)	0.029(2)	0.021(2)	0.003(2)	0.00027(192)	−0.003(1)
C(7)	0.3459(5)	0.0427(2)	0.0736(4)	0.030(2)	0.027(2)	0.026(2)	0.004(1)	0.004(1)	0.00068(193)
C(8)	0.4280(6)	0.1222(3)	0.0732(5)	0.036(2)	0.030(2)	0.036(2)	0.001(2)	0.011(2)	−0.00027(214)
C(9)	0.9612(6)	−0.1260(3)	0.6897(5)	0.033(2)	0.031(2)	0.036(2)	−0.004(2)	0.00066(219)	−0.002(2)
C(10)	0.4084(5)	−0.0214(2)	0.1856(5)	0.036(2)	0.026(2)	0.033(2)	0.00060(204)	0.005(2)	0.001(2)
C(11)	0.7566(6)	−0.2562(3)	0.7277(5)	0.036(2)	0.034(2)	0.034(2)	−0.004(2)	0.006(2)	0.002(2)
C(12)	0.6862(5)	−0.1919(3)	0.6310(4)	0.027(2)	0.038(2)	0.028(2)	−0.001(2)	0.00047(194)	−0.001(2)
C(13)	0.1990(6)	0.0252(3)	−0.0398(5)	0.037(2)	0.033(2)	0.036(2)	0.00024(217)	0.001(2)	−0.001(2)
C(14)	1.0184(6)	−0.1936(3)	0.7840(5)	0.030(2)	0.038(2)	0.036(2)	0.003(2)	−0.006(2)	−0.00063(227)
C(15)	0.1342(6)	0.0845(3)	−0.1479(5)	0.041(2)	0.049(3)	0.036(2)	0.013(2)	−0.004(2)	0.003(2)
C(16)	0.3602(7)	0.1817(3)	−0.0352(5)	0.059(3)	0.031(2)	0.045(3)	−0.001(2)	0.015(2)	0.007(2)
C(17)	0.7290(6)	−0.0504(3)	0.5092(5)	0.034(2)	0.032(2)	0.031(2)	0.005(2)	0.003(2)	0.003(2)
C(18)	0.2150(7)	0.1628(3)	−0.1441(5)	0.059(3)	0.042(3)	0.040(3)	0.019(2)	0.008(2)	0.015(2)

Table 3.9 Final atomic coordinates and anisotropic mean-square displacement parameters ($Å^2$) for non-hydrogen atoms of SBH

Atom	x	y	z	U_{11}	U_{22}	U_{33}	U_{12}	U_{13}	U_{23}
O(1)	1.0726(5)	0.1424(2)	0.1781(5)	0.038(2)	0.037(2)	0.049(3)	−0.013(2)	−0.00006(240)	−0.002(2)
O(2)	1.2984(6)	0.0195(2)	0.5293(5)	0.051(3)	0.032(2)	0.056(3)	−0.010(2)	−0.016(2)	0.007(2)
N(3)	1.0914(6)	−0.0691(3)	0.3947(5)	0.034(3)	0.031(2)	0.025(2)	0.004(2)	−0.005(2)	0.005(2)
N(4)	1.0366(6)	−0.0048(3)	0.2933(5)	0.035(3)	0.027(2)	0.027(3)	0.005(2)	−0.00007(258)	0.002(2)
C(5)	1.4199(6)	−0.2583(3)	0.8035(5)	0.017(3)	0.014(2)	0.017(2)	0.003(2)	−0.006(2)	0.005(2)
C(6)	1.2899(7)	−0.1250(3)	0.6103(6)	0.032(3)	0.027(3)	0.022(3)	0.002(2)	−0.00038(276)	−0.003(2)
C(7)	0.8457(7)	0.0426(3)	0.0735(6)	0.029(3)	0.025(3)	0.026(3)	0.004(2)	0.003(2)	0.001(2)
C(8)	0.9281(8)	0.1223(4)	0.0730(6)	0.037(3)	0.030(3)	0.035(3)	0.00076(296)	0.009(3)	0.00098(296)
C(9)	1.4615(8)	−0.1260(4)	0.6898(6)	0.032(3)	0.033(3)	0.037(3)	−0.003(2)	−0.002(3)	−0.003(3)
C(10)	1.2576(8)	−0.2563(4)	0.7286(6)	0.045(4)	0.031(3)	0.036(3)	−0.004(3)	0.011(3)	0.002(3)
C(11)	0.6992(8)	0.0251(4)	−0.0396(7)	0.037(3)	0.032(3)	0.038(3)	0.002(2)	0.002(3)	−0.00076(304)
C(12)	1.1857(7)	−0.1919(4)	0.6310(6)	0.028(3)	0.035(3)	0.028(3)	−0.001(2)	0.002(2)	−0.001(2)
C(13)	0.9084(7)	−0.0215(3)	0.1859(6)	0.036(3)	0.024(3)	0.033(3)	0.001(2)	0.003(3)	0.00064(280)
C(14)	1.5178(8)	−0.1944(4)	0.7844(7)	0.032(3)	0.043(4)	0.033(3)	0.010(3)	−0.008(3)	−0.003(3)
C(15)	0.6342(8)	0.0844(4)	−0.1483(7)	0.041(4)	0.046(4)	0.035(3)	0.010(3)	−0.005(3)	0.004(3)
C(16)	0.7154(9)	0.1629(4)	−0.1442(7)	0.059(4)	0.042(4)	0.039(4)	0.019(3)	0.006(3)	0.015(3)
C(17)	0.8606(9)	0.1819(4)	−0.0352(7)	0.059(4)	0.031(3)	0.043(4)	−0.002(3)	0.015(3)	0.008(3)
C(18)	1.2293(8)	−0.0502(4)	0.5097(6)	0.035(3)	0.034(3)	0.032(3)	0.006(3)	0.002(3)	0.002(2)

bond angles are given in Table 3.10 and 3.11 along with the molecular structures shown in Figure 3.31–3.33.

Table 3.10 Bond distances for some hydrazones studied

pycPIH	Bond Lengths (Å)	SIH	Bond Lengths (Å)	SBH	Bond Lengths (Å)
O(1)–C(17)	1.44	O(1)–C(8)	1.36	O(1)–C(8)	1.37
O(2)–C(14)	1.22	O(2)–C(17)	1.23	O(2)–C(18)	1.23
N(3)–N(4)	1.38	N(3)–N(4)	1.38	N(3)–N(4)	1.38
N(3)–C(9)	1.29	N(3)–C(17)	1.36	N(3)–C(18)	1.36
N(4)–C(14)	1.36	N(4)–C(10)	1.29	N(4)–C(13)	1.29
O(5)–C(10)	1.35	N(5)–C(11)	1.34	N(5)–C(10)	1.34
N(6)–C(18)	1.34	N(5)–C(14)	1.34	N(5)–C(14)	1.33
N(6)–C(19)	1.33	C(6)–C(9)	1.42	C(6)–C(9)	1.41
C(7)–C(9)	1.46	C(6)–C(12)	1.40	C(6)–C(12)	1.41
C(7)–C(10)	1.41	C(6)–C(17)	1.50	C(6)–C(18)	1.49
C(7)–C(12)	1.41	C(7)–C(8)	1.40	C(7)–C(8)	1.40
C(8)–C(13)	1.38	C(7)–C(10)	1.46	C(7)–C(11)	1.42
C(8)–C(19)	1.39	C(7)–C(13)	1.42	C(7)–C(13)	1.47
C(10)–C(15)	1.40	C(8)–C(16)	1.39	C(8)–C(17)	1.39
N(11)–C(15)	1.30	C(9)–C(14)	1.40	C(9)–C(14)	1.41
N(11)–C(20)	1.33	C(11)–C(12)	1.40	C(10)–C(12)	1.40
C(12)–C(17)	1.51	C(13)–C(15)	1.39	C(11)–C(15)	1.39
C(12)–C(20)	1.38	C(15)–C(18)	1.40	C(15)–C(16)	1.41
C(13)–C(14)	1.50	C(16)–C(18)	1.40	C(16)–C(17)	1.39
C(13)–C(16)	1.39				
C(15)–C(21)	1.50				
C(16)–C(18)	1.40				

Table 3.11 Bond angles for some hydrazones studied

pycPIH	Bond angles (degrees)	SIH	Bond angles (degrees)	SBH	Bond angles (degrees)
N(4)–N(3)–C(9)	119.1	N(4)–N(3)–C(17)	116.8	N(4)–N(3)–C(18)	117.2
N(3)–N(4)–C(14)	115.9	N(3)–N(4)–C(10)	116.2	N(3)–N(4)–C(13)	116.3
C(18)–N(6)–C(19)	118.2	C(11)–N(5)–C(14)	118.2	C(10)–C(5)–C(14)	118.4
C(9)–C(7)–C(10)	121.7	C(9)–C(6)–C(12)	119.0	C(9)–C(6)–C(12)	118.9
C(9)–C(7)–C(12)	120.9	C(9)–C(6)–C(17)	117.3	C(9)–C(6)–C(18)	117.6
C(10)–C(7)–C(12)	117.4	C(12)–C(6)–C(17)	123.7	C(12)–C(6)–C(18)	123.5
C(13)–C(8)–C(19)	118.8	C(8)–C(7)–C(10)	123.6	C(8)–C(7)–C(11)	118.3
N(3)–C(9)–C(7)	117.1	C(8)–C(7)–C(13)	118.3	C(8)–C(7)–C(13)	123.6
O(5)–C(10)–C(7)	122.6	C(10)–C(7)–C(13)	118.1	C(11)–C(7)–C(13)	118.0
O(5)–C(10)–C(15)	118.5	O(1)–C(8)–C(7)	120.9	O(1)–C(8)–C(7)	120.7
C(7)–C(10)–C(15)	118.9	O(1)–C(8)–C(16)	118.5	O(1)–C(8)–C(17)	118.7
C(15)–N(11)–C(20)	119.0	C(7)–C(8)–C(16)	120.6	C(7)–C(8)–C(17)	120.6
C(7)–C(12)–C(17)	122.4	C(6)–C(9)–C(14)	117.3	C(6)–C(9)–C(14)	117.1
C(7)–C(12)–C(20)	117.8	N(4)–C(10)–C(7)	118.3	C(5)–C(10)–C(12)	123.1
C(17)–C(12)–C(20)	119.8	N(5)–C(11)–C(12)	123.1	C(7)–C(11)–C(15)	121.3
C(8)–C(13)–C(14)	124.9	C(6)–C(12)–C(11)	118.6	C(6)–C(12)–C(10)	118.3
C(8)–C(13)–C(16)	118.5	C(7)–C(13)–C(15)	121.1	N(4)–C(13)–C(7)	118.2
C(14)–C(13)–C(16)	116.6	N(5)–C(14)–C(9)	123.7	C(5)–C(14)–C(9)	124.2
O(2)–C(14)–N(4)	122.9	C(13)–C(15)–C(18)	119.5	C(11)–C(15)–C(16)	119.3
O(2)–C(14)–C(13)	121.3	C(8)–C(16)–C(18)	120.3	C(15)–C(16)–C(17)	119.9
N(4)–C(14)–C(13)	115.8	O(2)–C(17)–N(3)	123.8	C(8)–C(17)–C(16)	120.7
C(10)–C(15)–N(11)	122.8	O(2)–C(17)–C(6)	121.9	O(2)–C(18)–N(3)	123.2
C(10)–C(15)–C(21)	119.1	N(3)–C(17)–C(6)	114.3	O(2)–C(18)–C(6)	122.1
N(11)–C(15)–C(21)	118.1	C(15)–C(18)–C(16)	120.2	N(3)–C(18)–C(6)	114.7
C(13)–C(16)–C(18)	118.9				
O(1)–C(17)–C(12)	112.4				
N(6)–C(18)–C(16)	122.4				
N(6)–C(19)–C(8)	123.2				
N(11)–C(20)–C(12)	124.1				

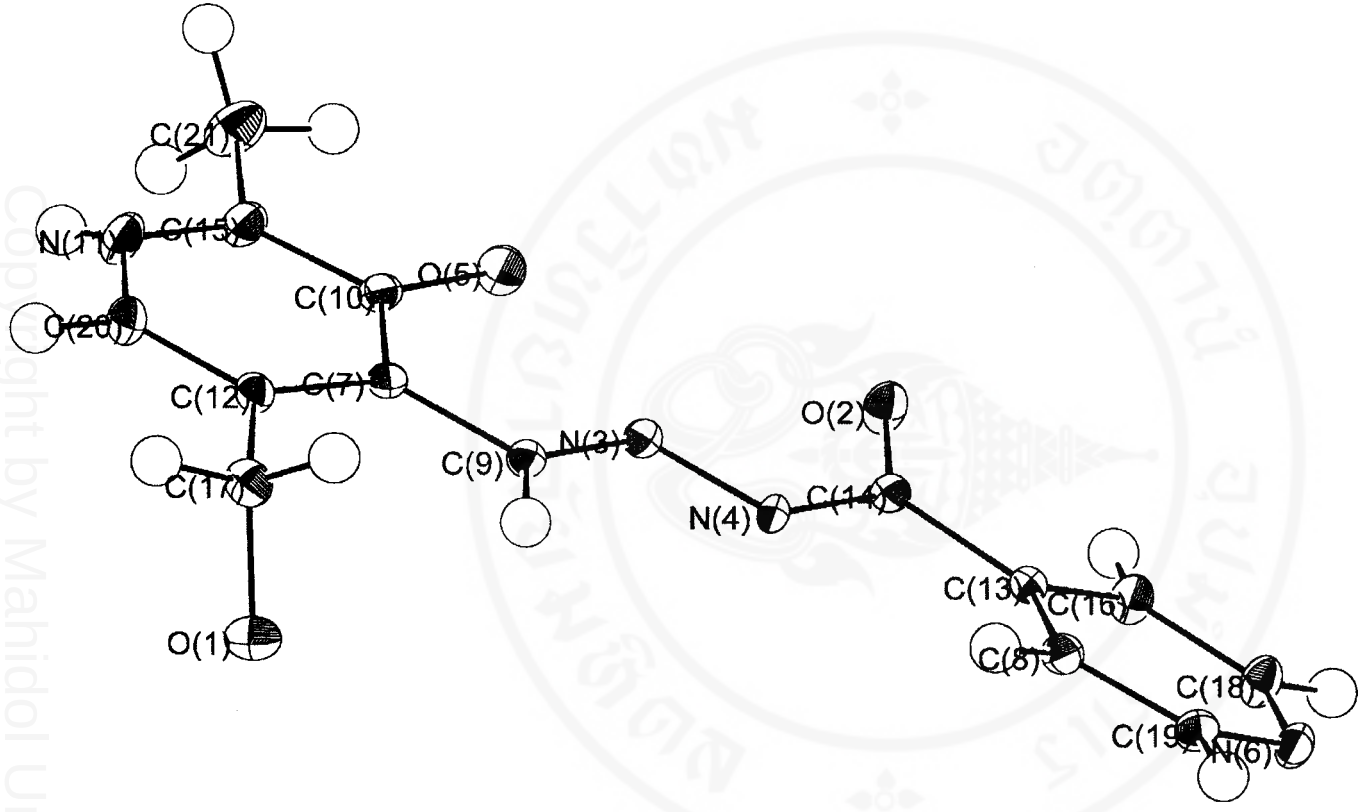

Figure 3.31 ORTEP drawing of PIH showing the atom numbering scheme. The thermal ellipsoids are drawn at 50% probability level and the hydrogen atoms are drawn as spheres. Numbers of hydrogen atoms are omitted for clarity.

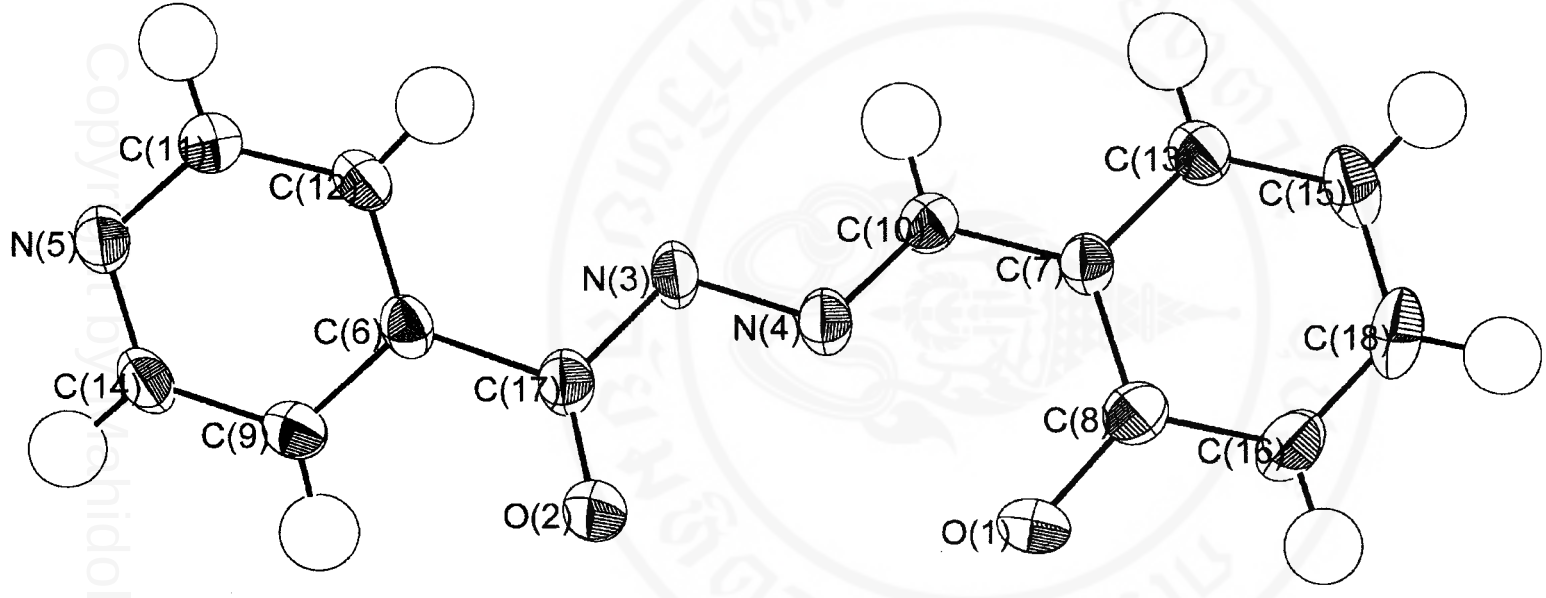

Figure 3.32 ORTEP drawing of SIH showing the atom numbering scheme. The thermal ellipsoids are drawn at 50% probability level and the hydrogen atoms are drawn as spheres. Numbers of hydrogen atoms are omitted for clarity.

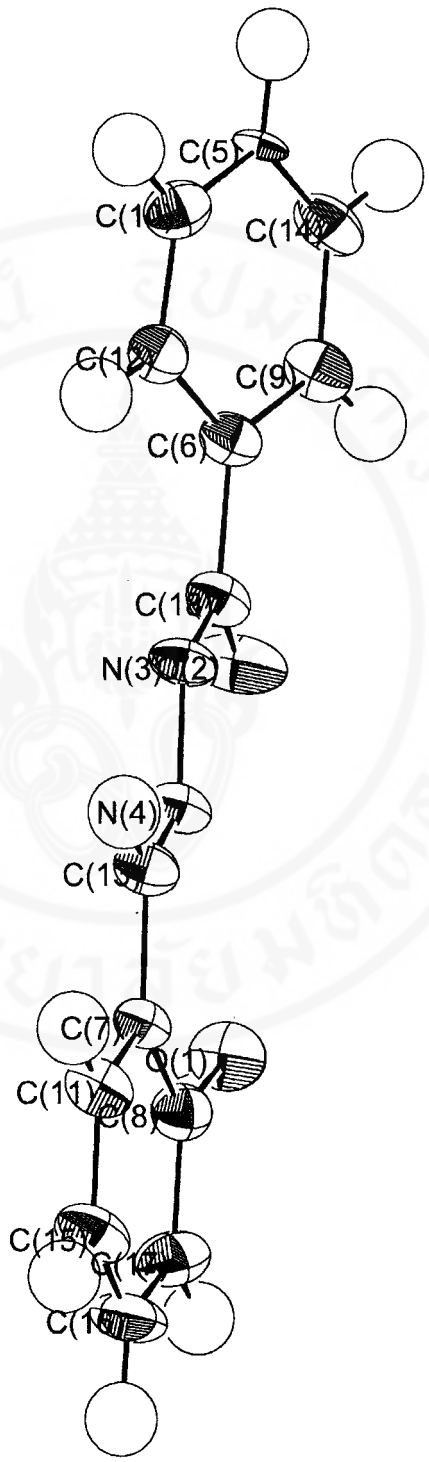

Figure 3.33 ORTEP drawing of SBH showing the atom numbering scheme. The thermal ellipsoids are drawn at 50% probability level and the hydrogen atoms are drawn as spheres. Numbers of hydrogen atoms are omitted for clarity.

3.6 Kinetic studies of PIH and related compounds

In this section, the results of studies of the rates of the cis-trans isomerization reactions of PIH and other structurally related compounds *viz* PBH, PSH, BIH, BBH, BSH, SIH, SBH and SSH in methanolic solutions at temperature 25.0, 30.0, 35.0 and 40.0 °C are reported.

The cis to trans geometrical isomerization is the reverse reaction of the photochemical trans to cis isomerization reaction (Equation 3.1). It is carried out by irradiating the solution of these compounds with sunlight or UV-lamp to initiate the *trans*- and *cis*-interconversion (Equation 3.1), and halting irradiation to attain only the irreversible thermal cis to trans isomerization (Equation 3.2). Since this reaction is rather slow, a UV-visible spectrophotometer can therefore be used to follow the change of reaction with time.

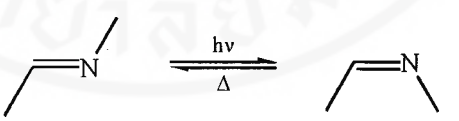

(3.1)

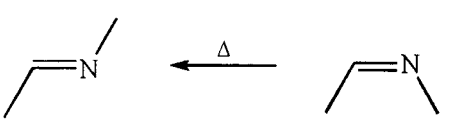

(3.2)

***trans*-isomer** ***cis*-isomer**

The experimental conditions for the kinetic studies of each hydrazone are listed in Table 3.12 below.

For each hydrazone, the experimental kinetic data are obtained as plots of the optical absorbance of the reacting system versus time at various temperatures.

Table 3.12 Experimental conditions for the kinetic studies of each hydrazone

Compound	Concentration (M)	Monitoring wavelength (nm)	Irradiated source
PIH	5.0×10^{-5}	300.0	Sunlight
PBH	5.0×10^{-5}	296.0	UV-Lamp
PSH	5.0×10^{-5}	297.0	UV-Lamp
BIH	5.0×10^{-5}	301.0	UV-Lamp
BBH	5.0×10^{-5}	296.0	Sunlight
BSH	5.0×10^{-5}	300.0	Sunlight
SIH	5.0×10^{-5}	288.0	Sunlight
SBH	5.0×10^{-5}	286.0	Sunlight
SSH	5.0×10^{-5}	289.0	Sunlight

Since the thermal cis-trans geometrical isomerization is a unimolecular reaction [72-75], it is first-order in *cis*-isomer and the rate equation becomes

$$\ln \frac{[cis\text{-isomer}]}{[cis\text{-isomer}]_0} = -kt \qquad (3.3)$$

where $[cis\text{-isomer}]$ is the concentration at time t and $[cis\text{-isomer}]_0$ is the concentration at $t = 0$. The difference in absorbance at $t = 0$ and at $t = \infty$, $A_\infty - A_0$, is proportional to the concentration of *cis*-isomer initially present in the solution. Likewise, the difference $A_\infty - A$, where A is the absorbance of *cis*-isomer at time t, is proportional to the instantaneous concentration $[cis\text{-isomer}]$. The rate equation can now be expressed as

$$\ln \frac{A_\infty - A}{A_\infty - A_0} = -kt \qquad (3.4)$$

Rearranging this equation, we obtain

$$A = (A_\infty - A_0)(1 - e^{-kt}) + A_0 \quad (3.5)$$

Equation 3.5 shows that the absorbance of the reacting system, A, increases exponentially with time, from an initial value of A_0 to a final value of A_∞.

The value of the rate constant k can be obtained by fitting the absorbance as a function of time to Equation 3.5. The method of non-linear least-squares will give a best-fit estimate of the rate constant, k. **Enzfitter**, a non-linear regression data analysis programme, was used to obtain the values of the parameters.

The kinetic results of the first-order cis-trans isomerization reaction of PIH and structurally related compounds in methanol at various temperatures are shown in Table 3.13.

The rate constant k is related to the absolute temperature T by the Arrhenius equation

$$k = Ae^{-E_a/RT} \quad (3.6)$$

This exponential relation means that the reaction velocity is very strongly dependent on temperature and increases rapidly with increasing temperature.

Taking the common logarithm of both sides of Arrhenius equation, we obtain

$$\log k = \log A - \frac{E_a}{2.303RT} \quad (3.7)$$

From Equation 3.7 and the values of rate constant k and absolute temperature T for each hydrazone in Table 3.13, a plot of log k against $1/T$ is a straight line and is shown in Figure 3.34.

Table 3.13 Kinetic results for the thermal cis-trans isomerization of the hydrazones in methanol at various temperatures

Compound	Temperature (°C / K)	Half-life (s)	Rate constant (s^{-1})
PIH	25.0 / 298.2	34.32×10^2	2.01×10^{-4}
	30.0 / 303.2	18.48×10^2	3.75×10^{-4}
	35.0 / 308.2	12.06×10^2	5.75×10^{-4}
	42.0 / 315.2	6.60×10^2	10.5×10^{-4}
PBH	25.0 / 298.2	$(26.84 \pm 0.83) \times 10^0$	$(2.582 \pm 0.080) \times 10^{-2}$
	30.0 / 303.2	$(16.01 \pm 0.28) \times 10^0$	$(4.329 \pm 0.077) \times 10^{-2}$
	35.0 / 308.2	$(10.67 \pm 0.25) \times 10^0$	$(6.50 \pm 0.15) \times 10^{-2}$
	40.0 / 313.2	$(8.07 \pm 0.25) \times 10^0$	$(8.58 \pm 0.27) \times 10^{-2}$
PSH	25.0 / 298.2	$(20.25 \pm 0.60) \times 10^1$	$(3.42 \pm 0.10) \times 10^{-3}$
	30.0 / 303.2	$(11.83 \pm 0.30) \times 10^1$	$(5.86 \pm 0.15) \times 10^{-3}$
	35.0 / 308.2	$(7.83 \pm 0.28) \times 10^1$	$(8.86 \pm 0.31) \times 10^{-3}$
	40.0 / 313.2	$(5.49 \pm 0.16) \times 10^1$	$(12.63 \pm 0.36) \times 10^{-3}$
BIH	25.0 / 298.2	$(7.24 \pm 0.21) \times 10^2$	$(9.58 \pm 0.28) \times 10^{-4}$
	30.0 / 303.2	$(5.03 \pm 0.15) \times 10^2$	$(13.78 \pm 0.40) \times 10^{-4}$
	35.0 / 308.2	$(3.79 \pm 0.13) \times 10^2$	$(18.29 \pm 0.61) \times 10^{-4}$
	40.0 / 313.2	$(2.615 \pm 0.096) \times 10^2$	$(26.51 \pm 0.98) \times 10^{-4}$
BBH	25.0 / 298.2	$(29.255 \pm 0.084) \times 10^2$	$(2.3693 \pm 0.0068) \times 10^{-4}$
	30.0 / 303.2	$(16.954 \pm 0.061) \times 10^2$	$(4.088 \pm 0.015) \times 10^{-4}$
	35.0 / 308.2	$(10.113 \pm 0.033) \times 10^2$	$(6.854 \pm 0.022) \times 10^{-4}$
	40.0 / 313.2	$(6.488 \pm 0.017) \times 10^2$	$(10.683 \pm 0.028) \times 10^{-4}$
BSH	25.0 / 298.2	$(5.310 \pm 0.015) \times 10^3$	$(1.3053 \pm 0.0036) \times 10^{-4}$
	30.0 / 303.2	$(3.0138 \pm 0.0089) \times 10^3$	$(2.2999 \pm 0.0068) \times 10^{-4}$
	35.0 / 308.2	$(1.8917 \pm 0.0029) \times 10^3$	$(3.6642 \pm 0.0056) \times 10^{-4}$
	40.0 / 313.2	$(1.1223 \pm 0.0021) \times 10^3$	$(6.176 \pm 0.012) \times 10^{-4}$
SIH	25.0 / 298.2	$(7.664 \pm 0.098) \times 10^3$	$(9.04 \pm 0.12) \times 10^{-5}$
	30.0 / 303.2	$(7.093 \pm 0.082) \times 10^3$	$(9.77 \pm 0.11) \times 10^{-5}$
	35.0 / 308.2	$(5.101 \pm 0.066) \times 10^3$	$(13.59 \pm 0.18) \times 10^{-5}$
	40.0 / 313.2	$(3.446 \pm 0.075) \times 10^3$	$(20.12 \pm 0.44) \times 10^{-5}$
SBH	25.0 / 298.2	$(19.914 \pm 0.089) \times 10^3$	$(3.481 \pm 0.016) \times 10^{-5}$
	30.0 / 303.2	$(16.379 \pm 0.105) \times 10^3$	$(4.232 \pm 0.027) \times 10^{-5}$
	35.0 / 308.2	$(10.340 \pm 0.103) \times 10^3$	$(6.703 \pm 0.067) \times 10^{-5}$
	40.0 / 313.2	$(7.255 \pm 0.066) \times 10^3$	$(9.554 \pm 0.087) \times 10^{-5}$
SSH	25.0 / 298.2	$(8.208 \pm 0.042) \times 10^3$	$(8.444 \pm 0.043) \times 10^{-5}$
	30.0 / 303.2	$(5.113 \pm 0.036) \times 10^3$	$(13.555 \pm 0.094) \times 10^{-5}$
	35.0 / 308.2	$(3.049 \pm 0.032) \times 10^3$	$(22.74 \pm 0.24) \times 10^{-5}$
	40.0 / 313.2	$(1.834 \pm 0.023) \times 10^3$	$(37.80 \pm 0.47) \times 10^{-5}$

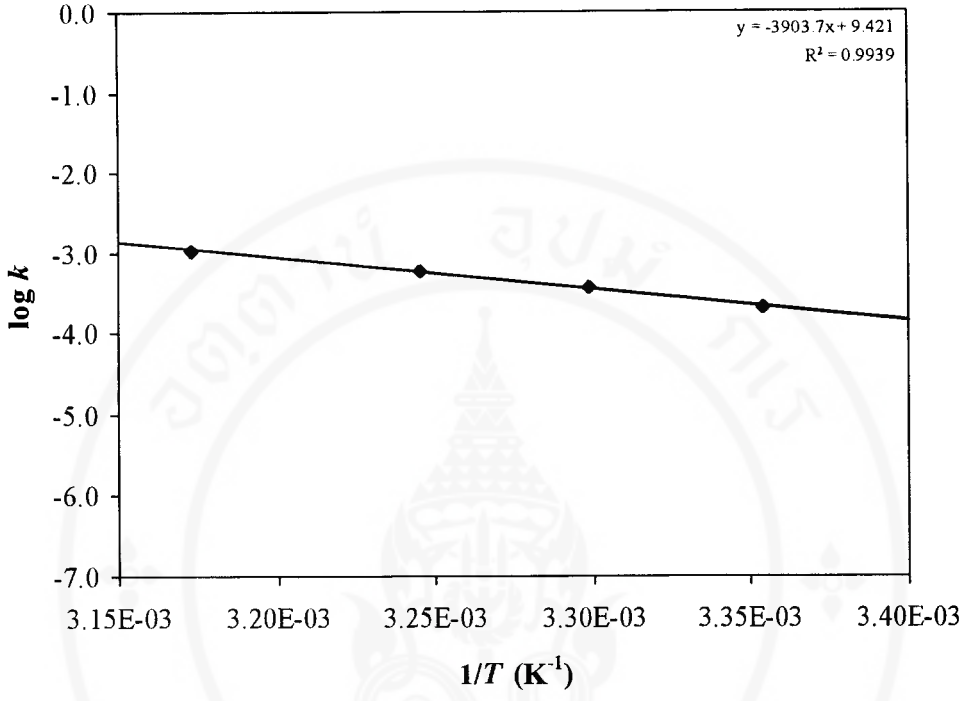

a)

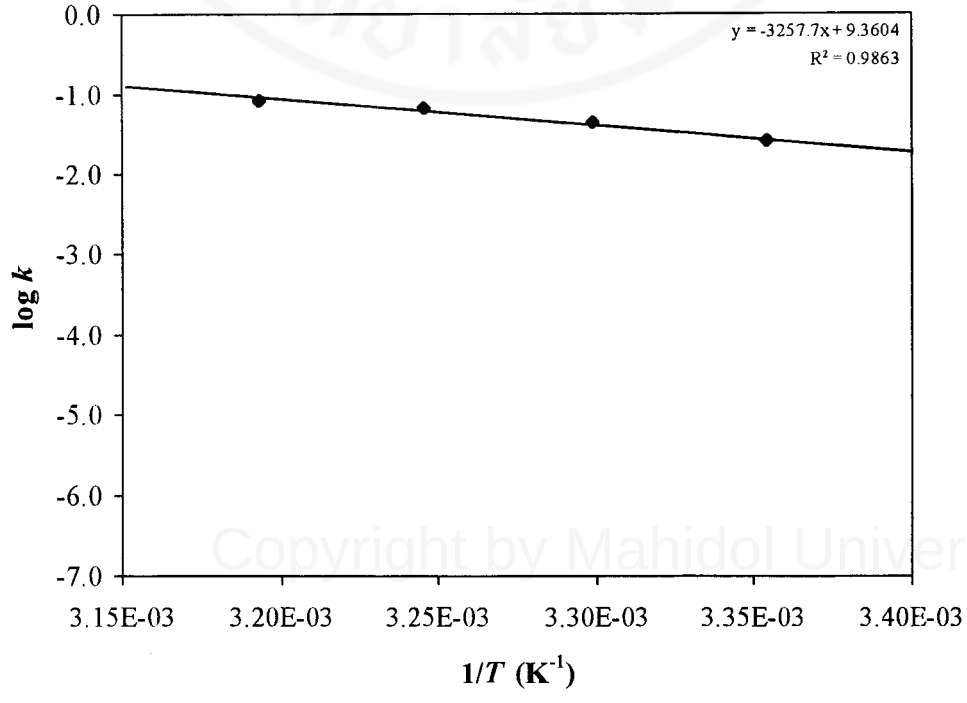

b)

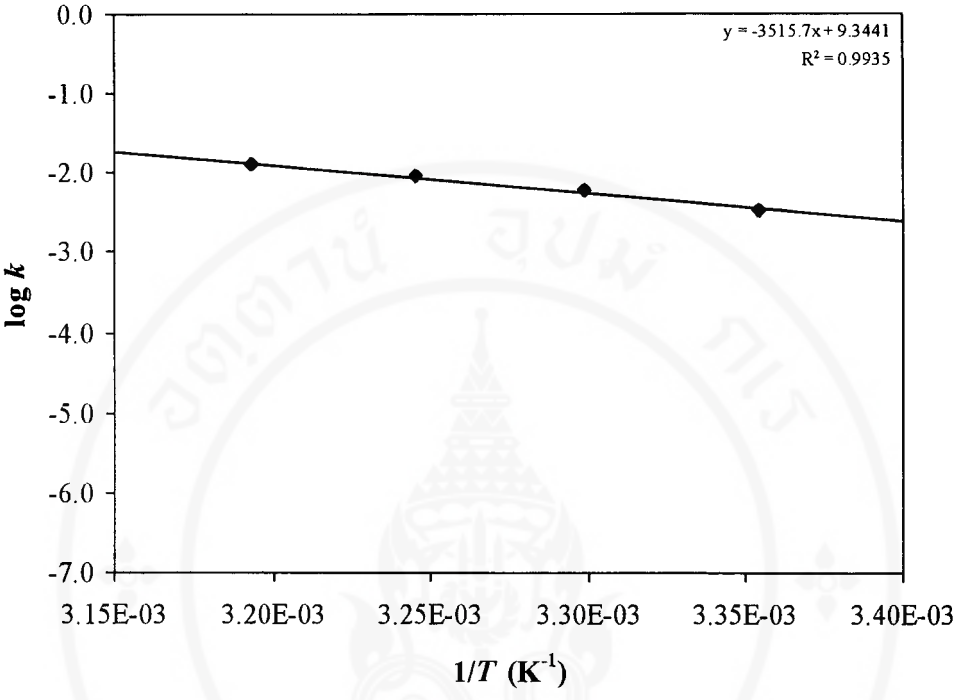

c)

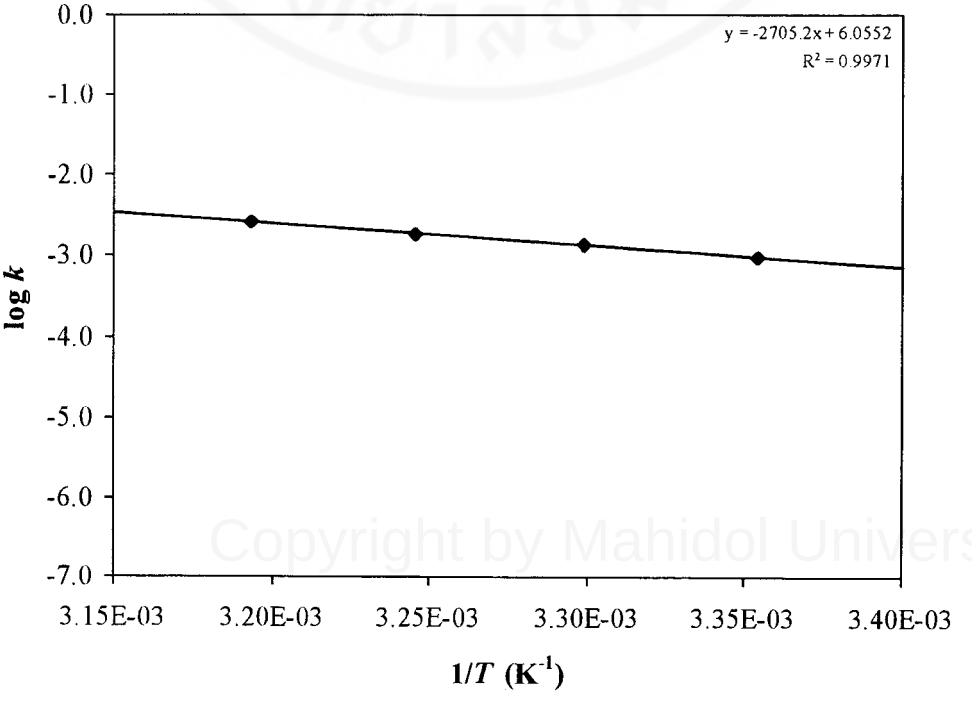

d)

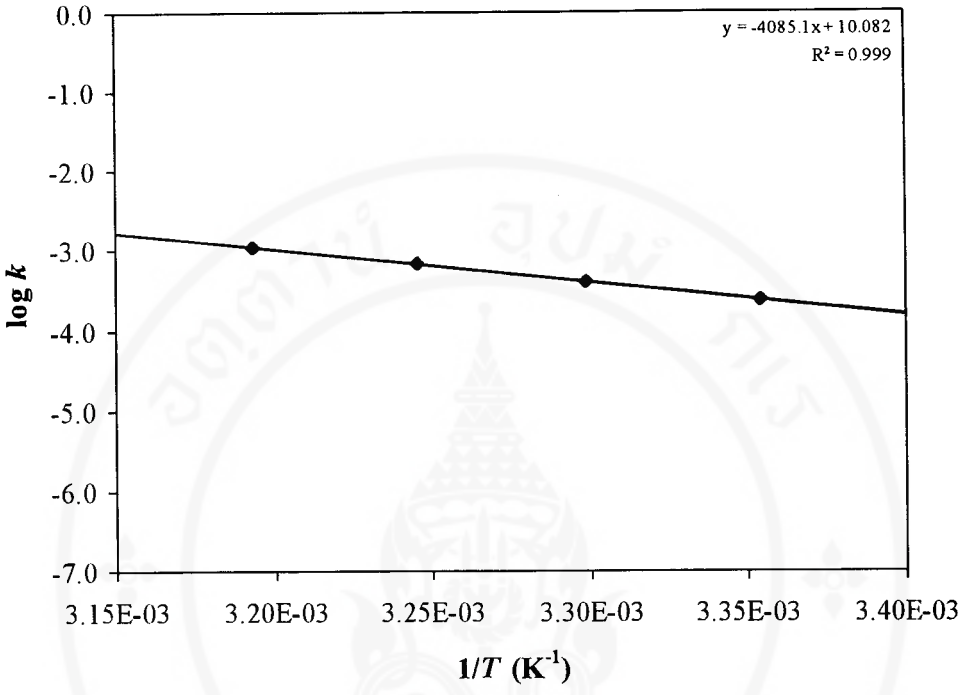

e)

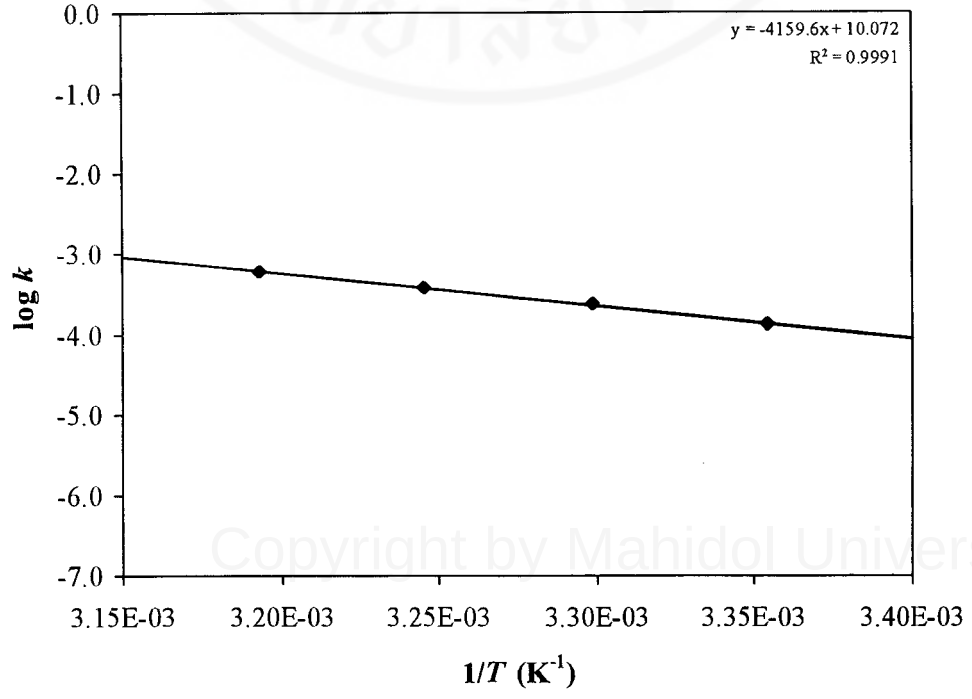

f)

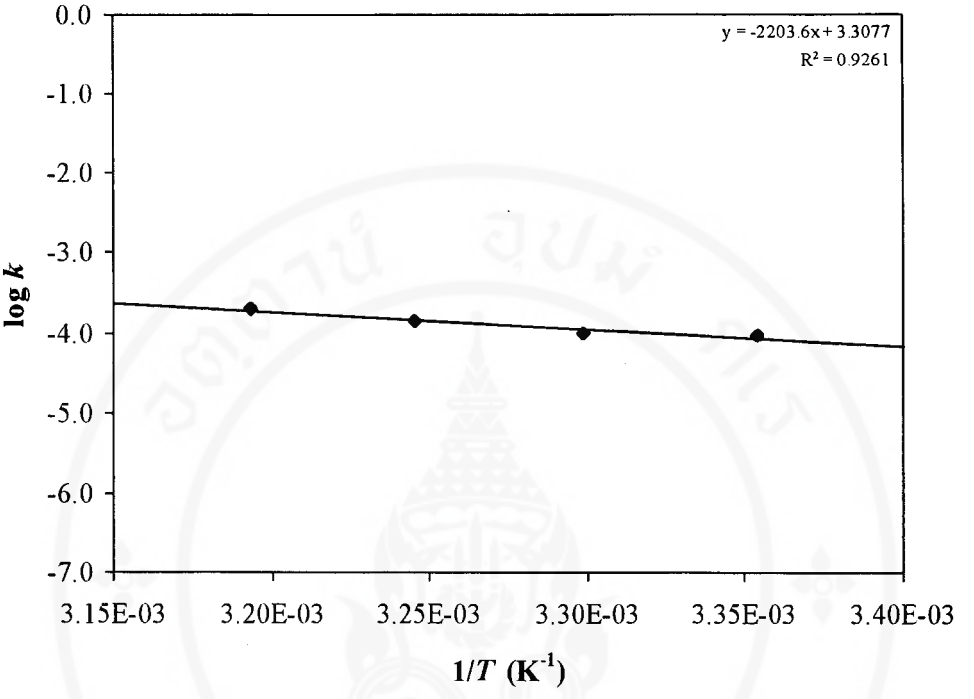

g)

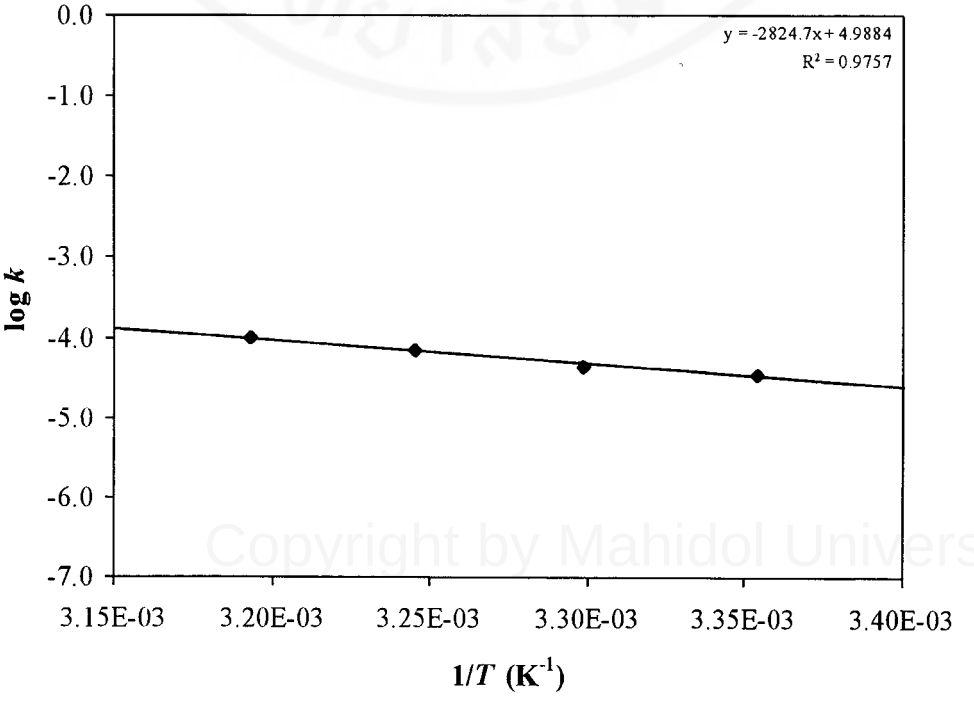

h)

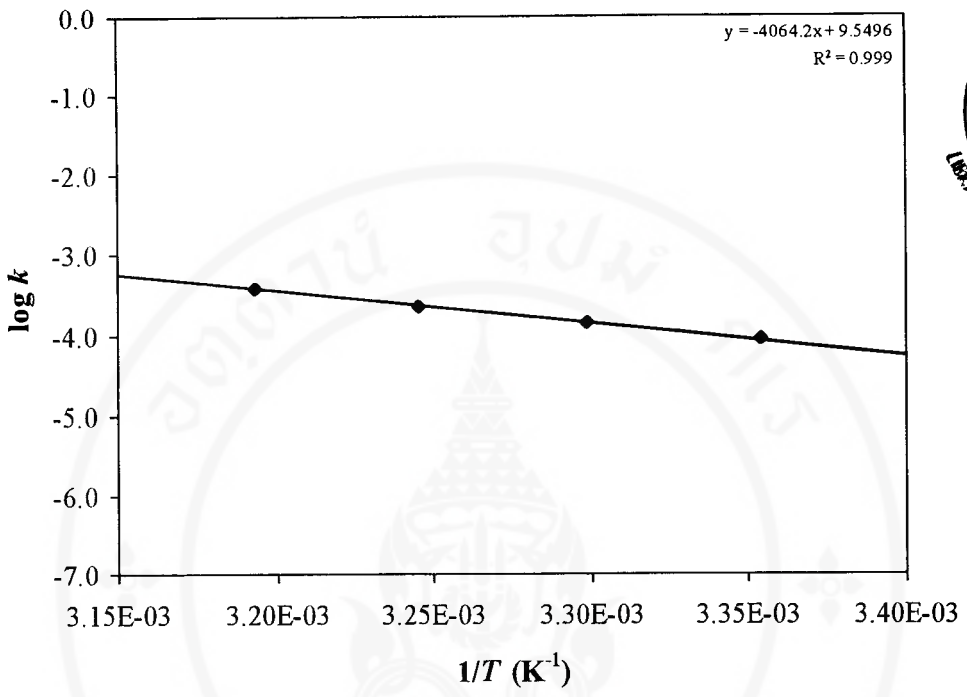

Figure 3.34 An Arrhenius plot of log k versus $1/T$ for the thermal cis-trans geometrical isomerizations of a) PIH, b) PBH, c) PSH, d) BIH, e) BBH, f) BSH, g) SIH, h) SBH and i) SSH in methanol.

From the Arrhenius plots, the activation energy E_a and the logarithm of preexponential factor log A of the thermal cis-trans isomerization reaction of each hydrazone can be calculated from the slope, $-E_a/2.303R$, and y-intercept, log A. Their values are given in Table 3.14 below.

Table 3.14 Activation energy (E_a) and logarithm of preexponential factor (log A) for the thermal cis-trans isomerization reaction of the hydrazones

Compound	E_a (kcal mol^{-1} / kJ mol^{-1})	log A
PIH	17.87 ± 0.99 / 74.7 ± 4.1	9.42 ± 0.71
PBH	14.9 ± 1.2 / 62.4 ± 5.2	9.36 ± 0.89
PSH	16.09 ± 0.92 / 67.3 ± 3.9	9.34 ± 0.66
BIH	12.38 ± 0.47 / 51.8 ± 2.0	6.06 ± 0.34
BBH	18.70 ± 0.42 / 78.2 ± 1.8	10.08 ± 0.30
BSH	19.04 ± 0.41 / 79.6 ± 1.7	10.07 ± 0.30
SIH	10.1 ± 2.0 / 42.2 ± 8.4	3.3 ± 1.4
SBH	12.9 ± 1.4 / 54.1 ± 6.0	5.0 ± 1.0
SSH	18.60 ± 0.42 / 77.8 ± 1.8	9.55 ± 0.30

CHAPTER IV

DISCUSSION

The first report of the existence of PIH as a cis-trans isomeric mixture was by Avramovici-Grisaru *et al.* [40]. The occurrence of two different coloured forms of PIH, a pale yellow crystal and a deep orange powder, when prepared by two different methods has also been found in this laboratory [69,76]. Therefore spectroscopic properties of the various forms of PIH were examined both as solids and in solution.

For the other structurally related hydrazones, namely PBH, PSH, BIH, BBH, BSH, SIH, SBH and SSH, which were prepared for the kinetic studies, investigations of their spectroscopic properties as a comparison and confirmation of results of PIH studies were carried out.

4.1 Solution study

4.1.1 Electronic absorption property of PIH and related compounds

Since PIH and some structural analogues are polyprotic acids, the pH of the solution has an important effect on the existence of various species of each hydrazone in aqueous solution, and hence the UV-visible spectrum [3,38,41,76-78]. To avoid this, methanol was used as solvent instead of the water throughout this research.

In electronic absorption studies, the UV-visible absorption spectra of the two types of PIH, namely a pale yellow crystal and a deep orange crystal obtained chloride free, by passing solution through a solid-state phase separation cartridge (Sep-pak C-18), were investigated. Both solids gave spectra that are very similar in methanolic solution. Likewise the deep orange powder, the hydrochloride of PIH, the same absorption pattern in aqueous and methanolic solutions has been reported [69]. Thus it may be concluded that the different coloured formed of PIH, when dissolved in methanol, give rise to the same structure, i.e. normal Schiff-base structure [69].

The UV-visible spectra obtained from PIH in methanol show the three major absorption bands at about 296, 340 and 400 nm, consistent with those proposed in the literature [35,40]. These absorption bands are attributed to electronic $\pi \rightarrow \pi^*$ (*K* band), $\pi \rightarrow \pi^*$ (*B* band) and $n \rightarrow \pi^*$ transitions, respectively, as shown in Table 3.1 (Section 3.1). The absorption maximum near 400 nm in the visible region of spectrum is characteristic of a typical yellow coloured solution.

For the other hydrazones, two classes of electronic absorption spectra are observed. Firstly, the UV-visible spectra show one major absorption band near 300 nm corresponded to electronic $\pi \rightarrow \pi^*$ transition (*K* band). Such compounds include BIH, BBH and BSH. There is no absorption maximum near 400 nm, and the methanolic solutions of these compounds are colourless. In the case of PBH, PSH, SIH, SBH and SSH, the UV-visible spectra similar to PIH are observed. The intense band at approximately 300 nm corresponds to electronic $\pi \rightarrow \pi^*$ transition (*K* band). For the medium and weak bands near 350 and 400 nm, they are due to electronic $\pi \rightarrow \pi^*$ (*B* band) transition of aromatic or heteroaromatic ring, and $n \rightarrow \pi^*$ transition, respectively. They are related to the existence of phenolic hydroxyl group in aldehydic

part of each hydrazone. The absorption maximum near 400 nm of these compounds in the visible region of spectra gives rise to the yellow colour of their methanolic solution.

In the case of PBH and PSH, the hydrochloride salt was used throughout this research. The existence of chloride ion should have no effect on their spectroscopic properties [69].

In the interpretation of the UV-visible spectra the electronic absorption spectra of the hydrazones were compared with the spectra of related, less highly substituted compounds. The model compounds were aminoacid-pyridoxal Schiff bases whose electronic absorption spectra have been investigated in some detail in methanol [55], alcohol/water and dioxane/water [56,57] and in buffer solutions at various pH values [56]. The spectra of starting materials for preparation of the hydrazones have been collected in various books [61-64].

4.1.2 Photochemical property of PIH and related compounds

It is found that PIH and the other related hydrazones exhibit the changes in electronic absorption spectra when their solutions are exposed to light. On storing in the dark, the spectra slowly revert to the original state. These behaviours are similar to photochromic properties of many carbon-nitrogen double-bond containing compounds which have been extensively investigated [4,5,14,52]. A list of such compounds includes anils, hydrazones, osazones and semicarbazones.

In the case of PIH, UV-irradiation has an effect on the increase of absorption spectrum at about 400 nm and the decrease of spectrum in region of 250–370 nm. These changes of the absorbance continue with further irradiation until the

photostationary state is reached. In this state UV-irradiation no longer has an influence on the spectral modification. The pale yellow crystal PIH and the deep orange crystal PIH purified from Sep-pak C-18 cartridge exhibit comparable spectral changes and isosbestic points (see Figure 3.3 and Table 3.2, Section 3.2). These isosbestic points indicate an equilibrium between two species of PIH in methanolic solution.

For the other hydrazones, the photochromic behaviours similar to PIH still occur with UV-irradiation. Their electronic spectra change to higher intensity at 400 nm but lower intensity at 250–380 nm. From this study, it is found that BBH is most photosensitive towards UV-light on account of its greatest change in absorption spectrum near 300 nm. On the contrary, PBH exhibits the least photosensitivity towards UV-light. The degree of photosensitivity from maximum to minimum is shown of Table 3.2 (Section 3.2). The extent of these changes depends on the wavelength of the light used for irradiation, with a definite equilibrium attained at each wavelength, irrespective of the *irradiation history* of the solution [52].

The photochromic behaviour of PIH and its analogues in methanolic solution is a reversible process. At room temperature, the spectrum slowly converts to the initial state in the dark. Since this change is somewhat slow, it is possible to follow this thermal reversion in solution state using normal UV-visible spectrophotometer. The studies show that the kinetics of the thermal isomerization of these compounds is first order, with activation energies of 10–19 kcal mol^{-1}, as calculated from the temperature dependence of this reaction in the range of 25–40 °C. The kinetics of these hydrazones will be reported again in Section 4.3.

In Schiff bases, it is believed that the stable isomer is the trans form around the carbon-nitrogen double bond [4-6]. X-ray diffraction of PIH has shown that in the

crystal the molecules are packed in the trans configuration [2,34,35,40,79] and in solution the trans isomer, which is essentially planar, is stabilized by strong hydrogen bonding [60], whereas the cis isomer lacks this ability to form a stabilizing hydrogen bond. Therefore, it is favoured to revert to the trans isomer on storage in the dark.

4.2 Solid-state study

Two methods of preparation, which differ in the starting materials, were used to give PIH solid. One is an indirect method. The starting material, pyridoxine hydrochloride, is oxidized in situ to pyridoxal before the aldehyde is subsequently reacted with isonicotinic acid hydrazide to obtain the required hydrazone, PIH. The second method is direct method. Pyridoxal hydrochloride is directly mixed with isonicotinic acid hydrazide to give PIH. Therefore this process may be called that condensation reaction. Both methods are carried out in sodium acetate buffer and the chloride-free pale yellow crystal and deep orange crystal PIH are obtained [3]. However, without sodium acetate buffer the deep orange powder PIH is obtained instead. The difference in the colour and form of PIH obtained from these synthetic methods is assumed to result from the different crystal structure. Consequently, investigation of physical properties probably will help to resolve this problem.

The salt and free-base forms of PIH have some variation in their physical properties. The colour of these compounds varies slightly from batch to batch and from the synthetic route. The colour ranges from deep orange to pale yellow. As expected, the hydrochloride is more soluble in water than the free-base form. There is also variation in the pattern of infrared spectrum which will be discussed in detail.

However the electronic absorption spectra and fluorescence emission spectra of PIH both in aqueous and methanolic solutions are found to be independent of the solid used to prepare the solution. These suggest that in solution PIH exists in the same form and the presence of chloride ion has no effect. These results indicate that the solid-state structure of PIH is the cause of their differences in colour and shape.

At the present time, it is known that the pale yellow crystal PIH exists in the normal Schiff-base (non-dipolar) form, and structurally assumes the trans configuration of the carbon-nitrogen double bond, with the trans, anti and *s*-transoid conformations for the aromatic carbon and imine carbon, imine nitrogen and hydrazidic nitrogen, and hydrazidic nitrogen and carbonyl carbon, respectively as shown in Figure 4.1. Although the structure of the pale yellow PIH have been extensively investigated and confirmed by a variety of spectroscopic techniques [2,34,35,40,79], little is known of the structure of deep orange solid PIH. It was thought that impurities and chloride ion are probably the cause of the deep orange colour in the solid. Avramovici-Grisaru's proposal that PIH exists in the solid state as a cis-trans isomeric mixture upon exposure to daylight [40], was also suggested to be the cause of deep orange colour. Therefore, various recrystallization steps were used to examine these hypotheses. The stages of crystallizations were reported in Section 3.4.2.

From recrystallization of the deep orange powder PIH hydrochloride in hot methanol, it is found that the deep orange PIH is still obtained. This shows that the impurities are not probably the cause of the deep orange colour. Although there are differences in the solid form and the infrared spectrum between the recrystallized PIH and the deep orange powder PIH, these only confirm that the crystal structure of PIH is modified after recrystallization. Likewise after recrystallization of the deep orange

powder PIH in hot water, the infrared spectrum is similar to that of the deep orange crystal PIH recrystallized from hot methanol but the solid form and colour are different. But in this case, the orange-yellow powder is obtained instead.

Since it is possible that the deep orange colour of the solid PIH probably results from the chloride ion, the deep orange powder PIH hydrochloride was therefore purified by passing through a solid-state phase separation cartridge (Sep-pak C-18) to remove the chloride ion. However the deep orange PIH was still obtained after purification. In addition, its infrared spectrum was identical with those of the deep orange crystal PIH obtained from recrystallization in hot methanol and water. Thus the chloride ion has an effect on the crystal structure of PIH, but it is not the cause of the deep orange colour. However, to eliminate the possible interference from chloride ion the chloride free deep orange crystal PIH was used for this work.

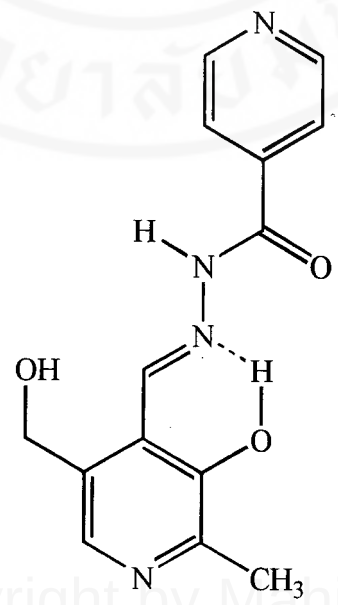

Figure 4.1 Normal Schiff-base (non-dipolar) form of the pale yellow PIH in the solid state. Schematic representation of the trans configuration and the trans, anti and *s*-transoid conformations of the most stable structure of PIH.

Deep orange PIH (chloride free) was still obtained after repeated recrystallization from hot methanol. This shows that the pale yellow PIH probably requires a particular condition to form. However if the deep orange PIH, dissolved in methanolic solution is induced to crystallize with 2–3 crystals of the pale yellow PIH, all the PIH crystals are obtained as the pale yellow colour and give the infrared spectrum as for the pale yellow PIH. The crystals of the pale yellow PIH behave as the nucleation sites for crystallization of PIH molecules in solution.

Avramovici-Grisaru *et al.* proposed that in the solid state PIH exists as the cis-trans isomeric mixture from the photochemical conversion of the trans isomer into the cis isomer on exposure to daylight at room temperature [40]. Since all recrystallizations were performed in the dark, PIH molecules exist as the trans forms in the solution would crystallize as the stable trans forms. If the deep orange colour results from the cis form of PIH in the solid, it would disappear after recrystallization. However the deep orange PIH was still obtained.

Upon exposure of solid to light the cis-trans geometrical isomerization may occur like other imine compounds [4-6,14] and the deep orange colour may develop. However there is no change in the solid colour observed for both the pale yellow PIH and the deep orange PIH even when exposed to daylight for a long time. This may be because the rotation around carbon-nitrogen double bond requires large modification in the crystal structure, as shown in Figure 4.2. In addition, the steric hindrance between hydrazidic proton and phenolic-hydroxyl group or primary alcoholic group in the molecule also inhibits this behaviour. Therefore, in the solid state the photochemical cis-trans isomerization of PIH does not probably occur at ambient temperature.

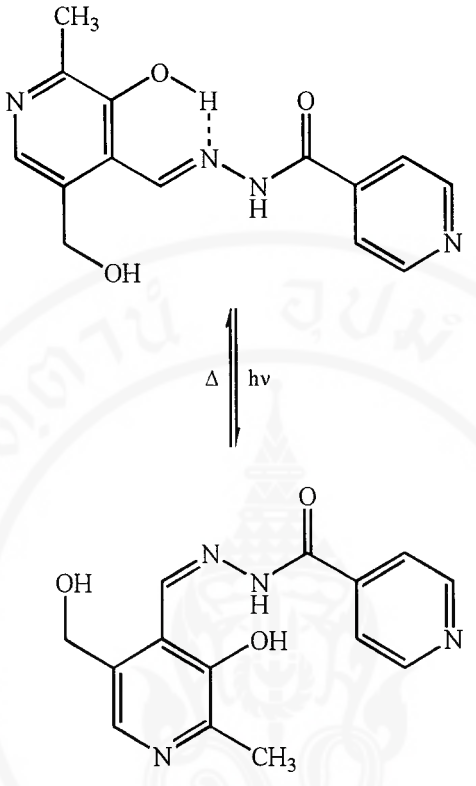

***trans*-PIH**

***cis*-PIH**

Figure 4.2 Cis-trans geometrical isomerization of PIH proposed to occur in the solid state on exposure to daylight at room temperature.

In addition, crystals of the deep orange PIH obtained from recrystallization show variation in form of the crystals. On the contrary, the pale yellow PIH has always the prismatic shape. Furthermore, optical microscopic studies reveal that the crystals of the pale yellow PIH have a smooth facet, a clear edge and corner, and a regular colour throughout the crystal. The deep orange PIH solid is not a single crystal but exists as groups of tiny crystals which have irregular shape and colour. This irregularity in colour of crystals indicates that the deep orange PIH does not crystallize with the same structure throughout the solid.

The crystallographic results of Webb *et al.* [80] show that in the presence of water PIH can crystallize in the hydrated form (1:1 PIH-to-water) as shown in Figure 4.3a. They also confirm that in the hydrated solid sample PIH exists in the dipolar form as shown in Figure 4.3b. In this structure PIH crystallize in the cis conformation around the ring carbon and imine carbon bond. This hypothesis was also expected to be the cause of deep orange colour. Therefore, infrared spectroscopy and X-ray diffraction were employed to examine and confirm the result above.

4.2.1 Infrared spectroscopy

Vibrational spectroscopy is a tool particularly well adapted to the study of the existence of the phenolic-hydroxyl group and of the amide group. Therefore this technique is used to study the structural differences of the solid hydrazones. It is hoped that the infrared spectra would reveal some structural details of the groups involved in tautomeric changes, besides providing additional evidence for the structure of these compounds [81].

Infrared study is generally restricted within the range of 2500–1200 cm^{-1}. Broad bands due to dimeric or polymeric associations hamper examination in the 3000 cm^{-1} area, and below 1200 cm^{-1} a great number of medium or weak bands makes assignments difficult [43,66].

In this section, the various types of PIH are discussed in conjunction with the structurally related compounds, namely PBH, PSH, BIH, BBH, BSH, SIH, SBH and SSH. The least substituted compound, BBH, is chosen as the reference compound.

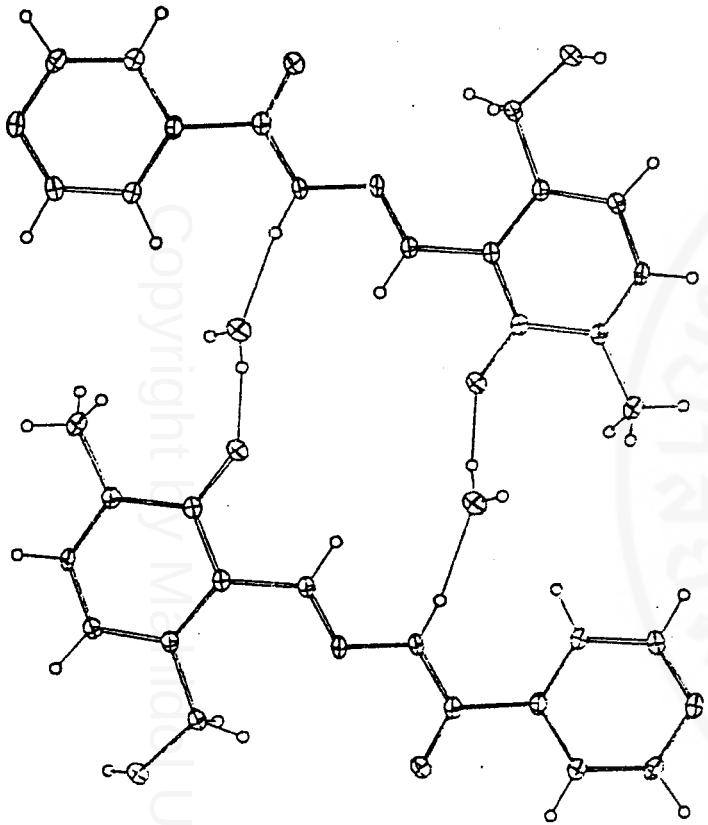

a)

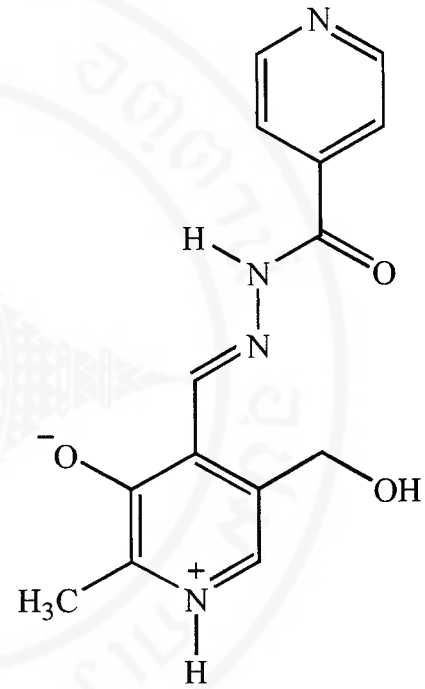

b)

Figure 4.3 Schematic representations of a) hydrated structure (1:1 PIH-to-water) of PIH dimer and b) pyridinium phenolate (dipolar) form of PIH, in the solid state.

4.2.1.1 Amide group identity

The amide group is distinctly identifiable by the amide I band (C=O stretching as the main contribution) at approximately 1680–1630 cm^{-1} and, to a lesser degree, by the amide II and III bands (combination of a N–H bending band and a C–N stretching band) at 1550 and 1360 cm^{-1}, respectively. In fact, the amide I band is intense whereas the amide II and III bands are of medium intensity and can be shifted according to the cis or trans conformation [63,64,67,42]. Moreover, the amide III band is next to the CH_3 in-plane bending band, which complicates interpretations. The N–H stretching band in the region of 3300 cm^{-1} is of little use, since it is not easy to distinguish the bands, particularly if the compounds are in hydrogen-bonded form.

Table 4.1 summarizes the vibrational absorption frequencies of amide groups for the hydrazones studied. In comparison with the C=O stretching frequency of the reference compound, BBH, it is found that in case of SBH the C=O stretching band (amide I band) shifts to higher frequency. This shows that the presence of the *ortho*-hydroxyl group probably has an effect on the resonance structures of SBH molecule, as shown in Figure 4.4. The partial positive charge on the imine nitrogen arising from intramolecular hydrogen bonding restricts the delocalization of the unpaired electrons from the amide nitrogen to the carbonyl oxygen, resulting in increased double-bond character of the carbonyl group. On the contrary, in the case of BSH the amide I band shifts to lower frequency relative to BBH. This is assumed to result from the intramolecular hydrogen bonding between the carbonyl group and the *ortho*-hydroxyl group in hydrazidic part of BSH molecule. From these infrared data, it appears that in the solid state, BSH, which is essentially planar [4], would exist in the form as shown in Figure 4.5a. For SSH which has the hydroxyl groups at the ortho positions both in

Table 4.1 Vibrational absorption frequencies of amide group for the hydrazones studied

Hydrazones	Wavenumbers (cm^{-1})			
	Amide I	**Amide II**	**Amide III**	**N–H stretching**
BBH	1642	1553	1365	3200, 3181
SBH	1674	1540	1357	3271
BSH	1630	1565	1381	3239
SSH	1638	1557	1374	3187
BIH	1693	1565	1355	3198
SIH	1685	1568	1355	3201, 3182
PBH	1676 (1648)	1542 (1560)	1348 (1364)	3221, 3209
PSH	1649	1548	1368	3223, 3173
Pale yellow PIH	1676	1559	1366	3157
Deep orange PIH	1656	1554	1363	
Deep orange powder PIH	1687	1550	1362	3221
Pale yellow sheet PIH	1677	1554	1361	

aldehydic and hydrazidic parts of molecule, the amide I band has the frequency between the C=O stretching frequencies of BBH and BSH. In the solid state the molecular structure of SSH is assumed to have the form as shown in Figure 4.5b.

In the cases of BIH and SIH, the presence of the pyridine ring in hydrazidic part of molecule has a significant effect on the increase of the C=O stretching frequency compared with BBH, as shown in Table 4.1. This large variation can be explained through the electron-withdrawing effect (inductive effect) and resonance effect which operate in opposite ways to influence the C=O stretching frequency, so that the carbonyl bond becomes stronger [63]. A higher-frequency (higher-energy) absorption results. However the interaction of these two effects is decreased when the *ortho*-

hydroxyl group is present, as in SIH molecule. Consequently, the C=O stretching band of SIH shifts to the lower frequency compared with BIH.

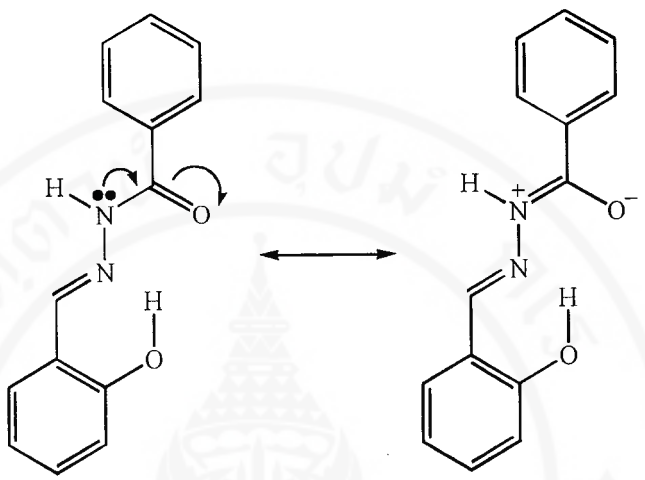

Figure 4.4 Resonance structures of SBH molecule with delocalization of unpaired electrons from amide nitrogen to carbonyl oxygen.

Like SBH, the existence of the phenolic-hydroxyl group in PBH molecule decreases the resonance effect arisen from the unpaired electrons on the nitrogen atom conjugated with the carbonyl group. Therefore its amide I band becomes somewhat stronger and absorbs at the higher frequency than of BBH. In case of PSH, the amide I band shifts to lower frequency compared with BBH. This results from the intramolecular hydrogen bond, similar to BSH. However PSH has the two hydroxyl groups both in aldehydic and hydrazidic parts, so it would be in the form like SSH, as shown in Figure 4.5c.

From observation of infrared spectra of PBH and PSH, it is found that their spectra are similar to that of the deep orange powder PIH the hydrochloride. The amide I band, which should be the most intense band, is weaker than the amide II band and the C–O stretching (and O–H bending) band. Since PBH and PSH are also

hydrochlorides, the presence of the chloride ion has probably an effect on the crystal structure and the absorption pattern of infrared spectrum [69]. In Table 4.1, the infrared absorption frequencies of PBH are compared with those reported in the literature (in the parentheses) [42].

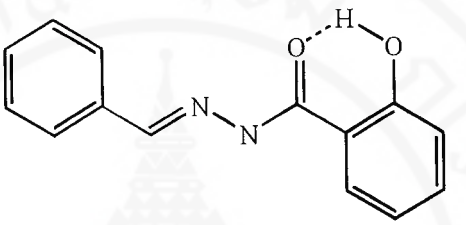

a)

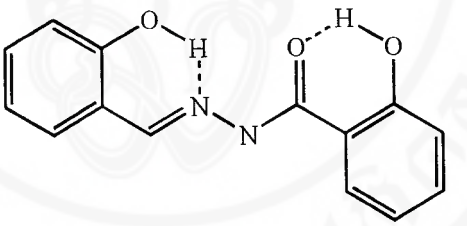

b)

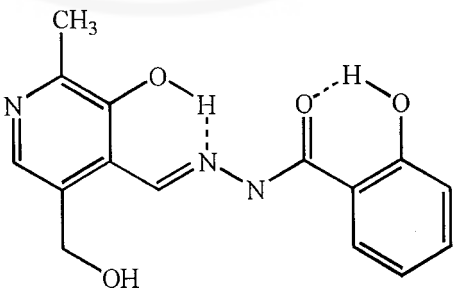

c)

Figure 4.5 Proposed structures of a) BSH, b) SSH and c) PSH in the solid state from infrared spectral data.

In addition to amide I band (C=O stretching as main contribution), the amide functional group also shows the amide II (mainly N–H bending, mixed with C–N stretching) and amide III (mainly C–N stretching, mixed with N–H bending) bands. Since these absorptions result from the interaction between the N–H bending and the C–N stretching of the C–N–H group, they tend to be modified in the same direction but opposite to the change of amide I band, as shown in Table 4.1. All the results can be explained on the basis of a contributive equilibrium between resonance structures **1** and **2**, as shown in Figure 4.6 [63].

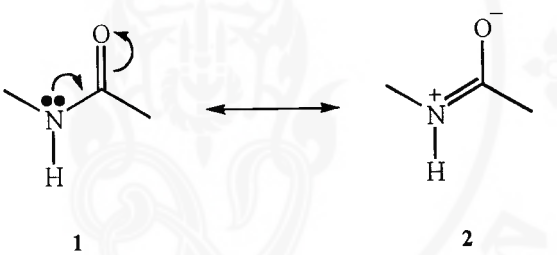

1 2

Figure 4.6 Resonance equilibrium of amide functional group in molecules of the hydrazones studied.

In the case of SBH, the amide II and III bands are shifted to lower frequencies compared with BBH. These show that the presence of the hydroxyl group in the ortho position of the aldehydic ring gives rise to the shift of resonance structure **2** to **1**. Such shift probably results from the substantial positive charge on the imine nitrogen which arises from the intramolecular hydrogen bonding between the hydroxyl group and the imine group and inhibits the delocalization of the lone-pair electrons from the amide nitrogen to the carbonyl oxygen. On the contrary, in case of BSH the presence of the hydroxyl group in the ortho position of the hydrazidic cycle leads to the contribution of resonance structure **2** and its amide II and III bands are shifted to higher

frequencies. These result from the intramolecular hydrogen bonding between the hydroxyl group and the carbonyl group of molecule. As expected, the amide II and III bands of SSH would appear at the higher frequencies compared with BBH and at the lower frequencies compared with BSH, because SSH has the hydroxyl groups both in aldehydic and hydrazidic parts.

Similar results are observed for BIH and SIH. However SIH gives the amide II and III frequencies not much different from BIH. This may results from the opposite interaction between the electron-withdrawing effect of the pyridine ring and the resonance effect of amide functional group, so that the *ortho*-hydroxyl group in aldehydic ring has not a significant effect on the shift of the amide II and III bands compared with BIH. For PBH and PSH, the shift of the amide II and III bands, and the amide I band in the opposite direction is also observed.

For various forms of PIH, four patterns of infrared spectra are observed and their amide absorption frequencies are listed in Table 4.1. For these characteristic absorptions, the vibrational bands of the pale yellow PIH are chosen as reference in comparison because of its known crystal structure [79].

It is difficult to explain variation of amide characteristic frequencies of various PIH. However, by comparison with the related hydrazone, SIH, it is found that the amide I and II bands of the pale yellow PIH are shifted to lower frequencies whereas the amide III band is shifted to higher frequency. This result is inconsistent with the basis of a contributive equilibrium of resonance structures previously stated but it notifies about an association which occurs on the hydrazidic hydrogen and has an effect on the contribution of resonance structures of the pale yellow PIH molecule. This association is assumed to be the intermolecular hydrogen bonding between the

hydrazidic hydrogen and the primary alcoholic-hydroxyl group of the pale yellow PIH, according to crystallographic data proposed in Section 4.2.2. For the deep orange PIH, the similar effect is also observed. However, its association probably involves the intermolecular hydrogen bonding between the hydrazidic hydrogen and the oxygen of a water molecule in crystal according to report of Webb *et al.* [80]. In addition, the shift of its carbonyl absorption band to lower frequency compared with that of the pale yellow PIH remarks that there is an additional association or hydrogen bonding on this group which probably results from a water molecule according to crystallographic data proposed by Webb *et al.* [80].

4.2.1.2 Phenolic- and alcoholic-hydroxyl group identity

The characteristic bands of phenolic- and alcoholic-hydroxyl groups result from O–H stretching and C–O stretching. These vibrations are sensitive to hydrogen bonding. The C–O stretching and O–H bending modes are not independent vibrational modes because they couple with the vibrations of adjacent groups [63,64].

The normal mode in the region 1280–1000 cm^{-1} corresponds to the deformation of the O–H group coupled to the elongation of the simple bond C–O. The C–O stretching (and O–H bending) band is, together with the amide I band, one of the most intense band in the spectrum of the hydrazones. It appears in the form of a multiplet; the component with the lowest frequency corresponds to the free O–H group, and the component situated at higher frequency corresponds to the deformation of the O–H group engaged in an association with an electron-donating group resulting from a chelation [42].

Table 4.2 Vibrational absorption frequencies of phenolic- and alcoholic-hydroxyl groups for the hydrazones studied

Hydrazones	Wavenumbers (cm^{-1})		
	C–O stretching (and O–H bending)		O–H stretching
BBH			
SBH	1274	1262	≈ 3000 (3400–2300)
BSH	1236	1216	≈ 3000 (3300–2400)
SSH	1231, 1272	1214	≈ 3000 (3300–2300)
BIH			
SIH	1291	1275	≈ 3000 (3300–2500)
PBH	1256 (1280, 1249)		≈ 3000 (3500–2300)
PSH	1257, 1217		≈ 3000 (3500–2200)
Pale yellow PIH	1281	1257	≈ 3000 (3400–2300)
Deep orange PIH	1276	1248	≈ 3000 (3600–2100)
Deep orange powder PIH	1270		≈ 3000 (3500–2400)
Pale yellow sheet PIH	1285		≈ 3000 (3600–2400)

In case of the O–H stretching band, hydrogen bonding shifts this band to lower frequency, especially if the bonding is with carbonyl or imine groups, very low frequency is observed. The O–H stretching band gives a little structural information, since its band width and intensity is complicated in the 3000 cm^{-1} area [63,64,67].

The characteristic vibrational frequencies of the phenolic- and alcoholic-hydroxyl groups for the hydrazones studied are summarized in Table 4.2. For the phenolic-hydroxyl group of the hydrazones, the C–O stretching (and O–H bending) band is shifted to higher frequency from normal value resulting from the intramolecular hydrogen bonding between the hydroxyl group with the imine and/or carbonyl groups. This band is located at different frequency depending on position of

phenolic-hydroxyl group in molecule. When the phenolic-hydroxyl group is at the ortho position in aldehydic part, like SBH, the C–O stretching (and O–H bending) band appears at approximately 1274 and 1262 cm^{-1}. This band occurs at about 1236 and 1216 cm^{-1} in case of BSH which possesses the phenolic-hydroxyl group at the ortho position in hydrazidic part. In the case of SSH, the C–O stretching (and O–H bending) bands which correspond to the phenolic-hydroxyl groups in both aldehydic and hydrazidic rings are observed.

For the O–H stretching vibration of the phenolic-hydroxyl group, a very strong and broad band is observed in the region of 3000 cm^{-1}. This results from the strong intramolecular hydrogen bonding (chelation) between the hydroxyl substituent with the imine group and/or the amide carbonyl group. Although similar broad bands are seen for both types of chelations, the bands have different intensity. The O–H stretching band of the hydroxyl group in the hydrazidic ring is more intense than that of the hydroxyl substituent in aldehydic ring. As expected, in the case of SSH and PSH which possess the two types of phenolic-hydroxyl groups, extremely broad band of the O–H stretching vibration is observed.

By comparison with the less substituted hydrazone, SIH, it is found that the pale yellow PIH gives the C–O stretching (and O–H bending) band of the phenolic-hydroxyl group at a slightly lower frequency. This probably results from the existence of the pyridine ring (electron-withdrawing group) and the additional substituents in the aldehydic part of the PIH molecule. However, the deep orange PIH appears at a slightly lower frequency compared with the pale yellow PIH. This indicates that there is a change in its structure, especially in the phenolic-hydroxyl group. From consideration of Webb's crystallographic result [80], this suggests that the

intramolecular hydrogen bonding of the imine group in the pale yellow PIH changes to an intermolecular hydrogen bond with a water molecule.

For the primary alcoholic-hydroxyl group in aldehydic ring of PIH molecule, the C–O stretching (and O–H bending) band is at approximately 1070–1040 cm^{-1} for the deep orange PIH and at about 1024–986 cm^{-1} for the pale yellow PIH. This results from the strong intermolecular hydrogen bonding occurred on the primary alcoholic-hydroxyl group of the pale yellow PIH. Crystallographic data, which explain clearly this effect, will be reported in next Section 4.2.2.

Upon association, the change, which is more clear than, is observed on the O–H stretching vibrational band. In the pale yellow PIH, this band is strong and broad than that of SIH. This result shows that an association (hydrogen bonding) is involved. However, from crystallographic data (Section 4.2.2) it is known that the similar association (intramolecular hydrogen bonding) occurs on the phenolic-hydroxyl group of the pale yellow PIH and SIH. Therefore the strong and broad band in spectrum of the pale yellow PIH probably results from the intermolecular hydrogen bonding on the primary alcoholic-hydroxyl substituent. More details about crystal structure of the pale yellow PIH will be given in Section 4.2.2. For the deep orange PIH, the O–H stretching band which is more strong and broad than of the pale yellow PIH is observed. This shows that there is the additional association on hydroxyl group of the deep orange PIH. From crystallographic data proposed by Webb [80], this association probably corresponds to the intermolecular hydrogen bonding between the phenolic-hydroxyl group and a water molecule.

4.2.1.3 Ring and substituent specific vibrations

In this research, the molecules studied possess two different aromatic parts: an aldehydic ring with an imine group, and a hydrazidic ring with a carbonyl group.

As stated in the literature [43], aromatic rings exhibit two types of characteristic C=C stretching vibrations: a quadrant mode (between 1600–1585 cm^{-1}) and a sextant mode (between 1500–1400 cm^{-1}). Unless restricted by symmetry, each type appears as doublets, with differing sensitivity to electronic effects of ring substituents.

For *ortho*-substituted cycle, four bands are expected: between 1620–1585, 1590–1565, 1510–1470 and 1465–1430 cm^{-1}. In principle, the second band only appears when ring is conjugated with unsaturated groups or groups having lone pair electrons. Conjugation intensifies all the first three peaks but positions are not affected. In addition, the intensities of the first and third bands are also strong, in the case of electron-donating substituents. The fourth band may overlap with CH_2 bending band.

In addition, four bands are expected for a *para*-substituted ring, located between 1620–1585, 1590–1565, 1525–1480 and 1420–1400 cm^{-1}. Intensities of the first two bands are directly related to the perturbations of electron density within the aromatic cycle: the more the difference of electronic effects between para substituents (inductive or mesomeric) the more intense are the bands. However, the second band generally remains weak, except in cases of conjugation or when the substituent is a halogen. Intensity of the third band increases for electron-donating substituents, but can vanish for electron-withdrawing groups. The fourth band is weak.

By comparison with the least substituted hydrazone, BBH, it is possible to study the shift and the intensity variations of the skeletal vibrational bands according to the

nature of the ring substituents. From the frequencies and intensities of the differing bands we can assign them (whenever possible) to an aldehydic ring or to a hydrazidic cycle as shown in Table 4.3.

Experimental results are in good agreement with the preceding literature observations [43]. However, of the eight expected bands, only some bands are observed since the overlap of their spectral ranges only allows for identification of the more intense components.

From Table 4.3, it is seen that the *ortho*-hydroxyl substituted hydrazone, SBH, exhibits some variations in the intensity in the skeletal bands compared with BBH. For instance, the decrease in the intensity of the second band (near 1579 cm^{-1}) probably results from the intramolecular hydrazone bonding between the *ortho*-hydroxyl group and the imine group. There are as well significant increase and decrease in intensities of the third and fourth bands (at approximately 1488 and 1444 cm^{-1}), respectively. They may arise from the introduction of the electron-donating substituent at the ortho position on aldehydic ring. For the very weak band at about 1414 cm^{-1} in BBH spectrum, it still appears as a weak band in spectrum of SBH.

In case of BSH, the splitting of the skeletal bands observed in spectrum probably result from the C=C stretching vibration of each the aromatic ring (aldehydic and hydrazidic rings). It may be assumed that the second band at 1585 cm^{-1}, missing in BBH, and the third and fourth bands at 1509 and 1457 cm^{-1}, which are very weak in BBH, are due to the *ortho*-substitution of the ring in the hydrazidic part. The intensification of these bands results from the electron-donating substituent, the hydroxyl group, in the hydrazidic ring. Thus substituents on each type of aromatic ring

Table 4.3 Vibrational absorption frequencies and relative intensities of aldehydic and hydrazidic rings for the hydrazones studied[a]

Hydrazones	Wavenumbers (cm^{-1})						
	AH(o/p)	AH(o/p)	H(p)	A(o)	H(o)	A(o)	H(p)
BBH	1601s	1577ms	1502vw	1487ms	1460vw	1447m	
SBH	1607s	1579m		1488s		1444w	1414mw
BSH	1611s	1585s, 1577s	1509m	1491ms	1457s	1448ms	1412vw
SSH	1611s	1572s		1488s	1454s		1412vw
BIH	1606mw, 1599m			1492m	1468vw	1449m	1412ms
SIH	1614s			1491ms		1459w	1408m
PBH	1587mw (1603)	(1578)	1512w	1491w (1483)		1450w (1441)	1428w
PSH	1604s			1489m		1458m	1426vw
Pale yellow PIH	1608mw	1594mw		1490mw		1446m	1414m
Deep orange PIH	1606mw	1581m				1431s	1421s
Deep orange powder PIH	1602s			1498w		1443w	1420m
Pale yellow sheet PIH	1604m	1573ms		1491w		1438mw	

[a]A : aldehydic ring, H : hydrazidic ring, o : ortho substituent, and p : para substituent; s : strong, ms : medium strong, m : medium, mw : medium weak, w : weak and vw : very weak

have a significant effect on the intensity variations of the skeletal bands, but they do not affect the position of these bands.

SSH shows the skeletal bands which are somewhat intense resulting from the *ortho*-hydroxyl substituents (electron-donating groups), in both aldehydic and hydrazidic rings. However, these are not split, as observed in the case of BSH. Although SSH gives the skeletal bands similar to those of BBH, it is interesting to note that its fourth band is due to, in contrast to BBH and SBH, the *ortho*-substitution in the ring of hydrazidic part. In addition, there is a decrease in intensity of the fourth band corresponding to the *ortho*-hydroxyl substituent in aldehydic part, so that only the band (near 1454 cm^{-1}) is observed in spectrum. The band at approximately 1412 cm^{-1}, it is still very weak as in the case of SBH and BSH.

By comparison with BBH, the existence of pyridine ring in hydrazidic part of BIH and SIH molecules has no significant effect on their skeletal bands, except at the vibrational band (near 1412 cm^{-1}) is greatly pronounced both in the spectra of BIH and SIH. It can be assumed that this band is due to the pyridine ring in hydrazidic part. Like the fourth band of a *para*-substituted ring, the electronic (inductive and mesomeric) effect of this heteroaromatic cycle can intensify this band as shown in Table 4.3. Like SBH, the presence of the *ortho*-hydroxyl substituent in the aldehydic part has an important effect on the intensities of the third and fourth bands (at approximately 1491 and 1459 cm^{-1}) in spectrum of SIH. The other skeletal bands of BIH and SIH are similar to those of the previous hydrazones.

Unlike the other hydrazones, the skeletal bands of PBH, corresponding to aromatic and heteroaromatic rings, are rather weak and complicated. However, their assignments to the aldehydic and hydrazidic rings are proposed and shown in Table

4.3 (compared with values in literature [42] displayed in parentheses). The frequencies observed from this experiment are in disagreement with the preceding literature observations. This probably results from the existence of the chloride ion in the solid sample of PBH. However chloride free PBH was not investigated in this study. In case of PSH, the similar feature is also observed, but with the skeletal bands which are more intense.

Unlike the other structurally related hydrazones, PIH contains pyridine rings both in aldehydic and hydrazidic parts of molecule. However, it still shows characteristic bands of the skeletal vibrations similar to the others.

Comparing the skeletal bands of the pale yellow PIH with those of the other forms PIH may give some information regarding the solid-state structure. On passing from the pale yellow PIH to the deep orange PIH, the intensities of the skeletal bands, especially the second band and the last two bands, increase. This indicates that this change occurs at heteroaromatic ring of the deep orange PIH. This result supports the formation of the zwitterionic form, according to crystallographic data proposed by Webb [80].

4.2.1.4 Other bands

The existence of the medium intensity absorption band at approximately 2060 cm^{-1} in infrared spectra of the deep orange PIH and the deep orange powder PIH (hydrochloride) indicates that an unsaturated amine group or an aromatic amine group contributes to their solid-state structures. The unsaturated amine ($-C=NH^{+}-$) gives three characteristic groups, namely the **ammonium band**, which are strong and broad, or relatively sharp, in the region of 2500–2300 cm^{-1}, the **immonium band** of medium

intensity, in the region of 2200–1800 cm^{-1}, and the $C=N^+$ stretching band at approximately 1680 cm^{-1} [67]. For the ammonium band, one is attributed to the NH^+ stretching vibration and the others are overtones and combinations. This band is clearly separated from the C–H stretching band of tertiary amine salts. Although the unsaturated amine shows the ammonium band like tertiary amine salts, it can be easily identified by the immonium band at about 2060 cm^{-1} (tertiary amine salts lack this band). The C=N stretching absorption which is shifted to higher frequencies upon salt formation is also an important factor.

The vibrational band at approximately 2060 cm^{-1} in infrared spectrum of deep orange PIH is the most significant structural feature that distinguishes it from the pale yellow PIH. This band is proposed to be due to the vibrational mode of the pyridinium group which is involved in the formation of the zwitterionic form of pyridoxal from the transfer of the phenolic proton to the pyridoxal nitrogen [35-37,70]. This assignment is consistent with the fact that the band is absent from the metal complexes as well as ligands of salicylaldehyde analogues [82] which have no pyridine nitrogen atom. Assignment of this band is shown in Table 3.4 (Section 3.4). Other characteristic bands of the pyridinium group are also expected to appear in the infrared spectrum. However, overlap of these bands with other intense bands, such as the hydrogen bonded O–H stretching band and the C=O stretching band, may interfere with their appearance.

Appearance of the medium intensity absorption band at approximately 3485 cm^{-1} in spectrum is another difference of great significance between the deep orange PIH and the pale yellow PIH, since this band is attributed to the O–H stretching vibration of a water which exists in the crystal of the deep orange PIH [67]. However, the weak

band in region of 1640–1615 cm^{-1} which corresponds to the H–O–H bending vibration is not observed [67]. This characteristic vibrational band of a water of crystallization indicates that PIH crystallizes in the dipolar form of the hydrated crystal structure (1:1, PIH:water) like that proposed by Webb *et al.* [80].

The geometry of the most stable conformer of each hydrazone studied is shown in Figure 4.7. For some hydrazones, this result will be confirmed again by crystallographic data in Section 4.2.2.

4.2.2 X-ray diffraction

As previously stated, attempt to determine the solid-state structure (molecular and crystal structures) of the deep orange PIH using X-ray diffraction technique was not successful. However, crystallographic data of the pale yellow PIH and some hydrazones were obtained.

From the crystallographic data of the pale yellow PIH given in Section 3.5 and reported by Sarel *et al.* [79], it can be seen that in the crystalline state, the pale yellow PIH exists as a tetramer of its non-dipolar form. The tetramer comprises a planar 16-membered ring dimer, to which two additional units of PIH are hydrogen-bonded, each at right angle and in an opposite direction, to the macrocyclic ring plane at the respective alcoholic hydrogens, H–O(1). This affords a three-dimensional supramolecular structure presented by Figure 4.8.

The observed bond angle of 119.0°, for the pyridoxal-ring C(15)–N(11)–C(20) angle (see Table 3.11, Section 3.5), is consistent with a non-dipolar rather than with a dipolar form for the pale yellow PIH, since the respective bond angle for the latter should have been larger by 5°, namely, to be approximately 124° [79]. The former is

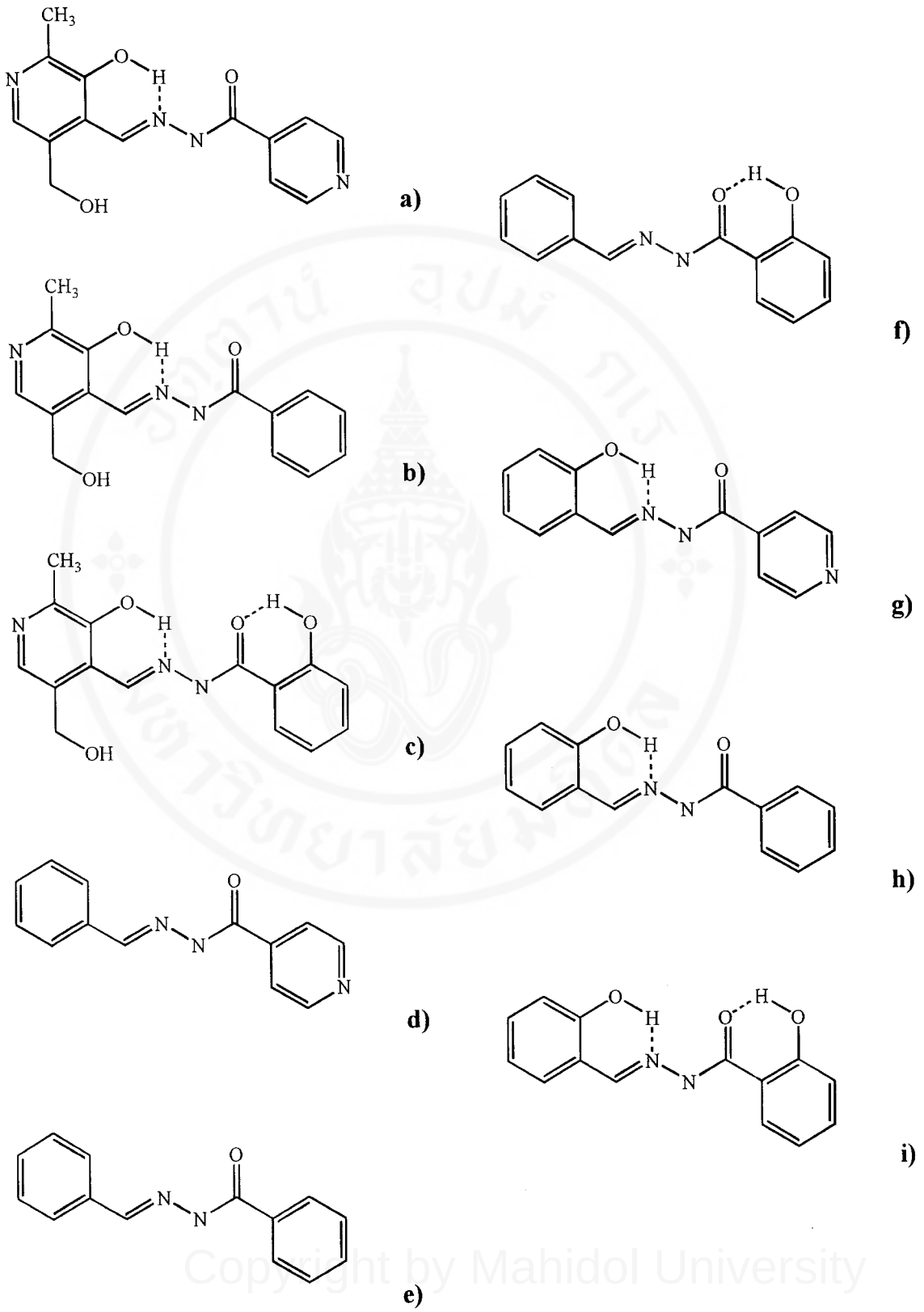

Figure 4.7 The most stable configurational and conformational forms of a) PIH, b) PBH, c) PSH, d) BIH, e) BBH, f) BSH, g) SIH, h) SBH and i) SSH in the solid state.

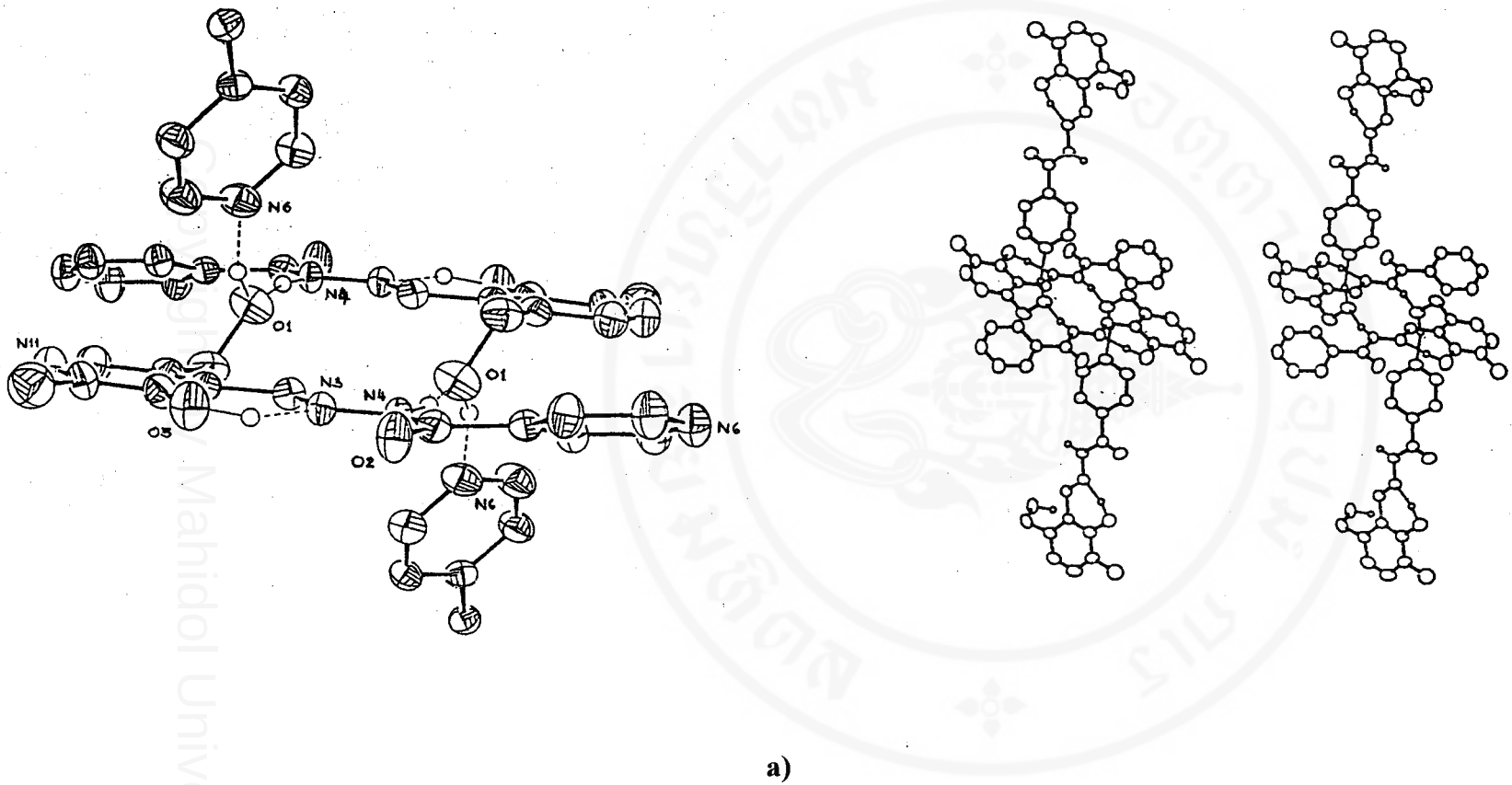

a) b)

Figure 4.8 Crystal structure of PIH in a) perspective view with the atom numbering scheme and b) stereoscopic view.

indicative also for the energetically favoured trans relationship between the hydrazidic, and the hydroxymethyl side-chains [45]. Furthermore, the crystal structure confirms a *s*-trans conformation for the hydrazide function, namely, that the carbonyl oxygen, O(2), and the hydrazidic hydrogen, H–N(4), are trans oriented.

Recent studies [79] of the hydrogen-bonded distances in the crystalline state of the pale yellow PIH have shown that the tetrameric assembly is stabilized by virtue of two distinctly different intermolecular modes of hydrogen bondings. One, is of a longer distance (1.850 Å), and of the *non-linear three-centred* type (bond angle around 133.09°, **3-C** bond) [21]. This mode allows the formation of a 16-membered ring dimer by linking two alcoholic oxygens, O(1), with two hydrazidic hydrogens, H–N (4). As with the water molecule, the **3-C** bond is energetically favoured due to *cooperative effect*.

The second mode, is of the *linear two-centred* type (**2-C** bond), characterized by its shorter length (1.726 Å), and its larger bond angle (159.84°). It is favoured for attaching two additional PIH units, to the protruding alcoholic hydroxyl groups at the upper and at the lower sides of the dimeric macrocycle plane. Thus, the alcoholic hydroxyl hydrogen, H–O(1), function as H-donors, whereas the hydrazidic-ring nitrogens N(6), function as H-acceptors. It is noteworthy that the pyridoxal alcoholic group in water-free PIH plays a pivotal role in aggregating the four molecules in a specific form to yield the observed tetrameric supramolecule (Figure 4.8a).

For SIH and SBH, the crystallographic data are summarized in Table 3.6, 3.8, 3.9, 3.10 and 3.11 (Section 3.5) and the molecular and crystal structures are shown in Figure 3.32 and 3.33 (Section 3.5). These evidently indicate that in the crystalline state molecules of SIH and SBH is nearly coplanar. In addition, they confirm the

energetically favoured cis conformation between the hydrazidic and the phenolic-hydroxyl side-chains, and the *s*-transoid conformation for the carbonyl oxygen and the hydrazidic hydrogen of the solid-state structures of SIH and SBH, as previously proposed from infrared studies.

4.3 Kinetic study: Factors influencing the thermal cis-trans geometrical isomerizations of the hydrazones

To study the molecular factors which affect the rate of the thermal cis-trans isomerization reaction of the hydrazone, a series of structurally related hydrazones were synthesized by reacting the three different aldehydes, *viz* pyridoxal hydrochloride, benzaldehyde and salicylaldehyde, with three acid hydrazides, *viz* isonicotinic acid hydrazide, benzoic acid hydrazide and salicyloyl hydrazide. The nine possible hydrazones, PIH, PBH, PSH, BIH, BBH, BSH, SIH, SBH and SSH were obtained as shown in Figure 1.8 (Section 1.4).

From preliminary kinetic experiments, it was found that the thermal cis-trans geometrical isomerizations of the hydrazones are somewhat slow and give rise to changes of optical absorbance of system in solution. Thus it was possible to follow the reactions using UV-visible spectrophotometric method. In the kinetic studies, the rate constants were measured at four temperatures, namely 25.0, 30.0, 35.0 and 40.0 °C, and the activation energies and the logarithm of preexponential factors calculated. The results are given in Table 3.13 and 3.14 (Section 3.6).

The activation energies of 10.1–19.0 kcal mol^{-1} observed for the thermal isomerizations are in good agreement with values obtained previously by Fischer *et al.*

[52], Wettermark *et al.* [4] and Anderson *et al.* [5], and are consistent with that reported for the isomerization about conjugated nitrogen-nitrogen double bond (23 kcal mol^{-1} for azobenzene) and conjugated carbon-carbon double bond (42 kcal mol^{-1} for stilbene).

Variations of substituents on aldehydic and/or hydrazidic rings of the hydrazones have a significant effect on the values of the rate constant, the activation energy and the logarithm of preexponential factor, as shown in Table 3.13 and 3.14 (Section 3.6). This result is consistent with previous investigations of factors influencing the ease of thermal isomerization about the carbon-nitrogen double bond. It has been shown that the interconversion barrier is remarkably sensitive to the attached substituent groups [50]. For instance, among imino compounds derived from benzophenone, changes in groups attached to nitrogen can produce a range of the rates of uncatalyzed isomerizations of greater than 14 powers of 10 [50]. However, it is noted that the hydrazones, which possess the *ortho*-hydroxyl group to the carbon-nitrogen double bond with the possibility of tautomerization, have activation energies and the log of preexponential factors of the same magnitude as the unsubstituted hydrazones [5].

To study the variation in the values of the activation energies and the preexponential factors, the hydrazones are categorized as follow:

1. Constant aldehydic part
    1.1 Constant benzaldehyde, i.e. BBH, BSH and BIH
    1.2 Constant salicylaldehyde, i.e. SBH, SSH and SIH
    1.3 Constant pyridoxal, i.e. PBH, PSH and PIH

2. Constant hydrazidic part

2.1 Constant benzoic acid hydrazide, i.e. BBH, SBH and PBH

2.2 Constant salicyloyl hydrazide, i.e. BSH, SSH and PSH

2.3 Constant isonicotinic acid hydrazide, i.e. BIH, SIH and PIH

When aldehydic part is constant, increasing values of the activation energies and the preexponential factors relating to the *cis*-molecular structures of the hydrazones are found, as shown in Figure 4.9. The results evidently show that there are some relationship between the molecular structure and the value of the activation energy and/or the preexponential factor of hydrazones. It is also seen that each group of hydrazones which have the hydrazidic part as salicyloyl hydrazide (SH) have activation energies greater than those of related hydrazones which have benzoic acid hydrazide (BH) in the hydrazidic part. From Figure 4.9, the activation energies of BSH, SSH and PSH are greater than those of BBH, SBH and PBH, respectively. Hydrazones which have isonicotinic acid hydrazide (IH) as the hydrazidic part, have the lowest activation energies observed, except PIH.

Similar variation in the preexponential factors with the molecular structures is also observed. Hydrazones which have SH in the hydrazidic part have values of the preexponential factors greater than or approximately equal to those of related hydrazones with BH in the hydrazidic part. Hydrazones which possess the hydrazidic part as IH, BIH and SIH show the least values of the preexponential factors in the group and the largest value is seen for PIH.

To discuss the rates of the thermal cis-trans isomerizations of the hydrazones relating to the molecular structures, the activation energy and the preexponential factor must be considered together. From Figure 4.9, it is found that the values of the

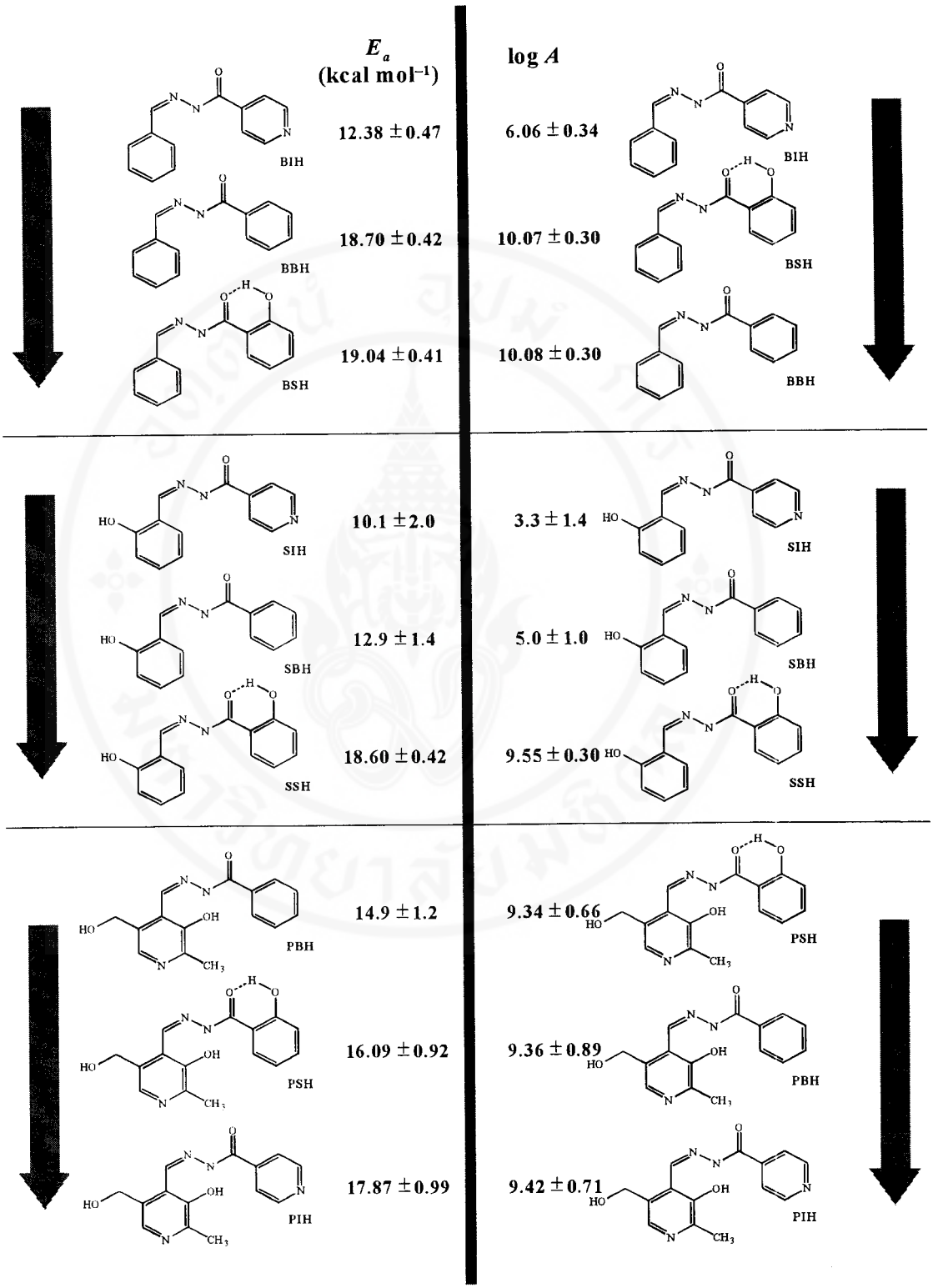

Figure 4.9 Figure showing the molecular structures of the *cis*-isomer of hydrazones together with their activation energies (E_a) and logarithm of the preexponential factors (log A). The aldehydic part of the hydrazone is constant and the hydrazidic group varied. The numerical values increase from top to bottom.

activation energies and the preexponential factors of the hydrazones for each group changes in the same direction. However, the third group, PBH, PSH and PIH, have preexponential factors of the same order. Their rates of the thermal relaxations are thus only dependent on the values of the activation energies. By comparing these values, the rates of the thermal relaxations for these hydrazones can be predicted. As well, results show that the rates of the thermal relaxations of BBH and BSH in the first group only depend on the activation energy. BBH has faster isomerization rate than BSH, as the activation energy of BBH is less than that of BSH.

In the case of constant hydrazidic part, increasing values of the activation energies and the preexponential factors relating to the *cis*-molecular structures of the hydrazones are shown in Figure 4.10. The same variation in the values of the activation energies and the preexponential factors relating to the molecular structure of hydrazones are observed in this group. However, values of the preexponential factors for PBH and BBH, and PSH, SSH and BSH are nearly the same. Thus their rates of the thermal cis-trans isomerization can be compared by considering only the values of the activation energies. Consequently, PBH isomerizes faster than BBH, as its activation energy is less than that of BBH. For the second group, the rates of the thermal relaxation are in order as follow: PSH > SSH > BSH. In addition, consideration of the variation in the values of the activation energies and the preexponential factors relating to the molecular structure shows that hydrazones, which have the aldehydic part as benzaldehyde (B), possess the activation energies and the preexponential factors greater than those of related hydrazones which have salicylaldehyde (S) in the aldehydic part.

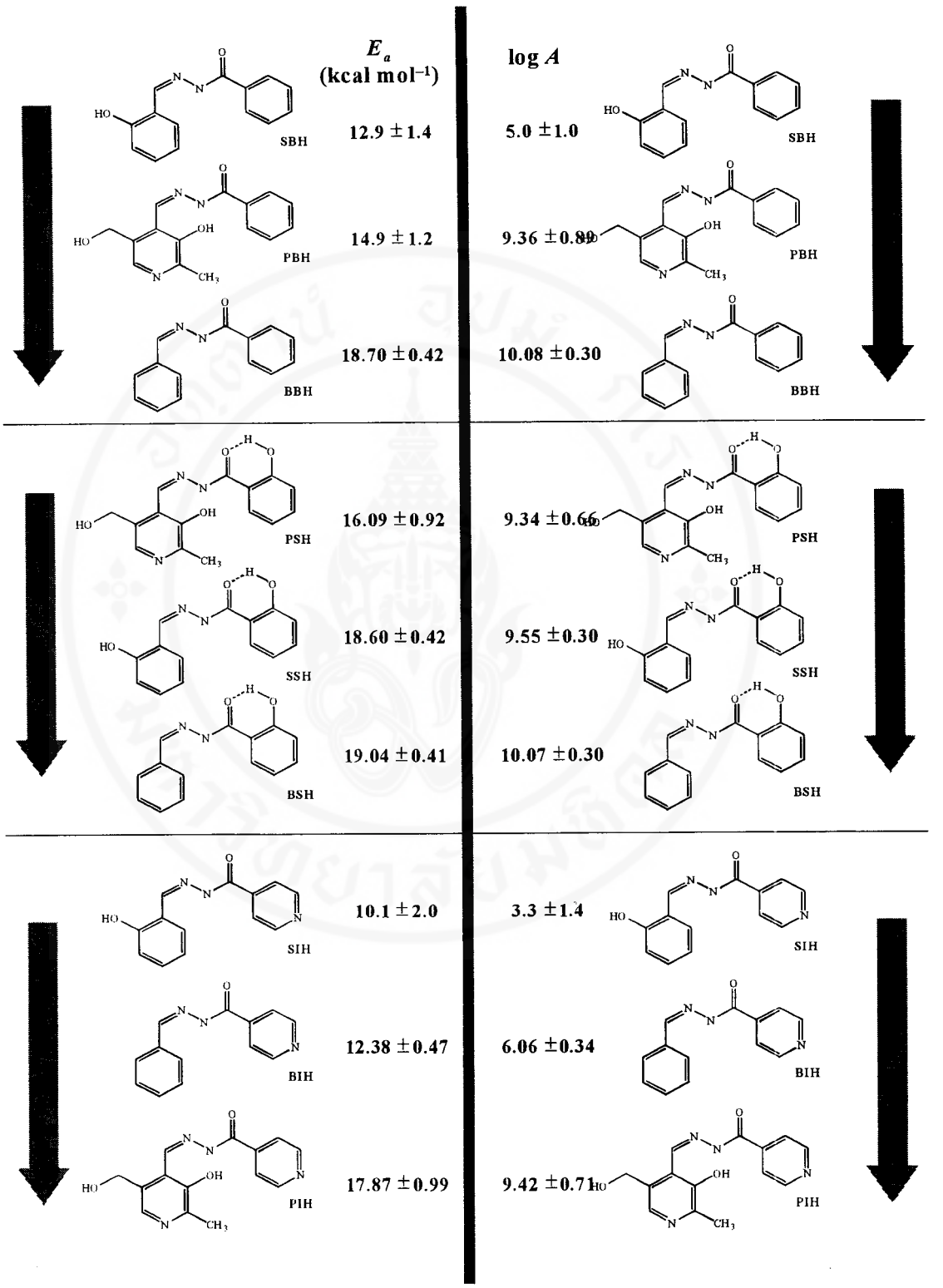

Figure 4.10 Figure showing the molecular structures of the *cis*-isomer of hydrazones together with their activation energies (E_a) and logarithm of the preexponential factors (log A). The hydrazidic part of the hydrazone is constant and the aldehydic group varied. The numerical values increase from top to bottom.

The temperature dependence of the first-order rate constant $k(T)$ can also be analyzed using the **Activated Complex Theory** (the transition state theory) of reaction rate. This states that

$$k(T) = \left(\frac{k_B T}{h}\right) e^{-\Delta G^{\ddagger}/RT} \qquad (4.1)$$

with $\Delta G^{\ddagger} = \Delta H^{\ddagger} - T\Delta S^{\ddagger}$

Where $\Delta G^{\ddagger}$ = standard free energy of activation

$\Delta H^{\ddagger}$ = standard enthalpy of activation

$\Delta S^{\ddagger}$ = standard entropy of activation

k_B = Boltzmann constant = 1.38066×10^{-23} J K^{-1}

and h = Planck constant = 6.626076×10^{-34} J s

In order to evaluate $\Delta H^{\ddagger}$ and $\Delta S^{\ddagger}$ from the measured rate constants $k(T)$, Equation 4.1 can be re-written as:

$$\left[\ln k(T) - \ln\left(\frac{k_B T}{h}\right)\right] R = \Delta S^{\ddagger} - \frac{\Delta H^{\ddagger}}{T} \qquad (4.2)$$

Thus a plot of the left-hand side of the above equation against $1/T$ will give a straight line of slope $-\Delta H^{\ddagger}$ and intercept of $\Delta S^{\ddagger}$.

The results of the least-squares linear regression of Equation 4.2 are given in Table 4.4.

Comparison of the values of $\Delta H^{\ddagger}$ and $\Delta S^{\ddagger}$ obtained using the Arrhenius equation and the Activated Complex Theory shows small differences in their values (see Tables 4.4 and 4.5). However the variation in $\Delta H^{\ddagger}$ and $\Delta S^{\ddagger}$ with the structure of the hydrazones still shows the same pattern.

Table 4.4 Standard enthalpy of activation ($\Delta H^{\ddagger}$) and standard entropy of activation ($\Delta S^{\ddagger}$) for the thermal cis-trans isomerization reaction of the hydrazones (calculated using the Activated Complex Theory)

Hydrazones	k (s^{-1}) at 25.0 °C	$\Delta H^{\ddagger}$ (J mol^{-1})	$-\Delta S^{\ddagger}$ (J K^{-1} mol^{-1})
SBH	$(3.481 \pm 0.016) \times 10^{-5}$	$(51.5 \pm 6.0) \times 10^{3}$	$(1.58 \pm 0.20) \times 10^{2}$
SSH	$(8.444 \pm 0.043) \times 10^{-5}$	$(75.3 \pm 1.8) \times 10^{3}$	$(7.06 \pm 0.57) \times 10^{1}$
SIH	$(9.04 \pm 0.12) \times 10^{-5}$	$(39.6 \pm 8.4) \times 10^{3}$	$(1.90 \pm 0.28) \times 10^{2}$
BSH	$(1.3053 \pm 0.0036) \times 10^{-4}$	$(77.1 \pm 1.7) \times 10^{3}$	$(6.06 \pm 0.57) \times 10^{1}$
PIH	2.01×10^{-4}	$(72.2 \pm 4.1) \times 10^{3}$	$(7.3 \pm 1.4) \times 10^{1}$
BBH	$(2.3693 \pm 0.0068) \times 10^{-4}$	$(75.7 \pm 1.8) \times 10^{3}$	$(6.04 \pm 0.58) \times 10^{1}$
BIH	$(9.58 \pm 0.28) \times 10^{-4}$	$(49.3 \pm 2.0) \times 10^{3}$	$(1.375 \pm 0.065) \times 10^{2}$
PSH	$(3.42 \pm 0.10) \times 10^{-3}$	$(64.8 \pm 3.9) \times 10^{3}$	$(7.5 \pm 1.3) \times 10^{1}$
PBH	$(2.582 \pm 0.080) \times 10^{-2}$	$(59.8 \pm 5.2) \times 10^{3}$	$(7.4 \pm 1.7) \times 10^{1}$

Table 4.5 Standard enthalpy of activation ($\Delta H^{\ddagger}$) and standard entropy of activation ($\Delta S^{\ddagger}$) for the thermal cis-trans isomerization reaction of the hydrazones (calculated using the Arrhenius equation)

Hydrazones	k (s^{-1}) at 25.0 °C	$\Delta H^{\ddagger}$ (J mol^{-1})	$-\Delta S^{\ddagger}$ (J K^{-1} mol^{-1})	$\Delta G^{\ddagger}$ (J mol^{-1})
SBH	$(3.481 \pm 0.016) \times 10^{-5}$	$(54.1 \pm 6.0) \times 10^{3}$	$(1.49 \pm 0.23) \times 10^{2}$	$(9.863 \pm 0.044) \times 10^{4}$
SSH	$(8.444 \pm 0.043) \times 10^{-5}$	$(77.8 \pm 1.8) \times 10^{3}$	$(6.21 \pm 0.17) \times 10^{1}$	$(9.632 \pm 0.049) \times 10^{4}$
SIH	$(9.04 \pm 0.12) \times 10^{-5}$	$(42.2 \pm 8.4) \times 10^{3}$	$(1.82 \pm 0.51) \times 10^{2}$	$(9.63 \pm 0.12) \times 10^{4}$
BSH	$(1.3053 \pm 0.0036) \times 10^{-4}$	$(79.6 \pm 1.7) \times 10^{3}$	$(5.21 \pm 0.13) \times 10^{1}$	$(9.517 \pm 0.026) \times 10^{4}$
PIH	2.01×10^{-4}	$(74.7 \pm 4.1) \times 10^{3}$	$(6.46 \pm 0.41) \times 10^{1}$	9.398×10^{4}
BBH	$(2.3693 \pm 0.0068) \times 10^{-4}$	$(78.2 \pm 1.8) \times 10^{3}$	$(5.19 \pm 0.13) \times 10^{1}$	$(9.368 \pm 0.027) \times 10^{4}$
BIH	$(9.58 \pm 0.28) \times 10^{-4}$	$(51.8 \pm 2.0) \times 10^{3}$	$(1.290 \pm 0.056) \times 10^{2}$	$(9.03 \pm 0.26) \times 10^{4}$
PSH	$(3.42 \pm 0.10) \times 10^{-3}$	$(67.3 \pm 3.9) \times 10^{3}$	$(6.60 \pm 0.39) \times 10^{1}$	$(8.70 \pm 0.26) \times 10^{4}$
PBH	$(2.582 \pm 0.080) \times 10^{-2}$	$(62.4 \pm 5.2) \times 10^{3}$	$(6.57 \pm 0.52) \times 10^{1}$	$(8.20 \pm 0.25) \times 10^{4}$

CHAPTER V

CONCLUSIONS

Although PIH has been extensively investigated for its possible use as iron chelating drug, it also possesses several interesting chemical properties. Attempt to elucidate the chemical properties regarding variation in the solid-state colour of PIH obtained from different preparation methods have been carried out.

In methanol, various types of PIH including pale yellow crystal, deep orange crystal purified from Sep-pak C-18 cartridge, deep orange powder (the hydrochloride of PIH) etc. give the same electronic absorption and fluorescence excitation and emission spectra. These suggest that in solution all types of solid PIH exist in the same form, i.e. normal Schiff-base form (non-dipolar form). From previous experimental evidence this structure is assumed as the trans configuration in carbon-nitrogen double bond, and the trans, anti and *s*-transoid conformations for the aromatic carbon and imine carbon, imine nitrogen and hydrazidic nitrogen, and hydrazidic nitrogen and carbonyl carbon, respectively. The presence of chloride ion has no effect on these spectroscopic properties. These results indicate that the solid-state structure of PIH is the cause of their differences in colour and form.

In solid state, experimental and spectroscopic techniques, including recrystallization, infrared spectroscopy and X-ray diffraction were employed to examine and confirm the various hypotheses concerning variation in colour and form of PIH.

1. Impurities are the cause of the deep orange colour of PIH in the solid state.
2. Chloride ion may result in the orange colour in crystal of PIH.
3. Existence of PIH in the solid state as a cis-trans isomeric mixture upon exposure to daylight, is the cause of deep orange colour (Avramovici-Grisaru *et al.*).
4. The existence of the dipolar form of PIH in the hydrated solid sample (1:1-PIH:H_2O) results in the orange colour (Webb *et al.*).

In this study, results of recrystallizations indicate that impurities, chloride ion and cis-trans isomeric mixture are not the cause of the deep orange colour. Therefore, only the last proposal is possible as the cause of this behaviour. From investigation of the solid-state structures of the various types of PIH using infrared spectroscopy, it is suggested that in the presence of water PIH can crystallize in the hydrated form (1:1 PIH-to-water) with the existence of molecule as the pyridinium phenolate (dipolar form), which generates the orange colour in the crystalline state. Unfortunately, crystallographic technique which was exploited to obtain additional information and to confirm infrared spectral data, regarding the molecular and crystal structures of the deep orange PIH (chloride free) are not available. Consequently, the exact solid-state structure is not known.

Although the solid-state structure of the deep orange PIH can not be definitely known from only infrared spectral data, the results are sufficient to confirm that the formation of the zwitterionic form of the pyridoxal due to the transfer of the phenolic proton to the pyridoxal nitrogen is the significant cause of the deep orange colour in the crystal of PIH.

Another interesting chemical property of PIH is the thermal- and photo-interconversions of the cis and trans isomers associated with the carbon-nitrogen double bond. It prompted investigation in aspects of both the photochemical cis-trans isomerization reaction and the kinetics of the thermal cis-trans geometrical isomerization. Other structurally related hydrazones, namely PBH, PSH, BIH, BBH, BSH, SIH, SBH and SSH were synthesized for the kinetic study.

From photochemical studies, it was found that PIH and structurally related compounds exhibit change in electronic absorption spectra when their solutions are exposed to light. On keeping in the dark, the spectra slowly convert to the initial spectra. This behaviour is proposed to be configurational change of the two diastereomers associated with the carbon-nitrogen double bond.

In the kinetic studies, it was found that the thermal cis-trans isomerization reactions of PIH and structurally related compounds are first order, with the activation energies of 10–19 kcal mol^{-1} and the common logarithm of preexponential factors of 3–10, calculated from the temperature dependence of these reactions in the range of 25–40 °C.

Variations of substituents on aldehydic and/or hydrazidic rings of the investigated hydrazones have a significant effect on the numerical values of the rate constant, the activation energy and the preexponential factor. However, it is noted that

the hydrazones, which possess the *ortho*-hydroxyl group to the imine bond with the possibility of tautomerization, have the activation energies and the preexponential factors of the same magnitude as the unsubstituted hydrazones.

The activation energies and the preexponential factors are related to the *cis*-molecular structures of the hydrazones. It is difficult to compare the rates of the thermal cis-trans isomerizations of hydrazones. However, for hydrazones which have the same value of the preexponential factors, their rates of reactions can be compared.

The temperature dependence of the first-order rate constant $k(T)$ has also been analyzed using the **Activated Complex Theory** (the transition state theory) of reaction rate. Comparison of the values of $\Delta H^{\ddagger}$ and $\Delta S^{\ddagger}$ obtained using the Arrhenius equation and the Activated Complex Theory shows small differences in their values. However, the variation in $\Delta H^{\ddagger}$ and $\Delta S^{\ddagger}$ with the structure of the hydrazones still shows the same pattern.

REFERENCES

1. Ponka P, Borova J, Neuwirt J, Fuchs O. Mobilization of iron from reticulocytes: Identification of pyridoxal isonicotinoyl hydrazone as a new iron chelating agent. FEBS Letters 1979;97(2):317-21.
2. Ponka P, Borova J, Neuwirt J, Fuchs O, Necas E. A study of intracellular iron metabolism using pyridoxal isonicotinoyl hydrazone and other synthetic chelating agents. Biochim. Biophys. Acta 1979;586:278-97.
3. Vitolo LMW. New chelating agents for the treatment of thalassemia [Ph.D. Thesis]. Australia: School of Mathematical and Physical Sciences, Murdoch University, 1984.
4. Wettermark G, Dogliotti L. Transient species in the photolysis of anils. J. Chem. Phys. 1964;40(6):1486-7.
5. Anderson DG, Wettermark G. Photoinduced isomerizations in anils. J. Am. Chem. Soc. 1965;87(7):1433-8.
6. Cohen MD, Schmidt GMJ. Photochromy and thermochromy of anils. J. Phys. Chem. 1962;66:2442-5.
7. Suppan P. Chemistry and light. Cambridge: The Royal Society of Chemistry, 1994.
8. Alarcón SH, Olivieri AC, Labadie GR, Cravero RM, González-Sierra M. Tautomerism of representative aromatic α-hydroxy carbaldehyde anils as studied by spectroscopic methods and AM1 calculations. Synthesis of 10-hydroxyphenanthrene-9-carbaldehyde. Tetrahedron 1995;51(16):4619-26.

9. Alarcón SH, Olivieri AC, Nordon A, Harris RK. Solid-state electronic absorption, fluorescence and ^{13}C CPMAS NMR spectroscopic study of thermo- and photo-chromic aromatic Schiff bases. J. Chem. Soc., Perkin Trans. 2 1996;2293-6.

10. Alarcón SH, Olivieri AC, González-Sierra M. ^{13}C NMR spectroscopic and AM1 study of the intramolecular proton transfer in anils of salicylaldehyde and 2-hydroxynaphthalene-1-carbaldehyde. J. Chem. Soc., Perkin Trans. 2 1994;1067-70.

11. Hadjoudis E, Vittorakis M, Moustakali-Mavridis I. Photochromism and thermochromism of Schiff bases in the solid state and in rigid glasses. Tetrahedron 1987;43(7):1345-60.

12. Ogawa K, Kasahara Y, Ohtani Y, Harada J. Crystal structure change for the thermochromy of *N*-salicylideneanilines. The first observation by X-ray diffraction. J. Am. Chem. Soc. 1998;120(28):7107-8.

13. Becker RS, Richey WF. Photochromic anils. Mechanisms and products of photoreactions and thermal reactions. J. Am. Chem. Soc. 1967;89(6):1298-1302.

14. Padwa A. Photochemistry of the carbon-nitrogen double bond. Chem. Rev. 1977;77(1):37-68.

15. Crichton RR. Inorganic biochemistry of iron metabolism. Chichester: Ellis Horwood, 1991.

16. Bothwell TH, Charlton RW, Cook JD, Finch CA. Iron metabolism in man. Oxford: Blackwell, 1979.

17. Gordeuk VR, Bacon BR, Brittenham GM. Ann. Rev. Nutr. 1987;7:485-508.

18. Powell L, Halliday J. In: Jacobs A, Worwood N, editors. Iron in biochemistry and medicine II. London: Academic Press, 1980. Ch. 13.

19. Jacobs A. In: Jacobs A, Worwood N, editors. Iron in biochemistry and medicine II. London: Academic Press, 1980. Ch. 12.

20. Weatherall DJ, Clegg JB. The thalassemia syndromes. 3rd ed. Oxford: Blackwell Scientific Publication, 1981.

21. Martell AE, Anderson WF, Badman DG, editors. Development of iron chelators for clinical use. Proceedings of the Second Symposium on the Development of Iron Chelators for Clinical Use; 1980 August 23-24; San Francisco, California. New York: Elsevier North Holland; 1981.

22. Peter HH. In: Spik G, Montreuil J, Crichton RR, Mazurier J, editors. Proteins of iron storage and transport. Amsterdam: Elsevier, 1985. p. 293-303.

23. Herschko C, Weatherall DJ. CRC Crit. Rev. Clin. Lab. Sci. 1988;26:303-45.

24. Porter J. Eur. J. Haematol. 1989;43:271-85.

25. Bickel H, Gäumann E, Keller-Schierlein W, Prelog V, Vischer E, Wettstein A, Zähner H. Ueber eisenhaltige Wachstums-factoren, die Sideroamine and ihre Antagonisten, die eisenhaltigen Antibiotika Sideromycine. Experimentia 1960;16:129.

26. Waxman HS, Brown EB. Clinical usefulness of iron chelating agents. In: Brown EB, Moore CV, editors. Progress in Hematology, Vol. VI. New York: Grune & Stratton, 1969. p. 338.

27. Keberle H. The biochemistry of desferrioxamine and its relation to iron metabolism. Ann. N. Y. Acad. Sci. 1964;119:758.

28. Keller-Schierlein W. Chemistry of iron chelating agents from microorganisms; development and characterization of desferrioxamine B. In: Anderson WF, Hiller MC, editors. Proceedings of a Symposium: Development of Iron Chelators for Clinical Use. DHEW Publication No. (NIH) 76-994, 1976. p. 53.

29. Modell B. Advances in the use of iron chelating agents for the treatment of iron overload. In: Brown EB, editor. Progress in Hematology, Vol. XI. New York: Grune & stratton, 1979. p. 267.

30. Cikrt M, Ponka P, Necas E, Neuwirt J. Biliary iron excretion in rats following pyridoxal isonicotinoyl hydrazone. Br. J. Haematol. 1980;45:275-83.

31. Hershko C, Avramovici-Grisaru S, Link G, Gelfand L, Sarel S. Mechanism of in vivo iron chelation by pyridoxal isonicotinoyl hydrazone and other imino derivatives of pyridoxal. J. Lab. Clin. Med. 1981;98:99-108.

32. Hoy T, Humphrys J, Jacobs A, Ponka P. Effective iron chelation following oral administration of an isoniazid-pyridoxal hydrazone. Br. J. Haematol. 1979;43:443-9.

33. Johnson DK, Pippard MJ, Murphy TB, Rose NJ. An in vivo evaluation of iron-chelating drugs derived from pyridoxal and its analogs. J. Pharmacol. Exp. Ther. 1982;221(2):399-403.

34. Murphy TB, Johnson DK, Rose NJ, Aruffo A, Schomaker V. Structural studies of iron(III) complexes of the new iron-binding drug, pyridoxal isonicotinoyl hydrazone. Inorg. Chim. Acta 1982;66:L67-L68.

35. Murphy TB, Rose NJ, Schomaker V, Aruffo A. Syntheses of iron(III) aroyl hydrazones containing pyridoxal and salicylaldehyde. The crystal and

molecular structure of two iron(III)-pyridoxal isonicotinoyl hydrazone complexes. Inorg. Chim. Acta 1985;108:183-94.

36. Heinert D, Martell AE. Pyridoxine and pyridoxal analogs. II. Infrared spectra and hydrogen bonding. J. Am. Chem. Soc. 1959;81:3933.

37. Bellamy LJ. The Infrared spectra of complex molecules. 3rd ed. New York: John Wiley & Sons, 1975.

38. Richardson DR, Vitolo LMW, Hefter GT, May PM, Clare BW, Webb J, Wilairat P. Iron chelators of the pyridoxal isonicotinoyl hydrazone class. Part I. Ionisation characteristics of the ligands and their relevance to biological properties. Inorg. Chim. Acta 1990;170:165-70.

39. Vitolo LMW, Hefter GT, Clare BW, Webb J. Iron chelators of the pyridoxal isonicotinoyl hydrazone class. Part II. Formation constants with iron(III) and iron(II). Inorg. Chim. Acta 1990;170:171-6.

40. Avramovici-Grisaru S, Sarel S, Link G, Hershko C. Syntheses of iron bis (pyridoxal isonicotinoylhydrazone)s and the in vivo iron-removal properties of some pyridoxal derivatives. J. Med. Chem. 1983;26:298-302.

41. Dubois JE, Fakhrayan H, Doucet JP, El Hage Chahine JM. Kinetic and thermodynamic study of complex formation between iron(II) and pyridoxal isonicotinoylhydrazone and other synthetic chelating agents. Inorg. Chem. 1992;31(5):853-9.

42. Colonna C, Cossé-Barbi A, Massat A, Doucet JP. IR studies of iron complexes with pyridoxal isonicotinoyl hydrazone and three other similar chelating agents. Spectr. Letters 1993;26(6):1065-72.

43. Colonna C, Doucet JP, Cossé-Barbi A. Infrared study of seven potential siderophores analogous to salicylaldehyde benzoyl hydrazone (SBH). Spectr. Letters 1994;27(9):1153-63.

44. Colonna C, Doucet JP, Cossé-Barbi A. Infrared study of complexes between iron, salicylaldehyde benzoyl hydrazone and seven analogous derivatives. Transition Met. Chem. 1995;20:338-43.

45. Doungdee P, Sarel S, Ringel I, Gibson D, Wongvisetsirikul N, Avramovici-Grisaru S. Iron chelators of the pyridoxal 2-pyridyl hydrazone class. Part III. Ionisation and conformational characteristics of the ligands. Heterocycles 1995;40(1):241-8.

46. Doungdee P, Sarel S, Wongvisetsirikul N, Avramovici-Grisaru S. Iron chelators of the pyridoxal 2-pyridyl hydrazone class. Part 4. pK_a Values of the chelators and their relevance to biological properties. J. Chem. Soc., Perkin Trans. 2 1995;319-23.

47. Turro NJ. Modern molecular photochemistry. Menlo Park (CA): The Benjamin/Cummings Publishing, 1978.

48. Turro NJ. Molecular photochemistry. New York: W. A. Benjamin, 1965.

49. Patai S, editor. The chemistry of the carbon-nitrogen double bond. New York: Interscience, 1969.

50. Curtin DY, Grubbs EJ, Gordon McCarty C. Uncatalyzed syn-anti isomerization of imines, oxime ethers, and haloimines. J. Am. Chem. Soc. 1966;88(12):2775-86.

51. Wettermark G. Sven. Kem. Tidskr. 1967;79:249.

52. Fischer E, Frei Y. Photoisomerization equilibria involving the C=N double bond. J. Chem. Phys. 1957;27:808-9.

53. Archer S, Auerbach ME. Pyridoxal isonicotinoyl hydrazone. US Patent 2, 775, 598. Dec 25, 1956.

54. Sah PPT. Nicotinyl and isonicotinyl hydrazones of pyridoxal. J. Am. Chem. Soc. 1954;76:300.

55. Matsushima Y, Martell AE. J. Am. Chem. Soc. 1967;89:1322.

56. Metzler DE, Snell EE. Spectra and ionization constants of the vitamin B_6 group and related 3-hydroxypyridine derivatives. J. Am. Chem. Soc. 1955;77:2431-37.

57. Nakamoto K, Martell AE. Pyridoxine and pyridoxal analogs. III. Ultraviolet absorption studies and solution equilibria of 2- and 4-hydroxymethyl-3-hydroxypyridines and pyridine-2, 3- and 4-aldehydes. J. Am. Chem. Soc. 1959;81:5857-63.

58. Davis L, Roddy F, Metzler DE. Metal chelates of imines derived from pyridoxal and amino acids. J. Am. Chem. Soc. 1961;83:127-34.

59. Metzler DE. Equilibria between pyridoxal and amino acids and their imines. J. Am. Chem. Soc. 1957;79:485-90.

60. Freedman HH. Intramolecular H-bonds. I. A spectroscopic study of the hydrogen bond between hydroxyl and nitrogen. J. Am. Chem. Soc. 1961;83:2900.

61. Lang L, editor. Absorption spectra in the ultraviolet and visible region. Vol. I-IV, 1962.

62. Calvert JG, Pitts JN. Photochemistry. New York: John Wiley & Sons, 1966.

63. Pavia DL, Lampman GM, Kriz GS. Introduction to spectroscopy: A guide for students of organic chemistry. 2nd ed. Fort Worth: Saunders College Publishing, 1996.

64. Silverstein RM, Bassler GC, Morrill TC. Spectrometric identification of organic compounds. 5th ed. New York: John Wiley & Sons, 1991.

65. Sala LF, Martell AE, Motekaitis RJ. Spectral properties and desmotropy of the Schiff base of diethylaminomalonate and pyridoxal hydrochloride. Inorg. Chim. Acta 1987;135:123-7.

66. Hadži D. Absorption spectra and structure of some solid hydroxyazo-compounds. J. Chem. Soc. 1956;2143-50.

67. Nakanishi K. Infrared absorption spectroscopy: Practical. San Francisco: Holden-Day, 1962.

68. Shriner RL, Hermann CKF, Morrill TC, Curtin DY, Fuson RC. The systematic identification of organic compounds. 7th ed. New York: John Wiley & Sons, 1998.

69. Srisorrachatr S. Kinetics and thermodynamics of complex formation reaction of hydrazones with some metal ions in aqueous solution [Ph.D. Thesis in Physical Chemistry]. Bangkok: Faculty of Graduate Studies, Mahidol University, 1988.

70. Singh G, Shastry PSSJ, Lonibala RK, Rao TR. Coordination behaviour of pyridoxalisonicotinoyl hydrazone towards some 3d-metal ions. Synth. React. Inorg. Met. -Org. Chem. 1992;22(7):1041-59.

71. Furniss BS, Hannaford AJ, Smith PG, Tatchell AR. Vogel's textbook of practical organic chemistry. 5th ed. Essex: Longman Group UK, 1989.

72. Fleck GM. Chemical reaction mechanisms. New York: Holt, Rinehart and Winston, 1971.

73. Levine IN. Physical chemistry. 4th ed. New York: McGraw-Hill, 1995.

74. Laidler KJ, Meiser JH. Physical chemistry. 3rd ed. Boston: Houghton Mifflin, 1999.

75. Silberberg M. Chemistry: the molecular nature of matter and change. St. Louis: Mosby-Year Book, 1996.

76. Sangma C. Study on chemical and physical properties of some isonicotinoyl hydrazone compounds [M.S. Thesis in Physical Chemistry]. Bangkok: Faculty of Graduate Studies, Mahidol University, 1984.

77. Fakhrayan H, Doucet JP, El Hage Chahine JM. The prototropic structural transformations of pyridoxalbenzoylhydrazone and other synthetic chelating ligands. Bull. Soc. Chim. Belg. 1993;102(6):377-89.

78. Chetuphon S. Kinetic study of Fe(III) ion with some isonicotinoyl hydrazones [M.S. Thesis in Physical Chemistry]. Bangkok: Faculty of Graduate Studies, Mahidol University, 1985.

79. Sarel S, Cohen S, Avramovici-Grisaru S. Iron chelators of the class of pyridoxal acylhydrazone. Part 5. Crystal structure and patterns of hydrogen bonding in pyridoxal isonicotinoyl hydrazone (PIH). Heterocycles 1998;47(2):1033-42.

80. Webb J, Vitolo ML. Birth Defects 1988;5B 23:63.

81. Johnston SF. Fourier transform infrared: A constantly evolving technology. Chichester: Ellis Horwood, 1991.

82. Narang KK, Aggarwal A. Indian J. Chem. 1975;13A:1072.

BIOGRAPHY

NAME	Mr. Opas Tojira
DATE OF BIRTH	March 8, 1974
PLACE OF BIRTH	Bangkok, Thailand
INSTITUTIONS ATTENDED	Mahidol University, 1992–1996: Bachelor of Science (Chemistry)
	Mahidol University, 1996–2000: Master of Science (Physical Chemistry)
RESEARCH GRANT / FELLOWSHIP	Institutional Strengthening Program supported by the National Science and Technology Development Agency (NSTDA) and Faculty of Science, Mahidol University; 1996–1998
	Teaching Assistant Scholarship Supported by Faculty of Graduate Studies, Mahidol University; 1998